Regulation of γTuRC-mediated microtubule nucleation studied *in vitro*

Tanja Consolati

University College London
&
The Francis Crick Institute

Supervised by Thomas Surrey

A thesis submitted for the degree of
Doctor of Philosophy

University College London
UK
April, 2019

Declaration

I Tanja Consolati, confirm that the work presented in this thesis is my own. Where information has been derived from other sources, I confirm that this has been indicated in the thesis.

Abstract

Microtubules are cytoskeletal filaments central to a wide range of cellular processes: they serve as tracks for intracellular transport, provide mechanical support, serve as building blocks for flagella and cilia and drive the separation of the genomic material for cell division. The organization of the microtubule cytoskeleton into different architectures is crucial for its function. Cells regulate the formation of these microtubule arrays by tight temporal and spatial control over the nucleation of new microtubules.

The main microtubule nucleator *in vivo* is the γ-tubulin ring complex (γTuRC), a multi-subunit complex conserved in all eukaryotic cells. Currently, the molecular mechanism of γTuRC-mediated microtubule nucleation is poorly understood. This is in part due to the difficulty to purify γTuRCs with good yields, in particular from higher eukaryotes, and the lack of an assay able to visualize and quantify microtubule nucleation kinetics in real time.

In cells, the γTuRC interacts with a multitude of proteins important for γTuRC localization and/or activation. In addition, it has emerged that γTuRC nucleation efficiency can be modulated by microtubule binding proteins via their effects on microtubule dynamics. What is missing is a framework to understand how these different factors regulate the γTuRC activity and how they can mechanistically work together to control γTuRC-mediated microtubule nucleation in cells.

To address this question, I established a new method for the purification of human γTuRCs from a stable cell line and developed a new real-time dynamic TIRF microscopy-based microtubule nucleation assay. The activity of purified γTuRCs was studied in the presence and in the absence of potential regulators and microtubule binding proteins in order to better understand the mechanism of microtubule nucleation and its regulation.

Für meine Eltern

Acknowledgement

I would like to thank Thomas Surrey for taking me on as a PhD student. Thank you for the support and mentorship that you have given me throughout my PhD. And thanks for always taking time to discuss. I would also like to thank Anne Straube and Anthony Roberts for agreeing to examine my thesis. Lastly I would like to thank my thesis committee, Guillaume Charras, Neil McDonald and Nathan Goerhing, for their support and helpful comments. Thanks for never doubting that something will come out of this project.

I would like to thank all current and past members of the Surrey lab for sharing this roallercoaster ride with me: Claire, Julian, Nic, Jamie, Jono, Franck, Christian, Iris, Rupam and Jayant. Specials thanks to Gil, Wei Ming and Christel for being the most amazing coffee buddies. Most importantly, I wish to thank Johanna Roostalu, for teaching me literally everything I know, for being a living microtubule library, your incredible patience and for always being there for me. It has been a pleasure to work with you and this thesis would not exist without you.

Science apart, I would also like to thank all of the friends I made during my PhD here in London and the friends I left behind in Austria. Thanks to Oliver, Ania, Paula, Carlson, Daniel, Janneke, Amparo and Mar. You are amazing! Without you guys these years wouldn't have been the same. Thanks for all the dinner parties, BBQs, all the travels we did together… Thanks for introducing me to aerial silks, Ania! You gave me the best present of my life and probably my biggest addiction. Thanks for the sofa and the food, Carlson. I might have starved to death without you. Living with you and sharing time with you has been one of the best things that happened to me these past years. :-) Thanks to Jutta, Andrea, Sanel, Martin, Chris, Cristina and Juanma for always believing in me and making me feel as if I never left home when I came back to visit. Thanks to Carlos, Bea, Sara, StJohn, Stefan and Ainoah for all the nights out, concerts, Finsbury park, coffees, pub quizzes… Carlos, Carlson and Johanna, this PhD has been a crazy whirlwind and you managed to always pick me up, keep me calm and get me to push through it. Thanks for always having time for a drink to cheer me on :-)

Lastly, I would like to thank my parents, my grandparents and my sisters for their love and support, without which none of these would have been possible. Thanks to my sisters for their surprise visits and my mum for the highly appreciated austrian food deliveries. Liebe Mama, lieber Papa. Thanks for allowing me to succeed and fail. Thanks for letting me take my own decisions. Thanks for believing in me and thanks for always welcoming me back home.

Special thanks to the Nala Mochi, who never failed to distract me from work.

Impact statement

Microtubules are important cytoskeletal filaments and well known drug targets in disease like cancer. They are nucleated to a large part by the γ-tubulin ring complex (γTuRC), a multiprotein complex known to be tightly regulated in cells. The targeting of microtubules in cancer has often led to conditions known as chemotherapy-induced peripheral neuropathy (CIPN). A condition which leads to cancer survivor disability and limits drug dosage and/or duration. An alternative to targeting microtubules directly would therefore be the inhibition of γTuRCs or proteins which regulate the complex. It has been shown that siRNA depletion of γTuRC components sensitizes a lung cancer cell line at 1000-fold reduced doses of the known cancer drug paclitaxel. Moreover, NEDD1, a major γTuRC recruitment factor in cells, has been shown to potentiate the anti-mitotic activity of a Plk1 inhibitors.

Currently the mechanism of microtubule nucleation by γTuRCs and the regulation of the complex are poorly understood. In part, this is due to the difficulty to study γTuRC regulation in cells as a multitude of regulatory factors has been identified which often have multiple functions *in vivo*. On the other hand, *in vitro* studies have been hampered by the difficulty to purify γTuRCs from higher eukaryotes in sufficient amounts. In addition, the lack of an assay which allows the real-time study of γTuRC-mediated microtubule nucleation has limited the biochemical characterization of the complex and in turn the study of its regulation.

In this thesis, I present a new approach for the purification of human γTuRCs from a stable cell line and the development of a new microtubule nucleation assay which for the first time can directly measure the effect of regulatory proteins on γTuRC nucleation activity. Using this assay, I was able to dissect the mechanism of two important modulators of microtubule dynamics on γTuRC-mediated microtubule nucleation.

In the future, I hope that the new assay showed in here can be used to elucidate how cells control the efficiency of microtubule nucleation by γTuRCs and establish a framework for the regulation of the complex *in vivo*. A better understanding of the underlying mechanism of individual regulatory proteins on the activity of γTuRCs will consequently open up new avenues for the γTuRC or associated proteins as targets in disease like cancer.

Table of content

Table of Figures

List of Tables

Abbreviations

AKAP450	A-kinase anchoring protein 450
AS	Ammonium sulfate
ADP	Adenosine diphosphate
ATP	Adenosine triphosphate
Arp2/3 complex	actin-related protein 2/3 complex
APC	adenomatous polyposis coli
Bio-	Biotinylated
CDK5	Cyclin-dependent kinase 5
CAMSAP	Calmodulin-regulated spectrin-associated protein
CDK5Rap2	CDK5 Regulatory Subunit Associated Protein 2
Cep169	Centrosomal protein 169
Cep192	Centrosomal protein 192
chTOG	Colonic and hepatic tumor overexpressed gene protein
CLASPs	Cytoplasmic linker associated proteins
CM1	Centrosomin motif 1
Cryo-EM	Cryogenic electron microscopy
Cobl	cordon-bleu
DMEM	Dulbecco's Modified Eagle Medium
DNA	Deoxyribonucleic acid
DTT	Dithiothreitol
E. Coli	Escherichia coli
EB	End-binding protein
EB1	End-binding Protein 1
EB3	End-binding Protein 3
EDTA	Ethylenediaminetetraacetic acid
EGTA	Ethylene glycol-bis(β-aminoethylether)-N,N,N',N'-tetraacetic acid
GCPs	Gamma-tubulin component proteins
GDP	Guanosine diphosphate
GFP	Green fluorescent protein
GMPCPP	Guanylyl 5'-α,β-methylenediphosphate
GOPTS	(3-Glycidyloxypropyl)trimethoxysilane
Grip	γ-tubulin ring protein
GST	Glutathione-S-transferase

GTP	Guanosine triphosphate
FRET	Fluorescence resonance energy transfer
HA	Hemagglutinin
HAUS	Human Augmin-like Complex
HEK293	Human embryonic kidney 293 cells
HEPES	(4-(2-hydroxyethyl)-1-piperazineethanesulfonic acid)
HRP	Horseradish peroxidase
JMY	junction-mediating and regulatory protein
KCl	Potassium chloride
kDa	Kilo Daltons
KIF4a	Kinesin Family Member 4A
LB	Lysogeny Broth
LC	Liquid chromatography
Lmod	leiomodin
LGALS3BP	Galectic-3-binding protein
MAPs	Microtubule associated proteins
mBFP	Monomeric blue fluorescent protein
MS	Mass spectrometry
MSAs	Microtubule stabilizing agents
MTOC	Microtubule organizing center
Mzt1	Mozart 1 / Mitotic-spindle organizing protein 1
Mzt2	Mozart 2 / Mitotic-spindle organizing protein 2
NEDD1	Neural Precursor Cell Expressed, Developmentally Down-Regulated 1
NHS	N-hydroxysuccinimide ester
NPFs	nucleation promoting factors
NME7	Nucleoside diphosphate kinase 7
OD	Optical density
$p150^{Glued}$	150 kDa Dynein-Associated Polypeptide
PAGE	Polyacrylamide gel electrophoresis
PBS	Phosphate buffer saline
PBST	PBS supplemented with Tween
PCM	Pericentriolar material
PCR	Polymerase Chain Reaction
PEG	Polyethylene glycol
PIPES	Piperazine-N,N'-bis(2-ethanesulfonic acid)

PRC1	Protein regulator of cytokinesis 1
PVDF	Polyvinylidene difluoride
RanGTP	GTP-bound Ras-related Nuclear Protein
RCC1	Regulator of chromosome condensation 1
RHAMM	Receptor for Hyaluronan Mediated Motility
SAFs	Spindle assembly factors
SDS	Sodium dodecyl sulfate
Spc110	Spindle pole component 110
Spc72	Spindle pole component 72
TIPs	Microtubule end-tracking proteins
TIRF	Total Internal Reflection Fluorescence
TIRFM	Total Internal Reflection Fluorescence Microscopy
TOG	Tumor overexpressed gene
TPX2	Targeting protein for Xklp2
βME	β mercaptoethanol
γTuNA	γTuRC-mediated nucleation activator
γTuRC	γ-tubulin ring complex
γTuSC	γ-tubulin small complex

1. Introduction

1.1 The cytoskeleton

The cytoskeleton is an interconnected network of filamentous polymers and regulatory proteins which fulfils a variety of essential functions including the organization of the internal architecture of cells, the generation of forces to enable cells to move, change shape and undergo cell division. It provides a physical and biochemical link of the cells interior with the external environment. The building blocks of the cytoskeleton are three classes of filaments: intermediate filaments, actin filaments and microtubules (see Figure 1.1). They are dynamic filaments which can disassemble and reassemble into a variety of structures with diverse properties depending on the cellular needs. The main differences between the filaments are their mechanical stiffness, the dynamics of their assembly and polarity and the type of associated proteins with which they interact (Fletcher and Mullins, 2010; Vignaud et al., 2012).

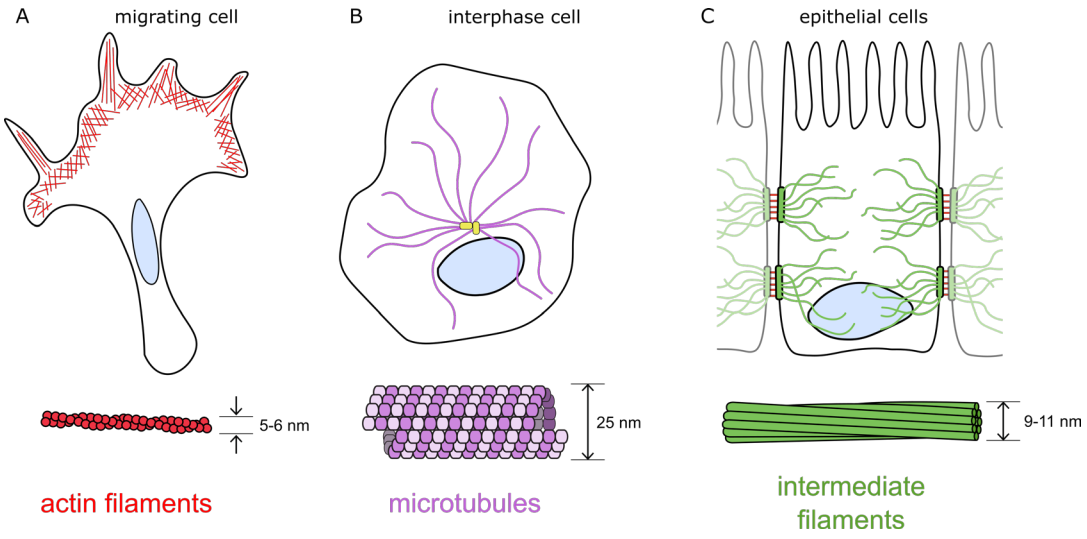

Figure 1.1: The building blocks of the cytoskeleton. (A) actin filaments depicted at the leading edge of a migrating cell. (B) Microtubules forming a radial interphase array. (C) the intermediate filament keratin at cell junctions between adjacent epithelial cells. A simplified structure of each type of filament is shown.

Intermediate filaments are nonpolar and do not interact with motor proteins (Robert et al., 2016). They have a high resistance to mechanical stress and are more flexible than microtubules and actin-filaments (Charrier and Janmey, 2016; Janmey et al., 1991). They are built from a diverse family of fibrous proteins that share structural

features (Eriksson et al., 2009; Geisler and Weber, 1982; Hesse et al., 2001; Steinert and Roop, 1988). Intermediate filaments assemble in a step-wise fashion which does not require energy. First, monomers assemble into tetramers which in turn laterally associate into a small filament. Filaments then grow by end to end association with other filaments (Herrmann and Aebi, 1998; Kirmse et al., 2007; Portet et al., 2009). Functionally, intermediate filaments form elaborate networks that connect the cell cortex to intracellular organelles and they are important tension bearing elements contributing to the mechanical and motile properties of cells (Cheng and Eriksson, 2017; Etienne-Manneville, 2018).

While intermediate filaments polymerize through self-assembly, the formation of both actin and microtubules is thermodynamically limited by a nucleation step (Mitchison, 1992; Tobacman and Korn, 1983; Voter and Erickson, 1984). In cells initiation of filament polymerization is tightly controlled through nucleation-promoting factors and regulators which promote faster or more sustained filament growth (Firat-Karalar and Welch, 2011; Tovey and Conduit, 2018). Both, actin and microtubule filaments can generate forces which are drivers for cell shape changes and together with motor proteins they are arranged in three-dimensional patterns and guide the organization of cellular compartments (Fletcher and Mullins, 2010; Vignaud et al., 2012).

Actin filaments are semi-flexible polymers which are important for processes including cell division, the establishment of cell polarity, morphogenesis and motility (May and Machesky, 2001; Pollard and Borisy, 2003; Pollard and Cooper, 2009). Bundles of actin filaments support filopodial protrusions involved in chemotaxis and cell-cell adhesion (Lidke et al., 2005; Mattila and Lappalainen, 2008; Vasioukhin et al., 2000). Many motile cells form networks of highly branched filaments at the leading edge to support movement or phagocytosis (Abraham et al., 1999; May et al., 2000). During cytokinesis actin filaments are central for cell rounding and the formation of the contractile ring for the abscission of the two daughter cells (Kamasaki et al., 2007; Reichl et al., 2008). Actin filaments (F-actin) are polar staggered double helices formed by nucleation and directional polymerization of monomeric globular actin molecules (G-actin) (Kasai et al., 1962; Wegner, 1976). Actin filaments grow through incorporation of ATP-actin at the barbed end followed by hydrolysis of the ATP and phosphate release within the filament lattice. ATP hydrolysis destabilizes the actin filaments and leads to their disassembly from the pointed end known as treadmilling behaviour (Fujiwara et al., 2002; Korn et al., 1987; Neuhaus et al., 1983).

Microtubules are the stiffest polymers with the most complex assembly and disassembly dynamics (Fletcher and Mullins, 2010; Gittes, 1993). They are assembled from tubulin dimers which stack into protofilaments to form a hollow

cylinder (Amos and Klug, 1974; Nogales, 2001). Their plus- and minus-ends exert a unique switching behaviour between phases of growth and shrinkage (Mitchison and Kirschner, 1984a). Microtubule nucleation is confined to a variety of different subcellular structures termed microtubule organizing centres (MTOCs). Each type of MTOC has the ability to support the assembly of a particular type of microtubule array through the local recruitment and activation of microtubule nucleators, motor proteins and regulators of microtubule dynamics (Teixidó-Travesa et al., 2012; Wu and Akhmanova, 2017). For example, microtubules nucleated from the centrosome form radial arrays, well suited for organelle positioning and providing tracks for vesicular transport (Gould and Borisy, 1977). In differentiated cells such as neurons, muscle cells or epithelial cells, non-centrosomal microtubule nucleation and organization gives rise to a variety of different arrays best serving the function of each cell type (Bartolini and Gundersen, 2006; Sanchez and Feldman, 2017). Most importantly, the microtubule cytoskeleton assembles the bipolar spindle crucial for chromosome segregation during cell division (Duncan and Wakefield, 2011).

1.1.1 Microtubule structure and dynamics

Microtubules assemble from αβ-tubulin dimers and usually consist of 13 linear protofilaments arranged into a pseudo-helical hollow tube of 25 nm in diameter (see Figure 1.2) (Beese et al., 1987; Evans et al., 1985; Nogales et al., 1999). Microtubules grow by the stochastic addition of GTP-loaded αβ-tubulin dimers in a head-to-tail fashion at microtubule ends (Amos and Klug, 1974; Cote and Borisy, 1981). Both, α- and β-tubulin bind to the nucleotide GTP (Weisenberg et al., 1968). While the GTP in the α-tubulin does not exchange, the GTP bound to the β-tubulin hydrolyses (David-Pfeuty et al., 1977; MacNeal and Purich, 1978; Spiegelman et al., 1977). New subunits are incorporated into the existing microtubule lattice through weak non-covalent bonds and GTP hydrolysis in the β-tubulin is stimulated by the formation of intersubunit contacts. This gives rise to a GDP microtubule shaft with a cap of GTP-bound β-tubulin at the polymerizing microtubule tip (Carlier and Pantaloni, 1981; Hyman et al., 1995). Tubulin dimers within protofilaments make longitudinal α-β-α-β and lateral α-α and β-β contacts. Protofilaments are slightly offset to each other adding a pseudo-helical arrangement to the microtubule. This is known as the ‘three-start lattice’ and results in a ‘seam’, which runs along the length of the microtubule. At the seam lateral contacts are replaced by α-β interactions (Kikkawa et al., 1994). The two ends of each microtubule are structurally different due to the orientation of the heterodimers which gives microtubules an intrinsic polarity. α-tubulin is exposed

at one end (minus-end) and β-tubulin at the other end (plus-end) (Allen and Borisy, 1974; Desai and Mitchison, 1997).

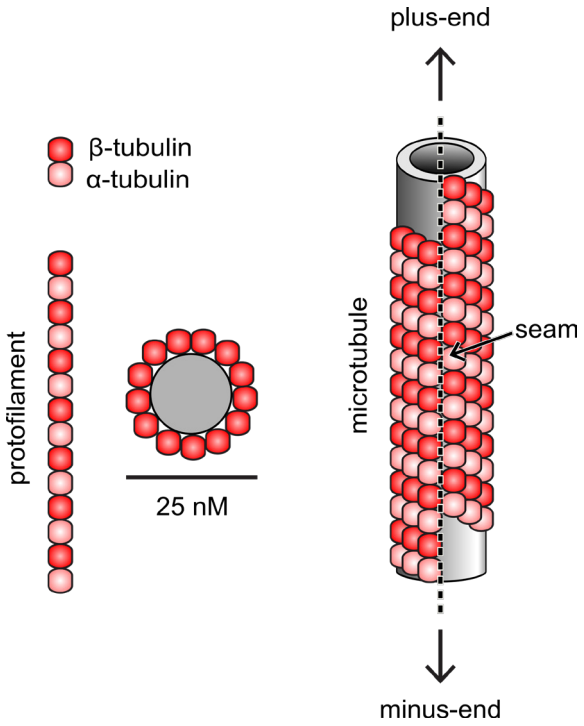

Figure 1.2: Schematic illustration of the microtubule structure.

Microtubules are inherently dynamic and switch stochastically between phases of growth and shrinkage, a behaviour known as dynamic instability (see Figure 1.3) (Mitchison and Kirschner, 1984a). Dynamic instability is crucial for microtubule functions *in vivo* as it allows the microtubular network to organize into different architectures and respond to intracellular and extracellular stimuli (Jordan et al., 1992; Kirschner and Mitchison, 1986). Dynamic instability is explained by the 'GTP cap model' (Carlier and Pantaloni, 1981; Mitchison and Kirschner, 1984a; Walker et al., 1988). Loss or reduction of the GTP cap induces microtubule shrinkage, called catastrophe. The opposite behaviour, the regaining of the cap and following transition from shrinkage to growth, is called rescue (Gardner et al., 2011; Schek et al., 2007; Walker et al., 1988).

Dynamic instability is crucial for the role of microtubules *in vivo* but a full understanding of this process is still lacking (Brouhard, 2015; Gardner et al., 2013). Based on cryo-EM reconstitutions and crystal structures it is thought that tubulin dimers undergo at least three different conformational changes during microtubule growth and shrinkage (Brouhard and Rice, 2014, 2018). Unpolymerized GTP-tubulin adopts a bent conformation in solution with a characteristic 12° kink at the intradimer interface (Gigant et al., 2000; Nawrotek et al., 2011; Ravelli et al., 2004; Rice et al.,

2008). When the tubulin dimer is incorporated at the growing microtubule end, the dimer straightens, followed by compaction upon GTP hydrolysis and phosphate release due to a movement of a subdomain of α-tubulin. The conformational change of tubulin within the lattice probably induces strain energy as the tubulins are held in an unfavourable conformation (Alushin et al., 2014; Wang and Nogales, 2005; Yajima et al., 2012; Zhang et al., 2015). When the GTP cap is lost from growing microtubule ends the unprotected GDP-tubulin relaxes back into the curved conformation. This relaxation weakens lateral contacts and leads to the outward curling of microtubule protofilaments (Atherton et al., 2018; Mandelkow et al., 1991).

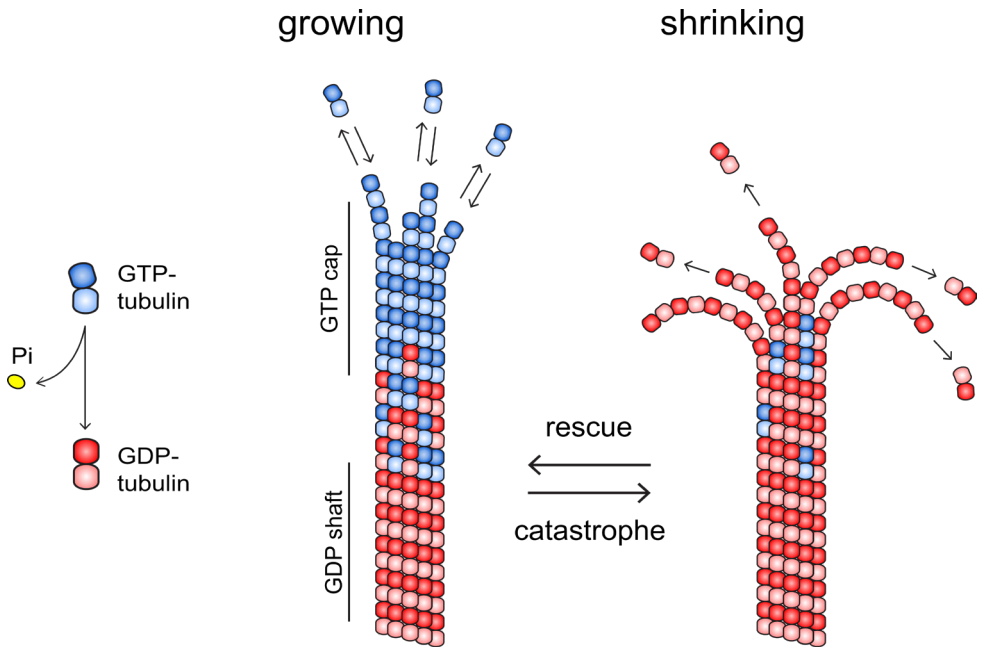

Figure 1.3: Schematic illustration of a growing and shrinking microtubule.

1.1.2 The structure of the microtubule end

Attempts to visualize the microtubule end by cryo-electron microscopy have shown a variety of different structures. Growing microtubules were found to be cylindrical with 'tapered' ends of protofilaments extending beyond each other or long 'sheets' of curved protofilaments which retain lateral connectivity (Atherton et al., 2017, 2018; Chrétien et al., 1995; Guesdon et al., 2016; Mandelkow et al., 1991; Vemu et al., 2017). Shrinking microtubules have unconnected protofilaments which unfurl outwards (Atherton et al., 2018; Mandelkow et al., 1991). A very recent publication using electron tomography to examine microtubule ends *in vitro* and in cells of different species reported that growing and shrinking microtubules consisted of well-separated outwardly curved protofilaments (McIntosh et al., 2018). Taken together, a

variety of different end structures have been reported in literature and it is currently not known how the microtubule end really looks like.

1.1.3 Microtubule cytoskeleton organization

Two properties of the microtubule cytoskeleton are crucial for its function *in vivo*: the dynamicity of the microtubule network and the ability to organize into arrays of defined geometry. Different types of microtubule architectures (see Figure 1.4) have been observed in cells and their organization can change depending on intracellular and environmental stimuli (Bartolini and Gundersen, 2006; Muroyama and Lechler, 2017; Sanchez and Feldman, 2017). For example, plant organ and tissue growth requires the fast rearrangement of cortical microtubule arrays, a process which can take place within minutes (Lindeboom et al., 2013). During cell division, the microtubule array of interphase cells is transformed into the bipolar spindle central for chromosome segregation and positioning of the cell-division plane (Helmke et al., 2013). The microtubule network of many types of differentiated cells and fungi are not organized in a radial manner but instead form parallel and antiparallel arrays (Horio, 2007; Muroyama and Lechler, 2017; Sawin and Tran, 2006). Neurons, for instance, contain polarised microtubule bundles which are distributed down the length of axons to facilitate unidirectional transport (Baas et al., 1988, 1989; Chen et al., 1992). In skeletal muscle cells, microtubules are organized parallel to the long axis of the cell important for myofibrillogenesis and cell shape (Bugnard et al., 2005; Ehler et al., 1999; Musa et al., 2003; Pizon et al., 2005; Tassin et al., 1985). Epithelial cells organize a mostly linear microtubule network along the apical-basal axis required for polarized microtubule-based transport (Bacallao et al., 1989; Bré et al., 1990; Müsch, 2004; Reilein et al., 2005). Understanding how such arrays are formed remains an open question but it most probably requires the combined effort of microtubule nucleation factors, proteins regulating microtubule dynamics and motor proteins (Dammermann et al., 2003; Hyman and Karsenti, 1998; Oriola et al., 2018).

Microtubule motor proteins control the precise arrangements of microtubules *in vivo* and can be distinguished into two major classes, the minus-end directed dyneins and the mostly plus-end directed kinesins (Cianfrocco et al., 2015; Cross and McAinsh, 2014; Hirokawa et al., 2009; Vale, 2003). This versatile group of proteins is responsible for the transport and rearrangement of microtubules by parallel and antiparallel sliding and cross-linking to align filaments and stabilize structures (Braun et al., 2009; Fink et al., 2009; Forth et al., 2014; Jolly et al., 2010; Lansky et al., 2015; Mollinari et al., 2002; Mountain et al., 1999; Sharp et al., 1999; van den Wildenberg

et al., 2008). Another key function is the efficient transport of cargos along existing microtubules, including other MAPs and nucleation factors (Franker and Hoogenraad, 2013).

Proteins that bind to microtubules can also regulate microtubule dynamics and stability. These proteins can be largely divided into microtubule stabilizing and destabilizing proteins and modulate microtubule dynamicity through different ways including promoting or preventing catastrophes and rescues and/or increasing or decreasing polymerization and shrinkage speeds (Cassimeris and Spittle, 2001; Vaart et al., 2009). Microtubule associated proteins (MAPs) such as microtubule polymerases and depolymerases, plus and minus-end tracking proteins (+TIPs and -TIPs), and proteins that regulate microtubule stability belong to this group (Brouhard et al., 2008; Dehmelt and Halpain, 2004; Jourdain et al., 1997; Mimori-Kiyosue et al., 2005; Moores et al., 2002, 2006; Newton et al., 2004; Reid et al., 2016; Steinmetz et al., 2000; Vitre et al., 2008).

The de novo formation of new microtubules is mediated by nucleation factors and their activity is restricted to specific subcellular sites such as the centrosome (Mitchison et al., 1986; Teixidó-Travesa et al., 2012). The best known microtubule nucleation factor *in vivo* is the γ-tubulin ring complex (γTuRC), a multi-protein complex that acts as a template from which microtubules can grow from (Khodjakov and Rieder, 1999; Moritz et al., 1995; Stearns et al., 1991).

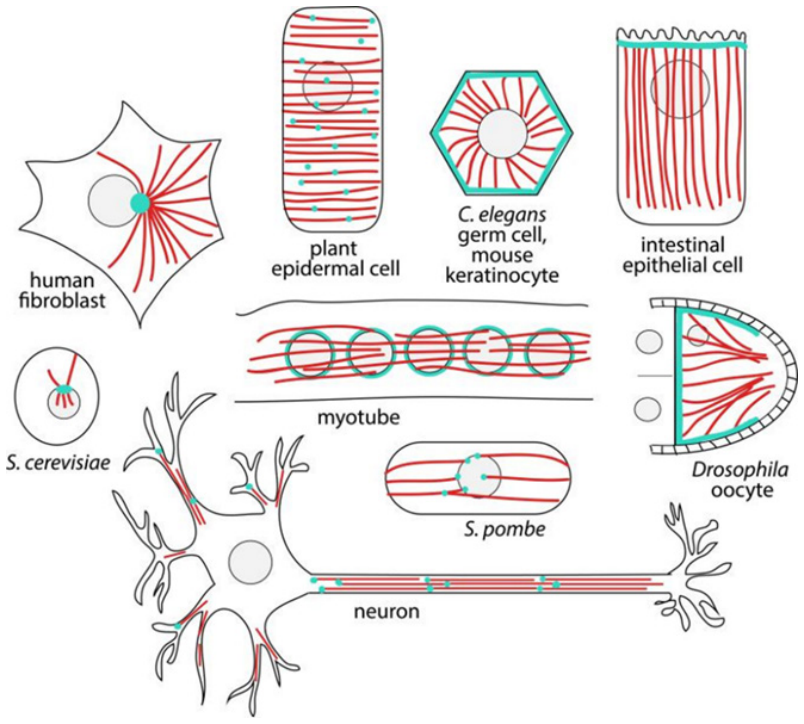

Figure 1.4: Organization of microtubule arrays in different cell types. MTOCs are shown in green and microtubules are shown in red. Taken from (Sanchez and Feldman, 2017).

1.2 γ-tubulin and the γ-tubulin ring complex

γ-tubulin was identified in a genetic screen in *Aspergillus nidulans* as a new member of the tubulin superfamily (Oakley and Oakley, 1989). It was subsequently shown to be a relatively unabundant but evolutionary conserved protein which is present in all eukaryotic cells (Akashi et al., 1997; Horio et al., 1991; Murata et al., 2005; Oakley et al., 1990; Sobel and Snyder, 1995; Stearns et al., 1991; Zheng et al., 1991). γ-tubulin was shown to oligomerize into higher order structures together with the γ-tubulin complex proteins (GCPs) (Murphy et al., 1998, 2001; Oegema et al., 1999; Zheng et al., 1995). There are species specific differences in the number and nomenclature of GCP proteins. In this thesis, I will use the human nomenclature for simplicity (see Table 1). Budding yeast and *Caenorhabditis elegans* only contain two GCPs: GCP2 and GCP3 (Kollman et al., 2010; Strome et al., 2001; Vinh et al., 2002). Other eukaryotes including humans have three additional GCPs: GCP4, GCP5 and GCP6 (Colombié et al., 2006; Fava et al., 1999; Gunawardane et al., 2000; Martin et al., 1998; Murphy et al., 1998, 2001; Vogt et al., 2006; Wiese, 2008; Zhang et al., 2000). Fission yeast, *Drosophila melanogaster* and *Aspergillus nidulans* express GCP4/5/6 but they are not essential for viability (Anders et al., 2006; Fujita et al., 2002; Goshima et al., 2007; Venkatram et al., 2004; Vérollet et al., 2006; Xiong and Oakley, 2009).

γ-tubulin and GCPs can form two types of complexes which are defined by size and protein composition: the γ-tubulin small complex (γTuSC) and the γ-tubulin ring complex (γTuRC) (Kollman et al., 2010; Oegema et al., 1999). The γTuSC is a heterotetramer which is assembled of two copies of γ-tubulin and two GCPs (Choy et al., 2009; Kollman et al., 2008; Oegema et al., 1999). The larger γTuRC consists of several γTuSCs arranged into a helical structure. The start and the end of the helix overlap after a single turn, giving the γTuRC its characteristic ring-like appearance in electron microscopy often described as a ‘lock washer’ (Figure 1.5) (Kollman et al., 2010, 2015; Moritz et al., 2000; Oegema et al., 1999). The exact stoichiometry and position of the GCPs in the γTuRC is currently not known.

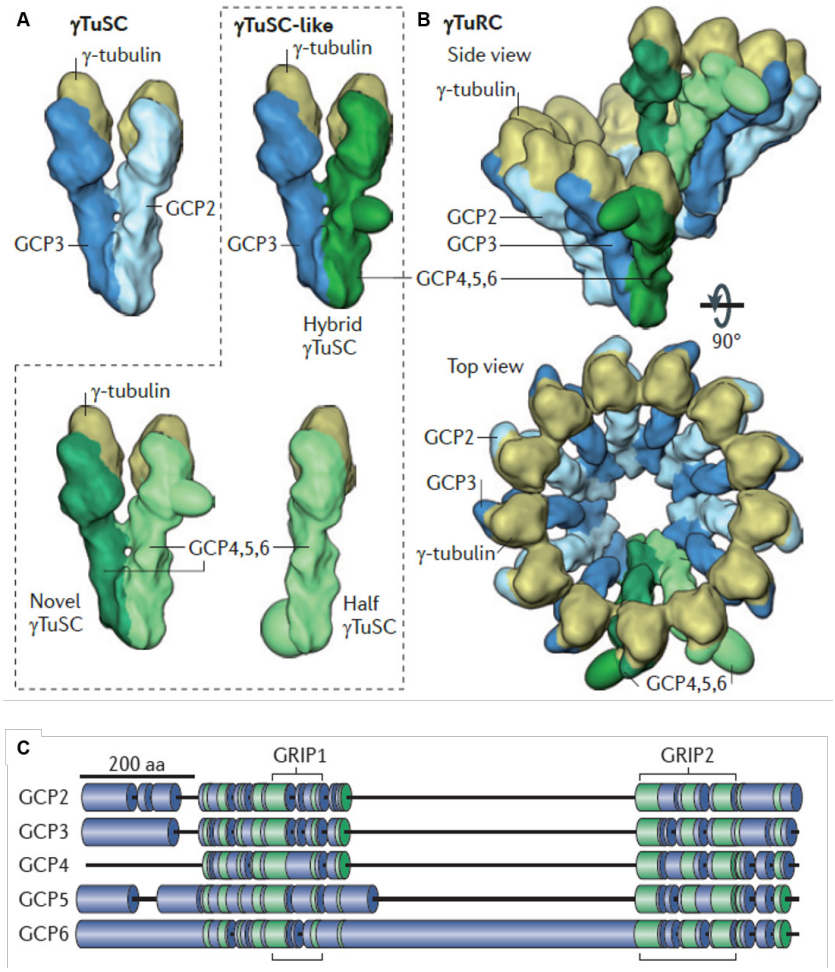

Figure 1.5: Schematic illustration of γTuRC assembly. (A) Two molecules of γ-tubulin, together with two of the GCP proteins (GCP2, GCP3, GCP4, GCP5 or GCP6) form a smaller subcomplexes termed γTuSC. (B) 14 γTuSCs come together to form the γTuRC with the first and the last γ-tubulin overlapping to give raise to a 13-protofilament microtubule. GCP4/5/6 are only present in higher eukaryotes and their exact position in the γTuRC is currently not known. (C) GCP2-6 contain two homologous regions, the grip1 (N-terminus) and grip2 (C-terminus) domains. Regions with more-distant homology are shown in green. Modified from (Kollman et al., 2011).

1.2.1 γTuRC core- and noncore-components

γ-tubulin and the GCPs are usually referred to as the core-components of the γTuRC as they have a structural role in γTuRC assembly (Farache et al., 2018; Kollman et al., 2011; Tovey and Conduit, 2018). The GCP proteins constitute a unique protein family with a very low overall sequence identity (overall less than 15%). Homology has only been predicted in two short segments, the γ-tubulin ring protein (grip) 1 domain and the grip2 domain (see Figure 1.5) (Gunawardane et al., 2000; Murphy et al., 2001). The grip1 domain is located in the N-terminal half of each protein and is important for lateral contacts between neighbouring GCPs. Grip2 is located at the C-

terminal half and mediates binding to γ-tubulin (Farache et al., 2016; Guillet et al., 2011; Gunawardane et al., 2000; Murphy et al., 2001). The overall size of GCP proteins varies by more than two fold (from ~70 to 210 kDa) due to insertions and unique sequence extensions at the N-termini of the different GCPs. GCP4 is the smallest and lacks almost any additional sequences outside the grip motifs (Guillet et al., 2011). Nevertheless, the protein fold and the function of GCPs is remarkably conserved between the different GCPs and also between different species (Guillet et al., 2011; Riehlman et al., 2013).

Several other proteins have been identified to copurify with γTuRCs but they are not required for γTuRC assembly and therefore not strictly core components of the complex. In the context of this thesis, these proteins will be referred to as γTuRC binders (see Table 1). In human cells five γTuRC-binders have been identified, i.e. CDK5Rap2, NEDD1, Mozart1, NME7 and LGALS3BP (Choi et al., 2010; Gunawardane et al., 2003; Hutchins et al., 2010; Liu et al., 2014a; Teixidó-Travesa et al., 2010). The role of LGALS3PB in γTuRC regulation or recruitment has not been investigated yet. All other proteins have important roles in γTuRC localization and anchoring to MTOCs and some of them seem to have a role in modulating γTuRC nucleation activity (Anders et al., 2006, 2006; Choi et al., 2010; Cota et al., 2017; Fong et al., 2008; Gomez-Ferreria et al., 2012; Lin et al., 2016, 2016, 2014; Lüders et al., 2006; Manning et al., 2010; Masuda and Toda, 2016; Masuda et al., 2013; Muroyama et al., 2016; Nakamura et al., 2012; Sdelci et al., 2012; Zhang et al., 2009).

1.2.2 Assembly of the γ-tubulin ring complex

Assembly of γTuSCs into γTuRCs is thought to be a prerequisite for efficient microtubule nucleation. The first step is the oligomerization of seven γTuSCs into the helical γTuRC which copies the geometry of a microtubule (Erlemann et al., 2012; Kollman et al., 2010). How γTuSCs assemble into γTuRCs is not well understood and the mode of assembly seems to be species and cell type specific (Farache et al., 2018; Petry and Vale, 2015).

In budding yeast and fission yeast, γTuSC oligomerization into γTuRC seems to be restricted to specific subcellular sites such as the spindle pole body (SBP). At those MTOCs, evolutionary conserved γTuRC-tethering proteins (see Table 1) are responsible for the assembly and anchorage of γTuRCs (Anders et al., 2006; Knop and Schiebel, 1997; Lin et al., 2015). For example, the budding yeast γTuRC-tethering protein Spc110 was shown by cryo-EM to form a scaffold which holds the γTuSCs spiral together (Kollman et al., 2010, 2015).

Other eukaryotes including humans contain the additional GCP4/5/6 molecules (Kollman et al., 2011). Originally it was believed that γTuRCs are built from a repeating ring of γTuSCs containing only GCP2/3. Similiarly to the γTuRC-tethering proteins mentioned above, the additional GCP4/5/6 were thought to form a stabilizing cap at the base of the spiral, responsible to hold the γTuSCs together (Moritz et al., 2000). This model was based on a low resolution electron-microscopic tomography structure of the *Drosophila melanogaster* γTuRC (Moritz et al., 2000). More recently it was shown that GCP4 can directly bind to γ-tubulin via the grip2 domain and that all other GCPs also contain the grip2 domain (Guillet et al., 2011; Gunawardane et al., 2000; Murphy et al., 2001). Now it is thought that all GCPs can each bind to a molecule of γ-tubulin, then lateraly associate via their grip1 motifs into γTuSCs and further into γTuRCs (Erlemann et al., 2012; Kollman et al., 2010, 2011, 2015).
Currently, it is thought that in human cells γTuRCs are pre-assembed in the cytoplasm but inactive and that activation occurs upon recruitment to MTOCs (Farache et al., 2018; Kollman et al., 2010; Teixidó-Travesa et al., 2012; Tovey and Conduit, 2018). Consistent with this idea, depletion experiments of GCP2-6 from human cells and *Drosophila melanogaster* have shown the appearance of smaller γTuSC sized subcomplexes in favour of γTuRCs in sucrose gradient fractionations of the cytoplasm (Cota et al., 2017; Farache et al., 2016; Vérollet et al., 2006). The depletion of GCP4/5/6 from human cells is usually accompanied by a reduced recruitment of γTuRCs to the centrosome and mitotic defects such as monopolar spindles and failures in centriole duplication (Bahtz et al., 2012; Cota et al., 2017; Farache et al., 2016; Fava et al., 1999; Murphy et al., 2001).
However, in somatic cells of *Drosophila melanogaster* the depletion of GCP4/5/6 does not interfere with the formation of bipolar spindles and γTuSCs are still recruited to centrosomes during mitosis (Vérollet et al., 2006; Vogt et al., 2006). This suggests that at least in *Drosophila melanogaster* γTuSCs might oligomerize at certain MTOCs by γTuRC-tethering proteins as described in fungi (Farache et al., 2018).

1.2.3 The structure of the γ-tubulin ring complex

For a better understanding of how the γTuRC mediates microtubule nucleation structural studies are essential. A first step towards that direction was the crystallography of human γ-tubulin and GCP4 as well as high resolution cryo-electron microscopy (cryo-EM) of budding yeast γTuSCs and γTuRCs (Kollman et al., 2011). The crystal structure of γ-tubulin revealed that γ-tubulin monomers make strong lateral contacts through regions identical to the lateral interactions between α-α- and

β-β-tubulin in the microtubule lattice. Overall γ-tubulin adopts a very similar fold to αβ-tubulin which is consistent with the expectation that it can form lattice-like contacts with microtubules. γ-tubulin also contains a nucleotide binding site and was shown to bind GTP with a similar preference as found for β-tubulin. GTP bound free γ-tubulin adopts a bent conformation. If γ-tubulin undergoes a conformation change, as found for αβ-tubulin, is currently not known (Aldaz et al., 2005).

The crystal structure of human GCP4 showed that the protein has a unique protein fold, which can be described as an elongated structure with a pronounced kink in the middle region (Guillet et al., 2011). Human GCP4 was found to fit surprisingly well into cryo-EM structures of budding yeast complexes, suggesting that the overall fold of the GCPs is highly conserved (Guillet et al., 2011; Kollman et al., 2011, 2015).

The budding yeast γTuSC has been analysed extensively by negative stain and cryo-EM. Structurally the γTuSC adopts the shape of a V with GCP2/3 forming the base and γ-tubulin at the tips. The two molecules of γ-tubulins are held apart from each other without making lateral contacts (Choy et al., 2009; Kollman et al., 2008). It was also shown that γTuSC adopts the same structure irrespective of the nucleotide state of γ-tubulin (Kollman et al., 2008).

The structure of the larger budding yeast γTuRC was obtained in the presence of a short fragment of the γTuRC-tethering protein Spc110 (see Table 1). This fragment stabilizes the assembly of purified γTuSCs into γTuRCs to such an extent that γTuSC rings grow into extended helical filaments of laterally associated complexes. Analysis of these γTuSC filaments by cryo-EM revealed six and a half γTuSCs per helical turn. This means that the first and the last γ-tubulin overlap and γTuRCs therefore present 13 γ-tubulins at the top of the ring. Oligomerization did not induce any major conformational changes to the individual γTuSCs, i.e. the γ-tubulins within each γTuSC are still held apart while γ-tubulins between neighbouring γTuSCs laterally bind to each other. Therefore, the symmetry of the γTuSC filaments is closely but not exactly resembling the structure of the microtubule (Kollman et al., 2010, 2015).

Artificially induced structural rearrangements were able to close the gap between the γ-tubulins and the resulting closed structure was shown to match 13-protofilament microtubule geometry. The conformational change required GCP2 to slightly bend and GCP3 to slightly straighten, suggesting that all GCPs might be flexible (Kollman et al., 2015).

1.2.4 The stoichiometry of γTuRC

The precise stoichiometry of the γTuRC is not known because high resolution structures were so far only obtained for the budding yeast complex (Kollman et al., 2011). Since budding yeast γTuRCs do not contain GCP4/5/6 their number and exact position within the ring could not be determined. Nevertheless, biochemical studies of purified γTuRCs from *Drosophila melanogaster*, *Xenopus laevis* and human cells estimated that the complex contains all GCPs simultaneously and that the majority of the complex is formed by γ-tubulin and GCP2/3 (Choi et al., 2010; Fava et al., 1999; Murphy et al., 2001; Oegema et al., 1999; Zheng et al., 1995). The most recent estimation proposes the following subunit composition: 14 copies of γ-tubulin, 12 copies of GCP2/3, 2-3 copies of GCP4, one copy of GCP5 and less than one copy of GCP6 (Choi et al., 2010).

This estimation of γTuRC subunit stoichiometry suggests that not all complexes contain GCP6. However, if the subunit composition of γTuRCs can vary between complexes of the same species or cell types remains to be determined.

The position of the GCPs within the ring is even less well understood. Analysis of the crystal structure of GCP4 revealed two highly charged sites which are located at lateral contact positions (Guillet et al., 2011). It was suggested, that GCP4 might act as γTuRC initiator or terminator as the charged sites could potentially interfere with the assembly of the complex in only one direction (Farache et al., 2018; Guillet et al., 2011; Kollman et al., 2011). *In vivo* fluorescence resonance energy transfer (FRET) analysis and cross-linking experiments found direct lateral binding between GCP2/3 and GCP4/5 but no other interactions were analysed (Farache et al., 2016).

1.2.5 Specific roles of GCPs

Little is known about the individual roles of GCPs within the γTuRC or the function of their unique sequence extensions. A recent publication in human cells showed by expression of chimera proteins that the C-terminus of the GCPs is exchangeable whereas the N-terminus is not (Farache et al., 2016). Consequently, GCPs might have specific regulatory functions mediated by their N-termini and some *in vivo* studies have been carried out to identify distinct roles for different GCPs (Farache et al., 2018; Kollman et al., 2011; Tovey and Conduit, 2018).

For example, GCP4/5/6 which are present but not essential for viability in fission yeast, fruit flies and filamentous fungi still seem to have specific roles. GCP4/5/6 in *Drosophila melanogaster* are important for microtubule anchoring at the centrosome

and accurate chromosome segregation and GCP4/6 are essential in male and female germlines (Schnorrer et al., 2002; Vérollet et al., 2006; Vogt et al., 2006). Deletion mutants in fission yeast show reduced microtubule nucleation specifically from the interphase MTOCs (Anders et al., 2006; Fujita et al., 2002; Venkatram et al., 2004). In *Aspergillus nidulans* GCP4/5/6 seem to be important for the fidelity of chromosome segregation (Xiong and Oakley, 2009).

In human cells, phosphorylation of GCP6 has been shown to be necessary for centriole duplication and recruitment to keratin intermediate filaments (Bahtz et al., 2012; Oriolo et al., 2007). Phosphorylation of GCP5 might be involved in centrosome localisation of γTuRC (Izumi et al., 2008). Other GCPs also contain several phosphorylation sites but their function remains unclear (Teixidó-Travesa et al., 2012).

Consistently, results indicate that apart from their structural role in γTuRC assembly, GCPs might also have a more unique function to mediate spatio-temporal regulation of γTuRC activity.

1.3 γTuRC localization to MTOCs

Temporal and spatial control over microtubule nucleation in cells is achieved by the recruitment and local activation of the γTuRC at distinct subcellular locations (Farache et al., 2018; Teixidó-Travesa et al., 2012). For example, the nucleation rate of centrosomes was quantified to be up to 7-fold higher during mitosis compared to interphase and this increase in nucleation capacity was shown to correlate with the amount of γ-tubulin at centrosomes (Khodjakov and Rieder, 1999; Piehl et al., 2004; Zheng et al., 1991).

Apart from the centrosome several other sites and pathways of microtubule nucleation have been identified in cells, including the Golgi apparatus, plasma membranes or the vicinity of mitotic chromatin (Bugnard et al., 2005; Chabin-Brion et al., 2001; Guerin and Kramer, 2009; Rivero et al., 2009; Scrofani et al., 2015; Torosantucci et al., 2008). The γTuRC is a known component of all described microtubule nucleation pathways (Sulimenko et al., 2017; Teixidó-Travesa et al., 2012; Wu and Akhmanova, 2017). However, very little is known about the relative contributions of the different microtubule nucleation pathways to spindle assembly in different organisms and cell types (Gavilan et al., 2017, 2018; Hayward et al., 2014; Maia et al., 2013; O'Connell et al., 2009). I will now briefly discuss what is known about γTuRC localization to MTOCs in animal cells and mention the most important γTuRC recruitment factors.

Table 1: Orthologous of γTuRC. Adapted from (Sulimenko et al., 2017; Teixidó-Travesa et al., 2012; Tovey and Conduit, 2018).

	H. sapiens	**X. laevis**	**D. melanogaster**	**A. thaliana**	**C. elegans**	**C. albicans**	**A. nidulans**	**S. pombe**	**S. cerevisiae**
γTuSC	**γ**-tubulin[1]	**γ**-tubulin	**γ**Tub23C[1]	TUBG1[1]	Tbg1	Tub1	mipA	Tug1/Gtb1	Tub4
	GCP2	Xgrip110	Dgrip84	AtGCP2	Grip1/Gip1	Spc97	GCPB	Alp4	Spc97
	GCP3	Xgrip109	Dgrip91	AtGCP3	Grip2/Gip2	Spc98	GCPC	Alp6	Spc98
γTuRC	GCP4	Xgrip75/75s	Dgrip75	AtGCP4	?	?	GCPD	Gfh1	?
	GCP5	Xgrip133	Dgrip128	At1g80260	?	?	GCPE	Mod21	?
	GCP6	Xgrip195/210	Dgrip163	At3943610	?	?	GCPF	Alp16	?
γTuRC binders	NEDD1[2]	xNEDD1[2]	Grip71	Nedd1[2]	?	?	?	?	?
	Mzt1	Mzt1	Mzt1	GIP1a/b	Mzt1	Mzt1	MztA	Mzt1	?
	Mzt2A/B	?	?	?	?	?	?	?	?
	NME7	?	?	?	?	?	?	?	?
	LGALS3BP	?	?	?	?	?	?	?	?
CM1 domain γTuRC tethering proteins	CDK5Rap2[3]	?	Cnn	?	?	Spc110	PcpA	Pcp1	Spc110
	Myomegalin					Spc72	ApsB	Mto1/2	Spc72
	Pericentrin								
Microtubule binders	chTOG	XMAP215	Msps	?	Zyg9	?	?	Alp14	Stu2
	TPX2	TPX2	Mei38	TPX2	Tpxl-1	?	?	?	?

[1]known to express two isoforms of γ-tubulin, [2]NEDD1/GCP-WD, [3]CDK5Rap2/CEP215/KIAA1633

1.3.1 Nucleation from the centrosome

Centrosomes are the main MTOCs in animal cells (Bornens, 2012; Conduit et al., 2015; Schatten and Sun, 2010; Wu and Akhmanova, 2017). They are composed of two barrel-shaped centrioles surrounded by the pericentriolar material (PCM) (Avidor-Reiss and Gopalakrishnan, 2013; Chrétien et al., 1997; Dammermann et al., 2004). The PCM is a dense highly regulated network built from several hundreds of different proteins and the central site for microtubule nucleation and attachment (Andersen et al., 2003; Delgehyr et al., 2005; Lawo et al., 2012; Mennella et al., 2012; Mogensen et al., 2000).

Several proteins have been identified which contribute to γTuRC recruitment to centrosomes in animal cells including pericentrin, CDK5Rap2, NEDD1 and Mzt1 (Cota et al., 2017; Fong et al., 2008; Gomez-Ferreria et al., 2012; Haren et al., 2009; Lüders et al., 2006; Muroyama et al., 2016; Teixidó-Travesa et al., 2010; Zhang et al., 2009; Zimmerman et al., 2004). Other proteins which are core components of the PCM are implicated in centrosomal anchoring of γTuRCs, including pericentrin, CDK5Rap2, AKAP450, Cep192, Cep169 and ninein (Casenghi et al., 2003; Delgehyr et al., 2005; Dictenberg et al., 1998; Doxsey et al., 1994; Gomez-Ferreria et al., 2012; Mogensen et al., 2000; Mori et al., 2015a, 2015b; Takahashi et al., 2002; Zimmerman et al., 2004). The exact role of PCM core components and the interplay between the different γTuRC recruitment and anchoring factors at the centrosome is not well understood but apart from γTuRC anchoring, the PCM might also have a role in concentrating tubulin and other regulatory proteins to promote nucleation (Rale et al., 2018; Woodruff et al., 2017).

1.3.2 Nucleation from the Golgi apparatus

The second major MTOC in mammalian cells is the Golgi apparatus (Chabin-Brion et al., 2001; Efimov et al., 2007; Sanders and Kaverina, 2015). It is a central organelle in the eukaryotic secretory pathway performing functions central to cell growth, homeostasis and division (Rios, 2014; Wu and Akhmanova, 2017; Zhu and Kaverina, 2013). In most vertebrate cells the Golgi localizes close to the nucleus and surrounds the centrosome (Corthésy-Theulaz et al., 1992; Hurtado et al., 2011). Golgi-derived microtubule arrays are polarized to allow optimal secretory trafficking to and from the Golgi apparatus (Miller et al., 2009; Wu et al., 2016).

The Golgi apparatus uses a similar subset of proteins as the centrosome to recruit and anchor γTuRCs to the Golgi including AKAP450, CM130, CDK5Rap2 and

myomegalin (Rivero et al., 2009; Roubin et al., 2013; Wang et al., 2010b, 2014). γTuRC-mediated nucleation is probably confined to hot spots at the cis-Golgi possibly due to clustering and/or local activation of γTuRCs (Sanders et al., 2017).
CM130 is important to recruit AKAP450 to Golgi membranes and might be a key regulator of microtubule nucleation at the Golgi (Nakamura, 2010; Rivero et al., 2009). The γTuRC is probably recruited and anchored by AKAP450 (Rivero et al., 2009; Wang et al., 2010b). This protein is a major Golgi scaffolding protein and binds the complex via the γTuRC-binders CDK5Rap2, myomegalin or might also directly bind to γTuRCs (Roubin et al., 2013; Wang et al., 2010b, 2014; Wu et al., 2016).

1.3.3 Nucleation from the nuclear membrane and plasma membranes

Microtubule nucleation from the nuclear membrane and plasma membranes is poorly understood (Petry and Vale, 2015; Sulimenko et al., 2017; Wu and Akhmanova, 2017). Best characterized is the differentiation of skeletal muscle cells in which pericentrin, ninein and γTuRCs are recruited to the nuclear envelope by unknown mechanisms (Bugnard et al., 2005; Dyachuk et al., 2016; Fant et al., 2009).
In epithelial cells microtubules are anchored at the apical plasma membrane possibly through ninein (Mogensen et al., 2000). How the γTuRC is recruited to the plasma membrane in these cells is not known but it might involve binding of keratin to GCP6 (Oriolo et al., 2007).

1.3.4 Chromatin-mediated microtubule nucleation

Chromatin-mediated microtubule nucleation is an important pathway for acentrosomal microtubule nucleation (Meunier and Vernos, 2016). Acentrosomal microtubules have been shown to be sufficient for bipolar spindle assembly in cells naturally lacking centrosomes, such as oocytes or plant cells, and in cells where centrosomes were removed experimentally (Calarco, 2000; Courtois et al., 2012; Khodjakov et al., 2000; Mahoney et al., 2006).
The central player in chromatin mediated microtubule nucleation is the small GTPase Ran (Bischoff and Ponstingl, 1991a). Ran is an essential shuttling protein between the nucleus and cytoplasm in interphase (Görlich et al., 1996; Izaurralde et al., 1997; Melchior et al., 1993; Moore and Blobel, 1993). During mitosis, when the nuclear envelope breaks down, the chromatin-bound nucleotide exchange factor RCC1 generates a gradient of RanGTP which concentrates around mitotic chromatin (Bischoff and Ponstingl, 1991b; Bischoff et al., 1994; Carazo-Salas et al., 1999; Kalab

et al., 1999, 2002; Kaláb et al., 2006). RanGTP activates microtubule generation through the release of spindle assembly factors (SAFs) from importins (Nachury et al., 2001; Tsai et al., 2003; Wiese et al., 2001). Currently known SAFs are non-motile microtubule associated proteins and motor proteins (Ems-McClung et al., 2004; Gruss et al., 2001; Koffa et al., 2006; Silljé et al., 2006; Trieselmann et al., 2003; Wittmann et al., 2000).

One of the best studied SAFs is the anti-catastrophe factor TPX2 (Gruss and Vernos, 2004; Gruss et al., 2001, 2002; Reid et al., 2016; Schatz et al., 2003). Upon release from importins TPX2 activates the mitotic kinase Aurora A which in turn phosphorylates TPX2 (Bayliss et al., 2003; Eyers et al., 2003; Tsai et al., 2003). Apart from activating Aurora A, TPX2 was shown to form a complex with NEDD1, RHAMM and γTuRCs to mediate RanGTP dependent microtubule nucleation (Groen et al., 2004; Pinyol et al., 2013; Scrofani et al., 2015).

1.3.5 Nucleation from kinetochores

The γTuRC is recruited to kinetochores by a subset of nucleoporins (Nup107-160) and microtubule nucleation was shown to be RanGTP depended (Mishra et al., 2010). How γTuRCs function at kinetochores is currently not well understood and poses a conundrum, as γTuRCs would nucleate microtubules of opposite polarity to mature k-fibers. Nevertheless, the formation of short microtubules around kinetochores has been observed in mammalian and *Drosophila melanogaster* S2 cells (Khodjakov et al., 2003; Maiato and Sunkel, 2004; Sikirzhytski et al., 2018). Interestingly, TPX2 might also have a function in kinetochore microtubule nucleation, however, if TXP2 interacts with nucleoporins and/or γTuRCs was not investigated (Tulu et al., 2006).

1.3.6 Microtubule branching

Acentrosomal microtubule nucleation can also be mediated through a microtubule-dependent microtubule nucleation pathway (Goshima and Kimura, 2010; Sánchez-Huertas and Lüders, 2015). This pathway depends on the evolutionary conserved complex Augmin/HAUS and seem to have a role in controlling spindle density during mitosis (Goshima et al., 2008; Lawo et al., 2009; Liu et al., 2014b; Uehara et al., 2009; Wainman et al., 2009; Zhu et al., 2008). The molecular mechanism behind microtubule branching is not well understood but it involves the recruitment of γTuRCs to Augmin via NEDD1 (Chen et al., 2017b; Hsia et al., 2014; Song et al., 2018; Uehara et al., 2009; Zhu et al., 2008). Experiments in *Xenopus* egg extract suggest that the

Augmin-NEDD1-γTuRC complex is further regulated by TPX2 in a RanGTP dependent fashion (Alfaro-Aco et al., 2017; Petry et al., 2013).

1.3.7 γTuRC-independent microtubule nucleation

Growing evidence suggests that the γTuRC is not strictly needed for all nucleation events in cells. For example, γTuRC depletion does not completely block microtubule nucleation in budding yeast, fruit flies and moss cells and in these systems a significant proportion of microtubules does not colocalize with γTuRCs (Kitamura et al., 2010; Nakaoka et al., 2015; Nashchekin et al., 2016; Rogers et al., 2008). Depletion of γTuRCs in *Drosophila melanogaster embryos* and *Caenorhabditis elegans* perturbs spindle assembly but microtubules can still form (Hannak et al., 2002; O'Toole et al., 2012; Rogers et al., 2008; Sampaio et al., 2001; Strome et al., 2001; Wang et al., 2015).

The current γTuRC-centred model might therefore be incomplete and cells might contain other factors which cooperate or work in parallel with γTuRCs to nucleate microtubules *in vivo* (Oakley et al., 2015; Tovey and Conduit, 2018). Recent studies therefore focused on the role of MAPs in microtubule nucleation and several proteins have been identified including microtubule polymerases from the XMAP215-family and suppressors of microtubule dynamicity such as TPX2, doublecortin, CAMSAP/Patronin, CLASPs and the dynactin subunit $p150^{Glued}$ (Efimov et al., 2007; Hendershott and Vale, 2014; Horesh et al., 1999; Jiang et al., 2014; Lazarus et al., 2013; Moores et al., 2004, 2006; Reid et al., 2016; Roostalu et al., 2015; Taylor et al., 2000). Additionally, proteins belonging to the group of microtubule severing enzymes can help to increase microtubule number by breaking existing microtubules (McNally and Roll-Mecak, 2018).

1.4 Mechanism of microtubule nucleation

The molecular mechanism of γTuRC-mediated microtubule nucleation is still poorly understood. In the next chapter I will first summarize what is known about microtubule nucleation in general and how microtubule assembly can be stabilized. Then I will outline what is known about γTuRC-mediated microtubule nucleation and the regulation of the complex.

1.4.1 Spontaneous microtubule nucleation

It is well known that microtubules can nucleate spontaneously in vitro (Job et al., 2003; Weisenberg, 1972). However, spontaneous microtubule nucleation is inefficient and requires high concentrations of tubulin (≥20 μM) (Voter and Erickson, 1984; Weisenberg, 1972). The current model of spontaneous nucleation is a two-step process involving the rate-limiting formation of a stable oligomer followed by the elongation into a microtubule (Erickson and Pantaloni, 1981; Kuchnir Fygenson et al., 1995; Voter and Erickson, 1984). The difficulty for tubulin dimers to assemble into a stable oligomer is thought to be a consequence of the complex structure and dynamic instability of microtubules (Erickson and Pantaloni, 1981; Mitchison, 1992; Roostalu and Surrey, 2017). In terms of microtubule assembly, tubulin dimers collide stochastically and form unstable oligomers. These oligomers constantly assemble and disassemble until they reach a critical size. Above that size, which is described in the literature as the 'critical nucleus', the oligomer is thermodynamically stable and polymerizes. Spontaneous microtubule nucleation is therefore a cooperative process and much more favourable at higher tubulin concentrations (Figure 1.6) (Erickson and Pantaloni, 1981; Job et al., 2003).

The kinetics of microtubule assembly in solution containing purified tubulin and Mg2+ ions were measured previously by monitoring changes in turbidity resulting from the scattering of the incidient light by the microtubule polymer (Carlier and Pantaloni, 1978; Detrich et al., 1985; Himes et al., 1977; Johnson and Borisy, 1977; Lee and Timasheff, 1975, 1977; Robinson and Engelborghs, 1982, 1982; Voter and Erickson, 1984). The change in turbidity is caused by a combination of spontaneous microtubule nucleation and microtubule polymerization in solution (Borisy et al., 1972; Mirigian et al., 2013). In these 'bulk' assays a characteristic delay or lag phase was observed, followed by pseudo-first-order exponential increase in turbidity. The lag phase in different experiments varied between 50 seconds up to 10 min depending on experimental conditions (Carlier and Pantaloni, 1978; Caudron et al., 2000; Detrich et al., 1985; Himes et al., 1977; Johnson and Borisy, 1977; Lee and Timasheff, 1975, 1977; Robinson and Engelborghs, 1982; Voter and Erickson, 1984). The lag phase was found to be shorter at higher tubulin and GTP concentrations (Carlier and Pantaloni, 1978; Caudron et al., 2000; Voter and Erickson, 1984). Instead, turbidity measurements of microtubules polymerized from stabilized microtubule seeds showed that polymerization occurs immediately without the presence of a lag phase (Carlier and Pantaloni, 1978). For these reasons, the lag phase was interpreted as the kinetically unfavourable assembly step of the microtubules nucleus (Carlier and

Pantaloni, 1978; Erickson and Pantaloni, 1981; Oosawa and Asakura, 1975; Voter and Erickson, 1984).

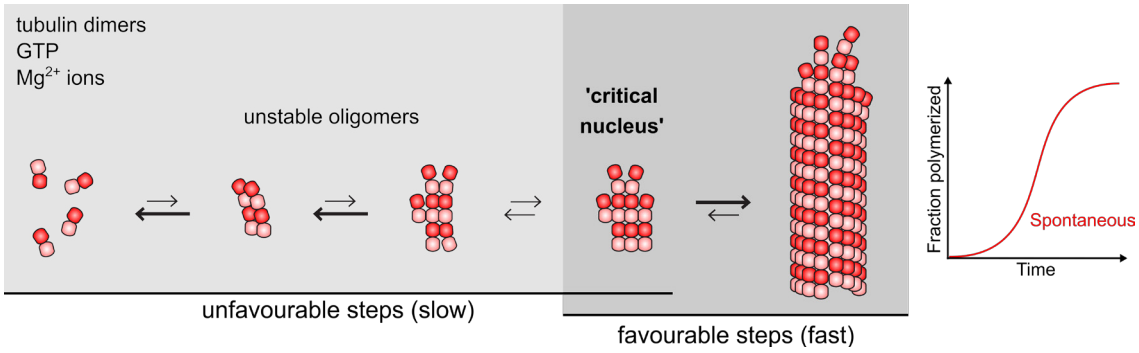

Figure 1.6: Hypthetical pathway of spontaneous microtubule nucleation. Spontaneous nucleation of microtubules in solutions containing GTP and Mg^{2+}. The thickness of the arrow indicates the likelihood of the reaction direction. It is thought that the process becomes favourable after a critical nucleus size has been reached. Redrawn from (Kollman et al., 2011; Roostalu and Surrey, 2017).

1.4.2 The structure of the microtubule nucleus

Very little is known about the size and shape of the microtubule nucleus (Brouhard and Rice, 2018; Roostalu and Surrey, 2017). First estimates of the nucleus size were obtained from above described kinetic bulk experiments and were reported to be in a range of 6 to 12 tubulin dimers (Carlier and Pantaloni, 1978; Caudron et al., 2000; Kuchnir Fygenson et al., 1995; Voter and Erickson, 1984). Complementary, different groups used negative stain electron microscopy in an attempt to visualize the microtubule nucleus. These experiments found small microtubule sheets or ribbon-shaped structures. These structures varied in size from three to a few tens of dimers in length and appeared like elongated structures consisting of a few parallel protofilaments (Mozziconacci et al., 2008; Portran et al., 2017; Voter and Erickson, 1984; Wang et al., 2005). These observations suggest, that similar to the microtubule lattice, longitudinal contacts in the nucleus are stronger than lateral contacts (Mandelkow et al., 1991; Roostalu and Surrey, 2017; Sui and Downing, 2010). To which extend these assemblies contain GTP or GDP is not known.

1.4.3 Stabilization of spontaneous microtubule nucleation by small molecules

Glycerol, GTP analogues and drugs that inhibit microtubule dynamics can increase microtubule nucleation efficiency *in vitro*, albeit through different mechanisms (Cao et

al., 2018; Hyman et al., 1992; Kellogg et al., 2017; Khrapunovich-Baine et al., 2011; Lee and Timasheff, 1975, 1977).

The best studied microtubule stabilizing agent (MSAs) is Taxol. Taxol binds to β-tubulin at the inner microtubule wall and prevents the conformational change upon GTP-hydrolysis and consequently microtubule depolymerisation (Arnal and Wade, 1995; Kellogg et al., 2017). While Taxol has the highest stabilizing effect on longitudinal interactions at the interdimer interface, other MSAs such as peloruside A and laulimalide, strongly stabilize lateral contacts (Khrapunovich-Baine et al., 2011). The effect of these two MSAs has been shown to be synergistic with Taxol suggesting that the simultaneous stabilization of longitudinal and lateral contacts can complement each other (Gapud et al., 2004; Hamel et al., 2006).

Glycerol is known for its property to promote protein folding and protein interactions (Gekko and Timasheff, 1981). When glycerol is added to solutions of tubulin it enhances the self-association of tubulin molecules as the system tries to decrease the area of solvent-protein contacts (Gekko and Timasheff, 1981; Lee and Timasheff, 1975, 1977). This nonspecific thermodynamic effect requires substantially higher concentrations than needed by MSAs to promote microtubule nucleation (Roostalu and Surrey, 2017).

Microtubules can grow without hydrolysing GTP but hydrolysis is required for microtubule shrinkage. GTP analogues can stabilize microtubule nucleation by preventing or slowing down GTP hydrolysis (Hamel et al., 1984; Hyman et al., 1992, 1995; Müller-Reichert et al., 1998). The non-hydrolysable GTP analogue guanosine-5‘-[α,β)-methyleno]triphosphate (GMPCPP) has been shown to decrease the energy barrier for nucleation (Hyman et al., 1992; Wieczorek et al., 2015). This suggests, that GTP hydrolysis leads to the disassembly of microtubule nucleation intermediates (Brouhard and Rice, 2018; Roostalu and Surrey, 2017; Wieczorek et al., 2015).

1.4.4 Microtubule binders promote spontaneous microtubule nucleation

Microtubule-associated proteins (MAPs) affect the dynamic properties of microtubules and can enhance microtubule nucleation by promoting microtubule assembly, preventing catastrophes and stabilizing tubulin-tubulin interactions (Roostalu and Surrey, 2017; Vaart et al., 2009). Two MAPs, TPX2 and XMAP215, were found to be of particular importance in non-templated microtubule nucleation ((Brunet et al., 2004; Ghosh et al., 2013; Popov et al., 2002; Roostalu et al., 2015; Schatz et al., 2003). XMAP215 and TPX2 will generally be referred to as microtubule binders in the context of this thesis.

XMAP215 family members are microtubule polymerases which contain two to five paddle-shaped evolutionary conserved αβ-tubulin binding domains (TOG-domains) at their N-terminus (Al-Bassam et al., 2007; Brouhard et al., 2008; Widlund et al., 2011). The TOG domains are separated by linkers and charged stretches which contribute to microtubule lattice binding (Al-Bassam and Chang, 2011; Al-Bassam et al., 2007; Ayaz et al., 2012). XMAP215 family members enhance microtubule growth rates by catalysing the addition of αβ-tubulin specifically to the microtubule plus-end (Brouhard et al., 2008; Gard and Kirschner, 1987; Podolski et al., 2014; Roostalu et al., 2015). Currently it is thought that one TOG domain tethers XMAP215 family members to weakly bound curved αβ-subunits at the microtubule end whereas the other TOG domain delivers free tubulin dimers to promote longitudinal protofilament growth. Once the tubulin straightens due to lattice incorporation XMAP215 is released from the end; a mechanism termed 'hand-off' which allows the polymerase to move forward and catalyse the addition of the next tubulin dimer. XMAP215 family members therefore bind only weakly to the microtubule lattice (Al-Bassam and Chang, 2011; Ayaz et al., 2012, 2014; Widlund et al., 2011). Depletion of XMAP215 in budding yeast, plant cells or the slime mould *Dictyostelium discoideum*, reduces cytoplasmic microtubule numbers and completely abolishes microtubule nucleation in *Xenopus* egg extract (Gräf et al., 2003; Groen et al., 2009; Kawamura et al., 2006; Kosco et al., 2001; Kronja et al., 2009; Tournebize et al., 2000).

TPX2 is a multifunctional protein and a key player in the RanGTP-dependent microtubule nucleation pathway around chromatin (Neumayer et al., 2014). Structurally, TPX2 is an elongated monomer and contains several microtubule binding domains and regions which are important for regulating the interaction of TPX2 with other proteins such as importins, Aurora A or mitotic kinases (Alfaro-Aco et al., 2017; Brunet et al., 2004; Roostalu et al., 2015; Trieselmann et al., 2003; Zhang et al., 2017). Functionally, TPX2 was shown to suppress microtubule catastrophes and reduce depolymerisation speed without affecting microtubule growth speeds (Reid et al., 2016; Roostalu et al., 2015; Wieczorek et al., 2015). TPX2 preferentially binds to growing microtubule ends but also to the microtubule lattice (Roostalu et al., 2015). Depletion of TPX2 completely abolishes chromatin-mediated microtubule nucleation in *Xenopus* egg extracts and reduces nucleation in mouse oocytes and cultured cells (Brunet et al., 2008; Gruss et al., 2001, 2002; Petry et al., 2013).

TPX2 and XMAP215 homologs can both stimulate microtubule nucleation in solutions containing purified tubulin and Mg^{2+} ions at significantly lower tubulin concentrations than needed for spontaneous assembly (Alfaro-Aco et al., 2017; Brunet et al., 2004; Ghosh et al., 2013; Roostalu et al., 2015; Schatz et al., 2003). XMAP215 and human

homologue chTOG mildly stimulate the nucleation of long microtubules *in vitro* while TPX2 was shown to stabilize short microtubule 'stubs' which usually fail to elongate into microtubules (Ghosh et al., 2013; Roostalu et al., 2015). Interestingly, when chTOG and TPX2 are combined *in vitro*, chTOG is able to elongate the TPX2-nucleated stubs into microtubules, thereby synergistically increasing the efficiency of spontaneous microtubule nucleation beyond the effect of the individual proteins (Roostalu et al., 2015). These experiments suggest, that the two proteins employ a different mechanism to enhance spontaneous microtubule nucleation (Brouhard and Rice, 2018; Roostalu and Surrey, 2017). XMAP215-family members most likely accelerate the protofilament growth of unstable microtubule oligomers. The fast increase in protofilament length most likely increases the possibilities for lateral interactions between protofilaments to form. XMAP215-family members therefore might promote the transformation of unstable oligomers into stable nuclei (Brouhard and Rice, 2018; Roostalu and Surrey, 2017). In contrast, TPX2 can directly promote microtubule stability by reducing catastrophe frequency and decreasing depolymerization speeds (Reid et al., 2016; Roostalu et al., 2015; Wieczorek et al., 2015). Furthermore, it has been shown by cryo-EM that TPX2 simultaneously binds to longitudinal and lateral tubulin interfaces (Zhang et al., 2017). This suggests that TPX2 might promote microtubule nucleation by promoting the association between tubulin subunits (Roostalu and Surrey, 2017; Zhang et al., 2017).

1.4.5 Templated microtubule nucleation

Microtubule nucleation can also be initiated by providing a template for microtubules to grow from. Commonly used nucleation templates are purified centrosomes with bound γTuRCs, axonemes containing existing microtubules which can be extended or short stabilized microtubule 'seeds' which can be polymerized (Johnson and Borisy, 1977; Mitchison and Kirschner, 1984b; Schnackenberg et al., 1998; Telley et al., 2011; Walker et al., 1988; Zheng et al., 1995).

A recent publication found that nucleation from centrosomes, axonemes and microtubule seeds is stochastic and that the porability to nucleate a microtubule increases with increasing tubulin concentration (Wieczorek et al., 2015). Nucleation from the templates was found to proceed with a tubulin concentrations (~6 µM) that is in between spontaneous microtubule nucleation in absence of a template (~20 µM) and the tubulin concentration required for the growth of already existing microtubules (1 µM) (Voter and Erickson, 1984; Wieczorek et al., 2015). Due to this observation it is now thought that similar to spontaneous microtubule nucleation, nucleation from

templates is also thermodynamically unfavourable and needs to overcome a kinetic barrier (Brouhard and Rice, 2018; Roostalu and Surrey, 2017; Wieczorek et al., 2015). The presence of the barrier for templated nucleation might be due to structural differences (curvature and raggedness) and/or differences in the nucleotide state (GTP versus GDP) between already growing microtubule ends and the template (Brouhard and Rice, 2018; Roostalu and Surrey, 2017; Wieczorek et al., 2015).
The size of a stable microtubule intermediate forming on stabilized microtubule seeds as template was recently estimated (Wieczorek et al., 2015). In these experiments the elongation of microtubules from seeds was measured at high time resolution using fluorescent tubulin. It was found that fluorescent tubulin first assembles on the seed and that this initial fluorescence signal remained stationary for a short time before elongation occurs. The initial stationary fluorescent signal corresponds on average to 250 tubulin dimers (Wieczorek et al., 2015). This estimate of the nucleus size for templated microtubule nucleation is considerably larger than the size of the nucleus approximated for spontaneous microtubule nucleation (Carlier and Pantaloni, 1978; Caudron et al., 2000; Kuchnir Fygenson et al., 1995; Mozziconacci et al., 2008; Portran et al., 2017; Voter and Erickson, 1984; Wang et al., 2005). This size difference might be due to the different methods used to estimate the nucleus size, i.e. kinetic data or cryo-EM for spontaneous microtubule nucleation versus fluorescence microscopy for microtubule seed templates (Carlier and Pantaloni, 1978; Caudron et al., 2000; Kuchnir Fygenson et al., 1995; Mozziconacci et al., 2008; Portran et al., 2017; Voter and Erickson, 1984; Wang et al., 2005; Wieczorek et al., 2015).

1.5 γTuRC-dependent microtubule nucleation

The γTuRC is so far the best studied template for microtubule nucleation in cells. The central role of γ-tubulin in microtubule nucleation is known for a long time from studies disrupting γ-tubulin function in *Aspergillus nidulans*, *Schizosaccharmoyces pombe* and human cells (Horio et al., 1991; Joshi et al., 1992; Martin et al., 1997; Oakley et al., 1990). Later, add back experiments with salt stripped centrosomes *in vitro* could directly show that γ-tubulin is essential for microtubule nucleation from centrosomes (Moritz et al., 1998; Schnackenberg et al., 1998). Currently, very little is known about the mechanism the γTuRC employes to initiate microtubule formation. Due to its ring-shaped structure, it was suggested that γTuRCs essentially act as a seed from which microtubules can elongate (Erickson, 2000; Job et al., 2003; Keating and Borisy, 2000; Kollman et al., 2010, 2015; Moritz et al., 1995, 2000). Microtubules could assemble on γTuRC templates by forming strong longitudinal bonds with incoming

αβ-tubulin dimers. Stabilization of these longitudinal bonds would in turn also enhance the formation of lateral bonds between the growing protofilaments, making γTuRC-templated nucleation more efficient than spontaneous nucleation (Figure 1.7) (Brouhard and Rice, 2018; Roostalu and Surrey, 2017).

Purified γTuRCs from different organisms stimulate microtubule nucleation in solutions of purified tubulin (Kollman et al., 2015; Murphy et al., 2001; Oegema et al., 1999; Zheng et al., 1995). However, purified γTuRCs are not constitutively active. *In vitro* experiments could show that γTuRC nucleation efficiency strongly depends on tubulin concentration and can further be tuned by regulatory factors (see Table 2 for details for *in vitro* microtubule nucleation studies with purified γTuRC) (Choi et al., 2010; Gombos et al., 2013; Gunawardane et al., 2000; Gunzelmann et al., 2018; Kollman et al., 2010, 2015; Lin et al., 2016, 2014; Liu et al., 2014a; Lyon et al., 2016; Muroyama et al., 2016; Oegema et al., 1999; Thawani et al., 2018; Vinh et al., 2002; Wiese and Zheng, 2000; Zheng et al., 1995)

In cells, microtubule nucleation is confined in space to MTOCs and is temporally controlled by coupling nucleation activity to the cell cycle or differentiation stage. Therefore, it might not be surprising that γTuRC activity is also tightly regulated. The activation of the complex should coincide with its recruitment to MTOCs where regulatory factors are concentrated. Several different possibilities of γTuRC regulation have been proposed and will be discussed below.

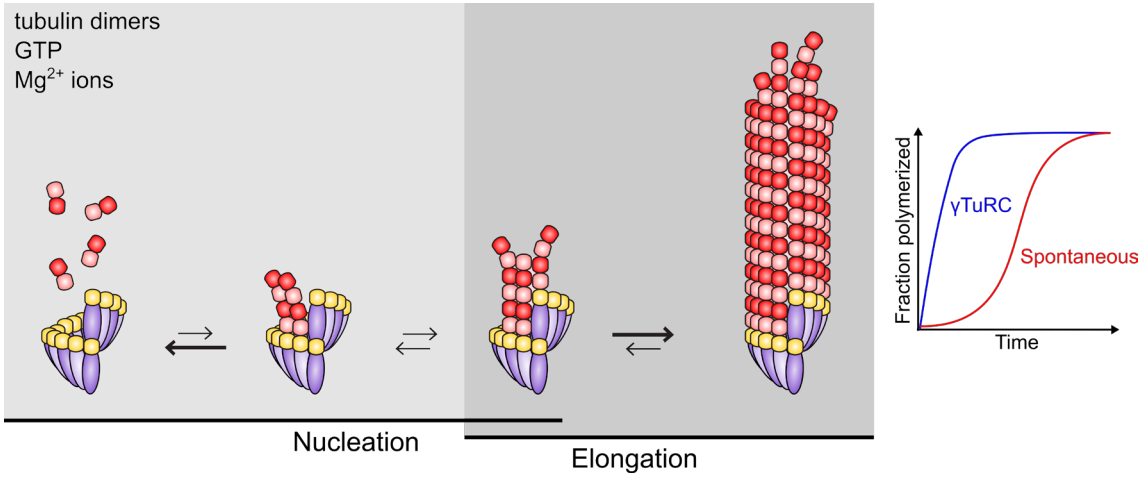

Figure 1.7: Schematic illustration of templated microtubule nucleation by γTuRCs. The thickness of the arrow indicates the likelihood of the reaction direction. It is thought that γTuRCs bypass the slow lag phase observed for spontaneous microtubule nucleation. Redrawn from (Kollman et al., 2011).

Table 2: Summary of *in vitro* microtubule nucleation assays with purified γTuRC

Type of Assay	Organism	γTuSC	γTuRC	γTuRC binder	Microtubule binder	Tubulin [μM]	Additives	Effect on *in vitro* nucleation activity	References
Turbidity	Human	-	?	-	-	3.9-9	-	γTuRC nucleates microtubules *in vitro*	(Murphy et al., 2001)
Solution nucleation microscopy		-	30 nM γ-tub	γTUNA[1] NγBD[2]	-	10	-	γTuNA stimulates nucleation, NγBD does not	(Muroyama et al., 2016)
		-	2 nM GCP5	CDK5Rap2 γTUNA	-	10	-	CDK5Rap2 and γTuNA stimulate nucleation	(Choi et al., 2010)
		-	2 nM GCP5	NME7	-	10	-	NME7 stimulates nucleation	(Liu et al., 2014a)
	X. laevis	-	3-6 nM GCP4	-	XMAP215	10-12	-	XMAP215 stimulates nucleation	(Thawani et al., 2018)
		-	4.3 μg/mL	-	-	2.5-30	-	γTuRC nucleates microtubules *in vitro*	(Zheng et al., 1995)
		-	?	-	-	32.5	-	γTuRC caps microtubule minus ends	(Wiese and Zheng, 2000)
	D. melanogaster	0.1-0.2 μM	-	-	-	40	-	γTuRC binds preformed microtubules	(Gunawardane et al., 2000)
		0.74 μM γ-tub	0.84 μM γ-tub	-	-	40	-	γTuRC is more active than γTuSC	(Oegema et al., 1999)
	C. albicans	1 μM	-	CaSpc110 CaSpc72N[3] CaMzt1	-	20	12.5% glycerol 1 μM taxol 150 mM KCl	Mzt1 stimulates nucleation	(Lin et al., 2016)
	S. pombe	?	-	Mto1/2[bonsai] Mzt1	-	20	-	Mzt1 stimulates nucleation	(Leong et al., 2019)

Type of Assay	Organism	γTuSC	γTuRC	γTuRC binder	Microtubule binder	Tubulin [μM]	Additives	Effect on *in vitro* nucleation activity	References
Solution nucleation microscopy	*S. cerevisiae*	0.3 μM	-	Spc110$^{1-220}$	-	20	25% glycerol	GTP binding to γ-tubulin stimulates nucleation	(Gombos et al., 2013)
		?	-	Spc110	-	?	20% glycerol 125 mM KCl	Ring closure stimulates nucleation, yeast tubulin enhances nucleation efficiency	(Kollman et al., 2015)
		150 nM	-	Spc110$^{1-220}$	-	12-20	25% glycerol	γTuSC oligomerization stimulates nucleation	(Kollman et al., 2010)
		3 μM	-	Spc110$^{1-220}$		20	25% glycerol	Spc110$^{1-220}$ phosphorylation stimulates nucleation	(Lin et al., 2014)
		25-50 nM	-	Spc110$^{1-220}$	-	15	20% glycerol 125 mM KCl	γTuSC oligomerization stimulates nucleation	(Lyon et al., 2016)
		?	-	-	-	20	-	γTuSC oligomerization stimulates nucleation	(Vinh et al., 2002)
		50 nM	-	Spc72N[3]	Stu2	12	12.5% glycerol	Stu2 stimulates nucleation	(Gunzelmann et al., 2018)

[1]γTuNA is the N-terminal γTuRC-binding domain of CDK5Rap2 containing the evolutionary conserved CM1 domain (amino acids 51-100), [2]NγBD is the C-terminal γTuRC-binding domain of NEDD1 (amino acids 597-660), [3]Spc72N is the N-terminal γTuRC-binding domain of Spc72 containing the CM1-motif (amino acids 1-267)

1.5.1 Regulation of γTuRC

Regulation of γTuRC assembly

The γTuRC is assembled from smaller subcomplexes (γTuSCs). Purified γTuSCs from *Saccharomyces cerevisiae* or *Drosophila melanogaster* were found to be either unable to form microtubules *in vitro* or only mildly stimulated microtubule nucleation (Kollman et al., 2010; Oegema et al., 1999; Vinh et al., 2002). When γTuSCs are assembled into γTuRCs a dramatic increase in microtubule nucleation efficiency has been found for both organisms. *Drosophila melanogaster* γTuRCs are ~150-fold more active per mole of complex than γTuSCs (Oegema et al., 1999). Similarly, budding yeast γTuRC nucleation efficiency is ~300-fold higher than γTuSCs (Kollman et al., 2015).

This strong effect on nucleation efficiency might be explained by the different structures of the complexes. γTuSCs are heterotetramers consisting of two molecules of γ-tubulin and two GCP proteins, while the fully assembled γTuRC resembles a ring which closely matches the diameter and helical pitch of a microtubule (Choy et al., 2009; Kollman et al., 2008, 2010, 2015; Vinh et al., 2002). Furthermore, structural studies with budding yeast complexes could show that the two γ-tubulins in the γTuSC are actually held apart from each other (Choy et al., 2009; Kollman et al., 2008, 2010). As a consequence, γTuSCs might not be able to efficiently stabilize the weaker lateral connections between two neighbouring protofilaments. Alternatively, a minimum of three laterally associated protofilaments might be required for a microtubule to nucleate on a template (Roostalu and Surrey, 2017).

Regulation of γTuRC by conformational change

Structural studies of budding yeast γTuRC revealed that even after oligomerization of γTuSCs into γTuRCs the two γ-tubulins within the same γTuSC are unable to form lateral contacts with each other while the γ-tubulins between neighbouring γTuSCs bind to each other (Kollman et al., 2010). This result was unexpected and was interpreted as γTuRC being in an ‘off state’ which requires activation by a conformational change (Kollman et al., 2010, 2015). The nucleation efficiency of the budding yeast γTuRC increased by 2-fold when γTuRC was artificially cross-linked to close the space between the γ-tubulins (Kollman et al., 2015). This experiment suggests that γTuRCs might be activated in cells by a conformational switch from an inactive to an active template (Kollman et al., 2011).

How this switch is regulated remains to be determined but allosteric activation could be a possibility. The evolutionary conserved γTuRC-tethering protein Spc110 is often mentioned as a candidate protein for allosteric regulation (Farache et al., 2018; Teixidó-Travesa et al., 2012; Tovey and Conduit, 2018). Spc110 is essential for the assembly of γTuRCs from γTuSCs in budding yeast and localizes the yeast γTuRC to the SPB (Knop and Schiebel, 1997; Kollman et al., 2010, 2015; Lin et al., 2015; Lyon et al., 2016). However, structural studies could show that the presence of a short fragment of Spc110 was not sufficient to trigger the conformational change needed to close the space between the two γ-tubulins within a γTuSC (Kollman et al., 2010, 2015; Lyon et al., 2016). *In vitro* experiments with purified proteins could show that phosphorylation of Spc110 and the presence of another γTuRC binder, Mozart1, increases budding yeast γTuRC nucleation efficiency (Lin et al., 2016, 2014). It is therefore possible that Spc110 has a dual role separated into γTuRC assembly and activation, which might be regulated by phosphorylation. Alternatively, Spc110 is driving the oligomerization while other proteins such as Mozart1 trigger the conformational change (Lin et al., 2016, 2014).
It is currently not known if the γTuRC in higher eukaryotes is also regulated by a structural change as high-resolution structures are currently unavailable. The γTuRC from higher eukaryotes contains additional GCPs (GCP4/5/6) which are missing in budding yeast. It is speculated that the additional GCPs have the role of yeast Spc110, i.e. holding the γTuSCs together in the ring shape (Kollman et al., 2011). Allosteric regulation might therefore not be required to activate γTuRCs in higher eukaryotes. Nevertheless, the γTuRC-thethering protein CDK5Rap2, which is not required for γTuRC assembly, was shown to increase the nucleation efficiency of human γTuRCs (Choi et al., 2010).

Regulation of γTuRC by phosphorylation

γ-tubulin as well as all other GCPs contain several phosphorylation sites, with some of them being specifically phosphorylated by mitotic kinases (Teixidó-Travesa et al., 2012; Tovey and Conduit, 2018). The phosphorylation sites studied so far in human cells have been implicated in γTuRC localization to centrosomes (GCP5) and keratin intermediate filaments (GCP6) as well as in centrosome duplication (γ-tubulin) and centriole biogenesis (GCP6) but do not seem to directly enhance γTuRC nucleation activity (Alvarado-Kristensson et al., 2009; Bahtz et al., 2012; Izumi et al., 2008; Oriolo et al., 2007).

The only evidence that γTuRC activity might be directly regulated by phosphorylation comes from *in vitro* assays with the γTuRC associated protein kinase NME7. NME7 co-purified with human γTuRCs in one study and was shown to enhance microtubule nucleation efficiency ~2.5-fold *in vitro*. This increase seem to be dependent on its kinase activity, however, a target for NME7 phosphorylation has not been identified yet (Liu et al., 2014a).

Regulation of γTuRC by activation via γTuRC binders

Several other proteins have been shown to copurify with γTuRCs and seem to have role in regulating γTuRC activity (Farache et al., 2018; Teixidó-Travesa et al., 2012; Tovey and Conduit, 2018).

γTuRC-tethering proteins (see Table 1) are the best studied proteins implicated in modulating γTuRC activity. These proteins contain an evolutionary conserved C-terminal CM1 (centrosomin 1) domain which mediates binding to γTuRCs (Lin et al., 2015). In yeast, CM1-containing proteins are crucial for the assembly of γTuSCs into γTuRCs (Lin et al., 2014; Lynch et al., 2014; Sawin et al., 2004). In higher eukaryotes, they do not have a role in complex assembly but mediate γTuRC recruitment and anchoring to different MTOCs including the centrosome and the Golgi. Depletion of CM1-containing proteins impairs centrosomal and acentrosomal microtubule nucleation *in vivo* (Chen et al., 2017a; Choi et al., 2010; Fava et al., 1999; Fong et al., 2008; Muroyama et al., 2016; Roubin et al., 2013; Takahashi et al., 2002; Wang et al., 2014; Zhang and Megraw, 2007; Zimmerman et al., 2004). Overexpression of γTuRC-tethering proteins in fission yeast and human cells induces cytoplasmic microtubule nucleation in a spatially random manner (Choi et al., 2010; Cota et al., 2017; Lynch et al., 2014). *In vitro* nucleation assays with purified human γTuRCs show that the CM1 domain of CDK5Rap2 (termed γTuNA; γTuRC-mediated nucleation activator) increases the number of nucleated microtubules by 7-fold in two independent studies (Choi et al., 2010; Muroyama et al., 2016). Budding yeast Spc110 increases microtubule nucleation of γTuRC dramatically due to the assembly of γTuSCs into γTuRCs. Phosphorylation of Spc110 at several positions increases the number of nucleated microtubules by another 3-fold suggesting that CM1 domain containing proteins have an evolutionary conserved role in regulating γTuRC activity (Lin et al., 2014).

NEDD1/GCP-WD is an important recruitment factor of γTuRCs to different MTOCs including centrosomes, spindle microtubules and chromatin (Gomez-Ferreria et al., 2012; Haren et al., 2006; Manning et al., 2010; Zhang et al., 2009). The localization

of NEDD1 to different MTOCs is regulated by phosphorylation in a cell-cycle dependent manner and NEDD1 depletion was shown to abolish γTuRC-mediated microtubule nucleation at centrosomes and chromatin (Gomez-Ferreria et al., 2012; Haren et al., 2009; Johmura et al., 2011; Liu and Wiese, 2008; Lüders et al., 2006; Manning and Kumar, 2007; Pinyol et al., 2013; Sdelci et al., 2012; Zhang et al., 2009; Zhu et al., 2008, 2009). Current evidence suggests that NEDD1 does not have a role in modulating γTuRC activity. Overexpression of NEDD1 displaces γTuRCs from centrosomes into the cytoplasm but unlike γTuNA it does not induce microtubule nucleation in the cytosol (Haren et al., 2006; Pinyol et al., 2013). In human keratinocytes, depletion of NEDD1 reduces the centrosomal localization of γTuRCs but does not affect microtubule nucleation activity from centrosomes and a purified fragment of NEDD1 does not stimulate γTuRC activity *in vitro* (Muroyama et al., 2016).

Another more recently identified γTuRC binder Mozart (Mzt1/GCP9) is implicated in modulating γTuRC assembly and regulation in different organisms. In some studies, Mzt1 is described as a core component of the γTuRC, which was overlooked in many previous characterizations of purified complexes due to its small size (~16 kDa) (Hutchins et al., 2010; Kollman et al., 2011; Teixidó-Travesa et al., 2010, 2012; Tovey and Conduit, 2018). Mzt1 is the most widely conserved γTuRC binder (see Table 1) but does not seem to be important in all organisms or cell types. For example in *Drosophila melanogaster*, Mzt1 is only expressed in the testes and *Arabidopsis thaliana* Mzt1 might only associate with a subset of γTuRCs (Nakamura et al., 2012; Tovey et al., 2018). Budding yeast does not seem to contain a Mzt1 homologue (Lin et al., 2016). Currently, it is not clear if Mzt1 has a direct effect on γTuRC microtubule nucleation efficiency. *In vitro* experiments with purified proteins from the yeast *Candida albicans* could show that Mzt1 is a bridging factor, which promotes the interaction between γTuSC and γTuRC-tethering proteins (Lin et al., 2016). *Candida albicans* Mzt1 is therefore thought to stabilize γTuSC oligomerizeriation by γTuRC-tethering proteins. The resulting more stable γTuRCs where shown to nucleate microtubules 3-fold more efficiently (Lin et al., 2016). Fission yeast Mzt1 does not interact with the γTuRC-tethering proteins Mto1/2 but prevents the aggregation of the GCP3 homologue Alp6 (Leong et al., 2019). Interestingly, both Mzt1 and Mto1/2 where needed for efficient microtubule nucleation by reconstituted fission yeast γTuRCs (Leong et al., 2019). Depletion of Mzt1 in human cells leads to a reduction of γ-tubulin specifically at centrosomes and induces monopolar spindles and mitotic arrest (Cota et al., 2017; Hutchins et al., 2010). It has been shown that Mzt1 interacts with the N-terminus of GCP3, GCP5, GCP6 and possibly GCP2 (Cota et al., 2017;

Lin et al., 2016). *In vivo* studies suggest that human Mzt1 might also function as a bridging factor similar to *Candida albicans* Mzt1. As mentioned above the overexpression of a short fragment of the γTuRC thethering protein CDK5Rap2 (γTuNA) results in spatially random microtubule nucleation in the cytoplasm (Choi et al., 2010; Cota et al., 2017). Simultaneous depletion of Mzt1 completely abrogates the effect of γTuNA overexpression suggesting that Mzt1 is needed for efficient activation of γTuRCs by γTuNA (Cota et al., 2017). Wheter Mzt1 has a role in stabilizing γTuRC assembly in human cells is currently not known. Knock down in HeLa cells does not seem to interfere with γTuRC integrity whereas in U2OS a significant decrease of fully assembled γTuRCs was found upon Mzt1 depletion (Cota et al., 2017; Lin et al., 2016). Nevertheless, the proposed bridging function of Mzt1 would be important to stabilize the interaction of γTuRCs with other intracellular regulators which could be important in modulating γTuRC activity at different subcellular locations (Cota et al., 2017; Tovey and Conduit, 2018). Less is known about the closely related Mzt2 A/B (GCP8 A/B) proteins. Mzt2 A/B seem to have an interphase specific role as their depletion interferes with γ-tubulin recruitment and microtubule nucleation at interphase centrosomes without inducing mitotic effects (Teixidó-Travesa et al., 2010).

Regulation of γTuRC by microtubule binders

Apart from regulation by ring assembly, conformational change and binding to regulatory proteins, γTuRC-mediated microtubule nucleation might also be regulated by MAPs. These proteins will be generally referred to as microtubule binders in the context of this thesis. Microtubule binders with functions in nucleation promote microtubule formation by modulating dynamic instability parameters and include proteins such as the microtubule polymerase XMAP215 or the anti-catastrophe factor TPX2.

Microtubule binders have been shown previously to reduce the time lag and the tubulin concentration needed to induce templated microtubule nucleation from stabilized microtubule seeds (Wieczorek et al., 2015). *In vitro* nucleation assays with purified budding yeast γTuRCs report a 3-fold increase in microtubule nucleation in the presence of the XMAP215 homologue Stu2 (Gunzelmann et al., 2018). XMAP215 increases the number of microtubules nucleated by purified *Xenopus laevis* γTuRCs in a dose-dependent manner (Thawani et al., 2018). Nucleation experiments in *Xenopus* egg extract suggest a direct link between TPX2 and γTuRCs in branching

microtubule nucleation and nucleation around chromatin (Alfaro-Aco et al., 2017; Petry et al., 2013; Scrofani et al., 2015).
Based on these observations a model was proposed which suggests that inefficient nucleation from templates might be explained by structural differences in the template (blunt and straight) compared to a growing microtubule end (tapered and curved). Addition of tubulin-dimers to blunt ends might be comparably inefficient due to the lack of 'corner' sites to form lateral contacts. Microtubule binders might help to tether curved tubulin dimers onto blunt ends and thus accelerating the transformation of a template into an elongation competent microtubule end (Brouhard and Rice, 2018; Roostalu and Surrey, 2017).

1.6 Actin filament nucleation by actin nucleators

G-actin and tubulin are quite distant at a protein structural level but there are several fundamental similarities between actin filaments and microtubules (Kabsch et al., 1990; Löwe et al., 2001; Mitchison, 1992; Wang et al., 2010a). Both, G-actin and tubulin assemble into polymers and hydrolyse nucleotides during polymerization (Amos and Klug, 1974; Carlier, 1989; Cote and Borisy, 1981; Kasai et al., 1962; Wegner, 1976). In both cases, nucleotides are exchangeable in the monomeric form while nucleotide exchange is blocked in the polymer (Carlier, 1989; Carlier and Pantaloni, 1981; Korn et al., 1987). Actin filaments and microtubules are polar due to their subunits pointing in the same direction within the lattice (Beese et al., 1987; Holmes et al., 1990; Nogales et al., 1999; Steinmetz et al., 1997). Both filaments also exhibit a kinetic barrier for nucleation *in vitro* and a linear dependence of the polymerization rate on the concentration of the respective monomers (Cooper et al., 1983; Erickson and Pantaloni, 1981; Oosawa and Asakura, 1975; Sept and McCammon, 2001; Voter and Erickson, 1984). On a structural and mechanistic level, however, actin filaments and microtubules differ substantially. As mentioned before, microtubules are stiff, hollow, thirteen-stranded filaments, whereas actin filaments are thin and flexible and have a two-stranded lattice (Beese et al., 1987; Evans et al., 1985; Gittes, 1993; Holmes et al., 1990; Nogales et al., 1999; Steinmetz et al., 1997). The structural differences between actin filaments and microtubules probably explain why the estimated size of the critical nucleus for actin polymerization, i.e. 3 to 4 G-actins, is smaller than the nucleus size estimated for microtubule nucleation (Cooper et al., 1983; Oda et al., 2016; Tobacman and Korn, 1983).
In cells, the spontaneous polymerization of G-actin into filaments is prevented by G-actin-binding and sequestering proteins, such as profilin and β-thymosin (Safer et al.,

1990; Schlüter et al., 1997). Therefore, cells use nucleation factors to nucleate actin filaments. However, while microtubules are primary nucleated by the γTuRC, actin filaments can be nucleated by several different actin nucleators. Currently there are three major classes of actin nucleators: (i) the Arp2/3 (actin-related protein 2/3) complex, (ii) formins and (iii) the more recently identified tandem-monomer-binding nucleators (see Figure 1.8) (Ahuja et al., 2007; Coutts et al., 2009; Firat-Karalar and Welch, 2011; Machesky and Insall, 1998; Machesky et al., 1994; Okada et al., 2010; Pruyne et al., 2002; Quinlan et al., 2005; Sagot et al., 2002a; Weston et al., 2012; Zuchero et al., 2009).

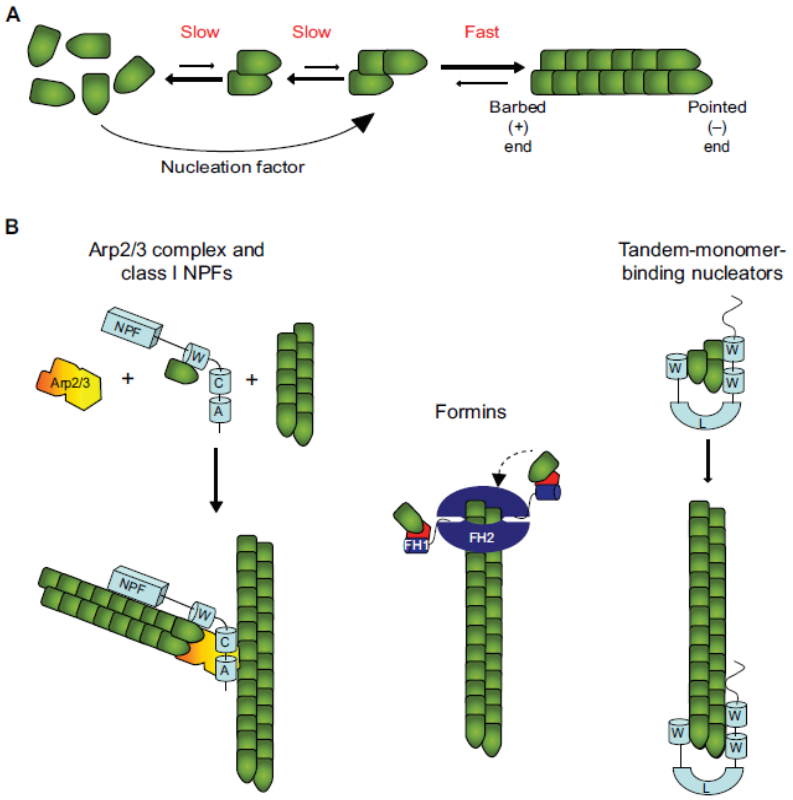

Figure 1.8: Scheme of actin nucleation by different actin nucleators. Taken from (Weston et al., 2012). (A) Actin filament assembly from G-actin. (B) Nucleation of new actin filaments from the side of an existing actin filament by the Arp2/3 complex after activation by NPFs, unbranched actin filament nucleation by formins and tandem-monomer binding nucleators.

The Arp2/3 complex is probably the actin nucleator most similar to the γTuRC. It contains Arp2 and Arp3, which are closely related to G-actin, and five additional subunits (Kelleher et al., 1995; Machesky and Insall, 1998; Machesky et al., 1994). The Arp2/3 complex is thought to act as a nucleation core by mimicking actin trimer formation upon the addition of an additional G-actin. Arp2/3 complexes, just like the γTuRC, therefore nucleate actin filaments from the minus (pointed) end and allow for actin polymerization from the plus (barbed) end (Rouiller et al., 2008; Smith et al.,

2013). By itself, the Arp2/3 complex is an inefficient nucleator. Activation requires the binding of the Arp2/3 complex to the side of an existing actin filament and allosteric activation by nucleation promoting factors (NPFs) (Ahuja et al., 2007; Derivery and Gautreau, 2010; Goley et al., 2010; Higgs and Pollard, 1999; Ismail et al., 2009; Lebensohn and Kirschner, 2009; Padrick et al., 2008; Smith et al., 2013; Suetsugu et al., 2001). Once activated, the Arp2/3 complex initiates branching of new actin filaments from already existing actin filaments at a 70° angle to form branched actin networks (Amann and Pollard, 2001; Mullins et al., 1998; Smith et al., 2013). The function of the Arp2/3 complex in initiating branched actin networks is similar to the function of the γTuRC in branched microtubule nucleation. However, whereas Arp2/3 complexes can bind to actin filaments by themselves, γTuRCs need Augmin and possibly NEDD1 and TPX2 to bind to existing microtubules (Alfaro-Aco et al., 2017; Chen et al., 2017b; Goshima et al., 2008; Hsia et al., 2014; Petry et al., 2013; Song et al., 2018; Uehara et al., 2009).

Unbranched actin filaments are nucleated by the second major class of actin nucleators, the formin proteins (Chesarone et al., 2010; Courtemanche, 2018). Formins are both nucleation factors and elongation factors (Pring et al., 2003; Pruyne et al., 2002; Romero et al., 2004; Sagot et al., 2002a). They are thought to nucleate actin filaments by stabilizing actin dimers and then stay processively associated with the elongating barbed end (Higashida et al., 2004; Kovar and Pollard, 2004; Pruyne et al., 2002; Romero et al., 2004; Sagot et al., 2002a). Formins protect actin filaments from capping proteins which would terminate the polymerization and simulatenously accelerate the addition of actin monomers to the barbed end thereby increasing the rate of actin polymerization (Harris et al., 2004; Kovar et al., 2005; Moseley et al., 2003; Romero et al., 2004; Sagot et al., 2002a). The function of formins might be similar to the function of microtubule polymerases. However, while formins are capable of nucleating actin filaments in cells, this has not been shown directly for microtubule polymerases (Chang et al., 1997; Evangelista et al., 2002; Feierbach and Chang, 2001; Kobielak et al., 2004; Sagot et al., 2002b; Schirenbeck et al., 2005; Severson et al., 2002). Nevertheless, XMAP215 and chTOG have been shown to nucleate microtubules *in vitro* probably by accelerating the transformation of spontaneously formed unstable tubulin oligomers into stable nuclei (Ghosh et al., 2013; Roostalu et al., 2015). In cells it is thought that microtubule polymerases work synergistically with γTuRCs to accelerate the elongation of microtubules nucleated by the complex (Gunzelmann et al., 2018; Thawani et al., 2018). The difference in the ability of formins and microtubule polymerases to act as nucleators might be explained by the more complex structure of microtubules compared to actin filaments.

The third class of actin nucleators are tandem-monomer-binding nucleators including Spire, cordon-bleu (Cobl), leiomodin (Lmod), junction-mediating and regulatory protein (JMY) and adenomatous polyposis coli (APC) (Ahuja et al., 2007; Coutts et al., 2009; Okada et al., 2010; Quinlan et al., 2005; Zuchero et al., 2009). While this group of actin nucleators is quite heterogeneous, they all contain tandem G-actin binding motifs which bring together G-actins to form an actin nucleation seed (Qualmann and Kessels, 2009). It was proposed that they form nuclei with distinct structural features. For example, Cobl, Lmod and APC stabilize cross-filament interactions along the short-pitch helix (Okada et al., 2010; Qualmann and Kessels, 2009). In contrast, Spire and JMY most likely stabilize monomers aligned along the long-pitch helix of the filament (Zuchero et al., 2009). However, how exactly tandem-monomer-binding nucleators nucleate actin filaments remains unknown. Proteins like TPX2, doublecortin, CAMSAP/Patronin and the dynactin subunit p150^{Glued} might have a similar function in microtubule nucleation. These proteins supress microtubule dynamicity and have been shown to nucleate microtubules *in vitro* most likely by stabilizing microtubule nucleation intermediates (Hendershott and Vale, 2014; Horesh et al., 1999; Jiang et al., 2014; Lazarus et al., 2013; Moores et al., 2004, 2006; Reid et al., 2016; Roostalu et al., 2015; Taylor et al., 2000). If these proteins can nucleate microtubules in cells in the absence of γTuRCs or rather promote microtubule nucleation from γTuRCs is not entirely known.

1.7 Aims

It is a major open question, how γTuRCs template microtubule nucleation and how the de novo formation of new microtubules by γTuRCs is regulated in cells. To answer these questions, several groups have attempted to study γTuRC-mediated microtubule nucleation *in vitro* using purified proteins. However, the purification of sufficient amounts of γTuRCs from native sources, in particular from higher eukaryotes, has proven to be difficult. Therefore, our understanding of γTuRC-mediated microtubule nucleation on a structural and mechanistic level largely stems from complexes of lower eukaryotes, such as yeast. Moreover, the current *in vitro* assays used to study γTuRC activity have a limited ability to measure the kinetics of microtubule nucleation by γTuRCs. Current assays able to follow γTuRC-mediated microtubule nucleation in real time cannot simultaneously visualize individual microtubules, whereas assays able to observe individual microtubules are unable to do this in real time.

In the context of this thesis my aim was to work towards a better understanding of γTuRC-mediated microtubule nucleation and the regulation of γTuRCs isolated from human cells. I established a new approach for purification of γTuRCs and developed a novel fluorescence microscopy-based microtubule nucleation assay. In chapter 2, I describe the new purification protocol for the affinity isolation of fluorescently tagged γTuRCs from a stable human cell line. In chapter 3, I describe the development of a new fluorescence microscopy-based assay which allows to observe the nucleation of individual microtubules by γTuRCs in real time. I will then show how this assay was successfully used to quantify microtubule nucleation kinetics under a variety of conditions. Lastly, in chapter 4, I will apply the new microtubule nucleation assay to study the regulation of human γTuRCs by different microtubule binders and γTuRC binders.

2. Purification of γTuRCs from human cells

2.1 Introduction

The biochemical study of γTuRC from higher eukaryotes has been hampered by the challenging purification of the complex from native sources. γTuRC isolation is difficult partly due to the low intracellular concentration of the complex (γ-tubulin amounts for 0.001-0.01% of total cellular protein) and its fragile nature as it tends to dissociate at higher salt concentrations limiting the type and number of conventional chromatography steps one can apply (Oegema et al., 1999; Stearns and Kirschner, 1994; Zheng et al., 1995, 1998). Although, *Drosophila melanogaster* and yeast γTuSC can be reconstituted by coexpression of all γTuSC subunits in insect cells, such methods have not been reported for γTuRC (Gunawardane et al., 2001; Vinh et al., 2002).

The majority of purification protocols for γTuRC from higher eukaryotes rely on the immunoaffinity isolation of the complex from native sources. This method was first reported for the purification of *Xenopus laevis* γTuRC (Zheng et al., 1995, 1998) and was later adapted to purify the γTuRC from a variety of different organisms (Table 3). Typically, the immunoaffinity isolation of γTuRC involves three steps: i) a precipitation step to preclear the γTuRC containing lysate followed by ii) affinity purification using a specific antibody which is usually directed against the C-terminus of γ-tubulin and lastly iii) sucrose gradient centrifugation to achieve higher purities and separate fully assembled γTuRCs from γTuSCs.

Apart from immunoaffinity isolation, two other methods for purification of γTuRC from human cells were reported (Choi and Qi, 2014; Choi et al., 2010; Liu et al., 2014a; Muroyama et al., 2016; Teixidó-Travesa et al., 2010). The first method bypasses the need of an antibody by exploiting the natural interaction between the complex and the conserved γTuRC-binding domain of the well-known centrosomal γTuRC localization and anchoring protein CDK5Rap2 (γTuNA) (Choi and Qi, 2014; Choi et al., 2010; Liu et al., 2014a). Since the interaction between γTuNA and γTuRC is rather weak γTuNA can be separated from the complex by sucrose gradient centrifugation. The same protocol was used to purify human γTuRC in a second independent study (Muroyama et al., 2016). Interestingly, in addition to affinity purification by γTuNA, authors were also able to purify the complex via the γTuRC-binding domain of another established intracellular γTuRC recruitment factor, NEDD1 (NγBD). Just like for γTuNA, the interaction between NyBD and γTuRC is weak and the protein fragment

can be separated from the complex using sucrose gradient centrifugation. The second method for the purification of γTuRC is based on human cells stably expressing γ-tubulin with a C-terminal mycTAP tag (Teixidó-Travesa et al., 2010). This method allows for direct affinity isolation of the complex by its own purification tag without the need of additional reagents. However, unlike native γTuRC purified with the above described methods, the tagged γTuRC was not tested for its microtubule nucleation activity *in vitro*. Also, the purified complex was not analysed by sucrose gradient centrifugation to assess if the tagging of γ-tubulin interferes with the stability of the complex or its assembly. Nevertheless, cells grow when overexpressing γ-tubulin-mycTAP and all known γTuRC subunits were found to copurify, suggesting that at least some γTuRC is functional and fully assembled.

Based on the protocols published and described above I decided to purify γTuRC from human cell lines by two different approaches. The first approach is the purification of the native complex using γTuRC binders (i.e. γTuNA and the C-terminus of NEDD1) following published protocols (Choi and Qi, 2014; Choi et al., 2010; Liu et al., 2014a; Muroyama et al., 2016). As a second approach, I developed a new method to purify a tagged version of human γTuRC from stable cell lines overexpressing a γTuRC subunit which is tagged with an affinity tag and a fluorescent marker protein. I did not attempt to purify γTuRC by immunoaffinity isolation since I was not able to produce a specific peptide antibody against one of the γTuRC subunits.

Table 3: Summary of purification protocols for γTuRC. This table is excluding protocols published for yeast, fungi and plant complexes.

Organism	Affinity purification	Precipitation	Refinement step	Starting amount	Final yield	Reference
Xenopus laevis	γ-tubulin antibody	15-25% ammonium sulphate	Size exclusion chromatography of crude extract, ion exchange of affinity column elution	25-30 mL	1-3 µg of γTuRC	(Wiese and Zheng, 2000; Zheng et al., 1995, 1998)
Xenopus laevis	γ-tubulin antibody	30% PEG	Sucrose gradient	10 mL	?	(Thawani et al., 2018)
Drosophila melanogaster	γ-tubulin antibody	-	-	?	?	(Wiese, 2008)
Drosophila melanogaster	γ-tubulin antibody	2% PEG	Sucrose gradient	20 g	?	(Gunawardane et al., 2001; Moritz et al., 2000)
Drosophila melanogaster	γ-tubulin antibody	2% PEG	-	30 mL	?	(Moritz et al., 2000)
Goat brain	γ-tubulin antibody	15-25% ammonium sulphate	-	?	?	(Thomas et al., 2010)
Sheep brain	γ-tubulin antibody	-	Sucrose gradient	?	0.005 µg of γ-tubulin	(Détraves et al., 1997)
HEK293	GCP2-antibody	9% PEG	-	?	?	(Murphy et al., 2001)
HEK293A or HEK293T cells	γTuNA[1]	-	Sucrose gradient	7 g	?	(Choi and Qi, 2014; Choi et al., 2010)
HEK293 cells	γTuNA[1] or NγBD[2]	-	Sucrose gradient	?	?	(Muroyama et al., 2016)
HeLa S3 (stable cells)	γ-tubulin-mycTAP	9% PEG	-	?	?	(Teixidó-Travesa et al., 2010)

[1]γTuNA is the N-terminal γTuRC-binding domain of CDK5Rap2 containing the evolutionary conserved CM1 domain (amino acids 51-100), [2]NγBD is the C-terminal γTuRC-binding domain of NEDD1 (amino acids 597-660)

2.2 Results

2.2.1 Purification of native γTuRC from human cells

2.2.1.1 Purification of native γTuRC via biotinylated γTuRC-binders

To purify γTuRC from human cells I designed a purification protocol essentially based on published methods (Choi and Qi, 2014; Choi et al., 2010; Liu et al., 2014a; Muroyama et al., 2016). γTuRC is purified by an affinity step exploiting the natural interaction of the complex with the γTuRC binding domain of an intracellular localization factor. After affinity purification the γTuRC binder is separated from the complex by sucrose gradient centrifugation which is possible due to their weak binding affinity.

Published protocols used fragments of two different γTuRC binders for purification: a short C-terminal fragment of NEDD1 (amino acids 597-660) and a short (amino acids 51-100) and a long (amino acids 51-200) fragment of CDK5Rap2. Both CDK5Rap2 fragments contain the conserved CM1-γTuRC binding domain (γTuNA).

From literature it is not clear if all γTuRC binders can purify a similar amount of γTuRC or if they have different affinities for the complex. Therefore, I first tested their γTuRC binding affinity in small scale. To this end, I cloned γTuNA$^{51-100}$, γTuNA$^{51-200}$ and the C-terminal half of NEDD1 (amino acids 364-660, ΔN-NEDD1) with an N-terminal AviTag. The aim of the thesis is to use the purified γTuRC in an *in vitro* microtubule nucleation assay. The AviTag on the γTuRC binders therefore has a dual function. AviTag is *in vivo* biotinylated and thus can be first used to affinity purify the γTuRC binders and second to immobilize them on glass surfaces used for the *in vitro* microtubule nucleation assay. Apart from the AviTag, all constructs also contain an N-terminal fluorescent maker, i.e. monomeric blue fluorescent protein (mBFP). The fluorescent maker will be used for visualization of the γTuRC binders in the fluorescence microscopy-based *in vitro* nucleation assay. From now on AviTag-mBFP-γTuRC binders will be referred to as Bio-γTuRC binders.

Bio-γTuNA51-100 and Bio-γTuNA51-200 were expressed and purified from E. coli, Bio-ΔN-NEDD1 was expressed and purified from insect cells. A scheme of the constructs and commassie stained protein gels of the purified proteins are shown in Figure 2.1. From 1 L of E. coli culture I was able to purify a total of 2 mg (1 mg/mL) Bio-γTuNA51-100 and 3 mg (1.5 mg/mL) Bio-γTuNA51-200. From 1 L of insect cell culture I could purify a total of 0.8 mg (0.4 mg/mL) Bio-△N-NEDD1.

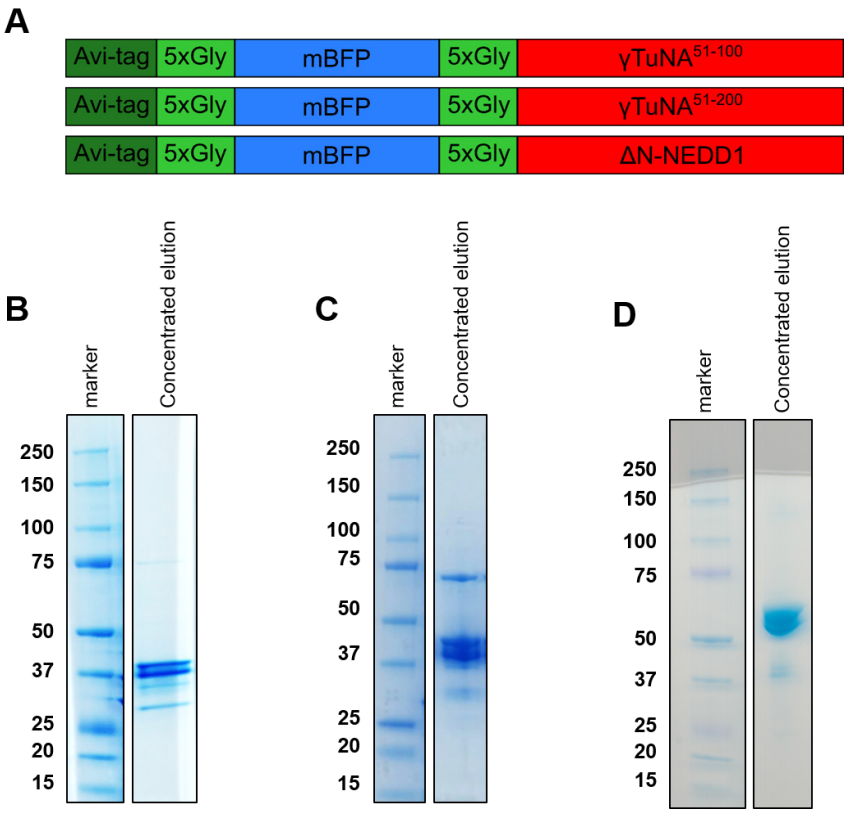

Figure 2.1: Purification of biotinylated γTuRC binders. (A) Constructs used for protein expression. Coomassie stained protein gels for purification of (B) Bio-γTuNA$^{51-100}$, (C) Bio-γTuNA$^{51-200}$ and (D) B-△N-NEDD1.

To compare the binding affinities of the different Bio-γTuRC binders, I tested them side-by-side in a small scale pull-down of native γTuRC from U2OS cells. Bio-γTuRC binders were bound to monomeric avidin agarose beads. Beads were incubated with cell lysate, washed to remove unspecific proteins and elution was performed using biotin. Western blots of eluates and beads after elution show that a substantial amount of γ-tubulin remains bound to the beads in all conditions (Figure 2.2 A). The bound γ-tubulin was also not eluted from the beads by a second elution step suggesting that the elution conditions might not be optimal. The first eluate for all Bio-γTuRC binders was analysed a second time by western blot for a more accurate comparison of binding efficiency between the different Bio-γTuRC binders. Band intensities were quantified using ImageJ and western blots show that Bio-γTuNA$^{51-200}$ binds around 55% more γ-tubulin than Bio-γTuNA$^{51-100}$ and around 62% more γ-tubulin than B-△N-NEDD1. The small scale pull-down was repeated once with the same result.

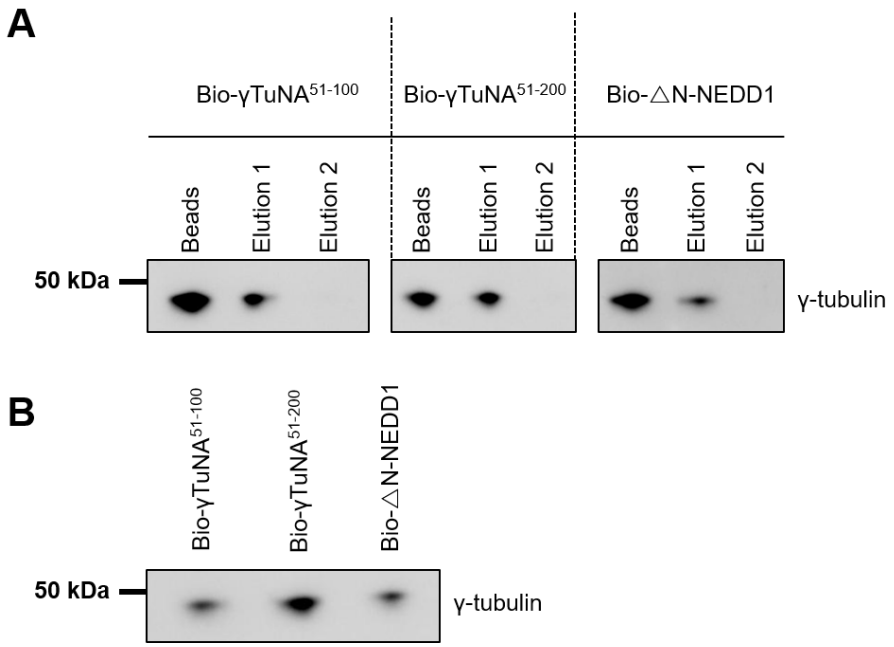

Figure 2.2: Comparison of different Bio-γTuRC-binders for purification of native γTuRC. (A) Western blots of elutates and monomeric avidin beads after elution detected with anti-γ-tubulin antibodies. (B) Comparison of γTuRC binding affinity for all tested Bio-γTuRC-binders. Elution 1 from (A) was loaded on a separate gel for comparison.

In the small scale pull-down, the highest amount of γ-tubulin was found in the eluate of Bio-γTuNA$^{51-200}$. It was previously shown that γTuNA$^{51-200}$ and NEDD1 do not bind to individual γTuRC subunits but only to the fully assembled γTuRC (Choi et al., 2010; Cota et al., 2017). Thus, western blot results suggest that γTuNA$^{51-200}$ binds a higher amount of γTuRC than the other two γTuRC-binders tested.

Next I tested Bio-γTuNA$^{51-200}$ in a large scale purification of native γTuRC from U2OS cell lysate. Purification steps are shown in Figure 2.3 A. Bio-γTuNA$^{51-200}$ was bound to monomeric avidin beads (Figure 2.3 B) and incubated with cell lysate, beads were washed and γTuRC bound to Bio-γTuNA$^{51-200}$ was eluted via biotin. Purification was followed by SDS-PAGE (protein gels) and western blot against γ-tubulin (Figure 2.3 C). Unexpectedly, Bio-γTuNA$^{51-200}$ failed to purify native γTuRC from human cell lysate at large scale. On protein gels no bands corresponding to γTuRC subunits can be detected. Analysis of the purification steps by western blot revealed that γ-tubulin did not bind to the column but instead was found in the flow through and completely removed in the first wash.

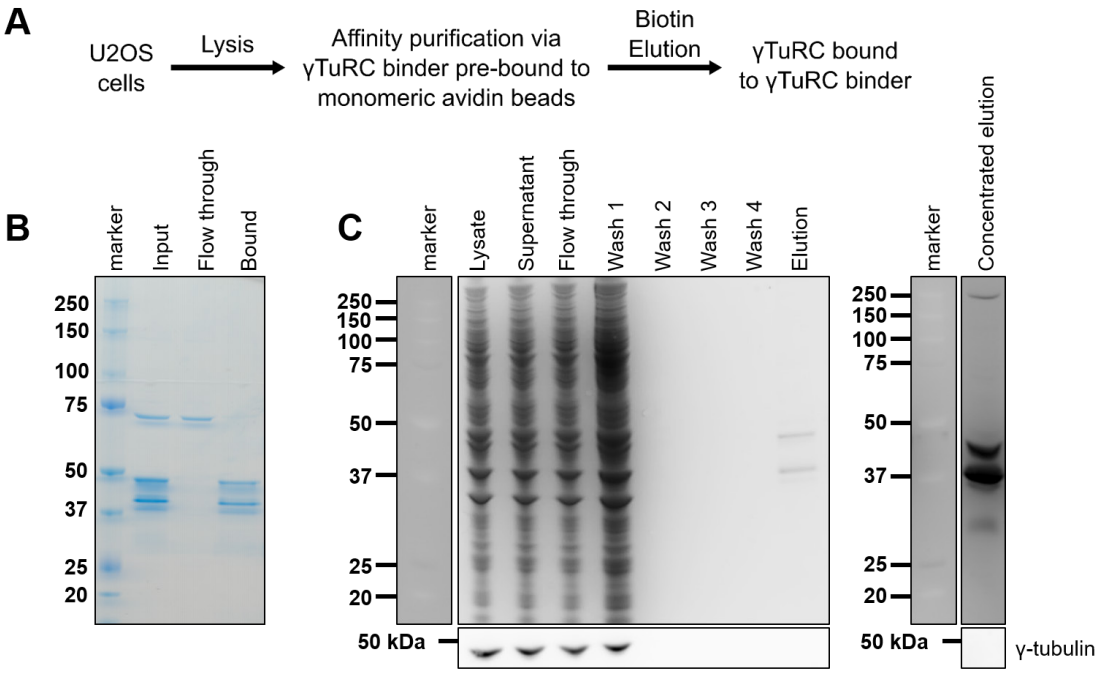

Figure 2.3: Large scale purification of γTuRC via Bio-γTuNA$^{51-200}$. (A) Purification steps (B) Coomassie gel of Bio-γTuNA$^{51-200}$ binding onto monomeric avidin beads. (C) Sypro ruby stained protein gels of purification steps and corresponding western blots detected with anti-γ-tubulin antibodies.

2.2.1.2 Optimization of lysis conditions

Bio-γTuNA$^{51-200}$ was able to pull-down native γTuRC at small scale but failed to do so at large scale. The main difference I found between the two conditions was the preparation of the cell lysate and the duration of the purification. Due to change in scale, the lysate was clarified at a different centrifugal force and the increase in volume also meant that the purification took significantly longer. γTuRC was previously reported to disassemble under certain conditions, such as high salt concentrations (Kollman et al., 2010; Lin et al., 2016; Oegema et al., 1999; Vogt et al., 2006). Therefore, I wondered if γTuRC might be unstable in the buffer conditions I chose or if centrifugation at high speed might sediment the complex together with the cell debris.

If γTuRC slowly disintegrates into γTuSCs, it could explain why Bio-γTuNA$^{51-200}$ failed to purify γTuRC at large scale as it only interacts with fully assembled complexes (Choi et al., 2010). Similarly, if γTuRC is lost from the sample because it sediments at high centrifugal force the remaining small complexes cannot be purified by Bio-γTuNA$^{51-200}$ affinity purification. Nevertheless, Bio-γTuNA$^{51-200}$ might also just be a weak interactor as it can reportedly be removed from the γTuRC by sucrose gradient centrifugation (Choi and Qi, 2014; Choi et al., 2010; Liu et al., 2014a; Muroyama et

al., 2016). Therefore, I next set out to optimize the lysis conditions. Table 4 summarizes the results of all experiments undertaken to optimize lysis conditions.

Table 4: Optimization of lysis conditions. Western blots for solubility tests are shown in Figure 2.4, western blots of size exclusion chromatography fractions in Figure 2.5.

Optimization	Buffer	Additives	Centrifugation	Result
Salt concentration and buffering agent	HEPES, pH 7.2 0.5% IGEPAL	150 mM KCl	278,088xg	No significant effect on GCP solubility or integrity of the γTuRC
		75 mM KCl	278,088xg	
	PIPES, pH 6.8 0.5% IGEPAL	150 mM KCl	278,088xg	
		75 mM KCl	278,088xg	
Variation of centrifugation speed and presence of detergent	HEPES, pH 7.2 150 mM KCl	±0.5% IGEPAL	278,088xg	Low speed centrifugation increases the γTuRC amount significantly. GCP6 solublity is lower in presence of IGEPAL
			17,000xg	
Enrichment of γTuRCs	HEPES, pH 7.2 150 mM KCl	±Ammonium sulfate	17,000xg	The γTuRC can be enriched in the lysate by ammonium sulfate precipitation.

Briefly, I first compared the solubility of γTuRC subunits in different lysis buffers and after clarification at different centrifugation speeds. Results were analysed by western blot against different γTuRC subunits, comparing the lysate and corresponding supernatant after centrifugation (Figure 2.4 A, C). Band intensities were quantified using ImageJ (Figure 2.4 B and D).

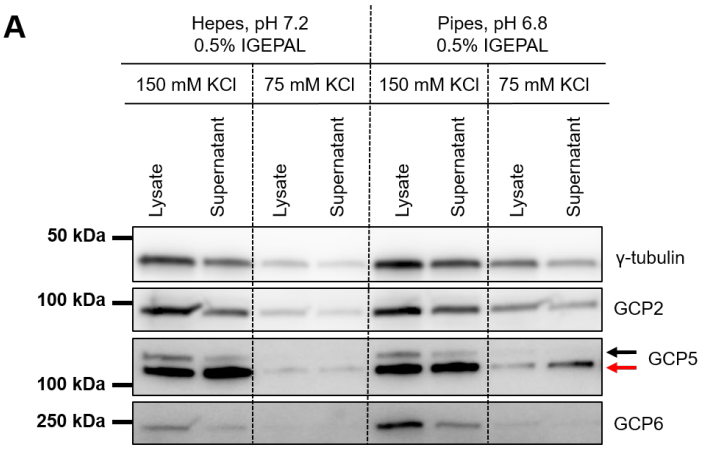

B

	Hepes, pH 7.2 0.5% IGEPAL			
	150 mM KCl		75 mM KCl	
	Lysate	Supernatant	Lysate	Supernatant
γ-tubulin	100	73	100	66
GCP2	100	65	100	67
GCP5	100	34	100	39
GCP6	100	46	100	35

	Pipes, pH 6.8 0.5% IGEPAL			
	150 mM KCl		75 mM KCl	
	Lysate	Supernatant	Lysate	Supernatant
γ-tubulin	100	81	100	63
GCP2	100	77	100	75
GCP5	100	32	100	16
GCP6	100	47	100	33

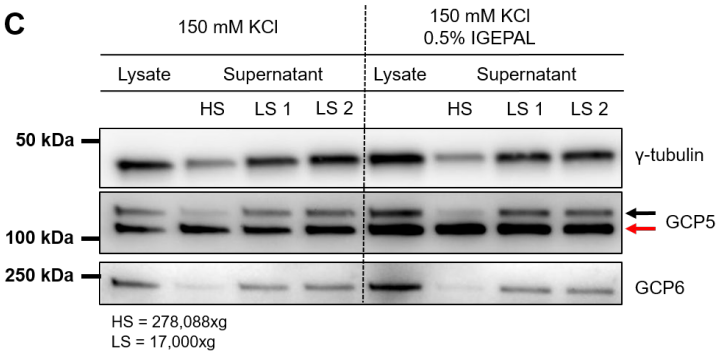

D

	150 mM KCl				150 mM KCl 0.5% IGEPAL			
	Lysate	Supernatant			Lysate	Supernatant		
		HS	LS1	LS2		HS	LS1	LS2
γ-tubulin	100	32	70	74	100	34	79	76
GCP5	100	27	67	63	100	19	61	57
GCP6	100	25	83	86	100	16	56	49

Figure 2.4: Comparison of different lysis conditions. (A, C) Western blot of U2OS cells before (lysate) and after spinning (supernatant) detected with antibodies against γTuRC subunits as indicated. (B, D) Quantification of band intensities normalized to corresponding lysate in percentage. Black arrow indicates GCP5, red arrow indicates unspecific protein detected by the anti-GCP5 antibody.

The solubility of γTuRC subunits was very similar in buffers of different salt concentration. However, GCP6 seems to be slightly more soluble in absence of the detergent IGEPAL. Centrifugation of U2OS cell lysates at high speed (large scale condition) decreased the amount of γTuRC subunits in the supernatant by ~72%. Low speed centrifugation (small scale condition) reduced the amount of γTuRC subunits only by ~26%. This result suggests that γTuRC sediments with cell debris at high centrifugation speeds. At low speed centrifugation less GCP6 was found in the supernatant in presence of IGEPAL (~20%) compared to buffer without IGEPAL (80%), suggesting that GCP6 is more soluble in the absence of the detergent.

The western blots of total protein in lysate and supernatant at different conditions do not inform about possible disintegration of the complex. Therefore, I next separated γTuRCs from γTuSCs using size exclusion chromatography and analysed the fractions by western blot (Figure 2.5). When lysates were centrifuged at high speeds a clear reduction of the amount of γTuRC was found in the corresponding size exclusion chromatography fractions (Figure 2.5 A-D versus Figure 2.5 E-F, γTuRC fractions are marked with a red square). This observation confirms that γTuRC sediments at high centrifugation speeds while γTuSC does so comparably less. Lowering the centrifugation speed therefore has a significant effect on the amount of γTuRC in the supernatant. Buffering agent and salt concentration showed little effect on γTuRC amount (Figure 2.5 A to D). The amount of GCP6 in buffer containing IGEPAL was lower in all fractions compared to lysate prepared in buffer without detergent (Figure 2.5 E-F). Interestingly, the size exclusion chromatography profiles for the other GCPs and γ-tubulin were not affected by the reduced amount of GCP6, suggesting that maybe not all of the soluble GCP6 is part of the complex or it can be replaced by other GCPs.

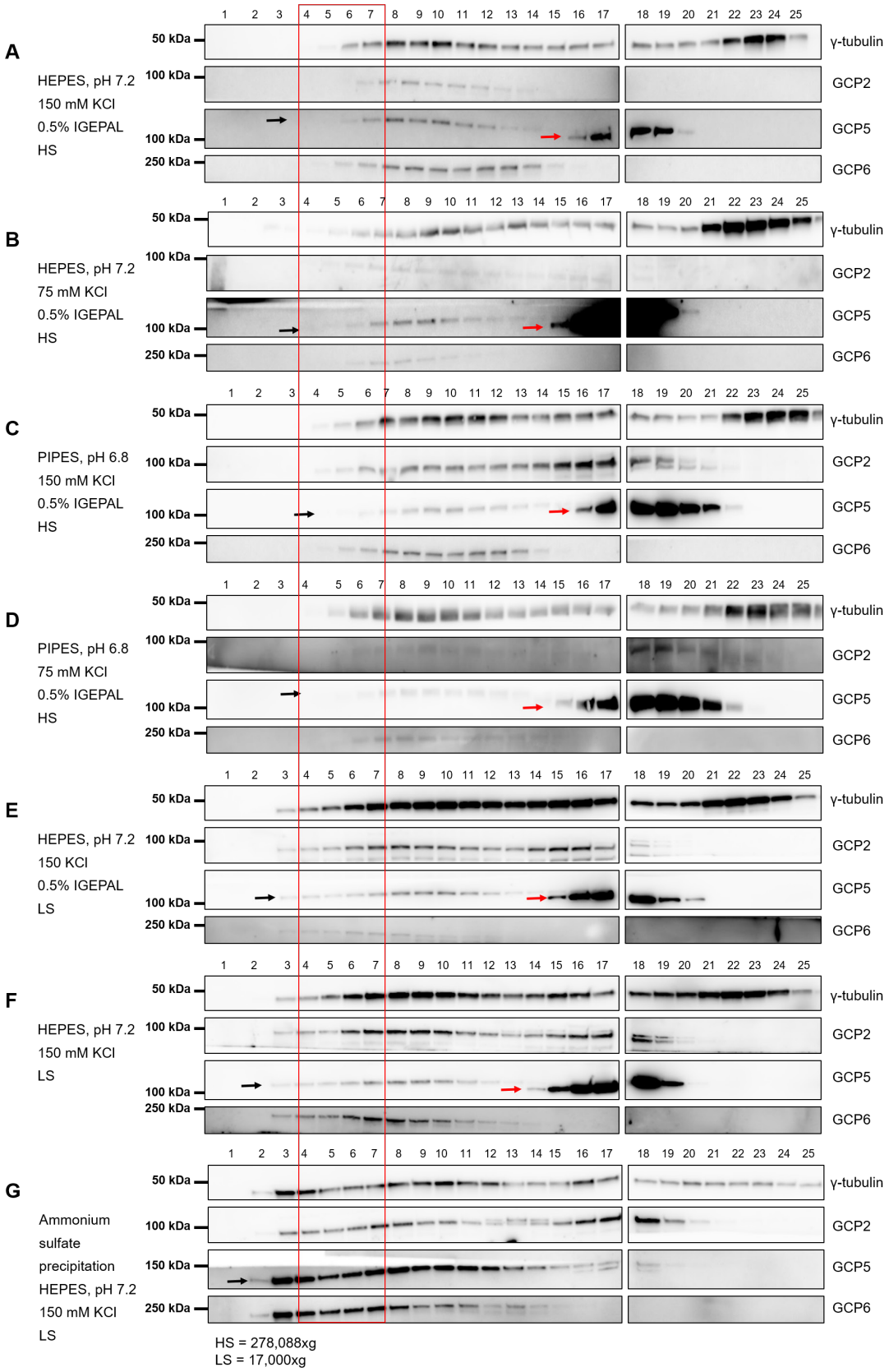

Figure 2.5: Size exclusion chromatography profiles of U2OS cell lysates. Western blots of size exclusion chromatography fractions (0.5 mL fraction size) for U2OS cell lysates prepared at the conditions indicated. The γTuRC peak fraction is marked in red. Western blots were detected with antibodies against the indicated γTuRC subunits. Black arrow indicates GCP5, red arrow indicates unspecific protein detected by the anti-GCP5 antibody.

As some protocols apply a precipitation step (ammonium sulphate or PEG precipitation, see Table 3) before the actual affinity purification, I also wanted to test if removal of unspecific proteins from the lysate before incubation with Bio-γTuNA$^{51-200}$ might help the interaction between the γTuRC-binder and the γTuRC. Therefore, I tested a previously described ammonium sulphate precipitation protocol to selectively precipitate the γTuRC from U2OS cell lysate (Zheng et al., 1998). This protocol involves two precipitation steps: i) the addition of a low amount of ammonium sulphate to remove unspecific proteins followed by ii) a second step at higher ammonium sulphate concentration to precipitate γTuRCs. An overview of the ammonium sulphate precipitation steps is shown in Figure 2.6 A. An exemplary ammonium sulphate precipitation of a 5 g U2OS cell pellet is shown in Figure 2.6 B.

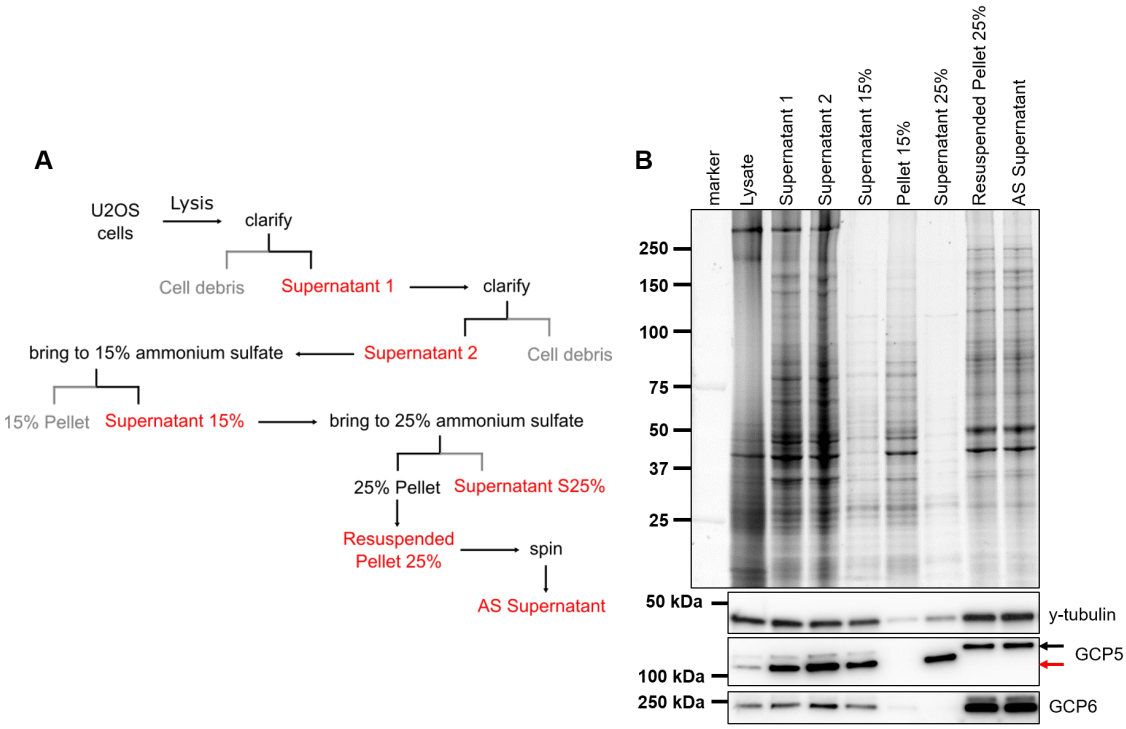

Figure 2.6: Ammonium sulphate precipitation of native γTuRCs from U2OS cells. (A) Overview of ammonium sulphate precipitation steps. (B) Sypro Ruby gel and corresponding western blots of all ammonium sulphate precipitation steps. Lysis buffer: 50 mM HEPES, pH 7.2, 150 mM KCl, 5 mM MgCl2, 1 mM EGTA, 1 mM DTT, 0.1 mM GTP.

Protein gels for all ammonium sulphate precipitation steps show a clear reduction of overall protein amount in the final sample compared to the crude lysate. Western blots show that γTuRCs largely remain in solution at low ammonium sulphate concentrations but precipitate in the second step, as reported previously (Zheng et al., 1998). Next, I analysed the integrity of the complex after ammonium sulphate precipitation by size exclusion chromatography and western blot. Ammonium sulphate precipitation increased the amount of γTuRCs (Figure 2.5 G, γTuRC

fractions are marked with a red square) and reduced the amount of γTuSCs and individual proteins, in particular γ-tubulin, from the sample.
Together, results show that the γTuRC is stable at all tested buffer conditions but partially removed from the lysate at high centrifugation speeds. The detergent IGEPAL is not required to solubilize the γTuRC during lysis but might actually have a negative effect on the solubility of individual GCPs, in particular GCP6. Selective precipitation of the γTuRC from cell lysates by ammonium sulphate precipitation removes unspecific proteins from the lysate without compromising the stability or yield of the γTuRC.

2.2.1.3 Optimization of γTuRC elution conditions

The affinity purification of γTuRC by Bio-γTuNA$^{51-200}$ relies on the binding of the biotinylated γTuRC-binder to monomeric avidin agarose beads followed by elution in biotin buffer. The small scale pull-down of γTuRC with different Bio-γTuRC-binders revealed that the amount of γ-tubulin remaining on the monomeric avidin beads after two rounds of elution is higher than in the eluate (see Figure 2.2 for western blots). With this low elution efficiency, the yield of the γTuRC purification will be substantially compromised. Therefore, I next tested if different elution conditions could improve the recovery of γTuRC. Table 5 summarizes the results of all experiments undertaken to optimize elution conditions.

Table 5: Optimization of elution conditions. Results are shown in Figure 2.7.

Optimization	Buffer	Beads	Result
Buffer condition	150 mM vs 250 mM KCl ± 0.5% IGEPAL	Monomeric avidin beads	Increase of salt and IGEPAL increase elution efficiency slightly
Bead material	250 mM KCl 0.5% IGEPAL	Agarose (porous) Polymethacrylate (porous) Magnetic (non-porous)	Bead material does not affect elution efficiency
Affinity purification tag	150 mM KCl	Glutathione beads	Change of N-terminal AviTag-mBFP to GST-AviTag greatly enhances elution efficiency

Briefly, I first tested different elution buffers in small scale pull-downs of γTuRC from U2OS cell lysate. Bio-γTuNA$^{51-200}$ was bound to monomeric avidin beads, beads were

incubated with cell lysates, washed to remove unspecific proteins, followed by elution via biotin. Eluate and beads after elution were analyzed by western blot (Figure 2.7 A) and band intensities were quantified using ImageJ (Figure 2.7 C). For all tested conditions, the amount of γ-tubulin remaining on the beads after biotin elution was substantial. Increasing the salt or detergent concentration in the elution buffer only had a mild effect on elution efficiency whereas increasing both simultaneously improved the elution efficiency from 2% to about half of γ-tubulin (~57%).

Since increasing the stringency of the elution buffer helped to release γ-tubulin from monomeric avidin beads I wondered if γTuRC and Bio-γTuNA$^{51-200}$ interact unspecifically with the purification matrix. The beads I used so far are porous monomeric avidin beads made of the organic polymer agarose. If the binding is unspecific due to the bead material, changing the beads might help to improve the elution efficiency. Therefore, I next compared the γTuRC elution efficiency from three types of monomeric avidin beads: i) the porous agarose beads used for previous experiments, ii) porous polymethacrylate beads (SoftLink) and iii) non-porous magnetic beads (BcMag). For this experiment, elution was performed using the improved elution buffer (high salt and detergent) supplemented with biotin.

Western blots show that monomeric avidin agarose beads have a higher binding capacity compared to the other two bead types. They bound significantly more Bio-γTuNA$^{51-200}$ (results not shown) and in turn more of the γTuRC subunits (Figure 2.7 B). I then compared for each type of bead the amount of γTuRC subunits remaining bound after elution with the amount found in the corresponding eluate. I found that the elution efficiency for all beads was the same. About half of γ-tubulin (on average ~45%) and 4-10% of GCP5/6 was eluted for all bead types (Figure 2.7 D).

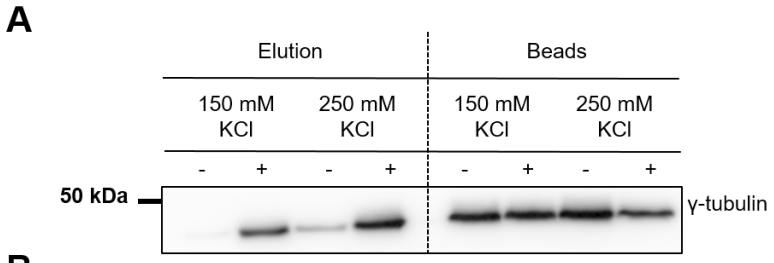

B

	Elution				Beads			
	150 mM KCl		250 mM KCl		150 mM KCl		250 mM KCl	
	-	+	-	+	-	+	-	+
γ-tubulin	2	39	14	57	98	61	86	43

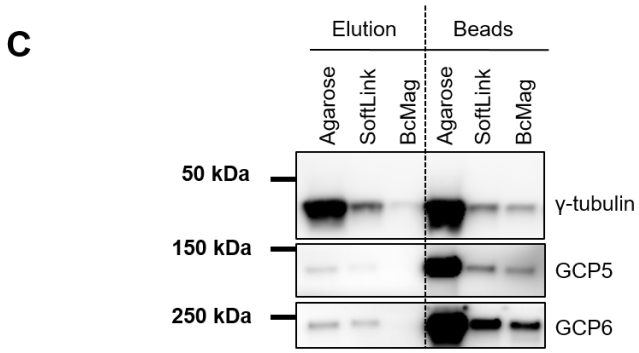

D

	Elution			Beads		
	Agarose	SoftLink	BcMag	Agarose	SoftLink	BcMag
γ-tubulin	44	41	50	56	59	50
GCP5	6	9	-	94	91	-
GCP6	4	4	-	96	96	-

Figure 2.7: Optimization of γTuRC elution conditions. Western blots of (A) elution from monomeric avidin beads at different buffer conditions and (C) elution from porous monomeric avidin beads (agarose) and SoftLink Soft Release resin (polymethacrylate) and non-porous BcMag monomeric avidin magnetic beads (magnetic). Bio-γTuNA$^{51-200}$ was used as γTuRC binder. Western blots were detected with antibodies against the indicated γTuRC subunits. Quantification of band intensities normalized to the sum of the combined signal of the eluate and beads after elution expressed in percentage.

To test if elution efficiency of γTuRC can be improved if a different type of affinity purification matrix is used, I next changed the N-terminal AviTag-mBFP affinity tag on γTuNA$^{51-200}$ to a GST-AviTag. GST-AviTag-γTuNA$^{51-200}$ was expressed and purified from *E. coli*. The construct and a coomassie stained protein gel of the purified protein are shown in Figure 2.8 A and B. From 1 L of *E. coli* culture I was able to purify a total of 1.5 mg (1.6 mg/mL) GST-AviTag-γTuNA$^{51-200}$ (GST-γTuNA$^{51-200}$).

I then repeated the small-scale pull down. GST-AviTag-γTuNA$^{51-200}$ was bound to glutathione agarose beads, beads were incubated with U2OS cell lysate, washed to

remove unspecific proteins and elution was performed using reduced glutathione (see Figure 2.8 C for western blots). The new affinity purification tag increased the elution efficiency for all γTuRC subunits substantially. 85% of γ-tubulin and all of GCP5/6 eluted from the beads at low salt buffer and in absence of detergent (Figure 2.8 D).

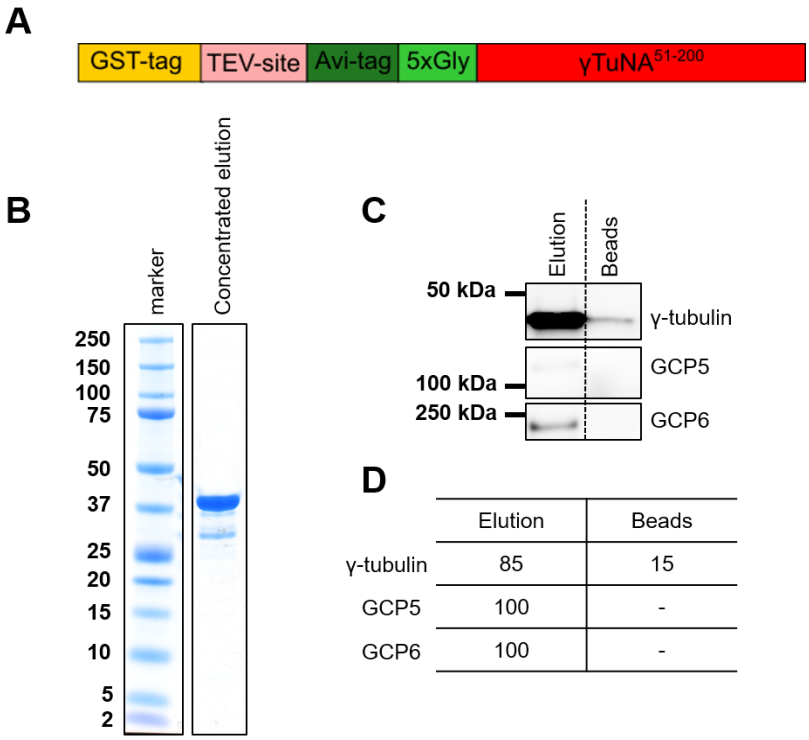

Figure 2.8: Pull-down of γTuRCs via GST-AviTag-γTuNA$^{51-200}$. (A) Construct used for expression of GST-AviTag-γTuNA$^{51-200}$. (B) Coomassie stained protein gel of purified GST-AviTag-γTuNA$^{51-200}$. (C) Western blots of eluates from glutathione beads containing prebound GST-γTuNA$^{51-200}$. Western blots were detected with antibodies against the indicated γTuRC subunits. (D) Quantification of band intensities normalized to the sum of the combined signal of the eluate and beads after elution expressed in percentage.

2.2.1.4 Large scale purification of native γTuRC via GST-γTuNA$^{51-200}$

As lysis and elution conditions have now been optimized, I next repeated the large scale purification of γTuRC by γTuRC-binders with appropriate modifications. Purification steps are summarized in Figure 2.9. Briefly, cells are lysed and ammonium sulphate precipitated. Then the lysate is incubated with glutathione beads containing prebound GST-AviTag-γTuNA$^{51-200}$ (from here on GST-γTuNA$^{51-200}$) to affinity purify γTuRC. Beads are washed and γTuRC bound to GST-γTuNA$^{51-200}$ is eluted using reduced gluthatione. Eluate is concentrated and separated by size exclusion chromatography to remove unspecific proteins and separate γTuRC from the γTuRC binder and γTuSC.

The binding of GST-γTuNA$^{51-200}$ to glutathione beads was confirmed using protein gels and is shown in Figure 2.10 A. Purification of γTuRC was followed by protein gels (Figure 2.10 B) and western blot (Figure 2.10 C). This time I was able to detect all γTuRC subunits in the eluate and concentrated eluate by western blot. The amount of γTuRC subunits remaining on the beads was very low after several consecutive elution steps indicating good elution efficiency from glutathione beads. However, a surprisingly high amount of γTuRC subunits were found to not bind to GST-γTuNA$^{51-200}$ in the affinity purification step as judged by comparing the input and flow through by western blot.

On protein gels apart from the prominent band most likely representing GST-γTuNA$^{51-200}$ (47 kDa, black arrow) I could also detect protein bands at around 50 kDa and 100 kDa (red arrows) which might correspond to γ-tubulin (50 kDa) and GCP2/3 (102 kDa/103 kDa).

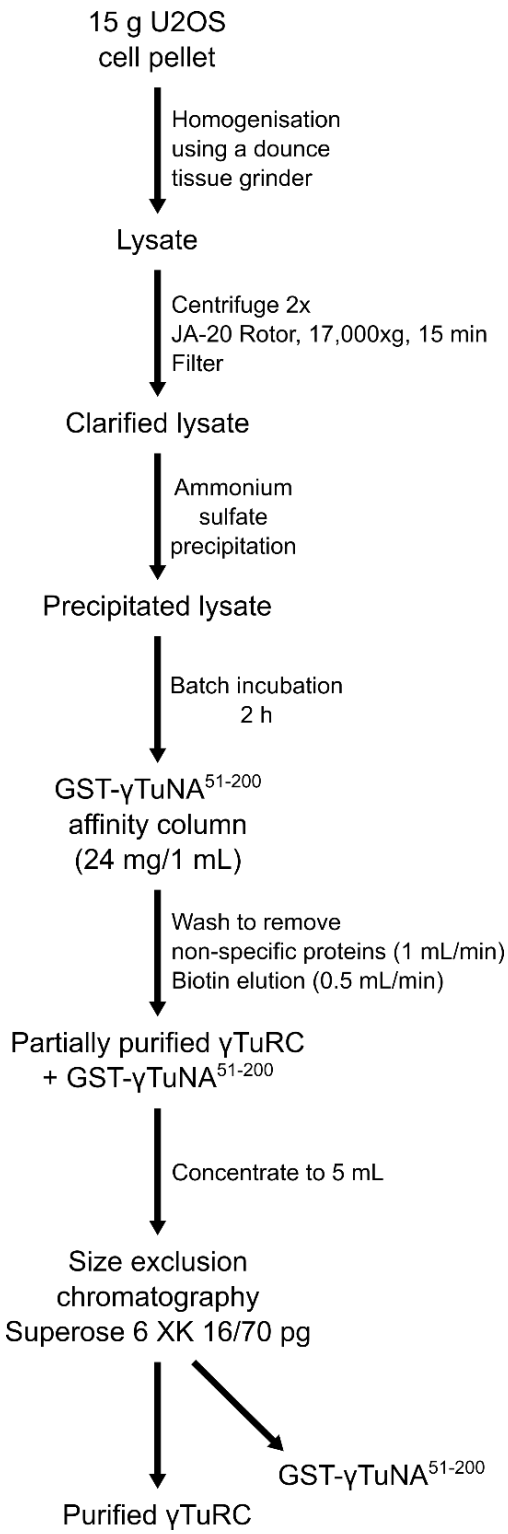

Figure 2.9: Overview of large scale purification of native γTuRCs via GST-γTuNA$^{51-200}$.

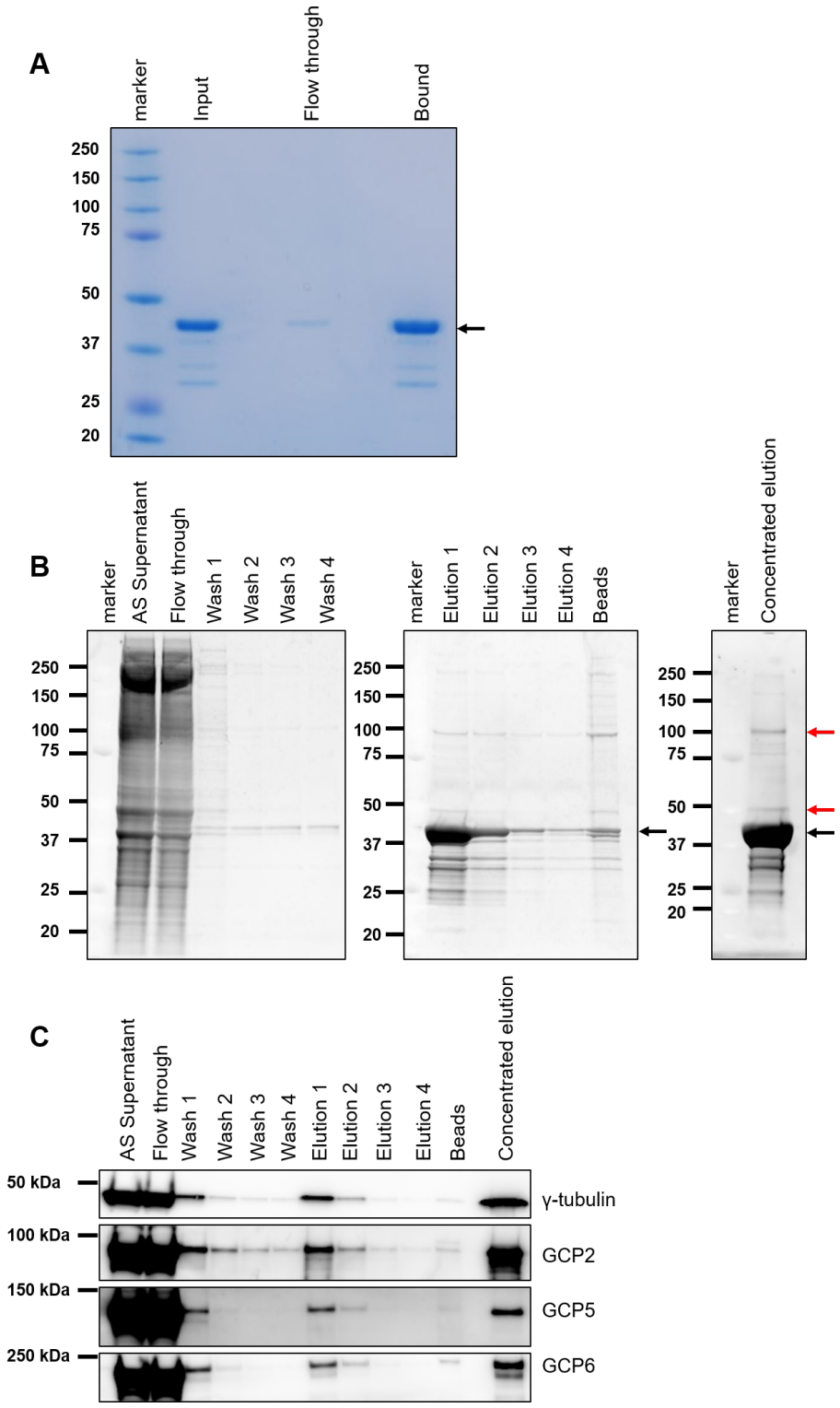

Figure 2.10: Affinity purification of native γTuRCs via GST-γTuNA$^{51-200}$. (A) Coomassie stained protein gel showing binding of GST-γTuNA$^{51-200}$ to glutathione beads. (B) Sypro Ruby stained protein gels for purification steps and (C) corresponding western blots detected with antibodies against γTuRC subunits as indicated. GST-γTuNA$^{51-200}$ is marked with a black arrow, γ-tubulin (50 kDa) and GCP2/3 (102 kDa/103 kDa) are marked with red arrows.

The concentrated partially purified γTuRC was subjected to size exclusion chromatography. The size exclusion chromatography profile is shown in Figure 2.11 A. γTuRC due to its large size (~2.1-megadalton) is expected to elute close to the void of the column. Western blots (Figure 2.11 C) show that γTuRC subunits are present in all fractions with the highest amount eluting at higher column volumes. This suggests that most of γTuRC in the elution is present as γTuSC or individual proteins instead of fully assembled complex. I expected GST-γTuNA$^{51-200}$ to elute towards the end of the column due to its small size (47 kDa). However, on protein gels (Figure 2.11 B) GST-γTuNA$^{51-200}$ can be detected in all fractions of the column. This suggests that unlike for sucrose gradient centrifugation, size exclusion chromatography might not be able to separate γTuRC from GST-γTuNA$^{51-200}$ and could indicate that it also binds to smaller subcomplexes which is in contrast to earlier reports (Choi and Qi, 2014; Choi et al., 2010; Cota et al., 2017; Liu et al., 2014a; Muroyama et al., 2016). On the other hand, GST-γTuNA$^{51-200}$ could also interact with another protein present in the lysate or form oligomers of higher molecular weight. No protein bands for γTuRC subunits could be detected by protein gel. Nevertheless, I concentrated the first peak close to the void of the column (Figure 2.11 B and C, red square) including the fractions with low signal by western blot but containing GST-γTuNA$^{51-200}$ according to protein gels.

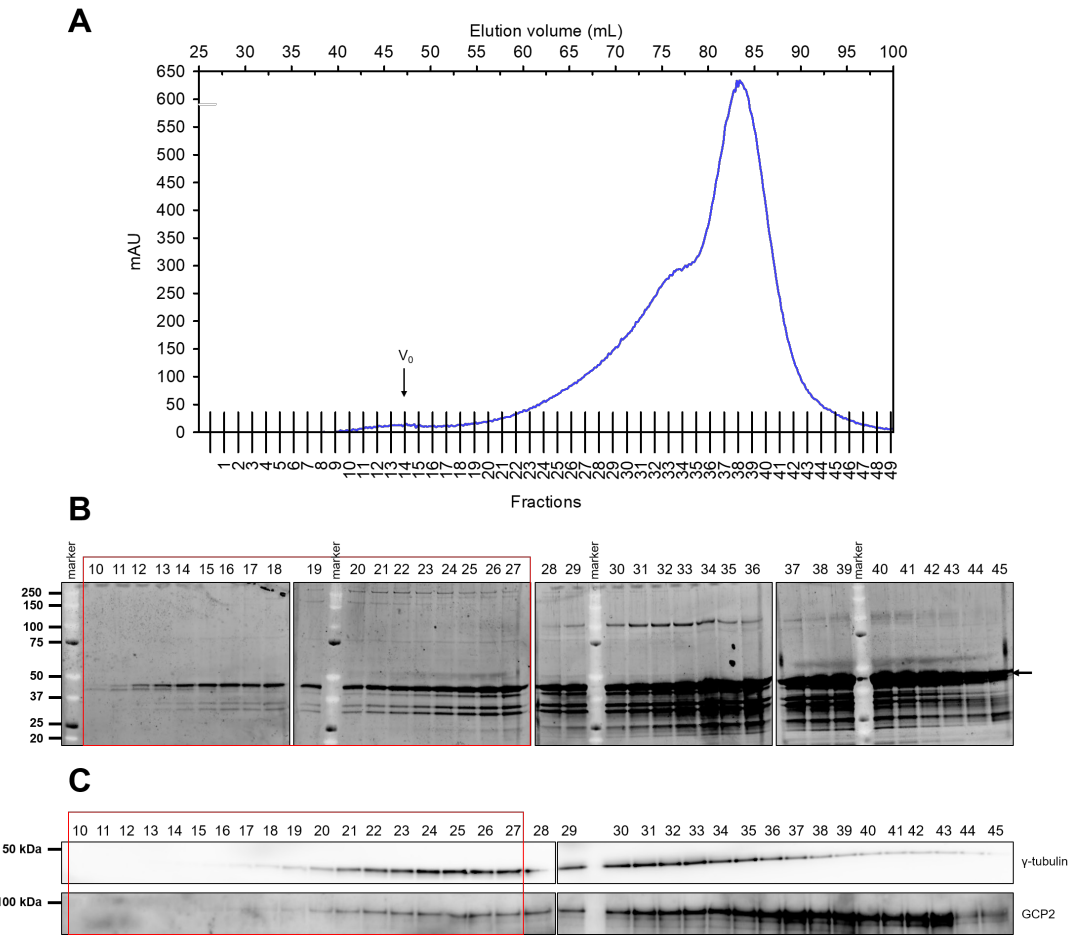

Figure 2.11: Size exclusion chromatography of native γTuRCs purified via GST-γTuNA$^{51-200}$. (A) Size exclusion chromatography profile showing the elution profile of total protein (blue line) from a Superose 6 XK 16/70 pg column. The void volume (V_0) of the column is indicated. (B) Sypro ruby gels of fractions and (C) corresponding western blots detected with antibodies against γ-tubulin and GCP2. Fraction size was 1.5 mL. Fractions that were pooled and concentrated are marked with a red square. GST-γTuNA$^{51-200}$ is marked with a black arrow.

The fractions as indicated in Figure 2.11 C (red square) were pooled and concentrated. γTuRC subunits were readily detected by western blot (Figure 2.12 B). However, apart from one prominent band, probably corresponding to GST-γTuNA$^{51-200}$, no other protein bands were detectable on protein gels (Figure 2.12 A). The protein gel used for this analysis was stained with commercial Sypro Ruby dye. This dye is very sensitive and can detect proteins at concentrations as low as 1 ng according to the manufacturer. Therefore, this result indicates a very low yield of γTuRC using the above described method for affinity purification of the complex.

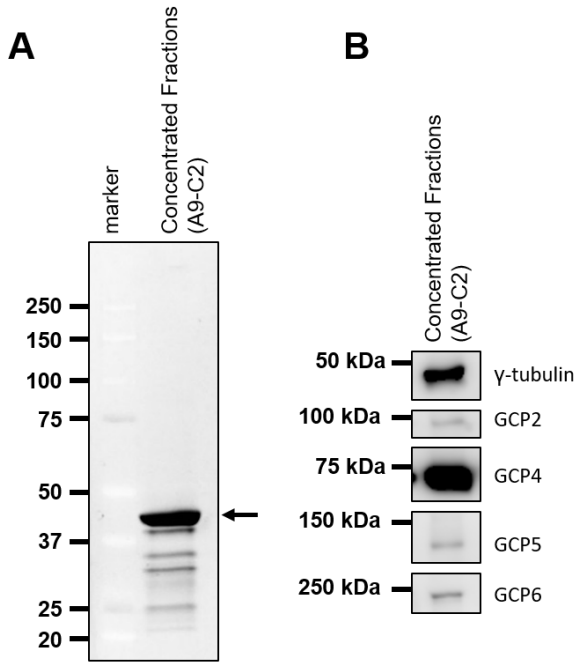

Figure 2.12: Analysis of native γTuRCs purified from U2OS cells via GST-γTuNA$^{51-200}$. (A) Sypro Ruby stained protein gel and (B) corresponding western blot detected with antibodies against γTuRC subunits as indicated.

The low yield found for γTuRC purification using this method can probably be explained by the weak binding affinity of γTuRC to GST-γTuNA$^{51-200}$. To improve the binding, I tested different conditions, i) incubating the lysate with soluble GST-γTuNA$^{51-200}$ in case pre-binding sterically hinders the interaction between γTuRC and the γTuRC-binder, ii) lowering salt concentration to reduce the stringency of the buffer during incubation, iii) leaving the lysate in contact with the beads for a longer time (2 h versus 16 hours) and iv) increasing the amount of GST-γTuNA$^{51-200}$ (results not shown). None of the above strategies was able to substantially improve the yield of the purification.

In summary, γTuNA$^{51-200}$ was able to affinity purify native γTuRC from U2OS cell lysates in amounts which were only detectable by western blot. In my opinion, the yield was too low to test the complex in *in vitro* nucleation assays for two reasons which are both crucial for reproducibility in the assay: i) it is difficult to accurately estimate protein concentration from western blots and ii) without being able to see the γTuRC and potential contaminants at least on protein gels stained with Sypro Ruby I cannot know the purity of each batch of purified γTuRC.

Nevertheless, the information collected from the optimization of lysis and elution conditions is very useful and can in principal be applied to other γTuRC purification protocols. Briefly, high speed centrifugation of the cell lysate sediments the γTuRC with the cell debris and thus decreases the amount of available complex for

purification significantly. γTuRC is soluble and does not disassemble in different buffer conditions, e.g. buffering agent, salt concentration and pH value. Lysis buffer supplemented with the detergent IGEPAL seems to have a negative effect on the solubility of GCP6 but does not stongly affect the integrity of the complex. For unknown reasons, γTuRC eluted worse from monomeric avidin beads compared to glutathione beads. Both γTuRC-binders elute efficiently from their corresponding affinity purification beads, suggesting that γTuRC might interact in an unspecific manner with monomeric avidin beads. With this in mind, I focused on the second strategy of γTuRC purification, i.e. the purification of fluorescently tagged γTuRC from stable cell lines, described below.

2.2.2 Purification of tagged γTuRC

2.2.2.1 Development of stable cell lines expressing tagged GCPs

The second approach for γTuRC purification involves the affinity isolation of tagged γTuRC from stable human cell lines. The γTuRC subunits will be tagged with an affinity purification tag (AviTag) and a fluorescent marker (mBFP). The advantage of this strategy is that γTuRC can be purified by affinity purification without relying on antibodies or γTuRC-binders. Additionally, the fluorescent labelling of the complex will allow me to visualize γTuRC directly in the fluorescence microscopy-based nucleation assays.

The first step was the development of stable HeLa Kyoto (HeLa-K) cell lines expressing tagged γTuRC subunits and to do this I worked together with Jayant Asthana and Wei Ming Lim (both Surrey group, The Francis Crick Institute).

I first designed constructs to tag two different γTuRC subunits, GCP2 and GCP4, with AviTag-mBFP. They were chosen based on published estimations of the subunit stoichiometry of γTuRC (Choi et al., 2010; Murphy et al., 2001; Zheng et al., 1995). Based on those quantifications, GCP2 is assumed to represents a major subunit of the γTuRC with around 6 copies per complex. Tagging of a high copy number subunit could increase the possibility of having at least one tagged GCP in the complex. There is the possibility that too many tagged subunits might disrupt complex formation. Therefore, apart from GCP2, I decided to tag GCP4, which is assumed to be a low copy number subunit (~2-3 molecules per complex).

Given the structural data available on budding yeast γTuRC the N-terminus of all GCPs should be located at the base of the complex while the C-terminus is close to the interphase between GCPs and γ-tubulin (Kollman et al., 2011). Therefore, tagging

of the N-terminus might be preferable, as it is located further away from the γ-tubulin binding site of the GCPs. A recent publication identified the N-terminus to be a key site for protein-protein interactions and binding of regulatory proteins (Farache et al., 2016). Thus, tagging of the N-terminus potentially interferes with the regulation of γTuRC by γTuRC binders. As a decision could not be taken at this point, I decided to initially prepare constructs for N- and C-terminal tagging of both proteins with AviTag-mBFP.

Constructs are shown in Figure 2.13. For *in vivo* biotinylation of the AviTag, a construct of the *E. coli* biotin ligase BirA was prepared. BirA was tagged with an N-terminal human influenza hemagglutinin (HA) tag for screening purposes.

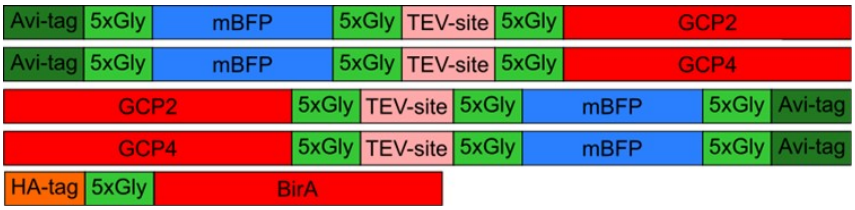

Figure 2.13: Constructs used to express tagged GCP2 and GCP4 in HeLa-K cells. As AviTag is biotinylated *in vivo* by *E. coli* biotin ligase BirA, cells were co-transducted with HA-tagged BirA.

Plasmids were cloned by Wei Ming Lim and HeLa-K cell lines was developed by Wei Ming Lim and Jayant Asthana (Cell culture, high throughput screen, fluorescence microscopy screen; both Surrey group, The Francis Crick Institute). Screening of HeLa-K cell lines by western blot was performed by myself together with Wei Ming Lim. Selection of the cell line is described in material and methods. Briefly, N-terminally tagged GCP2 did not express at sufficiently high amounts and cell lines were discarded. C-terminally tagged GCP2 expressed and two clones were selected for further analysis (Figure 2.14 A). N- and C-terminally tagged GCP4 was expressed but the biotinylation level varied among the different clones (Figure 2.14 C). Biotinylation was undetectable for all N-terminally tagged clones and cell lines were discarded. Two C-terminally tagged clones were chosen for further analysis.

A second western blot screen was conducted to choose the final cell lines for γTuRC purification. In this screen we compared the expression levels of GCP2/4 and BirA and the level of biotinylation for the selected clones. GCP2 was expressed and biotinylated similarly in both clones. I chose clone C15 as it co-expressed less BirA without affecting the level of biotinylation (Figure 2.14 B). Generally, the biotinylation for C-terminally tagged GCP4 (Figure 2.14 D) was lower compared to GCP2 and

difficult to detect by western blot. Nevertheless, I chose clone C18 as it expressed more GCP4, showed a higher level of biotinylation and co-expressed less BirA.

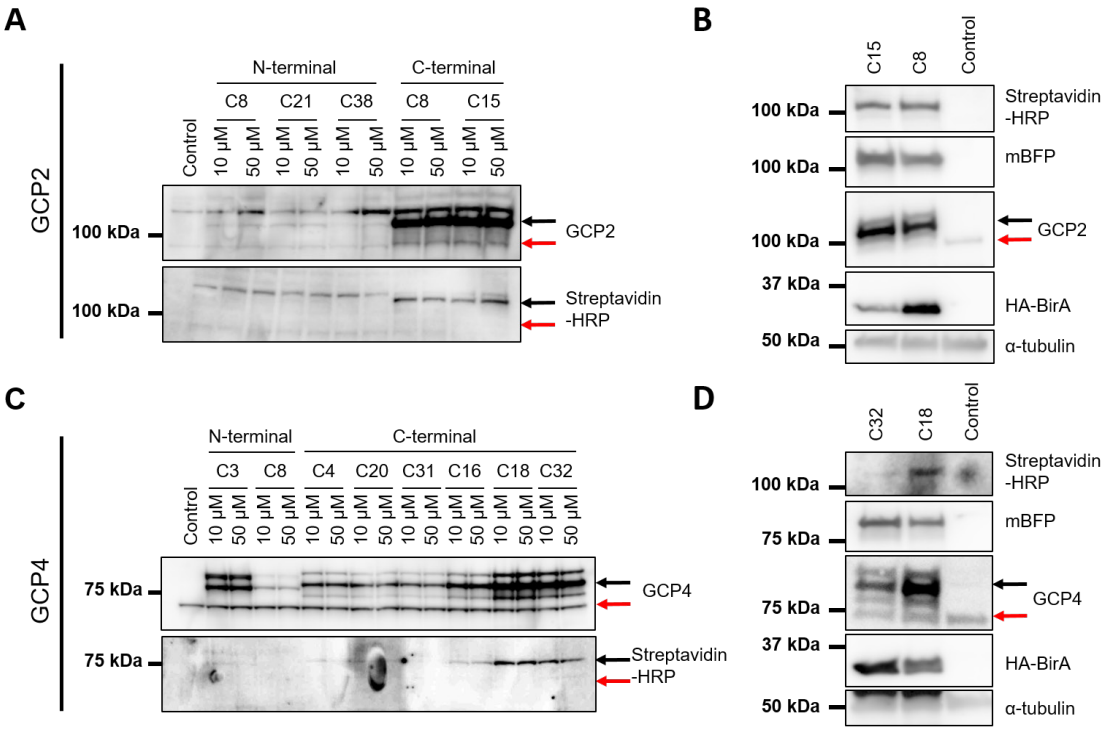

Figure 2.14: Western blot screen of tagged GCP2 and GCP4 expression in HeLa-K cells. First western blot screen for *in vivo* biotinylation of N- or C-terminal AviTag-mBFP tagged (A) GCP2 and (C) GCP4. Second western blot screen for selected C-terminally tagged clones for GCP2 (B) and GCP4 (D). α-tubulin was used as loading control. Tagged protein is highlighted with a black arrow, native protein with a red arrow.

I then verified that tagged proteins are integrated into fully assembled γTuRCs by size exclusion chromatography followed by analysis of the fractions by Western blots against different γTuRC subunits (Figure 2.15 A and B). I found that tagged proteins (black arrow) co-migrate with native γTuRC subunits in all fractions strongly suggesting that they are part of γTuRC. For both cell lines I could also detect native GCP2 and GCP4 (red arrow) in the γTuRC peak fractions (red square), indicating that tagged proteins (black arrow) do not completely replace their native counterpart in the complex or cells contain a mixture of fluorescently-tagged and untagged γTuRCs.

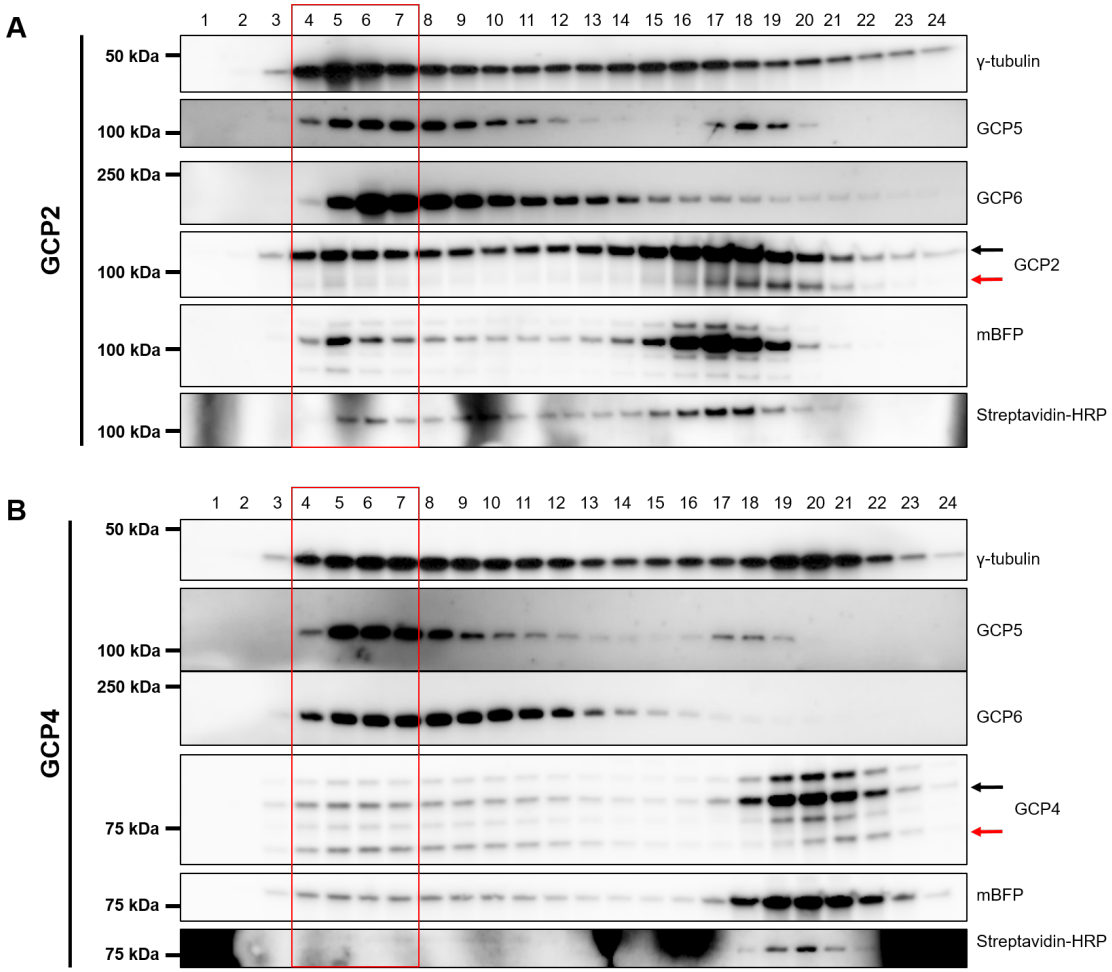

Figure 2.15: Size exclusion chromatography profiles of tagged HeLa-K cell lines. Western blots for size exclusion chromatography fractions for (A) GCP2-mBFP-AviTag and (B) GCP4-mBFP-AviTag cell lines. GCP2-mBFP-Avitag is highlighted with a black arrow, native GCP2 with a red arrow. Western blots were detected with antibodies against γTuRC subunits as indicated.

Finally, we analysed the subcellular localization of tagged proteins by fluorescence microscopy (Figure 2.16). GCP2 shows the expected centrosomal localization for γTuRC in interphase cells (Cota et al., 2017; Farache et al., 2016). For GCP4 we found a mixture of cells with normal localization and cells containing several bright fluorescence spots in the cytoplasm indicating aggregation or wrong localization of tagged γTuRCs in those cells. Therefore, the cell line expressing C-terminally tagged GCP4 was discarded.

The final selected cell line, i.e. HeLa-K stably expressing GCP2 with a C-terminal AviTag-mBFP (clone C15), was used for all further experiments. The fluorescently tagged GCP-mBFP-AviTag-γTuRC will be referred to as γTuRC in the next chapters.

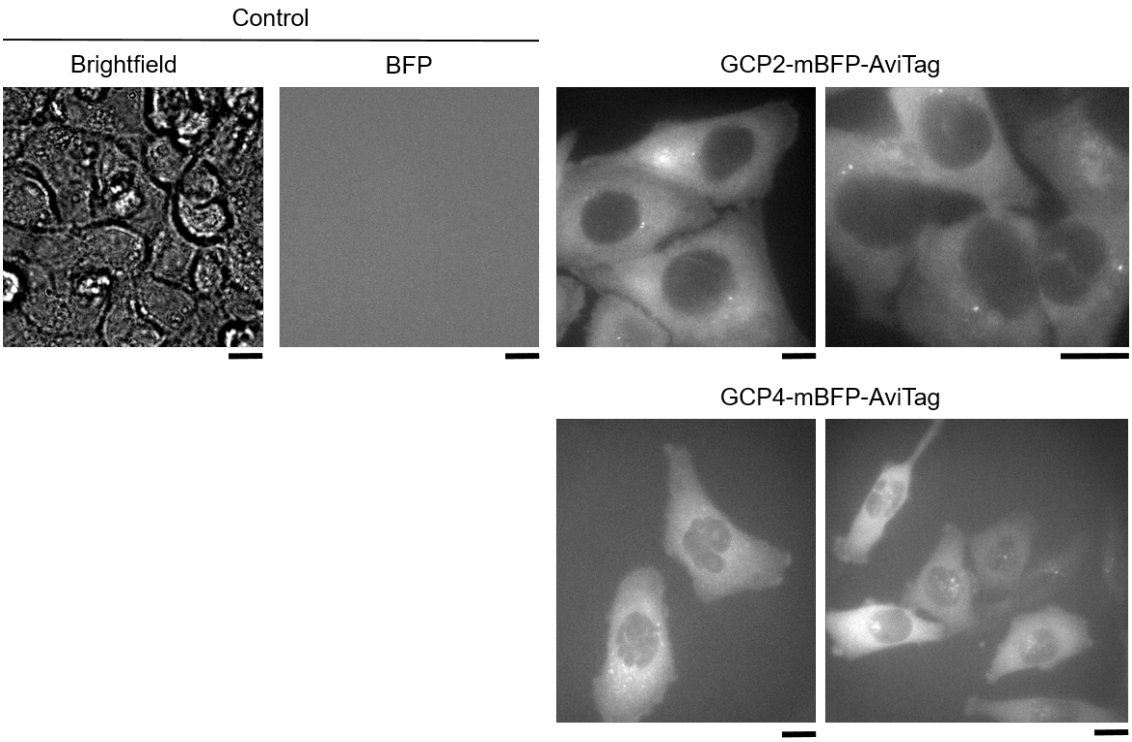

Figure 2.16: Microscopy images of mBFP fluorescence in interphase HeLa-K cells. Cells express either GCP2-mBFP-AviTag (clone C15) or GCP4-mBFP-AviTag (clone C18). Control shows brightfield image of cells and corresponding mBFP fluorescence channel. Scale bar = 10 µm.

2.2.2.2 Optimization of the purification of tagged γTuRC

The purification conditions for the first attempt to purify tagged γTuRC from the stable HeLa-K cell line was based on the purification protocol of native γTuRC from human cells as this protocol was previously optimized (see section 2.2.1). I therefore used the following purification steps: ammonium sulphate precipitation of the lysate, affinity purification via GCP2-mBFP-AviTag using monomeric avidin agarose beads, elution from the beads via biotin using the optimized elution buffer followed by size exclusion chromatography to separate γTuSCs from γTuRCs. Purification steps are shown in Figure 2.17 A. This time, western blots (Figure 2.17 C) showed a clear reduction in the amount of γTuRC subunits in the flow through of the monomeric avidin beads. As the affinity purification tag is on the GCP2, this result indicates that GCP2 is part of fully assembled γTuRCs. Western blots also show that γTuRC subunits are enriched in the eluate and concentrated eluate after the affinity purification and protein bands corresponding to γTuRC subunits by molecular weight can be detected on the Sypro Ruby stained protein gel (Figure 2.17 B). However, the concentrated eluate appeared as a smear on the protein gel and could not be loaded onto the size exclusion

chromatography column. This is probably due to the high concentration of IGEPAL needed to elute the γTuRC from monomeric avidin beads.

Therefore, I changed the purification protocol as follows: the high concentration of IGEPAL (0.5%) was replaced by a low concentration of Brij-35 (0.02%) as it eluted γTuRC subunits similarly well from monomeric avidin beads in a small scale pull down (results for the detergent screening are not shown). I replaced the ammonium sulphate precipitation step by a cation exchange column to which the γTuRC does not bind (Figure 2.17 D). This step helps to remove unspecific proteins from the highly concentrated lysate before loading the lysate on the affinity purification column without the need to precipitate the γTuRC from the lysate using ammonium sulphate. Lastly I changed the monomeric avidin beads to streptavidin mutein beads (Figure 2.17 E). As found for the purification of native γTuRC via γTuRC-binders (chapter 2 section 2.2.1), tagged γTuRC also eluted incompletely from monomeric avidin beads and required large elution volumes. Elution from streptavidin mutein beads was found to be complete and the elution volume was 15-fold lower, which in turn reduces the time for subsequent steps in the purification, e.g. concentration of the sample for size exclusion chromatography.

The final method to affinity purify the tagged γTuRC from a stable HeLa-K cell line is summarized in Figure 2.18. In the next chapter I will describe the final purification procedure for the tagged γTuRC from human cells in more detail.

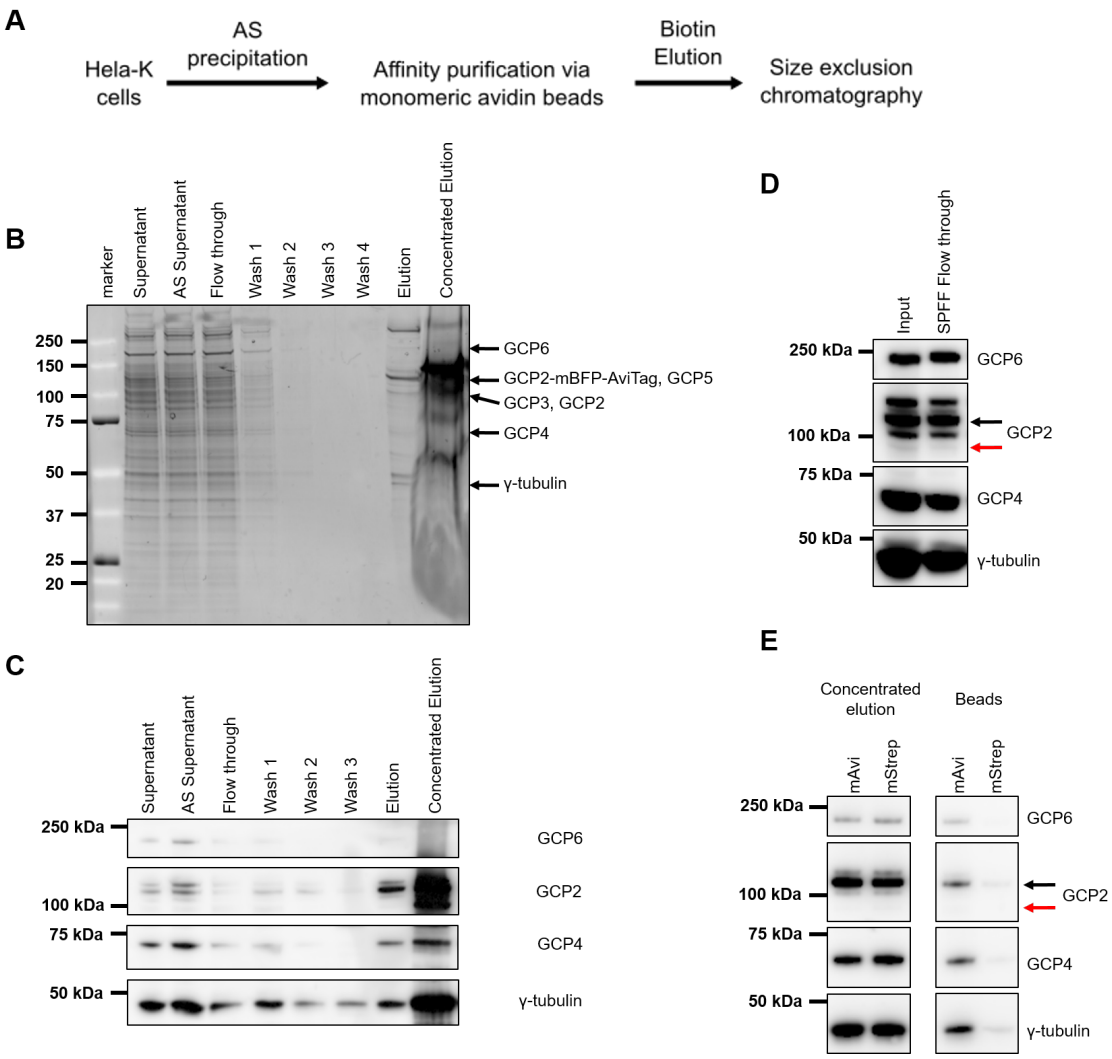

Figure 2.17: Optimization of the purification of GCP2-mBFP-AviTag-γTuRCs. (A) Overview of purification steps. (B) Sypro Ruby stained protein gel of γTuRC purification using 0.5% IGEPAL and 250 mM KCl in the elution buffer. (C) Western blots corresponding to the protein gel shown in B. (D) Representative western blot of input and flow through of lysate flown over a SP FF cation exchange column. (E) Comparison of the elution efficiency from monomeric avidin beads and streptavidin mutein matrix beads. Western blots were detected with antibodies against γTuRC subunits as indicated. GCP2-mBFP-Avitag is highlighted with a black arrow, native GCP2 with a red arrow.

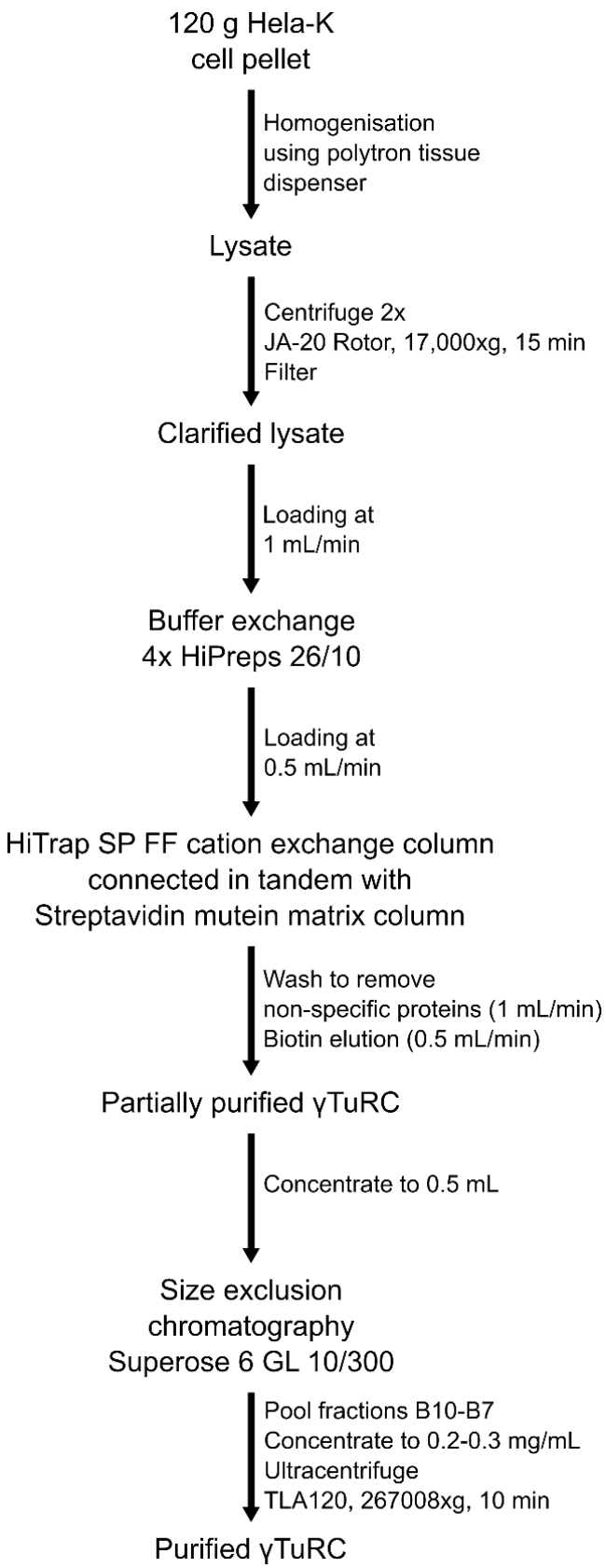

Figure 2.18: Overview of large scale purification of GCP2-mBFP-AviTag-γTuRCs.

2.2.2.3 Purification of tagged γTuRC

Tagged γTuRCs are purified following the method shown in Figure 2.18. Cells are lysed and buffer exchanged to remove biotin followed by a cation exchange step to remove unspecific proteins. Then lysate was affinity purified using a monomeric streptavidin mutein matrix column. Protein gels (Figure 2.19 A) show the removal of overall proteins from the lysate after the cation exchange step while the amount of γTuRC is not affected as judged from western blots (Figure 2.19 B). A clear reduction of the amount of γTuRC subunits can be detected in the flow through of the affinity purification column indicating binding of fully assembled γTuRC via GCP2-mBFP-AviTag subunit.

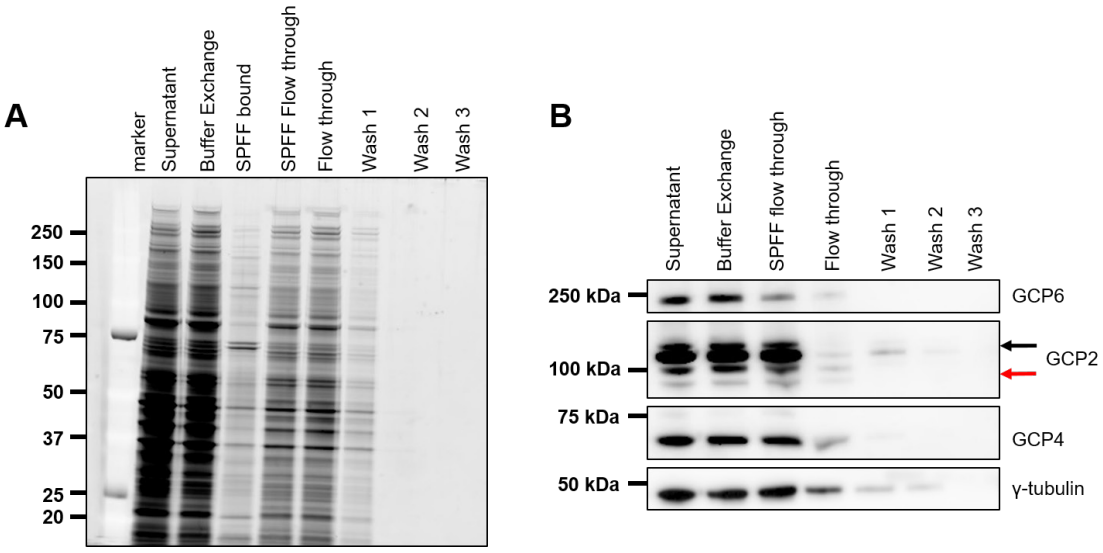

Figure 2.19: Affinity purification of GCP2-mBFP-AviTag-γTuRCs. γTuRCs were purified using a streptavidin mutein matrix column. (A) Sypro ruby stained protein gels of purification steps and (B) corresponding western blots detected with antibodies against γTuRC subunits as indicated. GCP2-mBFP-Avitag is highlighted with a black arrow, native GCP2 with a red arrow.

γTuRC is eluted from the affinity column via biotin elution. The elution profile (Figure 2.20 A) showed two overlapping peaks, both containing γTuRC subunits as found by western blot (Figure 2.20 C). The main fraction of the γTuRC can be found in fraction 2 and fraction 3 (Figure 2.20 B and C, purple arrows), followed by a tail of fractions containing a lower amount of γTuRCs. The two peaks are separated by a fraction containing the least amount of γTuRCs. This elution profile was unexpected but is most probably explained by the presence of different subpopulations of γTuRC which bind with different affinities to the purification resin. The γTuRC might contain different amounts of tagged GCP2 or subcomplexes of various sizes might be present at that stage of the purification.

The fractions containing the highest amount of all γTuRC subunits (Figure 2.20 B and C, purple arrows) were pooled, buffer exchanged and concentrated for the size exclusion chromatography step. Protein gels and western blots are shown in Figure 2.20 D and E.

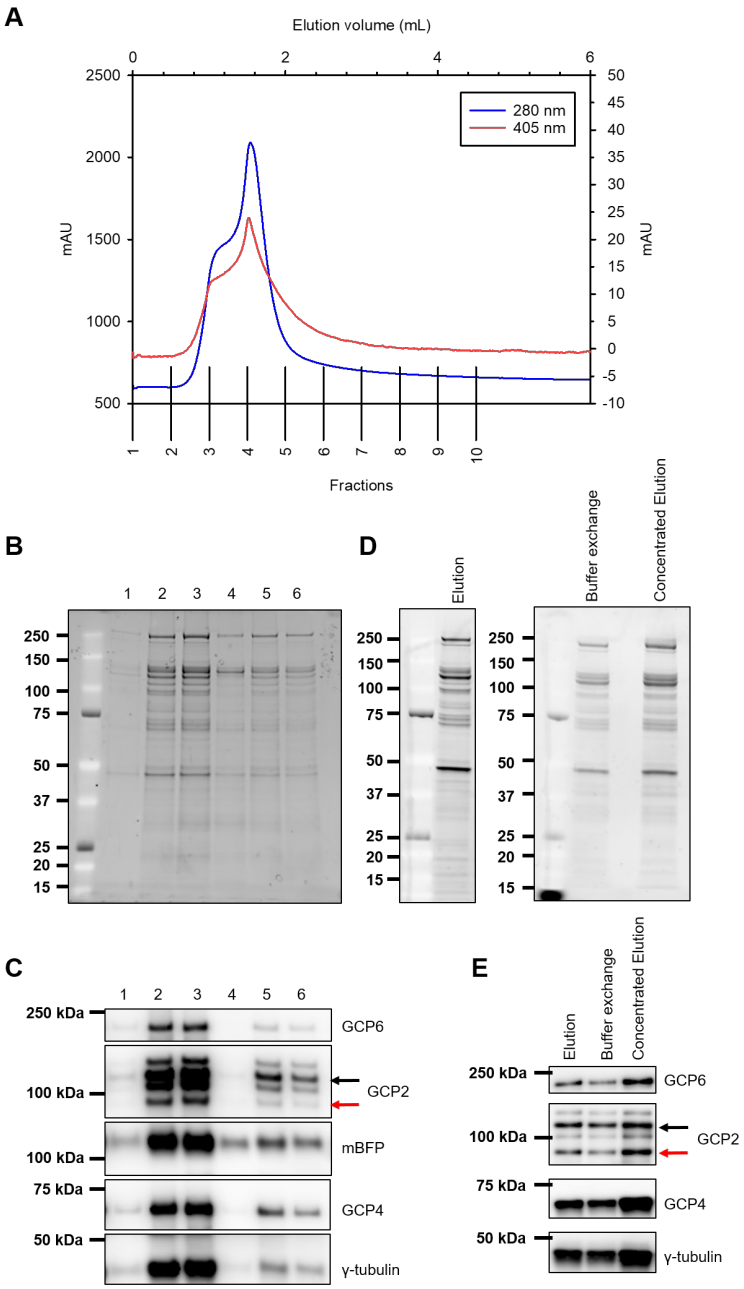

Figure 2.20: Elution profile of GCP2-mBFP-AviTag-γTuRCs. (A) Elution profile of total protein (blue line) and mBFP (red line) from streptavidin mutein matrix column. (B) Sypro Ruby stained protein gels for elution fractions and (C) corresponding western blots. (D) Sypro Ruby stained protein gels of pooled elution, buffer exchange and concentrated elution and (E) corresponding western blots. GCP2-mBFP-Avitag is highlighted with a black arrow, native GCP2 with a red arrow.

Concentrated eluate was subjected to size exclusion chromatography to separate γTuRCs from γTuSCs and other proteins. Size exclusion chromatography profile (Figure 2.21 A) reveals two peaks for total protein (blue line) and three peaks for mBFP (red line). The first peak most likely corresponds to fully assembled γTuRCs, while the second peak probably represents γTuSCs. The third peak most likely corresponds to single molecules of mBFP. Fractions were analysed for the presence of γTuRC subunits. Protein gels (Figure 2.21 B) show that mainly proteins of high molecular weight (150 kDa to 250 kDa) are separated from the complex by size exclusion chromatography. Western blots (Figure 2.21 A) show that the band intensities of the γTuRC subunits peak in fractions B10 to B7 (red square).

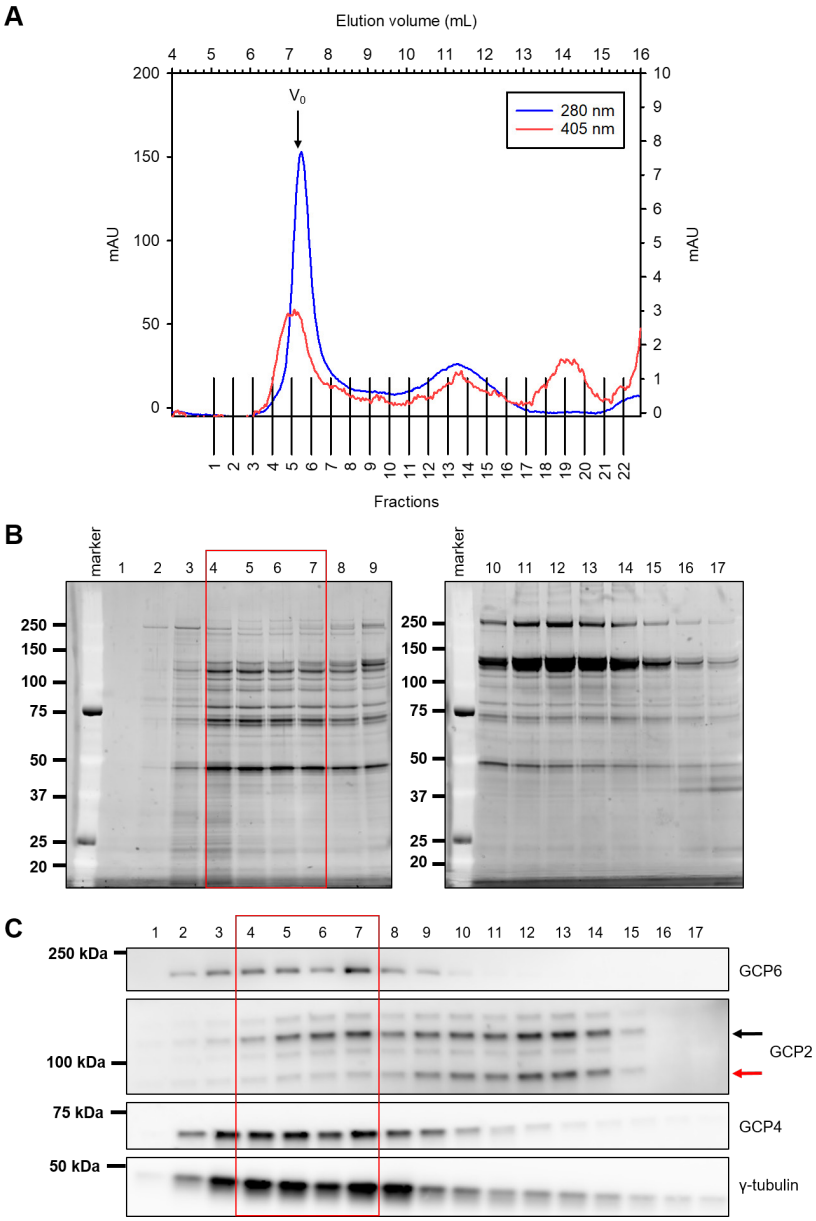

Figure 2.21: Size exclusion chromatography of GCP2-mBFP-AviTag-γTuRCs. (A) Size exclusion chromatography profile of γTuRC eluting from a Superose 6 10/300 GL column. Elution profile of total protein (blue line) and mBFP (red line) is shown. The void volume (V_0)

of the column is indicated. (B) Sypro ruby gels of fractions and (C) corresponding western blots. Fraction size was 0.5 mL. γTuRC peak fraction is marked with a red square. GCP2-mBFP-Avitag is highlighted with a black arrow, native GCP2 with a red arrow.

The peak fractions were collected and concentrated to 0.2-0.3 mg/mL. γTuRC was centrifuged to remove potential aggregates, aliquoted, snap frozen and stored in liquid nitrogen. Using the above described protocol on average a total of 200 µg of γTuRC can be purified from 30 g of cell pellet. The purity of the affinity isolated γTuRC was always analyzed by Sypro Ruby stained protein gels (Figure 2.22 A) and the presence of all γTuRC subunits was confirmed by western blot (Figure 2.22 B).

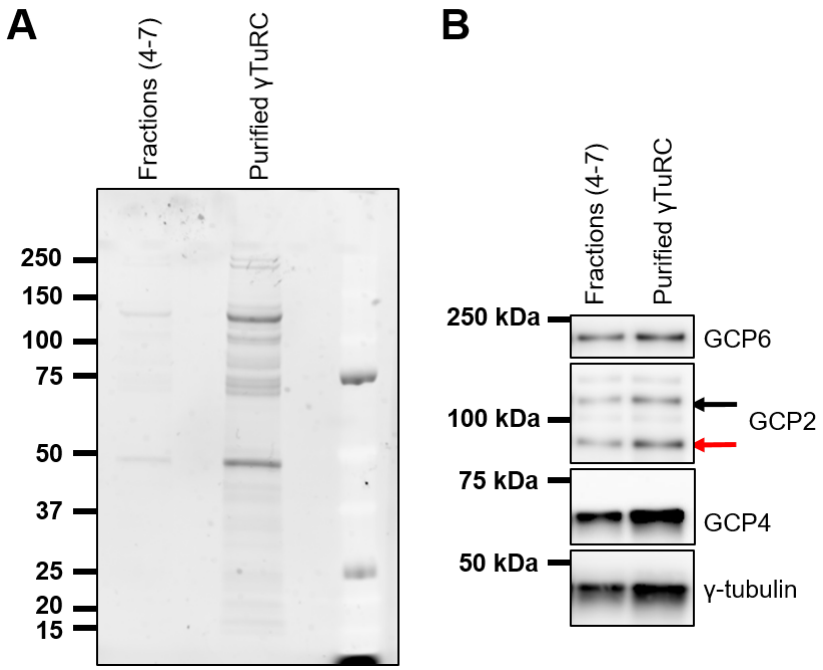

Figure 2.22: Analysis of purified GCP2-mBFP-AviTag-γTuRCs. (A) Sypro ruby gels for pooled size exclusion chromatography fractions and concentrated purified γTuRC and (C) corresponding western blots. GCP2-mBFP-Avitag is highlighted with a black arrow, native GCP2 with a red arrow.

2.2.2.4 Characterization of purified tagged γTuRC by mass spectrometry and negative-stain electron microscopy

The identity of the protein bands visible on Sypro Ruby stained protein gels was confirmed by mass spectrometry (Proteomics facility, The Francis Crick Institute). Coomassie-stained protein gel used for mass spectrometry analysis and the identity of the protein bands are shown in Figure 2.23 A. All γTuRC subunits were identified (see material and methods, Table 13). All other identified proteins are currently not known to play a role in microtubule regulation.

To confirm the presence of fully assembled γTuRC, purified complex was also analysed by negative stain electron microscopy in collaboration with Julia Locke

(Costa group, The Francis Crick Institute). A representative negative stain image is shown in Figure 2.23 B. Rings with a diameter of around 25 nm were found, as described for previous purifications of γTuRC from different organisms including human cells (Choi and Qi, 2014; Choi et al., 2010; Moritz et al., 2000; Zheng et al., 1995).

In summary, tagged fully assembled γTuRCs containing all known γTuRC subunits were successfully purified from a stable HeLa-K cell line using the new purification method.

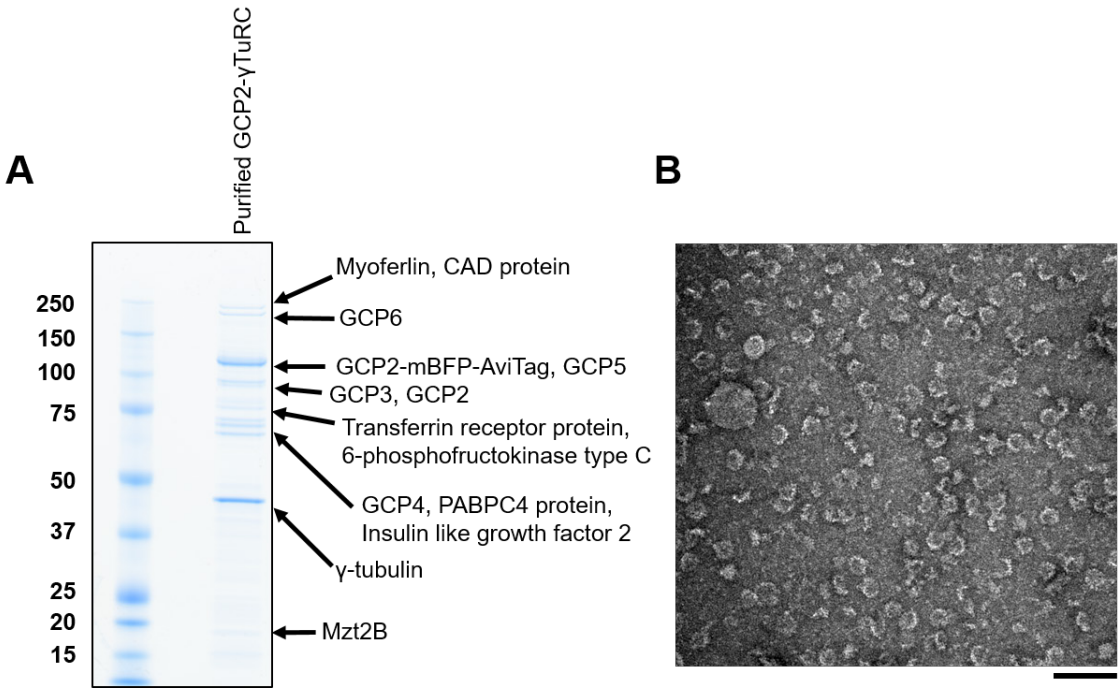

Figure 2.23: Characterization of GCP2-mBFP-AviTag-γTuRCs. (A) Coomassie stained gel of purified γTuRC. (B) Negative stain electron microscopy of purified γTuRC. Negative staining and image acquisition was performed by Julia Locke (Costa laboratory, The Francis Crick institute). Scale bar = 100 nm.

2.3 Discussion

In this chapter I tested two different approaches to purify γTuRC from human cells. I first attempted to reproduce published methods, then established a new purification protocol for the affinity isolation of fluorescently tagged γTuRC from stable cell lines.

2.3.1 Purification of native γTuRC

After multiple trials and substantial optimization of the purification procedure, I could not purify sufficient amounts of native γTuRCs using γTuRC-binders. For this purification, I closely followed the method described in one publication with only two modifications: the affinity tag on the γTuRC-binder (GST tag versus GST-AviTag used in this thesis) and the expression cell line used for purification (HEK293 cells versus U2OS cells) (Muroyama et al., 2016). A detailed comparison between the published protocol and my own method is difficult as neither the starting material nor the final yield were reported in the previous study. The affinity purification of the γTuRC by γTuRC-binders was first described by another group (Choi and Qi, 2014; Choi et al., 2010), and differs substantially from the approach described (Muroyama et al., 2016) and used by myself. In the original protocol, γTuRCs are purified from a mixture of untransfected cells and cells transiently expressing γTuNA. While it is not clear why a mixture of cells is used, the transient expression of γTuNA could be essential for this method to work. The binding of γTuNA to γTuRCs in the lysate might be weak as most of the complex was found in the flow through of the affinity purification column in my experiments. This suggests that there might be another intracellular factor needed for γTuNA to bind to the complex efficiently, and that this interaction might not happen anymore once the cells are lysed. Observations reported by different groups suggest a role for Mzt1, another γTuRC-binder, in modulating the interactions between γTuNA and γTuRCs (Cota et al., 2017; Dhani et al., 2013; Leong et al., 2019; Lin et al., 2016; Masuda and Toda, 2016). It could therefore be possible that both γTuRC-binders are needed for the efficient purification of native γTuRCs from human cell lysate.

It was previously shown that a phosphorylation at a specific site in γTuNA is required for the binding of γTuNA to γTuRCs (Choi et al., 2010; Cota et al., 2017). γTuNA used for purification of endogeneous γTuRCs in this thesis was expressed and purified from *E. coli*, while the γTuNA used in both published protocols was expressed in human cells (Choi and Qi, 2014; Choi et al., 2010; Muroyama et al., 2016). An

alternative explanation for the low γTuRC yield obtained in this thesis might therefore be the lack of phosphorylation on γTuNA.

2.3.2 Purification of tagged γTuRC

In the second part of this chapter I described the purification of γTuRCs from a stable HeLa-K cell line expressing GCP2-mBFP-AviTag. This method is so far the second strategy described for the purification of γTuRCs tagged with an affinity purification tag (Teixidó-Travesa et al., 2010). To my knowledge, this is the first strategy for the purification of fluorescently tagged γTuRCs. The purification protocol is based on the affinity purification of γTuRC by an overexpressed fluorescently labelled γTuRC subunit, i.e. GCP2. As indicated by the western blot and mass spectrometry results, the tagged GCP2 does not completely replace the endogenous protein. From my experiments it is not clear if each purified γTuRC contains copies of tagged and endogenous GCP2 or how many copies of tagged protein are present per complex. It is possible that my sample contains a mixture of complexes, with some containing only tagged GCP2s, some containing a mixture of tagged and endogenous GCP2 and some γTuRCs only containing endogenous protein. To distinguish between these possibilities, it would be interesting to perform nucleation experiments using individual γTuRCs and observe if all nucleated microtubules originate from a mBFP-labelled complex. Additionally, it would be interesting to perform quantitative mBFP-photobleaching experiments to quantify the copy number of fluorescent GCP2s within the different complexes.

Using this method, γTuRCs can be isolated from a moderate amount of cell pellet (120 g) at purities comparable with other published methods. It is difficult to compare the efficiencies of the different purification protocols as the amount of starting material and the final yield are usually not reported in the literature (see Table 3). Typically, I was able to purify 150-250 µg of γTuRCs from human cells. This is around 21-fold more complex than isolated by immunoaffinity from *Xenopus* egg extract (Zheng et al., 1995, 1998). I assessed the purity of the γTuRC sample using mass spectrometry (David Frith, The Francis Crick Institute, Proteomics facility) and identified all known subunits of human γTuRC and the known γTuRC-binder Mozart 2B (Mzt2B) (Hutchins et al., 2010; Murphy et al., 1998, 2001; Teixidó-Travesa et al., 2010). Mzt2B has been co-purified previously with γTuRC in three studies (Choi and Qi, 2014; Choi et al., 2010; Hutchins et al., 2010; Teixidó-Travesa et al., 2010). Other studies copurified Mzt1, a paralogue of Mzt2 (Hutchins et al., 2010; Thawani et al., 2018). Due to the

small size of Mzt1 and Mzt2 (8.5 and 16.2 kDa, respectively), it is thought that they might have been overlooked in previous purifications.

Apart from γTuRC subunits and Mzt2B I also identified several other proteins, which to my knowledge have no known roles in the assembly or regulation of γTuRCs (see Figure 2.23). These proteins have so far not been reported to co-purify with γTuRCs in other published studies (see Table 3 for references). Going forward, it could be interesting to determine if they have a specific role in γTuRC-mediated microtubule nucleation or if they represent remaining contaminants. To control for unspecific binding of these proteins to the column material, the column could be incubated with cell lysate from cells grown in the absence of D-biotin but overexpressing GCP2-mBFP-AviTag. In the absence of D-biotin, the AviTag is not biotinylated. This would prevent binding of the GCP2-mBFP-AviTag to the column, while proteins unspecifically interacting with the column matrix would still bind. Additionally, it would be interesting to re-analyse the purified γTuRC sample using a more quantitative mass spectrometry approach. This would allow me to determine the ratio of γTuRC subunits to other proteins and would be helpful to assess the purity of the sample. It would also be interesting to purify γTuRC from cells arrested in mitosis instead of asynchronous cells to see if I co-purify different additional proteins or if mitotis-specific post-translational modifications have a role in regulating γTuRC activity.

To confirm that I purify fully assembled complexes, I analysed the purified γTuRC using negative stain electron microscopy in collaboration with Julia Locke (Costa group, The Francis Crick Institute). The negative stain electron microscopy images revealed ring-like structures at the expected size of γTuRCs, indicating that fully assembled γTuRCs can be purified using the new purification method. We tried to further assess if some of the γTuRC rings were incomplete. However, it was difficult to confidently distinguish between a ‘broken’ γTuRC ring and γTuRCs being tilted (which might therefore appear ‘broken’). Currently, the exact stoichiometry and positions of the GCPs within the γTuRC are not known (Farache et al., 2018; Kollman et al., 2011; Tovey and Conduit, 2018). Given a relatively higher yield of γTuRC was achieved using the new purification approach, it would also be interesting to attempt cryo-electron microscopy (cryo-EM) to obtain structural information of human γTuRCs. Additionally, chemical cross-linking followed by mass spectrometry could be helpful to obtain insights into the interaction between different GCPs within the γTuRC.

In summary, the method presented in this chapter can be used to purify fluorescently labeled γTuRC from human cell lysates at quantities and purity sufficient for biochemical experiments.

3. γTuRC-mediated microtubule nucleation studied by TIRF-microscopy

3.1 Introduction

How the γTuRC mediates microtubule nucleation and how the complex is regulated is still poorly understood. To gain insight into the mechanism of γTuRC-templated microtubule nucleation and its regulation the development of a new real time fluorescence microscopy-based nucleation assay is crucial.

Previously, microtubule nucleation of purified γTuRC has been measured in most cases by fluorescence microscopy of fixed samples (see table Table 2 for references). In this approach, purified γTuRC is incubated with fluorescently labelled tubulin and GTP in solution to initiate the nucleation reaction. After incubation for a certain time, the reaction is chemically fixed, an aliquot is observed by fluorescence microscopy to count the number of nucleated microtubules. In this type of assay, it is important to distinguish between γTuRC-mediated microtubule nucleation and potential spontaneous microtubule nucleation in absence of the γTuRC under the same assay conditions. This has been done by comparing the microtubule numbers obtained in absence and presence of the complex.

In a second approach, the assay originally used to study spontaneous microtubule nucleation in solution has been applied to measure γTuRC-mediated microtubule nucleation by one group (Murphy et al., 2001). In this 'bulk' assay, purified γTuRCs are incubated with pure tubulin and GTP in solution and the increase of total polymer mass due to the combination of microtubule nucleation and polymerization is followed by turbidity measurements using a spectrophotometer. As for the fluorescence microscopy assay, the stimulatory effect of the γTuRC on microtubule nucleation is assessed in comparison to spontaneous nucleation occurring in the absence of γTuRC under the same assay conditions.

Both assays have limitations that restrict the amount of information one can obtain from each set-up. The fluorescence microscopy-based assay allows for the visualization of the individual microtubules and can be performed with sample sizes as small as 5 µL total volume. Therefore, one does not need large amounts of purified complexes but fixation might introduce artefacts. The bulk assay requires significantly larger volumes and has therefore limited applicability as typically the yield of γTuRCs purified from native sources is very low (see Table 2). Moreover, the bulk assay does not allow for the visualization of individual microtubules and the relative contribution

of microtubule nucleation and elongation on the turbidity measurement cannot be distinguished. Nevertheless, the real time measurement of the combined microtubule nucleation and elongation reaction permits direct kinetic measurements. In principle, the kinetic information of microtubule nucleation can also be obtained using the fluorescence microscopy assay by imaging samples fixed at different time points. However, to my knowledge this has not been described so far in the literature.

It appears, that in many of the previous nucleation experiments, the nucleation efficiency of γTuRC was presumably low as often very high tubulin concentrations were used and in several cases the reaction mixture was supplemeted with taxol and/or glycerol to stabilize microtubules nucleation (see Table 2).

Therefore, an improved nucleation assay is desireable, which ideally combines the advantages of the above described microtubule nucleation assays. In this chapter, I describe the development of a new total internal fluorescence (TIRF) microscopy-based assay for the study of microtubule nucleation by purified γTuRC. The new assay set-up is designed to measure the nucleation and elongation of individual microtubules by γTuRC in real time using fluorescence microscopy. This new assay set-up will then be used to study the kinetics of γTuRC-mediated microtubule nucleation in different conditions to better understand the mechanism of γTuRC-templated microtubule nucleation.

3.2 Results

3.2.1 Assay design

The real-time microtubule nucleation assay involves the surface immobilization of purified biotinylated γTuRCs to functionalized glass surfaces. Microtubule nucleation by immobilized γTuRCs in presence of pure tubulin and GTP and the elongation of nucleated microtubules can be observed in real time using total internal fluorescence (TIRF) microscopy. A functionalized glass slide and a passivated counterglass is used to build a flow cell to allow solution exchange. Microtubule nucleation is initiated by heating the flow cell to 33°C after exchanging the buffer for tubulin solution. The immobilization of γTuRCs on functionalized glass slides is based on previously described assay set-ups used to observe spontaneous microtubule nucleation in the absence of γTuRC and microtubule elongation from stabilized seeds (Bieling et al., 2007; Roostalu et al., 2015). Functionalized glass slides contain a brush of biotin-polyethylene glycol (biotin-PEG) to which NeutrAvidin can be bound. NeutrAvidin is a tetrameric protein containing four binding sites for biotin. This allows NeutrAvidin to mediate the binding of biotinylated molecules to the functionalized glass surface. The γTuRC purified in this thesis (see chapter 2) contains a biotinylated AviTag for surface attachment of γTuRC and a fluorescent marker protein to visualize the immobilization of γTuRC using fluorescence microscopy. The set-up of the assay is shown in Figure 3.1.

Microtubule nucleation by γTuRC is measured using TIRF microscopy. This technique allows for measurements at reduced fluorescence background as the excitation of fluorescent molecules is restricted to a thin section near the surface of the glass slide (evanescent field, ~200 nm) (Fish, 2009; Telley et al., 2011; Zwetsloot et al., 2018). This allows to image microtubule nucleation at high concentrations of fluorescently labelled tubulin and/or regulatory proteins as used in some of the assays performed in this thesis. The use of TIRF microscopy allowed me to measure up to four different fluorescently labelled proteins in a single experiment. I could image fluorescently labelled γTuRC, fluorescent tubulin and fluorescently labelled regulatory proteins at the same time using appropriate laser lines and emission filters.

The buffer used for assays contained low concentrations of methylcellulose (0.15%). Methylcellulose is a polymer that increases the viscosity of the solution, does not specifically interact with proteins, but creates a depletion force which promotes the alignment of microtubules close to the glass surface and thereby keeps them in the evanescent field (Farhadi et al., 2018; Inoue et al., 2015).

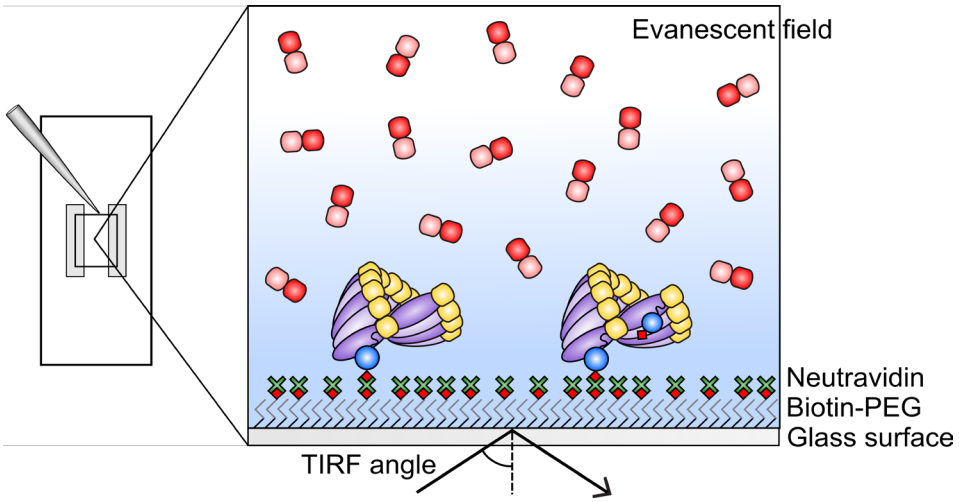

Figure 3.1: Schematic illustration of TIRF microscopy-based γTuRC microtubule nucleation assay. (LEFT) Flow cell created by attaching biotinylated functionalized glass slides to passivated counterglass using double sided tape. (RIGHT) Illustration of the biotinylated γTuRCs attached to the biotinylated functionalized glass slide by NeutrAvidin during a TIRF microscopy experiment. γTuRC and nucleated fluorescently labelled microtubules are undergoing illumination by a laser angled to create an evanescent field.

3.2.2 Validation of the *in vitro* microtubule nucleation assay

3.2.2.1 Attachment of the γTuRC to functionalized coverslips

The γTuRC used in all experiments is tagged on the C-terminus of GCP2 with a biotinylated affinity tag (AviTag) and monomeric blue fluorescent protein (mBFP) (see Figure 2.13 for construct design). The biotinylated γTuRC is bound to the biotinylated glass slide via NeutrAvidin (see Figure 3.1 for assay design).

I first tested if purified human γTuRCs can be immobilized on functionalized glass surfaces. To do this, I incubated a flow cell with buffer solution containing γTuRCs. After a short incubation time (5 min), I washed away unbound complexes and imaged the flow cell by TIRF microscopy using the mBFP fluorescence to detect potential attachment of γTuRCs on the surface. To know if the immobilization is specific I compared the mBFP fluorescence signal of γTuRC incubated with NeutrAvidin-coated glass slides and γTuRCs incubated with functionalized passivated glass slides without NeutrAvidin coating. I found that only glass slides with NeutrAvidin coating showed mBFP fluorescence (Figure 3.2 A). This result suggests, that the γTuRC can be immobilized on functionalized biotinylated glass slides specifically via the NeutrAvidin coating.

To test whether the mBFP density on the surface can be varied I incubated the glass surfaces with solutions containing different γTuRC concentrations ranging from 23 to

373 pM and repeated the above described experiment. I found that the mBFP fluorescence intensity increased when buffer solutions contained a higher concentration of γTuRCs during the incubation step (Figure 3.2 B).

The mBFP signal on the surface appeared grainy rather than homogenous for all conditions and the density of the mBFP signal decreased at lower γTuRC concentrations. I analysed the glass slides incubated with the lowest concentration of γTuRCs at higher magnification (Figure 3.2 B, red outline) and found individual fluorescent dots of mBFP on the surface, suggesting the presence of individual γTuRCs. Together, these observations indicate that the mBFP density is dependent on the γTuRC concentration in solution.

I then quantified the average mBFP fluorescence intensity in the field of view (164 µm x 164 µm) using ImageJ. By quantifying the signal intensity for repeated experiments for each γTuRC concentration I obtained an average mBFP fluorescence intensity, which was proportional to the amount of γTuRCs in the solution used for incubation with the glass slides (Figure 3.2 C). Linear regression analysis found a good fit as indicated by a high R^2 value of 0.87, which is a measure of linearity. The linear dependence of the mBFP signal on the γTuRC concentration suggests that the NeutrAvidin binding sites do not become saturated within the range of γTuRC concentrations tested.

I estimated the number of individual γTuRCs on the surface by counting the mBFP dots at 23 pM γTuRC at higher magnification (Figure 3.2 B, red outline). I found ~480 mBFP dots which would mean that ~0.1 molecules of bound γTuRC are bound per μm^2 at that concentration. The total number of surface immobilized γTuRC molecules in the field of view (164 µm x 164 µm) used for analysis therefore varies between 2,900 molecules for the lowest and 47,000 molecules for the highest concentration of γTuRC.

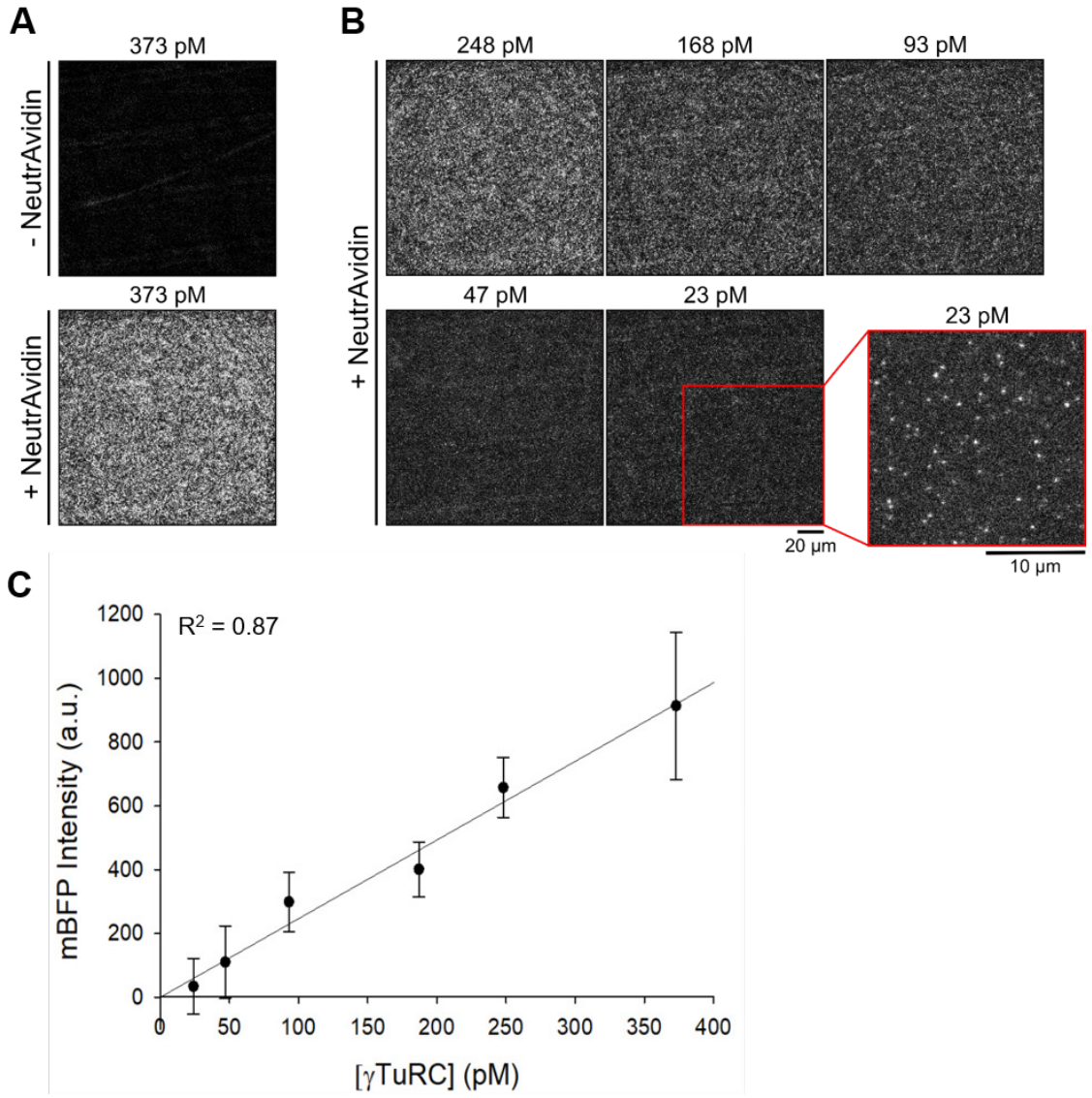

Figure 3.2: γTuRC attachment onto NeutrAvidin coated functionalized coverslips. (A) Representative mBFP fluorescence images of tagged γTuRCs bound to functionalized passivated coverslips with and without NeutrAvidin coating. (B) Representative images of mBFP fluorescence obtained for different concentrations of γTuRC. The lowest amount of γTuRC (23 pM) was additionally analysed at higher magnification to visualize individual complexes. Each condition was repeated at least three times. γTuRC concentrations as indicated in the Figure. Images are shown with the same absolute intensity scale. Intensities in the images are directly comparable. (C) Plot of the average γTuRC surface density (mBFP fluorescence intensity) (n=3) against γTuRC concentration. Plot shows linear regression and R^2 value. Quantification was performed using ImageJ. Field of view (164 µm x 164 µm). Error bars represent the standard deviation.

3.2.2.2 Characterization of tagged γTuRC microtubule nucleation activity

I next wanted to determine if immobilized γTuRCs are able to nucleate microtubules in solutions of pure tubulin and GTP. Therefore, I bound γTuRCs (373 pM in solution) to functionalized coverslips and exchanged the flow cell with assay buffer containing

a total of 10 µM purified tubulin (mixture of unlabelled and CF640R-fluorescently labelled tubulin). Microtubule nucleation was initiated by heating the flow chamber to 33°C and the reaction was followed by TIRF microscopy over time. To control for spontaneously nucleated microtubules I performed control assays using the same conditions but in the absence of surface immobilized γTuRCs. A time series of representative TIRF microscopy images is shown for the γTuRC assay and control assay in Figure 3.3 A. To confirm that γTuRC is able to stimulate microtubule nucleation above the level of spontaneous microtubule nucleation under my assay conditions, I quantified the number of microtubules at the end of each assay (20 min) in a field of view (164 µm x 164 µm). This experiment was repeated in total seven times on three different days and the average number of microtubules compared to three control assays performed in parallel in the absence of γTuRCs is shown in Figure 3.3 B. In the presence of γTuRCs, the number of microtubules nucleated after 20 min was 23-fold higher compared to spontaneous nucleation at the same tubulin concentration, suggesting that immobilized γTuRCs are able to stimulate microtubule nucleation *in vitro*.

As a control, snap shots of different areas of the flow cell were taken at the end of the microtubule nucleation reaction (~25 min after the flow cell was transferred onto the microscope) (Figure 3.3 C). Microtubule numbers and γTuRC amount on the surface were very similar between the field of views indicating that γTuRC binding and tubulin concentration are homogenously distributed throughout the flow chamber.

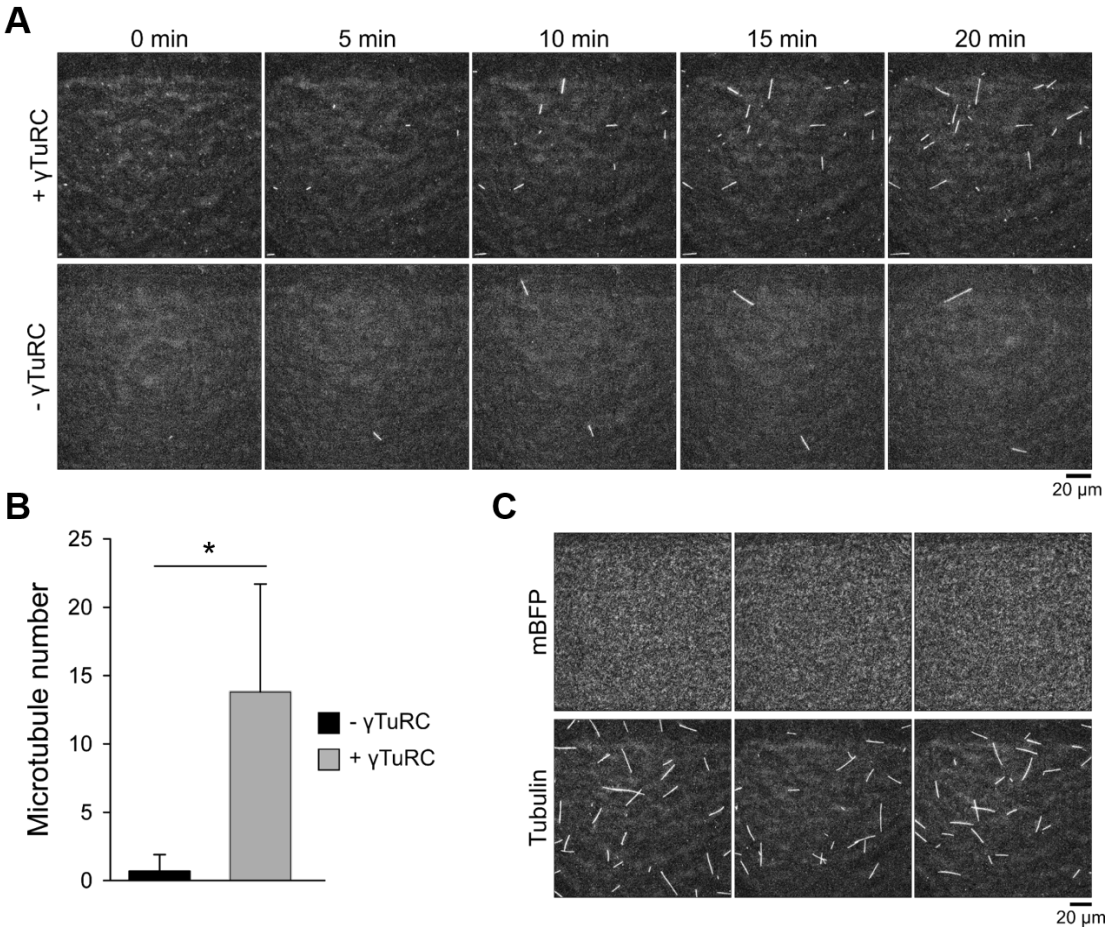

Figure 3.3: γTuRC-mediated microtubule nucleation in pure tubulin solutions followed by TIRF microscopy. (A) Representative time series of TIRF microscopy images of a microtubule nucleation reaction in the presence (upper panel) and in the absence (lower panel) of 375 pM γTuRC. Experiments were performed in the presence of 10 µM tubulin. (B) Quantification of the total number of microtubules nucleated in the presence (n=7, 15.1±7.4) and in the absence (n=3, 0.7±1.2) of γTuRC at t=20 min. Error bars represent the standard deviation. Statistical analysis was performed using unpaired t-test. Significant differences with unpaired t-test are shown (ns, not significant; *p<0.05; **p<0.01; ***p<0.001; ****p<0.0001). (C) Representative images of γTuRC surface density (upper panel) and nucleated microtubules (lower panel) of different fields of views within one flow cell. Images were taken 25 min after transfer of the flow cell onto the microscope. Assay conditions as described for (A). Field of view for all images (164 µm x 164 µm). Images are shown with the same absolute intensity scale. Intensities in the images are directly comparable.

The advantage of this assay is that the nucleation and elongation of individual microtubules can be observed in real-time. γTuRC is expected to template nucleation of microtubules from their minus-ends. Consequently, microtubules nucleated by γTuRC would grow only from their plus-end while the minus-ends should be capped by the immobilized complex at least for a while. To examine if microtubules only grow from one end, I closely observed the microtubules nucleated in the presence of γTuRC. A representative time series of four different microtubules nucleated in the presence of γTuRC is shown in Figure 3.4 A. Microtubules being nucleated in the

assay first appear as a dot followed by elongation. One end is growing while the other end is stable (purple arrow). Microtubules stay capped for the whole duration of the assay, as can be seen from representative kymographs (time space plots) (Figure 3.4 C).

To verify that the growing end represents the microtubule plus-end, I performed assays with short GMPCPP stabilized microtubules, commonly used as templates for dynamic growth *in vitro*. The microtubule 'seeds' can be bound to functionalized glass surfaces and in presence of free tubulin and GTP will grow from both ends, with the plus-end growing faster than the minus-end (Bieling et al., 2007, 2010).

I generated kymographs for γTuRC nucleation assays and 'seed' assays and quantified the microtubule growth velocities for both ends from the slopes of the kymographs (Figure 3.4 B, purple arrows indicate minus-ends). Representative kymographs for both assays are shown in Figure 3.4 C. In the microtubule seed assays both ends polymerize, with the faster growing plus-end growing at an average velocity of 20.0±4.4 nm s^{-1} and the slower minus-end at 4.5±1.6 nm s^{-1}. In assays containing γTuRCs the growing end polymerizes with an average growth velocity of 18.9±3.4 nm s^{-1}. I could not find a statistical difference in the plus-end growth speed between assays performed with microtubule seeds or γTuRCs indicating that the growing ends indeed represent the plus-ends. This result is in agreement with the expectation of γTuRC acting as a template to nucleate microtubules with their minus-ends being capped over time.

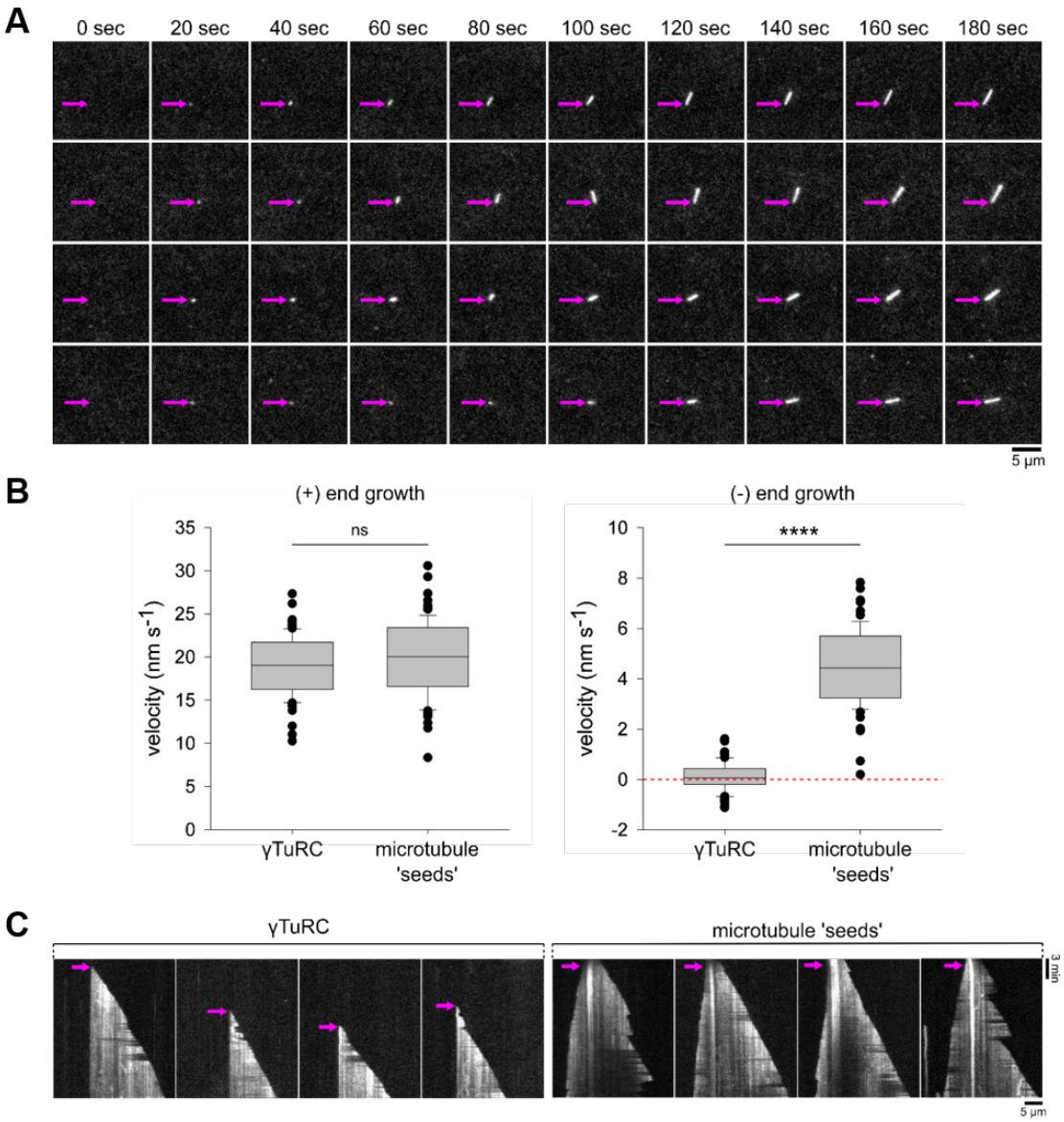

Figure 3.4: γTuRCs nucleate and cap microtubules from their minus-ends. (A) Representative time series of four individual microtubules nucleated in assays containing 373 pM γTuRC and 10 µM tubulin. Stable microtubule minus-ends are highlighted with a purple arrow (B) Quantification of microtubule plus-end (left) and minus-end (right) growth velocities. Error bars represent the standard deviation. Statistical analysis was performed using unpaired t-test. Significant differences are shown (ns, not significant; *p<0.05; **p<0.01; ***p<0.001; ****p<0.0001). (C) Representative kymographs for γTuRC nucleation assay and microtubule 'seed' assay performed under the same conditions as (A). Microtubule minus-ends are highlighted with a purple arrow. Images are shown with the same absolute intensity scale. Intensities in the images are directly comparable.

3.2.2.3 Quantification of γTuRC-mediated microtubule nucleation

The new real-time microtubule nucleation assay allows me to distinguish between microtubule nucleation and elongation. Consequently, by quantifying the number of

nucleation events over the duration of the assay I can directly obtain information about the kinetics of γTuRC-mediated microtubule nucleation.

Therefore, I counted the number of microtubules nucleated by γTuRCs at ten different time points in the same field of view (164 µm x 164 µm) over the duration of the assay (20 min). I found that a small number of microtubules clearly landed from solution instead of nucleating from the surface. These microtubules suddenly appear in the field of view and grow from both ends. These spontaneously nucleated microtubules were excluded from the analysis.

The number of γTuRC-nucleated microtubules quantified for seven individual assays performed at 10 µM tubulin in the presence of 373 pM γTuRC (same protein batch) on three different days was plotted against the time (Figure 3.5 A, black symbols). The average number of microtubules in all experiments and the corresponding standard deviation is shown in Figure 3.5 B (black symbols). Control experiments for spontaneous microtubule nucleation were performed in parallel but in the absence of γTuRC (Figure 3.5 A and Figure 3.5 B, grey symbols).

I observed a linear increase of γTuRC nucleated microtubules over time. Linear regression analysis revealed a good fit for each individual experiment with R^2 values above 0.90, indicating a constant nucleation probability for γTuRC in all assays. The slope of the linear regression represents the microtubule nucleation rate (r_{nuc} in Figure 3.5 A and B), which can be used to compare the efficiency of γTuRC-mediated microtubule nucleation between different experiments and conditions. Under these assay conditions, the nucleation rates varied for the different experimental repeats between 0.39 microtubules per min and 1.20 microtubules per min. To control if this relatively high variation in the nucleation rate can be explained by experimental differences between the repeats or due to the experiments being performed on different days I quantified the microtubule growth velocity (Figure 3.5 C) and BFP surface intensity as a measure of γTuRC density (Figure 3.5 D). I could not find a statistically significant difference between different days of experiments for both, the microtubule growth velocity or γTuRC density. These results demonstrate that the tubulin concentration was the same in all experiments and that a similar amount of γTuRC was immobilized on the glass surfaces.

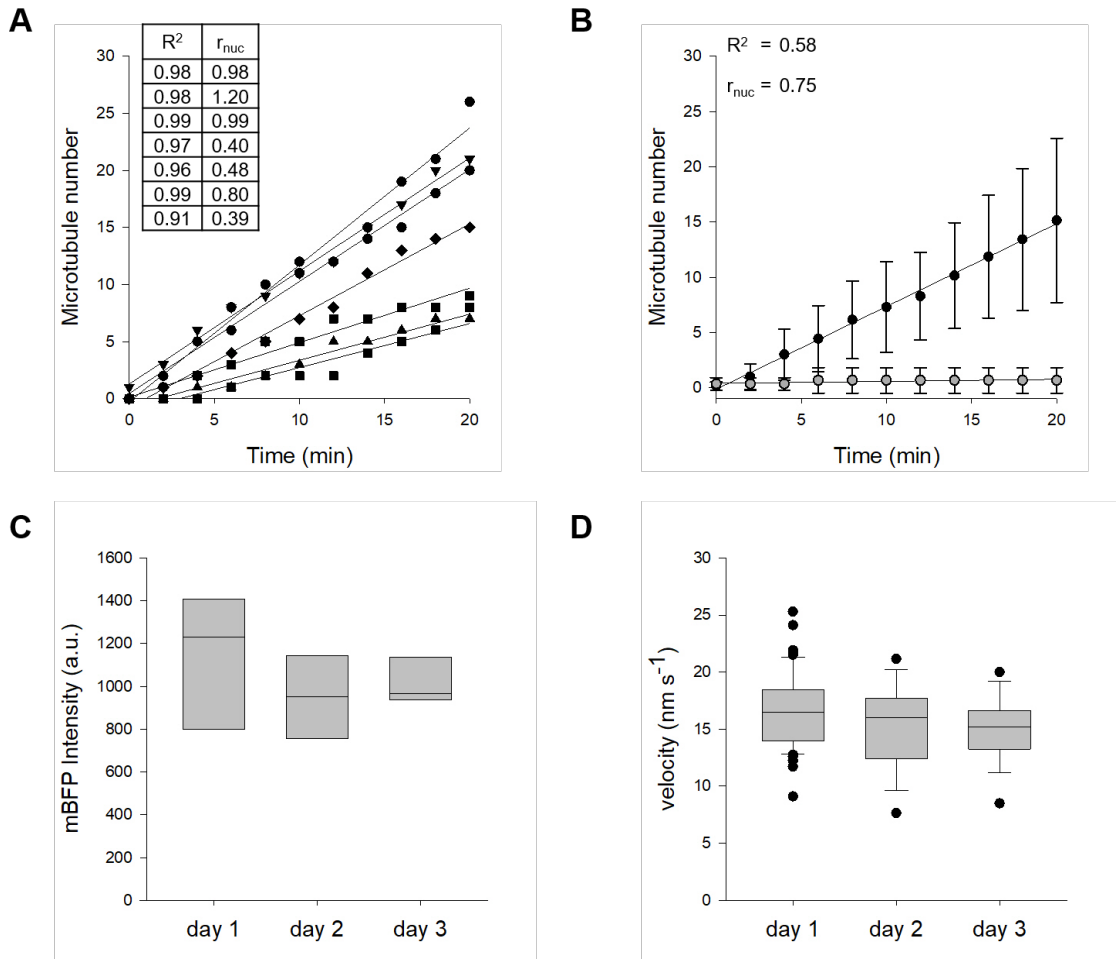

Figure 3.5: Quantification of γTuRC nucleated microtubules. (A) Plot of microtubule number over time in the presence of γTuRC (Black symbols) and in the absence of γTuRC (grey symbols). (B) Plot of the average microtubule number over time in the presence of γTuRC (n=7, black symbols) and in the absence of γTuRC (n=3, grey symbols). Error bars represent the standard deviation. Experiments were performed at 10 µM tubulin with 373 pM γTuRC. Lines represent the linear regression. R^2 and r_{nuc} are as indicated in the Figure. (C) Quantification of γTuRC surface densities: day 1 (n=3), day 2 (n=2), day 3 (n=3). (D) Quantification of microtubule plus-end growth velocities: day 1 (n=51), day 2 (n=16), day 3 (n=13). Quantification was performed using ImageJ. Field of view (164 µm x 164 µm). Statistical analysis was performed using F-test. Significant differences are shown (ns, not significant; *p<0.05; **p<0.01; ***p<0.001; ****p<0.0001).

In summary, for all experiments microtubule nucleation in the presence of γTuRCs was higher than spontaneous nucleation in the absence of γTuRCs. The results show that AviTag-mBFP tagged γTuRCs are active after immobilization onto functionalized glass slides and able to stimulate microtubule nucleation in solutions of pure tubulin and GTP over the level of spontaneous nucleation. On average, γTuRC-mediated microtubule nucleation was found to be 23-fold higher than spontaneous nucleation with an average nucleation rate of 0.75 microtubules per min. Taken together, the new TIRF microscopy-based microtubule nucleation assay is able to visualize the

nucleation and elongation of individual microtubules in real time and allows the quantification of microtubule nucleation kinetics. The assay can therefore be used to study γTuRC-mediated microtubule nucleation under different conditions.

3.2.3 Microtubule nucleation is dependent on γTuRC density

Next, I wanted to know if the amount of microtubules nucleating over time is dependent on the density of γTuRCs on the surface. For this experiment I increased the concentration of tubulin in the assay from 10 µM to 15 µM, expecting an increase in the nucleation efficiency similar to what has been shown for spontaneous microtubule nucleation in absence of γTuRC (Erickson and Pantaloni, 1981; Voter and Erickson, 1984).

I incubated functionalized glass slides with solutions containing a range of γTuRC concentrations from 23 pM to 373 pM. The plot showing the dependence of the mBFP fluorescence intensity on γTuRC concentration is shown in Figure 3.2 C. A time series showing representative TIRF microscopy images at three different γTuRC concentrations is shown in Figure 3.6 (top three rows).

I found that the number of microtubules nucleated over time was γTuRC concentration dependent. At the lowest γTuRC concentration only a few microtubule nucleation events could be observed whereas at the highest tested concentration, γTuRC strongly stimulated microtubule nucleation. For all tested γTuRC concentrations the number of nucleated microtubules was above the level of spontaneous nucleation in absence of γTuRC at the same tubulin concentration (Figure 3.6 bottom row).

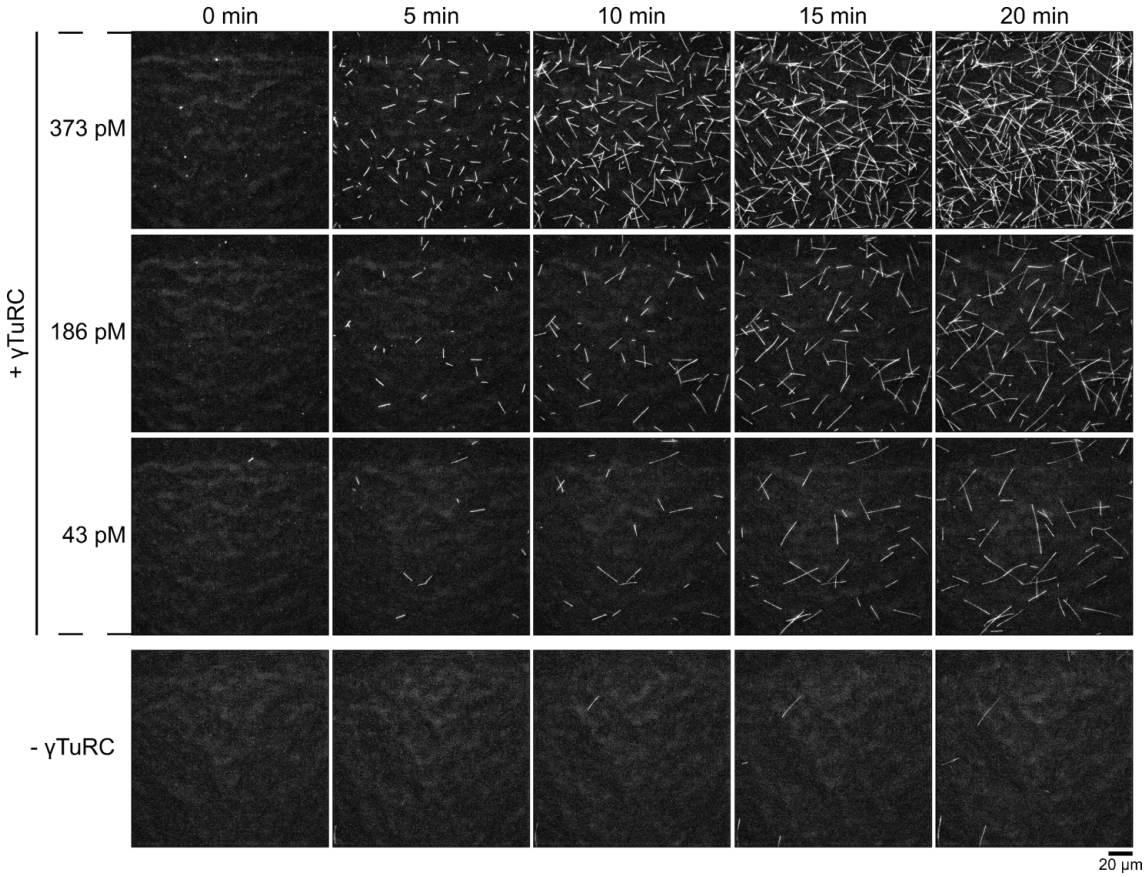

Figure 3.6: Microtubule nucleation efficiency is dependent on the γTuRC surface density. Representative time series of TIRF microscopy images of microtubule nucleation reactions performed in the presence of 15 µM tubulin at the indicated γTuRC concentrations. Spontaneous microtubule nucleation at the same tubulin concentration is shown for comparison (bottom panel). Field of view (164 µm x 164 µm). Images are shown with the same absolute intensity scale. Intensities in the images are directly comparable.

I quantified the number of microtubules nucleated at ten different time points in the field of view (164 µm x 164 µm) over the duration of the assay (20 min) for all conditions. At high concentrations of γTuRC, I instead quantified the number of microtubules for ten time points over a period of 15 min, as the density of microtubules was too high for quantification at later time points.

Figure 3.7 shows the average increase of microtubules over time. Error bars represent the standard deviation and each condition was repeated at least three times. For all γTuRC concentrations I found a linear increase of microtubule number over time with R^2 values above 0.75 for all conditions. Nucleation rates increased from 0.65 microtubules per min to ~14 microtubules per minute for the γTuRC density range tested. Note the different scales of the y-axis in Figure 3.7.

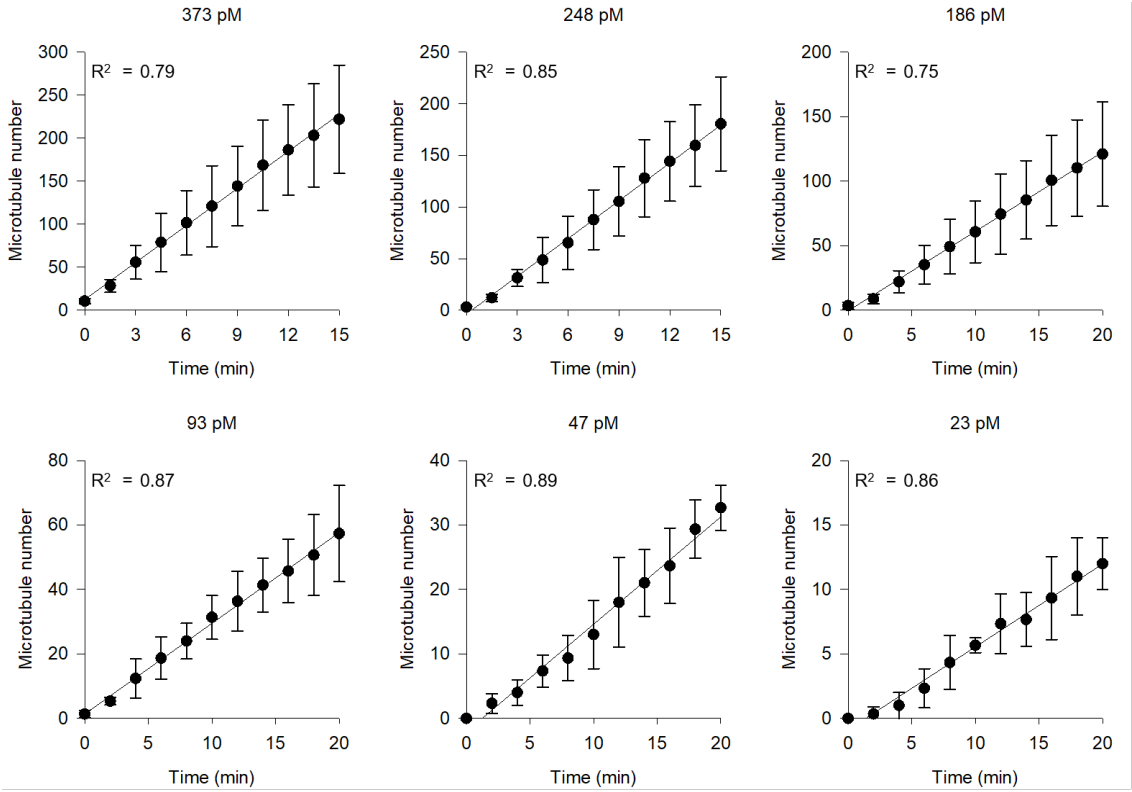

Figure 3.7: Quantification of microtubule nucleation rates for different γTuRC densities. Plots of the average microtubule number over time (n=3). Error bars represent the standard deviation. Experiments were performed at 15 µM tubulin. Lines represent the linear regression. γTuRC concentrations and R^2 values as indicated for each Figure.

For a better visualization of the different nucleation rates at all tested γTuRC concentrations, plots from Figure 3.7 are combined and shown at the same scale in Figure 3.8.

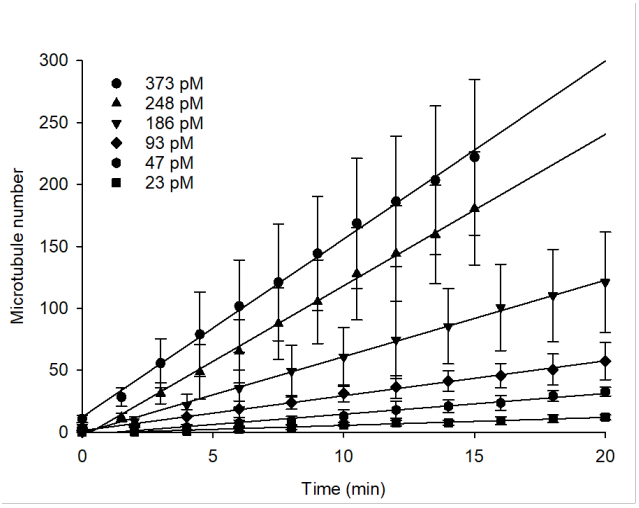

Figure 3.8: The rate of microtubule nucleation is dependent on the γTuRC surface density. Plot of the average microtubule number over time (n=3) in the presence of different γTuRC surface densities. Concentrations of γTuRC as indicated in the Figure. Error bars represent the standard deviation. Experiments were performed at 15 µM tubulin. Lines represent the linear regression.

I quantified the microtubule plus-end growth speed for all conditions and plotted the growth velocity against the density of γTuRC on the surface (Figure 3.9). As expected, the plus-end growth speed of the nucleated microtubules was the same for all γTuRC densities demonstrating that the tubulin concentration was the same in all experiments.

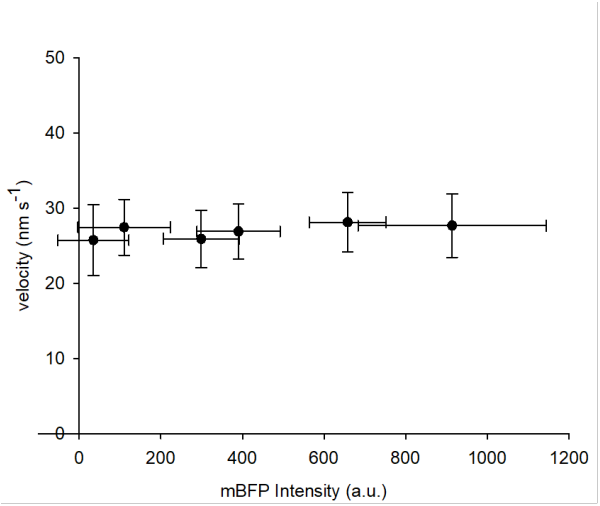

Figure 3.9: Quantification of microtubule plus-end growth in the presence of different γTuRC surface densities. Plot shows the average microtubule growth velocity against the average γTuRC surface density (n=3): 23 pM (n=28), 47 pM (n=65), 93 pM (n=97), 168 pM (n=192), 248 pM (n=161), 373 pM (n=303). Error bars represent the standard deviation.

I then plotted the microtubule nucleation rate against the mBFP intensity which is a measure of the γTuRC density (see Figure 3.2). Linear regression analysis found a good fit with a high R^2 value of 0.96 (Figure 3.10).

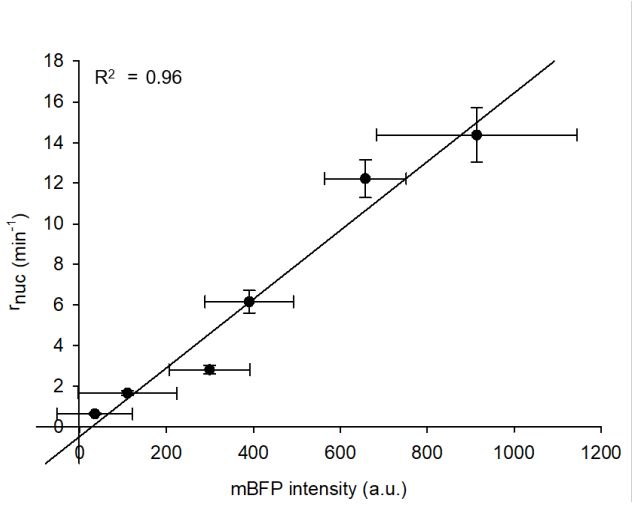

Figure 3.10: Linear dependence of microtubule nucleation rate on γTuRC surface density. Plot of the average microtubule nucleation rate (n=3) against the average γTuRC surface density (n=3). Error bars represent the standard deviation. Experiments were performed at 15 µM tubulin. Lines represent the linear regression. R^2 as indicated in the Figure.

In summary, I could show that purified human γTuRCs promote microtubule nucleation in a dose-dependent manner and that the nucleation rate was proportional to the γTuRC density on the surface.

3.2.4 Microtubule nucleation by γTuR is dependent on tubulin concentration

I next studied the dependence of γTuRC-mediated microtubule nucleation on the tubulin concentration. To do this I kept the γTuRC density on the functionalized glass surface constant by incubating flow chambers always with the same concentration of γTuRC in solution (373 pM). The tubulin concentration was varied between 6 µM and 20 µM. To confirm that the surface density of γTuRCs was similar for all assays I quantified the mBFP fluorescence intensity in each field of view (164 µm x 164 µm) that was also used to observe and quantify the microtubule nucleation reaction in all experiments (see Figure 3.11). No statistical difference in γTuRC density was found for different tubulin concentrations.

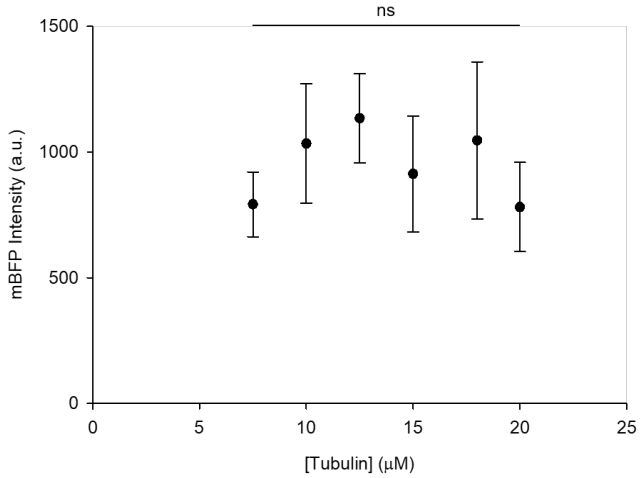

Figure 3.11: γTuRC densities on the glass surface are independent on tubulin concentration. Plot of the average γTuRC surface density (mBFP fluorescence intensity) (n=3) against tubulin concentration. Error bars represent the standard deviation. Quantification was performed using ImageJ. Field of view (164 µm x 164 µm). Statistical analysis was performed using F-test. Significant differences are shown (ns, not significant; *p<0.05; **p<0.01; ***p<0.001; ****p<0.0001).

For assays performed at a tubulin concentration of 6 µM, I could not detect any microtubule nucleation events. A time series showing representative TIRF microscopy images at three higher tubulin concentrations is shown in Figure 3.12 (top three rows). At 7.5 µM tubulin hardly any microtubules were nucleated during 20 min. This suggests that the minimum tubulin concentration for γTuRC to template microtubule nucleation under my assay conditions is ~7.5 µM tubulin. With increasing

tubulin concentration, the number of nucleated microtubules increased and at 20 µM tubulin the microtubule density after 8 min was so high that individual microtubules could not be distinguished.

For all tested tubulin concentrations, I made control experiments for spontaneous nucleation in absence of γTuRC by performing assays without complexes under otherwise same assay conditions. For all tested tubulin concentrations, γTuRC-mediated microtubule nucleation was above the level of spontaneous microtubule nucleation in the absence of γTuRCs. A representative time series for spontaneous microtubule nucleation at 20 µM tubulin in absence of γTuRCs is shown in Figure 3.12 (bottom row).

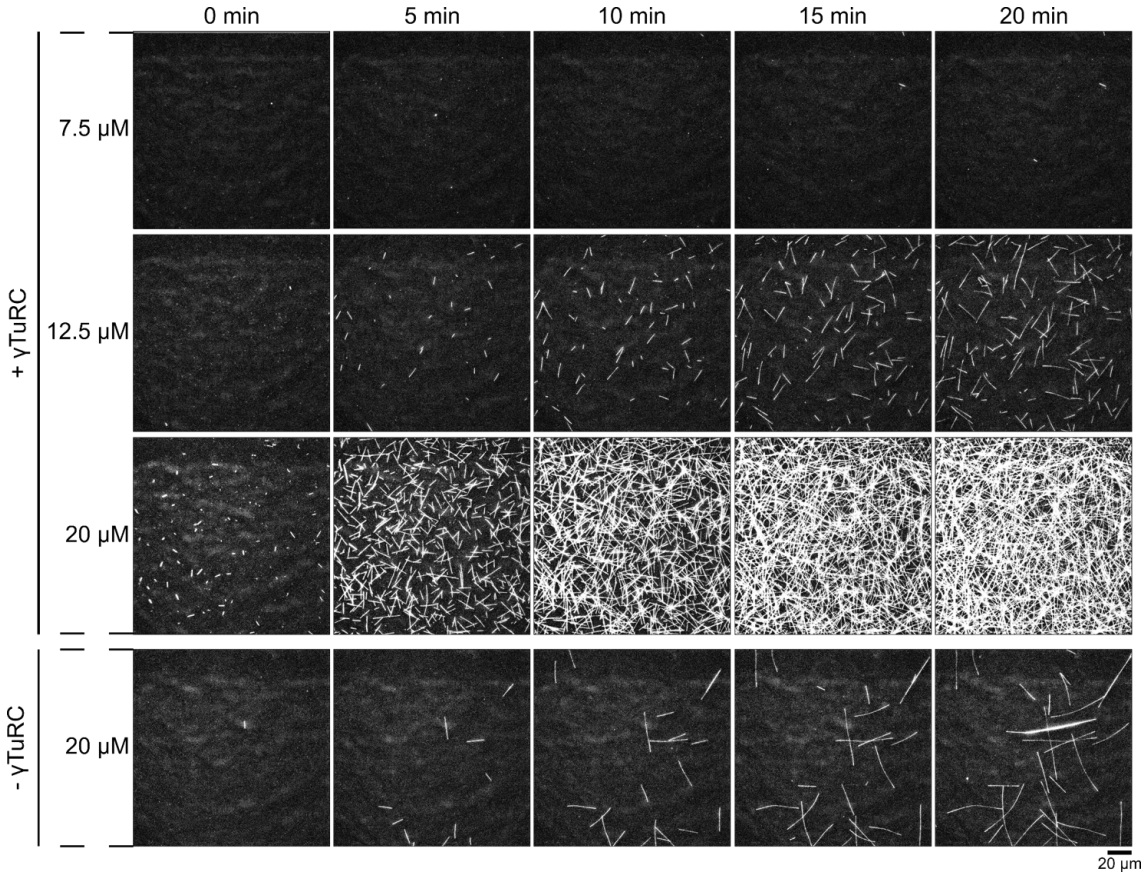

Figure 3.12: γTuRC-mediated microtubule nucleation efficiency is dependent on tubulin concentration. Representative time series of TIRF microscopy images of microtubule nucleation reactions performed in the presence of 375 pM γTuRC at the indicated tubulin concentration. Spontaneous microtubule nucleation at 20 µM tubulin is shown for comparison (bottom panel). Field of view (164 µm x 164 µm). Images are shown with the same absolute intensity scale. Intensities in the images are directly comparable.

Next I quantified the number of γTuRC nucleated microtubules at ten different time points over the duration of each assay (20 min). As before, I adjusted the time period

I used for counting the microtubule number depending on the density of microtubules in the assay (see x-axis of plots in Figure 3.13).

Again, the number of γTuRC nucleated microtubules increased linearly over time. Linear regression analysis revealed a better fit for for higher tubulin concentrations (higher R^2 value) as the number of nucleated microtubules fluctuated less in those experiments compared to lower tubulin concentrations.

The rates of microtubule nucleation by γTuRC depended strongly on the different tubulin concentrations. At 7.5 µM tubulin γTuRC nucleates ~0.09 microtubules per min whereas at 20 µM tubulin ~85 microtubules per min are nucleated.

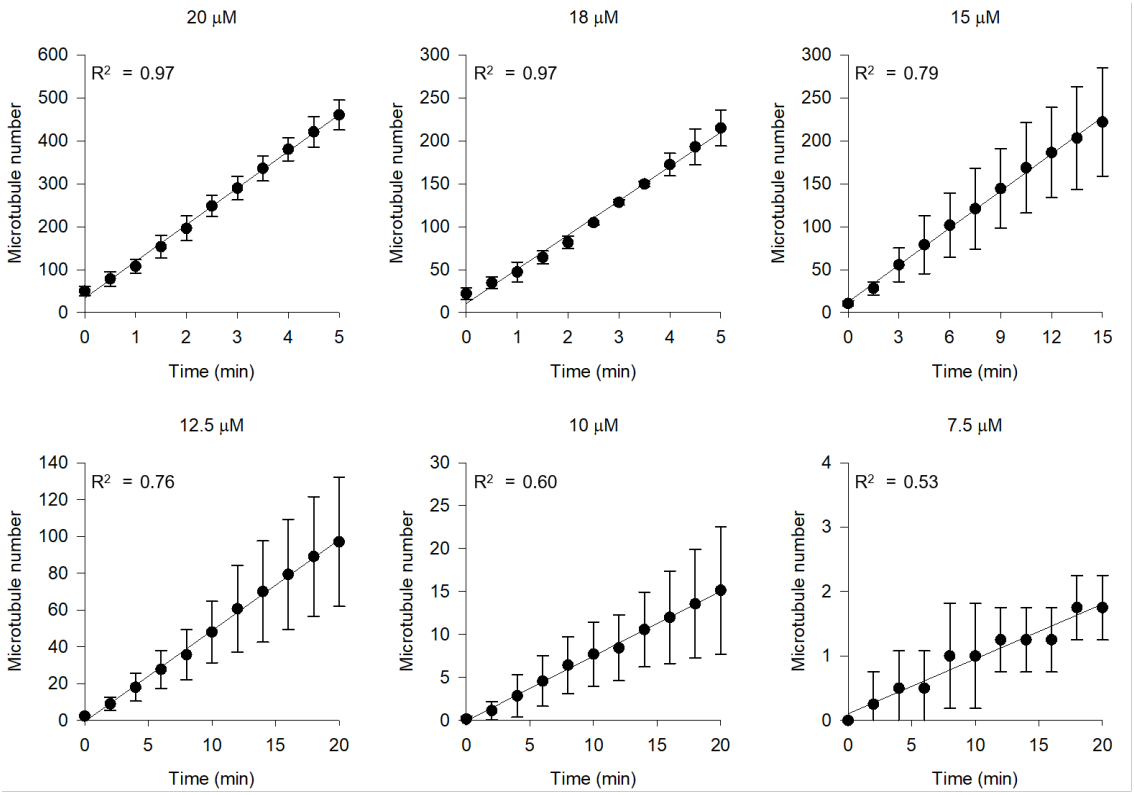

Figure 3.13: Quantification of microtubule nucleation rates at different tubulin concentration. Plots of the average microtubule number over time: 7.5 µM (n=4), 10 µM (n=7), 12.5 µM (n=3), 15 µM (n=3), 18 µM (n=3), 20 µM (n=3). Error bars represent the standard deviation. Experiments were performed at 373 pM γTuRC. Lines represent the linear regression. Tubulin concentrations and R^2 as indicated for each Figure.

For a better visualization plots from Figure 3.13 are combined and shown at the same scale in Figure 3.14.

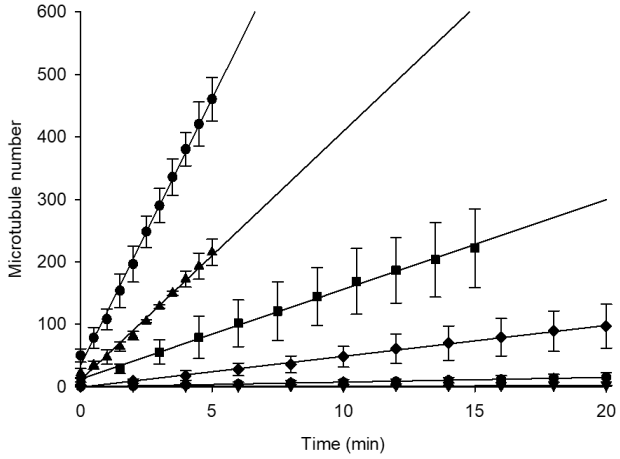

Figure 3.14: The rate of microtubule nucleation is dependent on the tubulin concentration. Plot of the average microtubule number over time in the presence of different tubulin concentrations: 7.5 µM (n=4), 10 µM (n=7), 12.5 µM (n=3), 15 µM (n=3), 18 µM (n=3), 20 µM (n=3). Concentrations of tubulin as indicated in the Figure. Error bars represent the standard deviation. Experiments were performed at 373 pM γTuRC. Lines represent the linear regression.

I then analysed the microtubule plus-end growth speeds of γTuRC nucleated microtubules for all tubulin concentrations by kymograph analysis. The plot of the measured growth velocities against the tubulin concentration revealed the expected linear dependence (Figure 3.15 A) (Drechsel et al., 1992; Gardner et al., 2011; Mitchison and Kirschner, 1984a; Wieczorek et al., 2015). I obtained an estimate for the 'critical tubulin concentration' (C_c) for microtubule growth from the extrapolation of the linear regression to the x-axis. The C_c is 2.25±0.04 µM tubulin, which is significantly lower than the lowest tubulin concentration (7.5 µM) for which I could observe microtubule nucleation by γTuRC, as expected (Wieczorek et al., 2015).
The plot of the γTuRC-mediated microtubule nucleation rate against tubulin concentration shows a steep non-linear increase (Figure 3.15 B). I fitted the curve of the measured nucleation rates (r_{nuc}) using a power function.

$$r_{nuc} = \frac{dn_{MT}}{dt} = r_0 \, c_{\gamma TuRC} \, c_{tub}^{n} = r \, c_{tub}^{n}$$

with r_{nuc} measured nucleation rate, n_{MT} number of microtubules, r_0 nucleation rate constant, $c_{\gamma TuRC}$ γTuRC density on the surface, c_{tub} tubulin concentration, n exponent indicating the molecularity of the reaction.

The exponent informs about the molarity or cooperativity of the reaction. n>2 indicates cooperativity. The fit of the equation to the curve gives an exponent n=6.8±0.3

suggesting that γTuRC-mediated microtubule nucleation is highly cooperative. In the case of microtubule nucleation, the exponent can be used to estimate the size of the 'critical nucleus' from microtubule nucleation kinetics data. Therefore, n represents the minimum amount of tubulin dimers that need to bind to γTuRC to form a stable enough oligomer for polymerization.

The plot of the average microtubule nucleation rates against the microtubule plus-end growth velocity also shows a steep non-linear increase (Figure 3.15 C). Microtubule nucleation by γTuRCs can be observed at a lowest plus-end growth speed of 13.3±1.8 nm s^{-1}.

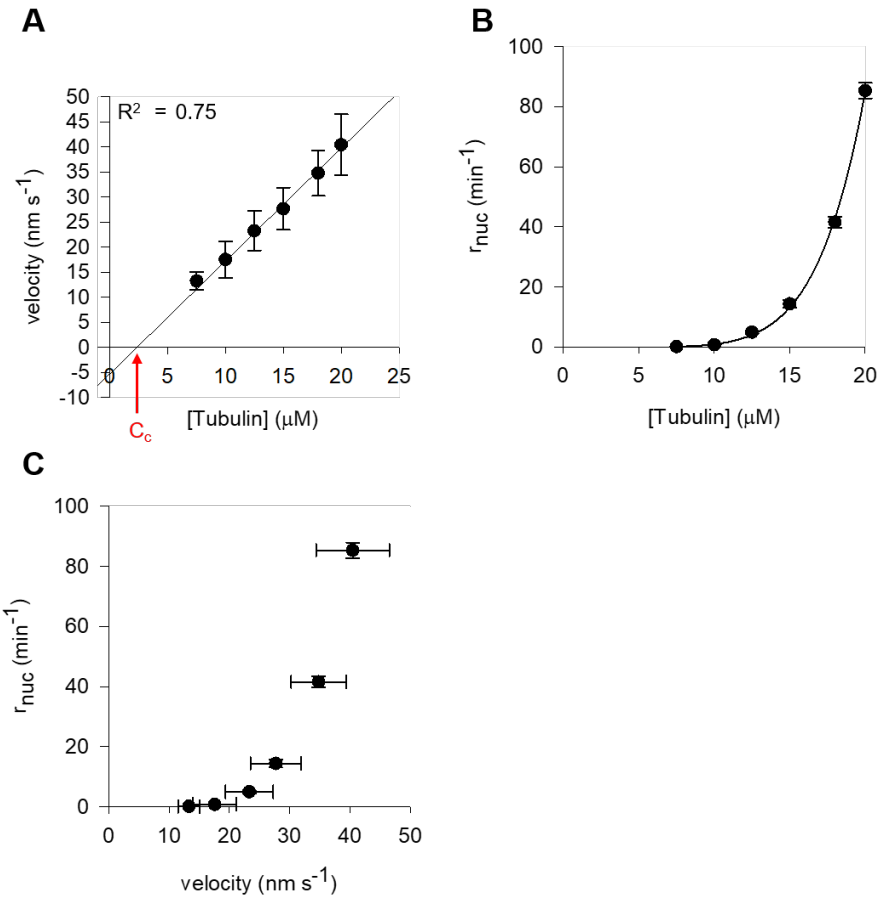

Figure 3.15: Characterization of γTuRC-mediated microtubule nucleation in the presence of different tubulin concentrations. (A) Plot of average microtubule plus-end growth velocity against tubulin concentration: 7.5 µM (n=10), 10 µM (n=177), 12.5 µM (n=211), 15 µM (n=303), 18 µM (n=168), 20 µM (n=245). (B) Plot of the average microtubule nucleation rate against tubulin concentration. Curve was fit with a power law function as described in the main text. (C) Plot of the average microtubule nucleation rate against the average microtubule plus-end growth velocity. All error bars represent the standard deviation. Experiments were performed at 373 pM γTuRC.

In summary, these results demonstrate that γTuRC-mediated microtubule nucleation, as has been found for spontaneous microtubule nucleation, is strongly dependent on

tubulin concentration (Erickson and Pantaloni, 1981; Voter and Erickson, 1984). The analysis of the dependence of the microtubule nucleation rate on tubulin concentration suggests that nucleation is very cooperative and that at least 7 tubulin dimers are needed to form a stable nucleus which can be elongated.

3.2.5 Time lag analysis

Using the new assay set-up to directly measure the microtubule nucleation kinetics of γTuRCs I found a linear increase of microtubule numbers over time. In some experiments there might be a short non-linear phase at the beginning of the nucleation reactions. Therefore, I wanted to investigate if this non-linear phase for γTuRC-mediated microtubule nucleation represents a time lag as previously reported for spontaneous microtubule nucleation in absence of γTuRCs and γTuRC-mediated microtubule nucleation when measured with a spectrophotometric bulk assay (Carlier and Pantaloni, 1978; Caudron et al., 2000; Detrich et al., 1985; Himes et al., 1977; Johnson and Borisy, 1977; Lee and Timasheff, 1975, 1977; Murphy et al., 2001; Robinson and Engelborghs, 1982; Voter and Erickson, 1984). To this end I quantified the potential time lags from the extrapolation of the linear regression for all plots of microtubule number over time for different γTuRC densities (Figure 3.7) and tubulin concentrations (Figure 3.13). Figure 3.16 A shows a plot of the average length of the lag times measured for all tested γTuRC densities and Figure 3.16 B shows a plot of the average length of the lag times measured for all tested tubulin concentrations. In the literature the length of the time lag was found to shorten with increasing tubulin or γTuRC concentration (Carlier and Pantaloni, 1978; Caudron et al., 2000; Detrich et al., 1985; Himes et al., 1977; Johnson and Borisy, 1977; Lee and Timasheff, 1975, 1977; Murphy et al., 2001; Robinson and Engelborghs, 1982; Voter and Erickson, 1984). I could not find a statistically significant difference of the length of the time lags at different γTuRC surface densities or the tubulin concentration in the assay.

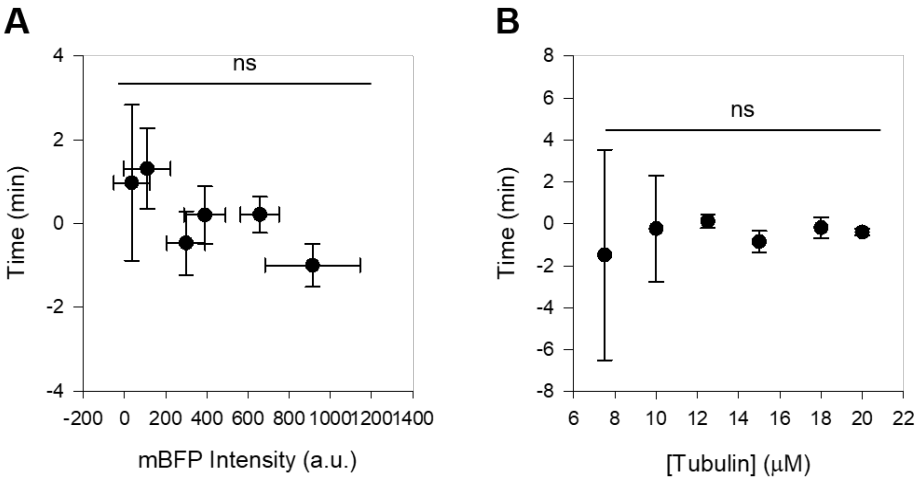

Figure 3.16: Dependence of a pontential time lag on γTuRC surface density or tubulin concentration. (A) Plot of the average time lag against γTuRC surface density: 23 pM (n=3), 47 pM (n=3), 93 pM (n=3), 168 pM (n=3), 248 pM (n=3), 373 pM (n=3). Experiments were performed at 10 μM tubulin. (B) Plot of the average time lag against tubulin concentration: 7.5 μM (n=4), 10 μM (n=7), 12.5 μM (n=3), 15 μM (n=3), 18 μM (n=3), 20 μM (n=3). Error bars represent the standard deviation. Experiments were performed at 373 pM γTuRC. Statistical analysis was performed using F-test. Significant differences are shown (ns, not significant; *p<0.05; **p<0.01; ***p<0.001; ****p<0.0001).

The efficiency of microtubule nucleation is known to be expontentially dependent on temperature (Fygenson et al., 1994). The nucleation reactions performed in this thesis are initiated by a temperature shift. I therefore measured the time it takes to reach thermal equilibrium within a flow cell using a thermistor. To accommodate the thermistor, the volume of the flow cell was increased by 6-fold. Figure 2.17 shows a plot of the increase of temperature over time within the flow cell. The start time of the nucleation experiments (time point zero) is marked with a red line. At the start of a nucleation experiment the temperature within the flow cell has reached about 96% of the final temperature (33°C).

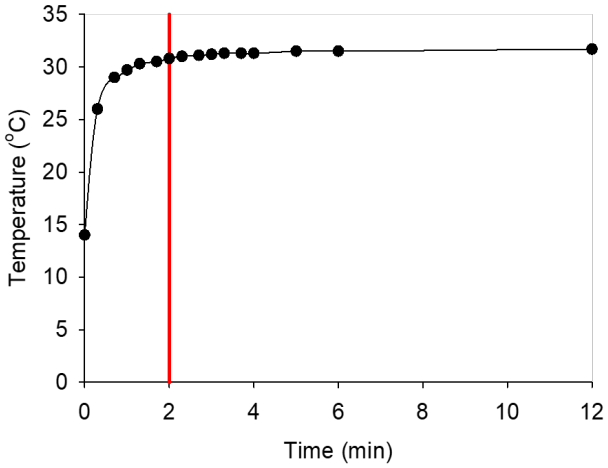

Figure 3.17: Temperature measurement in a modified flow cell. Flow cell volume is 6-fold higher compared to flow cells used for nucleation experiments. Temperature increase was followed using a thermistor. Experiment was performed as described for nucleation experiments (see material and methods section 6.11) but in the absence of proteins.

In summary, I could not find a dependence of the time lags onto γTuRC concentration or tubulin concentration. The short nonlinear phase visible for some experiments shown in Figure 3.7 and Figure 3.13 could potentially be explained by small differences in the time it takes to reach thermal equilibrium within the flow cell.

3.3 Discussion

In this chapter I described the development of a new TIRF microscopy-based assay to measure γTuRC-mediated microtubule nucleation in real-time. The tagged human γTuRC purified in this thesis enhanced microtubule nucleation over the level of spontaneous nucleation for all tested assay conditions, suggesting that the surface immobilized γTuRCs are active. Thus, the new assay set-up can for the first time distinguish microtubule nucleation by γTuRCs from microtubule elongation, and therefore allow direct quantification of the kinetics of γTuRC-mediated microtubule nucleation.

Purified human γTuRCs stimulated microtubule nucleation in a dose-dependent manner, and the number of nucleated microtubules increased linearly with increasing γTuRC densities. I found that the rate of γTuRC-mediated microtubule nucleation was proportional to the density of γTuRCs on the functionalized glass surface. This observation is in agreement with a previous study on γTuRC purified from *Drosophila melanogaster*, in which the number of microtubules nucleated at a given time point linearly correlated with the concentration of γTuRCs (Oegema et al., 1999).

In the literature, spontaneous microtubule nucleation in solution and γTuRC-mediated microtubule nucleation show a time lag for nucleation when measured by a spectrophotometric bulk assay (Carlier and Pantaloni, 1978; Caudron et al., 2000; Detrich et al., 1985; Himes et al., 1977; Johnson and Borisy, 1977; Lee and Timasheff, 1975, 1977; Murphy et al., 2001; Robinson and Engelborghs, 1982; Voter and Erickson, 1984). This time lag was interpreted as a kinetically unfavourable assembly step of the microtubule nucleus (Carlier and Pantaloni, 1978; Voter and Erickson, 1984). For spontaneous microtubule nucleation in the absence of γTuRC, the time lag was found to be in a range of 50 sec up to 10 min. The length of the time lag was shown to decrease with increasing tubulin concentration (Carlier and Pantaloni, 1978; Caudron et al., 2000; Detrich et al., 1985; Himes et al., 1977; Johnson and Borisy, 1977; Lee and Timasheff, 1975, 1977; Robinson and Engelborghs, 1982; Voter and Erickson, 1984). The time lag for γTuRC-mediated microtubule nucleation has been shown to decrease with increasing γTuRC concentration and ranges from 5 min to 10 min (Murphy et al., 2001). Using the new assay set-up to directly measure the microtubule nucleation kinetics of γTuRCs, I found that microtubule numbers increased linearly over time. In some experiments I found a short nonlinear phase at the beginning of the nucleation reaction. Analysis of this nonlinear phase revealed no correlations with the surface density of γTuRC or the tubulin concentration in the assay. Therefore, it is unlikely that such nonlinear

phase in the beginning of the nucleation assay represents a time lag for nucleation but rather other factors that affected the nucleation rate such as insufficient heating of the flow cell. This also explains the discrepancies of the lag phase duration between experiments. The different observations between the two assay set-ups may be caused by the fact that the bulk assay does not directly measuring nucleation kinetics. Rather, the bulk assay measures the change of turbidity in a sample caused by an overall increase of microtubule polymer mass due to nucleation and polymerization. The relative contribution of nucleation and microtubule polymerization to the final signal might be the reason for the time lag in bulk experiments. The presence of a time lag for these assays does not exclude that γTuRC nucleates microtubules at constant probability.

I estimated the number of γTuRC molecules in a field of view (164 µm x 164 µm) from measurements of mBFP fluorescence on the glass surface. At the highest γTuRC concentration (373 pM) used in this assay, ~47,000 molecules of γTuRC should be present. This would mean that under my assay conditions at the highest tubulin concentration tested (20 µM), around 1% of γTuRCs nucleate a microtubule during a period of 5 min. The low nucleation efficiency for the γTuRC found in this thesis is in agreement with previous attempts to reconstitute microtubule nucleation by purified complexes *in vitro*. Indeed, studies have shown that purified γTuRC was unable to fully recover microtubule nucleation from salt stripped centrosomes (Choi et al., 2010; Gunawardane et al., 2000; Gunzelmann et al., 2018; Kollman et al., 2010, 2015; Leong et al., 2019; Lin et al., 2016, 2014; Moritz et al., 1998; Oegema et al., 1999; Thawani et al., 2018; Tovey and Conduit, 2018; Zheng et al., 1995). The low efficiency of γTuRC-mediated microtubule nucleation *in vitro* was interpreted in the literature as the lack of regulatory factors that might activate the γTuRC for nucleation or promote microtubule nucleation from γTuRCs by regulating the dynamicity of microtubules (Farache et al., 2018; Kollman et al., 2011; Tovey and Conduit, 2018).

Nevertheless, the low nucleation efficiency found in this thesis could also be due to purified γTuRCs being 'damaged' or inactive. To differenciate between γTuRC-mediated microtubule nucleation being a stochastic process of low probability or γTuRCs being inactive, it would be interesting to directly observe microtubule nucleation from individual γTuRCs under my assay conditions. This would allow me to directly test if all γTuRCs are in principal able to nucleate a microtubule if given sufficient time. However, I did not see saturation of the quantified nucleation rates even at the highest tubulin concentration tested. Therefore, it is unlikely that a large fraction of the purified γTuRC is inactive. In summary, my results suggest that there is a finite and constant probability for γTuRC to produce a microtubule within a given

time period and assay conditions. This observation is also in agreement with a recent publication that found that nucleation from microtubule seed templates is stochastic (Wieczorek et al., 2015).

Recently it was suggested that templated microtubule nucleation, similar to spontaneous microtubule nucleation, faces a kinetic barrier (Wieczorek et al., 2015). In that study, the nucleation of microtubules from microtubule seeds occurred at a minimal tubulin concentration of 6 μM, which is substantially more efficient than spontaneous nucleation in absence of templates (>20 μM) but also significantly higher than the lowest tubulin concentration needed for the elongation of existing microtubules ~1 μM. This means that a microtubule seed has a reduced ability to elongate microtubules compared to a growing microtubule end, which indicates the presence of a kinetic barrier for microtubule nucleation from this type of template (Wieczorek et al., 2015). The authors tested this prediction by initiating microtubule nucleation from seeds at high tubulin concentrations (15 μM) and then exchanging the solution to a tubulin concentration below the critical concentration for nucleation (4 μM). Seeds readily nucleated at the high tubulin concentration and continued to elongate at the low tubulin concentration but failed to nucleate again after catastrophe occurred (Wieczorek et al., 2015).

Under my assay conditions, I found that γTuRCs fail to nucleate microtubules within 20 min if the tubulin concentration is below ~7.5 μM tubulin. However, the estimated critical tubulin concentration supporting microtubule growth under my assay conditions is around ~2 μM tubulin. This result suggests that the minimal concentration of tubulin required for microtubule nucleation from γTuRCs is also in between the concentration needed for microtubule elongation and the concentration supporting spontaneous microtubule nucleation. Together, these results indicate that γTuRC-mediated microtubule nucleation is also thermodynamically unfavourable, similar to microtubule seed templates. These results imply that a microtubule nucleus must assemble on the γTuRC before elongation can occur. Why templates might have a reduced ability to elongate a microtubule compared to an already growing microtubule end is not known. It was speculated that the kinetic barrier for templated microtubule nucleation is a consequence of a structural mismatch between curved tapered growing ends and blunt straight templates or differences in the nucleotide state (Brouhard and Rice, 2018; Wieczorek et al., 2015).

I estimated the size of the nucleus from the kinetic data obtained from γTuRC-mediated microtubule nucleation experiments at different tubulin concentrations and found that at least ~7 tubulin dimers need to assemble on the γTuRC before a microtubule can elongate. The nucleus size obtained for γTuRC-mediated

microtubule nucleation is similar to previous estimates of the nucleus size for spontaneous microtubule nucleation from kinetic bulk measurements (nucleus size between 5 to 20 tubulin dimers) (Flyvbjerg and Jobs, 1997; Voter and Erickson, 1984). This result indicated that the higher efficiency of γTuRC-mediated microtubule nucleation might be due to the more efficient formation of the nucleus on a template compared to nucleation in solution.

In summary, the TIRF microscopy-based γTuRC nucleation assay developed in this thesis represents a useful tool for the study of the mechanisms of templated microtubule nucleation by γTuRC. Measurement of individual microtubule nucleation events in real time allowed, for the first time, the direct quantification of the kinetics of γTuRC-mediated microtubule nucleation. To my knowledge, this is the most detailed kinetic study of purified γTuRC to date. I found that γTuRC-mediated microtubule nucleation is stochastic and that a kinetic barrier is apparently responsible for the low nucleation efficiency of the γTuRC *in vitro*.

The efficiency of γTuRC-mediated microtubule nucleation is proposed to be regulated by different mechanisms including a conformational change, activation by direct binding partners and proteins modulating microtubule dynamicity. In the next chapter I will apply the developed microtubule nucleation assay to study the regulation of γTuRC by intracellular factors proposed in the literature to promote microtubule nucleation from γTuRCs (Alfaro-Aco et al., 2017; Choi et al., 2010; Gunzelmann et al., 2018; Leong et al., 2019; Lin et al., 2016; Roostalu et al., 2015; Thawani et al., 2018; Wieczorek et al., 2015).

4. Study of γTuRC regulation

4.1 Introduction

In cells, γTuRC-mediated microtubule nucleation is tightly regulated in space and time. An open question is how cells achieve this level of control over the formation of new microtubules. As γTuRC activity is closely linked to its localization to MTOCs, a prominent hypothesis is that the γTuRC is activated by factors which attach the γTuRC to cellular structures (γTuRC binders). Cells might also regulate γTuRC activity by MAPs, such as microtubule polymerases or anti-catastrophe factors, to support microtubule nucleation by γTuRCs (microtubule binders). The molecular mechanism of regulation and the interplay between the different regulatory factors of the γTuRC are not well understood. To establish a framework for γTuRC regulation several groups have started to dissect the complex intracellular regulatory network by *in vitro* studies (see Table 2 for an overview of *in vitro* studies performed with purified proteins from different organisms). Here I focus on the regulation of the γTuRC from higher eukaryotes, particularly of human γTuRC.

Among the γTuRC-binders, CDK5Rap2 is a strong candidate for the regulation of the human γTuRC. This protein is implicated in the centrosomal attachment of γTuRCs in cells and contains an evolutionary conserved domain termed γTuNA (CM1-domain). γTuNA was previously shown to stimulate γTuRC-mediated microtubule nucleation *in vitro* in two independent studies using purified proteins from human cells (Choi et al., 2010; Muroyama et al., 2016). It has also been reported that overexpression of γTuNA induces spatially random nucleation when overexpressed in human cells and fission yeast (Choi et al., 2010; Cota et al., 2017; Lynch et al., 2014). A current hypothesis suggests that CDK5Rap2 might induce the conformational change needed for the γTuRC to switch from an ‘off-state’ into a nucleation active template (Kollman et al., 2011).

More recently, the γTuRC binder Mozart1 (Mzt1) has been found to have a function in γTuRC regulation (Cota et al., 2017; Lin et al., 2016). This small protein copurifies with the γTuRC from higher eukaryotes and was shown to bind directly to γTuRC subunits at their N-terminal regions (Cota et al., 2017; Cukier et al., 2017; Dhani et al., 2013; Janski et al., 2012; Lin et al., 2016; Masuda et al., 2013; Nakamura et al., 2012). So far, *in vitro* studies have only been performed with purified proteins from *Candida albicans* and a stimulatory effect of Mzt1 on γTuRC-mediated microtubule nucleation was found (Lin et al., 2016). The interpretation of this observation proved

to be difficult as Mzt1 is also an essential stabilizer for the assembly of γTuSC into γTuRC, i.e. for the first step in the formation of a nucleation competent template (Lin et al., 2016; Masuda and Toda, 2016; Masuda et al., 2013). In human cells Mzt1 seems to modulate the interaction of γTuRC with other regulatory proteins, including CDK5Rap2 (Cota et al., 2017). If Mzt1 is also needed for γTuRC assembly, similar to the yeast γTuRC, is not known and contradicting results have been published (Cota et al., 2017; Lin et al., 2016). Therefore, the function of Mzt1 in the regulation of human γTuRCs remains to be determined.

Apart from activation of the complex itself, evidence from *in vivo* studies suggest that γTuRC-mediated microtubule nucleation is also promoted by the microtubule binders TPX2 and XMAP215 (Brunet et al., 2008; Garrett et al., 2002; Gruss et al., 2001, 2002; Popov et al., 2002; Tournebize et al., 2000; Wittmann et al., 2000). These two proteins can stimulate microtubule nucleation on their own or from stabilized microtubule seeds by different mechanisms explained by their distinct biochemical properties. While XMAP215 is thought to induce microtubule nucleation by processively catalysing the microtubule plus-end growth, TPX2 is an anticatastrophe factor known to stabilize lateral and longitudinal tubulin-tubulin interactions (Al-Bassam and Chang, 2011; Brouhard and Rice, 2018; Brouhard et al., 2008; Roostalu and Surrey, 2017; Roostalu et al., 2015; Schatz et al., 2003; Wieczorek et al., 2015; Zhang et al., 2017). It has been proposed that TPX2 and XMAP215 accelerate the maturation of blunt templates such as the γTuRC into tapered structures similar to growing microtubule ends (Brouhard and Rice, 2018; Wieczorek et al., 2015).

In vitro, the budding yeast XMAP215 homologue Stu2 increases the efficiency of γTuRC-mediated microtubule nucleation by 3-fold. *Xenopus laevis* XMAP215 was also shown to increase γTuRC-mediated microtubule nucleation. Both publications also reported that the deletion of a potential γTuRC-binding domain on the C-terminus of the microtubule polymerases completely abolishes the stimulatory effect of XMAP215/Stu2 on γTuRC activity. The hypothesis was proposed that binding of XMAP215 to γTuRC is a prerequisite for efficient synergistic microtubule nucleation (Gunzelmann et al., 2018; Thawani et al., 2018).

The effect of TPX2 on γTuRC-mediated microtubule nucleation has not yet been studied *in vitro* with purified proteins. Nevertheless, studies in *Xenopus* egg extract have shown that TPX2 is important for the regulation of γTuRC activity in microtubule branching and nucleation around chromatin (Alfaro-Aco et al., 2017; Petry et al., 2013; Scrofani et al., 2015). A recent domain analysis of *Xenopus laevis* TPX2 revealed a γTuRC-binding motif with sequence similarity to γTuNA at the C-terminus of TPX2. This domain was shown to be sufficient to induce branching microtubule

nucleation in Xenopus egg extract in the presence of γTuRCs. TPX2 was reported to bind directly to γTuRCs through a newly identified γTuNA-like motif. A phosphorylation deficient mutant of this motif surprisingly did not disrupt binding of TPX2 to γTuRC but completely abolished branching microtubule nucleation in extract (Alfaro-Aco et al., 2017).

Another major family of microtubule binders are end binding (EB) proteins which are known to selectively track the ends of growing microtubules (+TIP tracking proteins) *in vivo* (Akhmanova and Steinmetz, 2008; Busch and Brunner, 2004; Jiang and Akhmanova, 2011; Ligon et al., 2002; Mimori-Kiyosue et al., 2000). EBs contain a microtubule binding domain which is connected to a dimerization domain important for recruitment of other +TIP proteins (Bu and Su, 2003; Gimona et al., 2002; Hayashi and Ikura, 2003; Honnappa et al., 2005, 2009; Slep et al., 2005). Mammalian cells contain three differentially expressed members of the EB family (EB1, EB2 and EB3), which are implicated in different cellular functions and were recently shown to bind to spatially distinct sites at the microtubule tip (Ferreira et al., 2014; Gouveia and Akhmanova, 2010; Roth et al., 2019; Su and Qi, 2001). The tracking of growing microtubule ends by EBs depends on their ability to sense a conformational change within the tubulin lattice, which is linked to the GTPase cycle of tubulin. Currently it is speculated that EBs preferentially bind to the GDP-Pi-state, which represents a GTP post hydrolysis state with the phosphate not yet released (Maurer et al., 2011, 2012; Zanic et al., 2009; Zhang et al., 2015). Upon phosphate release, EBs lose their affinity to bind to the MT lattice, which leads to the well-known comet-like accumulation of EBs at the growing microtubule ends. Interestingly, higher EB concentrations were found to shrink the size of the comet and increase the catastrophe frequency of microtubules (Bieling et al., 2007; Maurer et al., 2011). A prominent hypothesis suggests that EBs are maturation factors which cause compaction of the microtubule lattice, thereby increasing the GTP hydrolysis rate. Consequently the GTP cap size decreases and leaves the microtubule more susceptible for catastrophe (Maurer et al., 2014; Vitre et al., 2008; Zhang et al., 2015). The role of EB proteins in microtubule nucleation is not well understood. In cells, EBs are implicated in the microtubule plus-end tracking of several γTuRC binders and microtubule binders including myomegalin, CDK5Rap2 and XMAP215 (Fong et al., 2017; Grimaldi et al., 2015; Kim and Park, 2018; Kronja et al., 2009; Li et al., 2012; Zanic et al., 2013). One study showed that EB1 and γTuRC are both important for spindle orientation and seem to have antagonizing effects (Bouissou et al., 2009). In line with this observation, EB1 was shown in a recent *in vitro* study to decrease the efficiency of templated microtubule nucleation from stabilized microtubule seeds (Wieczorek et al., 2015).

In summary, γTuRC-mediated microtubule nucleation can in principle be stimulated by two different mechanisms: i) the direct activation of γTuRC by the binding of regulatory proteins and ii) the effect of proteins on microtubule dynamics. The new real-time TIRF microscopy-based nucleation assay presented in this thesis will be applied in this chapter to study the effect of different γTuRC binders (γTuNA and Mzt1) and microtubule binders (chTOG, TPX2 and EB3) on the nucleation activity of human γTuRC. The new assay allows for the first time the simultaneous observation of individual microtubule nucleation events and microtubule elongation and therefore should help to elucidate the underlying mechanism of γTuRC regulation by different intracellular factors.

4.2 Results

4.2.1 γTuRC regulation by γTuRC-binders

I first tested if γTuRC-mediated microtubule nucleation can be stimulated by γTuRC binders. Two γTuRC binders are of particular interest, CDK5Rap2 and Mozart1 (Mzt1). CDK5Rap2 was previously reported to stimulate the activity of human γTuRC through binding to the complex via a small evolutionary conserved domain termed γTuNA. The effect of Mzt1 on γTuRC-mediated microtubule nucleation is less clear. While it seems to stimulate the nucleation efficiency of C. albicans γTuRC, the effect of Mzt1 on human γTuRC has not been investigated yet.

I purified GST-tagged γTuNA (amino acids 51-200) from *E. coli* and was able to purify a total of 34.8 mg (3.17 mg/mL) GST-γTuNA$^{51-200}$. Julian Gannon (Surrey group, The Francis Crick Institute) purified a total of 12.5 mg (3 mg/mL) GST-Mzt1 from 1 L of *E. coli* culture. A scheme of the constructs and commassie stained protein gels of the purified proteins are shown in Figure 4.1.

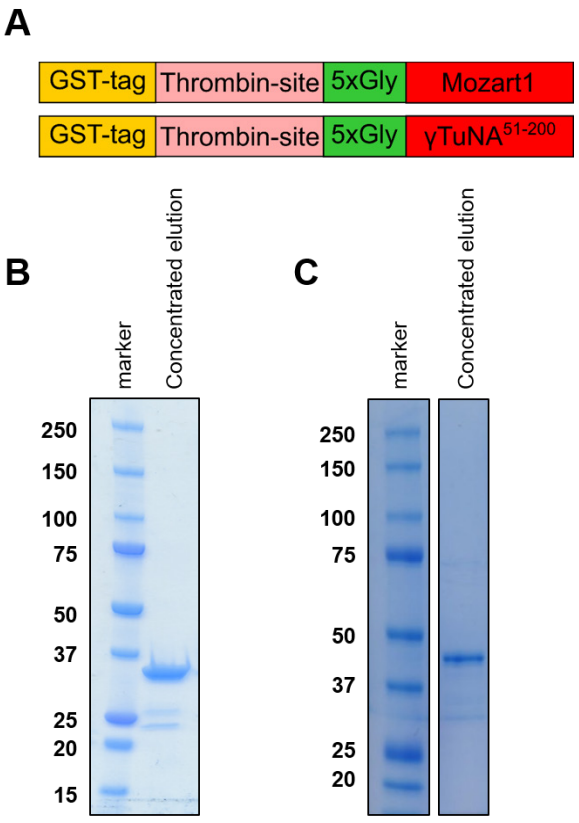

Figure 4.1: Purification of GST-tagged γTuRC binders. (A) Constructs used for protein expression. Coomassie stained protein gels of purified proteins. (B) GST-γTuNA$^{51-200}$ and (C) GST-Mzt1.

To study the function of regulatory proteins on γTuRC activity, proteins were included in the nucleation assay described in chapter 3 and the activity of γTuRC in the presence and in the absence of regulatory proteins was measured. Additionally, in control experiments I also measured the potential stimulation of spontaneous microtubule nucleation in the absence of γTuRCs but in the presence of the regulatory protein. A representative time series of microtubule nucleation by human γTuRC in the presence of either γTuNA or Mzt1 is shown in Figure 4.2. These experiments were performed at 10 µM tubulin with a γTuRC surface density obtained by preincubation of the functionalized glass surface with a γTuRC containing solution at a concentration of 373 pM. For comparison, a control in the presence of γTuRC but in the absence of either γTuNA or Mzt1 is shown (Figure 4.2, top panel). I could not observe a major stimulatory effect of any of the two proteins on γTuRC-mediated microtubule nucleation even though comparably high concentrations of the two proteins were used (500 nM). They also did not induce spontaneous microtubule nucleation (Figure 4.2, bottom panel).

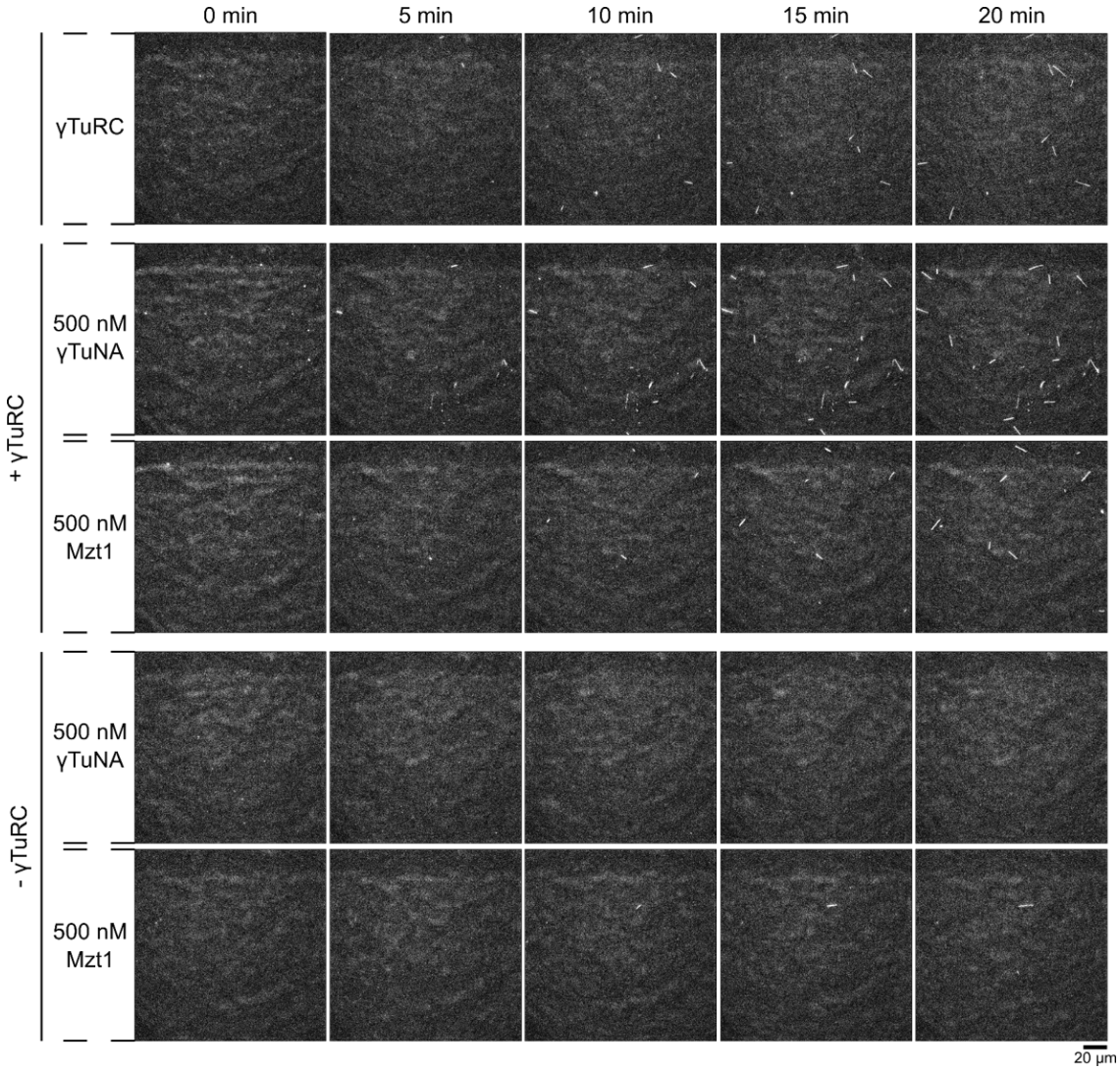

Figure 4.2: γTuRC-mediated microtubule nucleation in the presence of different γTuRC-binders. Representative time series of TIRF microscopy images of a microtubule nucleation reaction performed in the presence of 500 nM GST-Mzt1 or 500 nM GST-γTuNA at 10 µM tubulin and at a surface density corresponding to 373 pM γTuRC. Microtubule nucleation in the presence of γTuRCs but in the absence of γTuRC-binders (top panel) and spontaneous microtubule nucleation in the presence of 500 nM GST-Mzt1 or 500 nM GST-γTuNA (bottom panel) is shown for comparison. Field of view (164 µm x 164 µm). Images are shown with the same absolute intensity scale. Intensities in the images are directly comparable.

I quantified the number of nucleated microtubules at ten different time points in the field of view (164 µm x 164 µm) over the duration of the assay (20 min) and obtained the nucleation rates from linear regression analysis for assays performed in the presence of γTuRC-binders (Figure 4.3 A and B, black symbols). For comparison I quantified the nucleation rate for parallel controls performed in the presence of γTuRC but in the absence of γTuRC-binders (Figure 4.3 A and B, grey symbols). I found that γTuNA increased γTuRC nucleation efficiency by 1.3-fold. For Mzt1 I could not observe a statistically significant effect on γTuRC-mediated microtubule nucleation

under my assay conditions (Figure 4.3 E). To control for possible variations in the assay conditions I verified that the density of γTuRCs was comparable between the different experiments. I found no significant difference in the mBFP fluorescence intensity between different assays (Figure 4.3 C). I then measured the microtubule plus-end growth speeds to test if γTuRC binders have an effect on the microtubule growth velocity (Figure 4.3 D). I could not find a significant difference for microtubule growth speeds between the different assays, suggesting that γTuRC-binders have no effect on microtubule growth velocities.

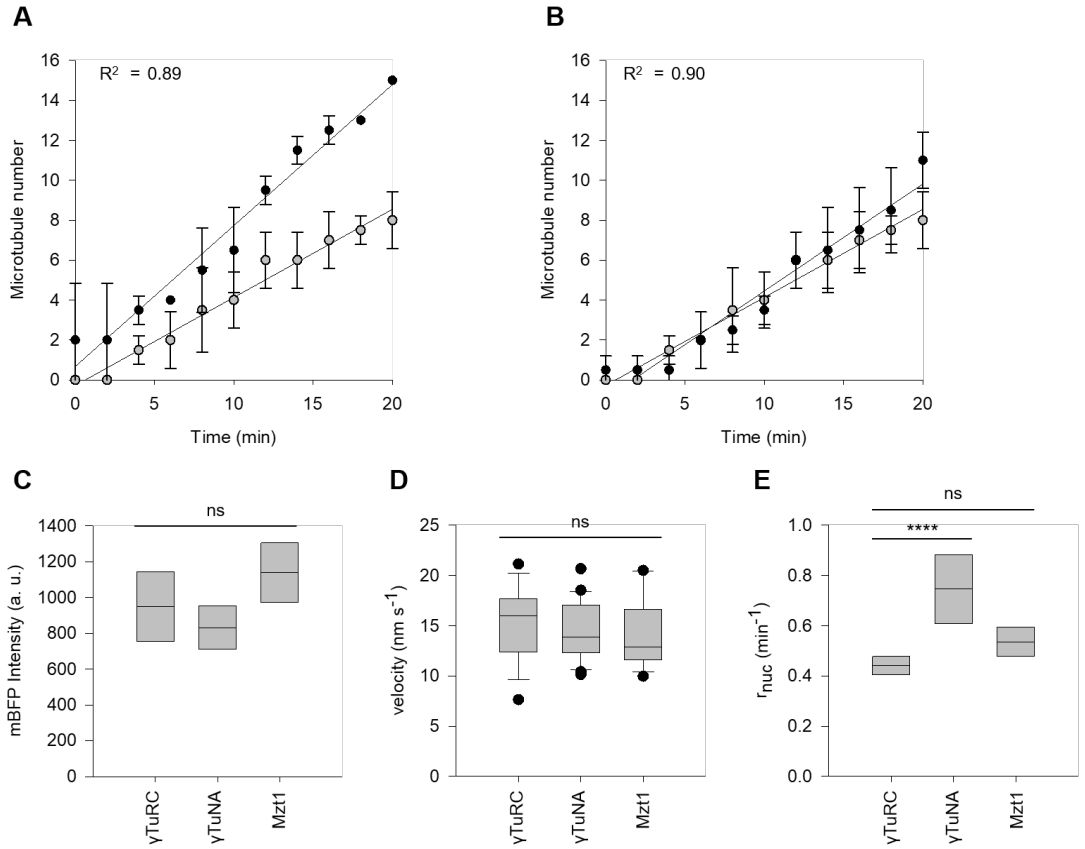

Figure 4.3: Quaracterization of γTuRC-mediated microtubule nucleation in the presence of γTuNA and Mzt1. Plot of the average microtubule number over time (n=2) in the presence of (A) 500 nM GST-γTuNA (black symbols) or (B) 500 nM GST-Mzt1 (black symbols) or in the absence of γTuRC-binders (grey symbols). Lines represent the linear regression. (C) Plot of the average γTuRC surface density (n=2) for each experiment. (D) Plof of the average microtubule plus-end growth velocity for each experiment: γTuRC control (n=18), 500 nM γTuNA (n=23), 500 nM Mzt1 (n=13). (E) Plot of the average microtubule nucleation rate. Experiments were performed at 10 µM tubulin in the presence of 373 pM γTuRC. Quantification was performed using ImageJ. Field of view (164 µm x 164 µm). All error bars represent the standard deviation. Statistical analysis was performed using F-test or unpaired t-test. Significant differences are shown (ns, not significant; *p<0.05; **p<0.01; ***p<0.001; ****p<0.0001).

In summary, γTuNA weakly stimulated γTuRC-mediated microtubule nucleation at relatively high protein concentration (500 nM). Mzt1 did not have an effect on the

efficiency of γTuRCs to nucleate microtubules under my assay conditions. Both proteins did not have an effect on the microtubule plus-end growth velocity.

4.2.2 γTuRC regulation by microtubule binders

4.2.2.1 chTOG promotes γTuRC-mediated microtubule nucleation in vitro

I next studied chTOG, a microtubule polymerase, which was suggested to enhance γTuRC-mediated microtubule nucleation by accelerating microtubule growth speeds. I supplemented the assay buffer with varying concentrations of mGFP-tagged chTOG (6.25 nM to 100 nM). chTOG-mGFP (from here onwards chTOG) was provided by Johanna Roostalu (Surrey group, The Francis Crick Institute). The construct is shown in Figure 4.4.

Figure 4.4: Scheme of cloning construct of chTOG-mGFP used in this thesis. Purification of chTOG-mGFP was conducted as described (Roostalu et al., 2015).

A representative time series of microtubule nucleation by human γTuRCs (373 pM) in the presence of three different chTOG concentrations and 10 µM tubulin is shown in Figure 4.5 (top three rows). I found that increasing the concentration of chTOG increased the number of microtubules nucleated by γTuRCs. Microtubules also grew faster and are longer in the presence of chTOG, which is in agreement with the function of chTOG as a microtubule polymerase (Brouhard et al., 2008; Roostalu et al., 2015). As reported previously, chTOG in the absence of γTuRCs only mildly induces spontaneous microtubule nucleation (Figure 4.5, bottom row) (Roostalu et al., 2015; Widlund et al., 2011). Interestingly, the background GFP-fluoresence intensity was higher in the control assay (absence of γTuRCs) compared to assays performed in the presence of γTuRCs at the same chTOG concentration (Figure 4.5, bottom two panels). For comparison, a parallel control in the presence of γTuRC but in the absence of chTOG is shown (Figure 4.5, top panel).

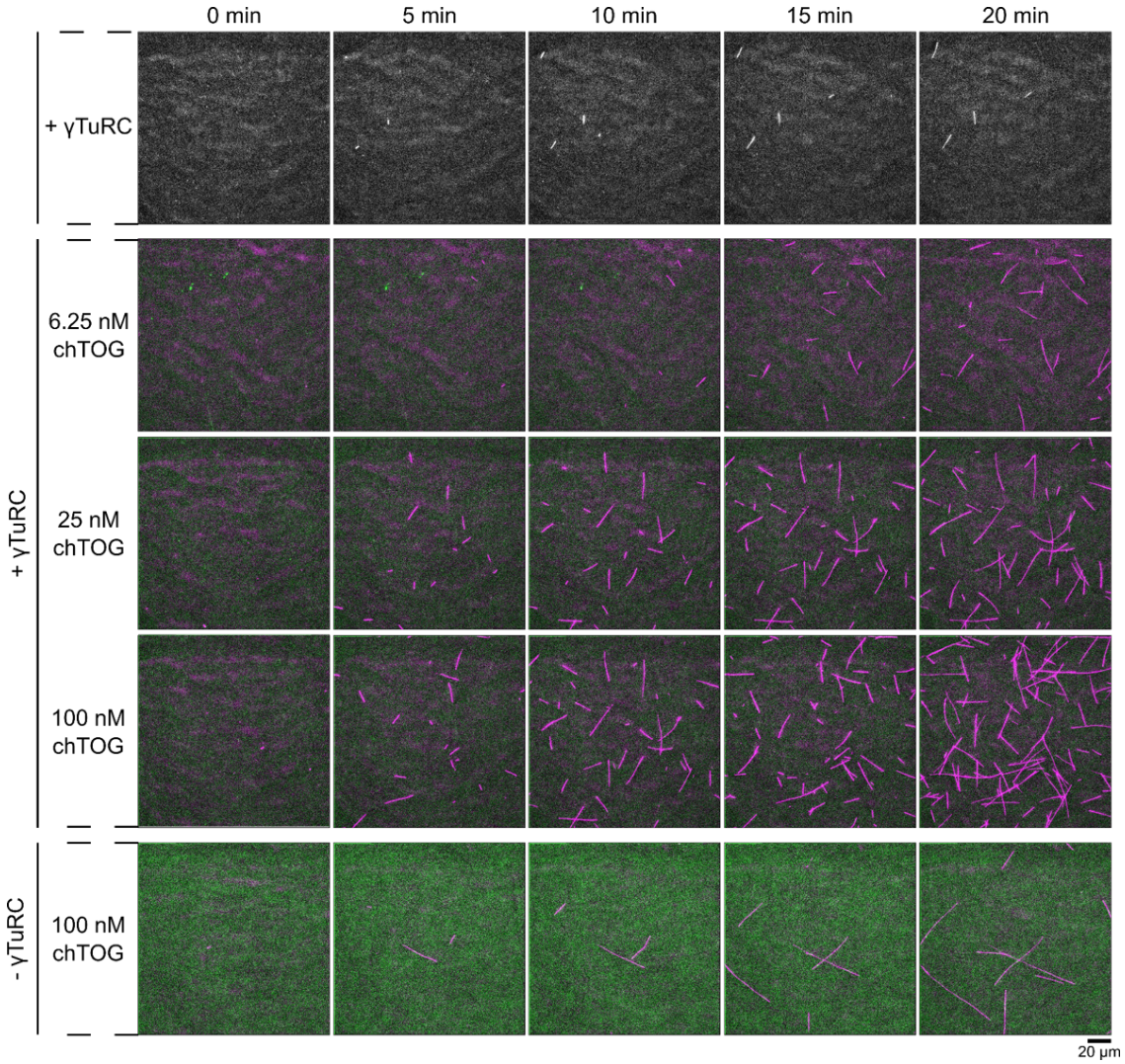

Figure 4.5: chTOG promotes microtubule nucleation by γTuRCs. Representative time series of merged TIRF microscopy images of a microtubule nucleation reaction performed in the presence of the indicated concentration of chTOG. Experiments were performed with mGFP-labelled chTOG at 10 µM tubulin and at a surface density corresponding to 373 pM γTuRC. Microtubule nucleation in the presence of γTuRCs but in the absence of chTOG (top panel) and spontaneous microtubule nucleation in the presence of 100 nM chTOG (bottom panel) is shown for comparison. Field of view (164 µm x 164 µm). Microtubules are shown in magenta, chTOG-mGFP is shown in green. Images are shown with the same absolute intensity scale. Intensities in the images are directly comparable.

The plot of microtubule number over time did not deviate from linearity for any of the tested chTOG concentrations (Figure 4.6, R^2 values as indicated). Nucleation rates were dependent on the chTOG concentration (note the different scales of the y-axis in Figure 4.6.) and increased from 1.1 to 5.4 microtubules per min from the lowest (6.25 nM) to the highest (100 nM) chTOG concentration. In other words, γTuRCs nucleate microtubules up to 12-fold more efficient in the presence of chTOG. The rate of microtubule nucleation by γTuRCs in the absence of chTOG is around 0.46 microtubules per min and is shown for comparison (grey symbols).

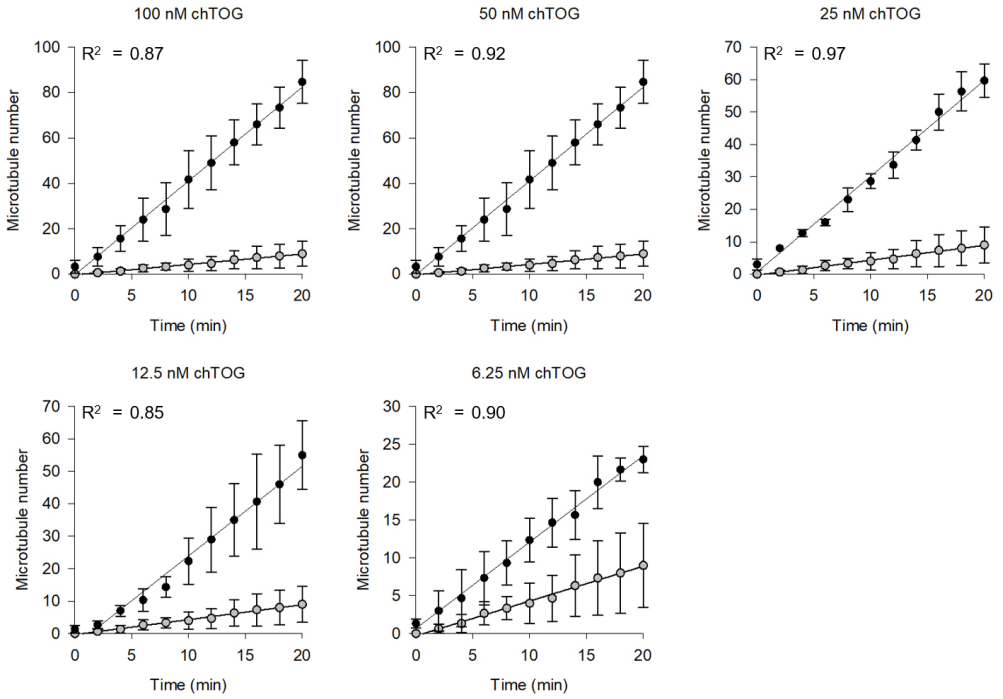

Figure 4.6: Quantification of γTuRC microtubule nucleation rates in the presence of different concentrations of chTOG. Plots of the average microtubule number over time (n=3) in the presence of different concentrations of chTOG (black symbols) and in the absence of chTOG (grey symbols). Experiments were performed at 373 pM γTuRC and 10 µM tubulin at the indicated chTOG concentration. Error bars represent the standard deviation. Lines represent the linear regression. R^2 as indicated.

For better visualization of the different nucleation rates obtained at different chTOG concentrations all plots from Figure 4.6 are combined and shown at the same scale in Figure 4.7 A. To confirm that the γTuRC surface densities were the same between the different chTOG concentrations and controls, I quantified the mBFP fluorescence intensity in the field of view (164 µm x 164 µm) and found no statistical difference between experiments (Figure 4.7 B).

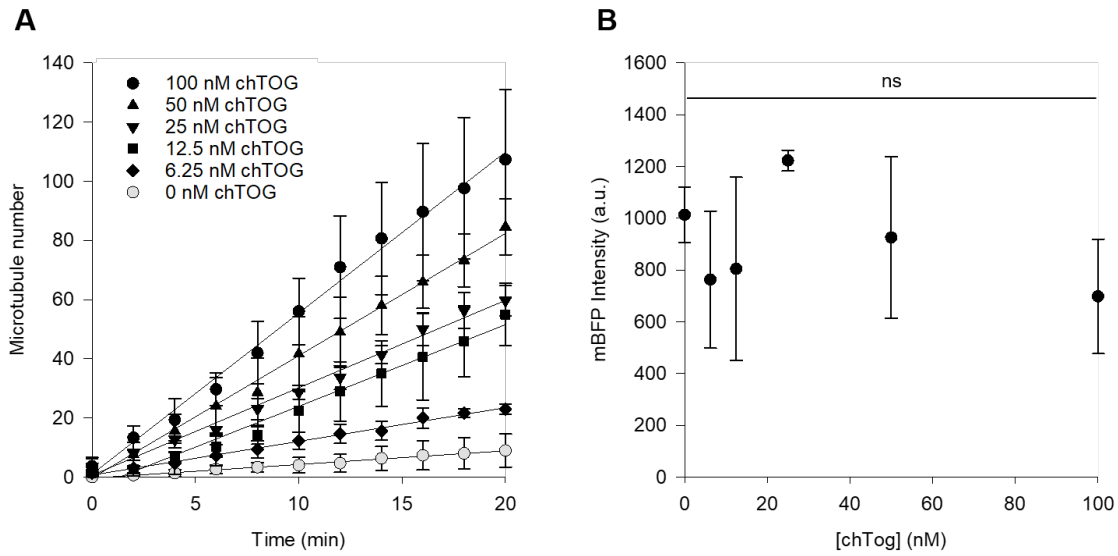

Figure 4.7: The microtubule nucleation rate is dependent on the chTOG concentration. (A) Plots of the average microtubule number over time (n=3) in the presence of different concentrations of chTOG (black symbols) and in the absence of chTOG (grey symbols). Concentrations of chTOG as indicated in the Figure. Experiments were performed in the presence of 10 µM tubulin and 373 pM γTuRC. Lines represent the linear regression. (B) Plot of the average γTuRC density (n=3) at different chTOG concentrations. Quantification was performed using ImageJ. Field of view (164 µm x 164 µm). All error bars represent the standard deviation. Statistical analysis was performed using F-test. Significant differences are shown (ns, not significant; *p<0.05; **p<0.01; ***p<0.001; ****p<0.0001).

Next I measured the microtubule plus-end growth rates for γTuRC-nucleated microtubules and plotted the velocity against the chTOG concentration (Figure 4.8 A). I found that microtubule plus-end growth increased with chTOG concentration with the curve starting to saturate at ~100 nM chTOG as expected from literature (Roostalu et al., 2015). Representative kymographs for all tested chTOG concentrations are shown in Figure 4.8 C. Higher chTOG concentrations showed a higher catastrophe frequency.

I found that the rate of microtubule nucleation by γTuRCs and the growth speeds show a very similar dependence on chTOG concentration. The nucleation rate increases steeply at lower chTOG concentrations and starts to saturate at ~100 nM chTOG (Figure 4.8 B).

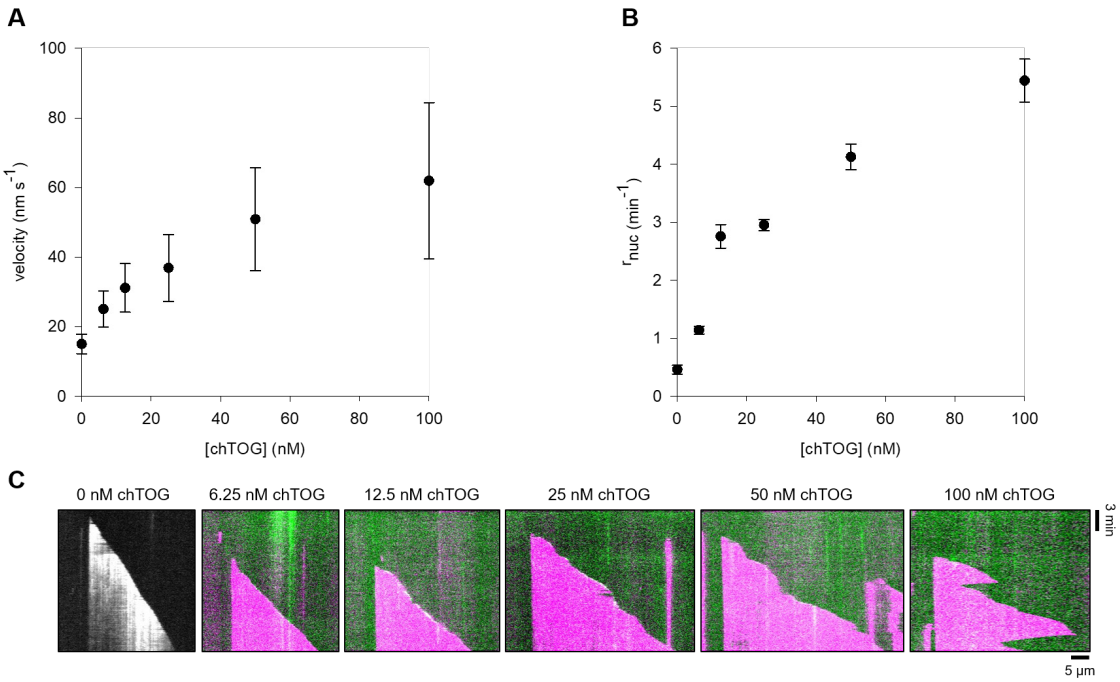

Figure 4.8: Dependence of growth speed and microtubule nucleation rate on the chTOG concentration. (A) Plot of the average microtubule plus-end growth velocity against chTOG concentration: 0 nM chTOG (n=19) 6.25 nM chTOG (n=50), 12.5 nM chTOG (n=138), 25 nM chTOG (n=125), 50 nM chTOG (n=204), 100 nM chTOG (n=194). (B) Plot of the average microtubule nucleation rate (n=3) against chTOG concentration. All error bars represent the standard deviation. (C) Representative kymographs for each chTOG concentration. Microtubules are shown in magenta, chTOG-mGFP is shown in green. Intensity is adjusted for best contrast and are not directly comparable.

To better understand how the change of growth speed by chTOG affects γTuRC-mediated microtubule nucleation, I plotted the nucleation rates against the growth velocity (Figure 4.9). I found that the increase in nucleation rate depends linearly on the growth velocity (R^2 value of 0.97), strongly suggesting that chTOG enhances microtubule nucleation by γTuRCs through its function as a microtubule polymerase. The extrapolation of the linear regression gives a growth velocity of 10.2 nm s^{-1}. This is lower than the growth velocity measured for the lowest tubulin concentration (7.5 µM) at which I could observe γTuRC-mediated microtubule nucleation within 20 min under my assay conditions.

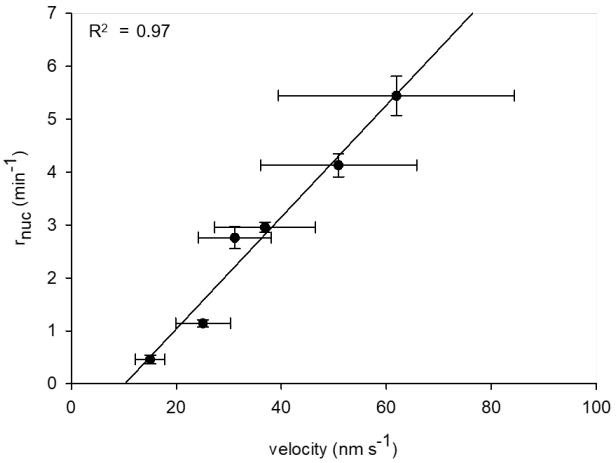

Figure 4.9: Dependence of γTuRC nucleation rate on microtubule plus-end growth velocity at different chTOG concentrations. Plot of the average nucleation rate (n=3) against the average microtubule plus-end growth velocity measured in the presence of different chTOG concentrations (6.25 to 100 nM). Error bars represent the standard deviation. The line represents the linear regression. R^2 value as indicated.

In agreement with recent publications on the effect of microtubule polymerases on γTuRCs from other organisms, I found that chTOG is able to stimulate microtubule nucleation by human γTuRCs in a dose-dependent manner (Gunzelmann et al., 2018; Thawani et al., 2018). Using the new microtubule nucleation assay I was able for the first time to directly demonstrate that microtubule nucleation by γTuRC is directly proportional to microtubule growth speeds in the presence of different chTOG concentrations. These results suggest that the acceleration of tubulin addition to the nascent microtubule formed on the γTuRC template promotes microtubule nucleation.

4.2.2.2 TPX2 promotes γTuRC-mediated microtubule nucleation in vitro

Next, I studied the effect of TPX2 on γTuRC-mediated microtubule nucleation. TPX2 was reported in the literature to enhance microtubule nucleation from stabilized microtubule seeds by preventing catastrophes (Wieczorek et al., 2015). To my knowledge, wheter TPX2 can directly promote microtubule nucleation by γTuRCs *in vitro* has not been studied yet.

To study TPX2 together with γTuRC in the new microtubule nucleation assay, I supplemented the assay buffer with mGFP-tagged TPX2 in a concentration range from 47 nM to 390 nM. mGFP-TPX2 (from here onwards, TPX2) was provided by Johanna Roostalu (Surrey group, The Francis Crick institute). The construct is shown in Figure 4.10.

Figure 4.10: Scheme of cloning construct of mGFP-TPX2 used in this thesis. Purification of mGFP-TPX2 was conducted as described (Roostalu et al., 2015).

A representative time series of microtubule nucleation by human γTuRCs (373 pM) in the presence of three different TPX2 concentrations and 10 µM tubulin is shown in Figure 4.11 (top three rows). I found that an increase in TPX2 concentration also increased the number of microtubules nucleated over time. TPX2 was found to bind to the microtubule lattice at all tested concentrations. The microtubules that nucleated in the presence of TPX2 did not undergo catastrophes and did not seem to grow faster than in control assays in absence of TPX2. Microtubules were found to bend in the presence of TPX2 as observed previously (Roostalu et al., 2015).

TPX2 is known to stabilize microtubule nucleation intermediates ('stubs') *in vitro* which fail to elongate into microtubules when nucleated by surface immobilized TPX2 (Roostalu et al., 2015). In my experiments, I could also observe some stubs on the surface. The formation of these stubs was independent on the presence of γTuRCs but dependent on the concentration of TPX2. I could also see microtubules growing from TPX2-stabilized stubs under my assay conditions. These microtubules grow from both ends in contrast to microtubules nucleated by γTuRCs and were excluded from the analysis. The spontaneous background nucleation for the highest TPX2 concentration in absence of γTuRC is shown in (Figure 4.11 bottom row). For comparison, a parallel control in the presence of γTuRC but in the absence of chTOG is shown (Figure 4.11, top panel).

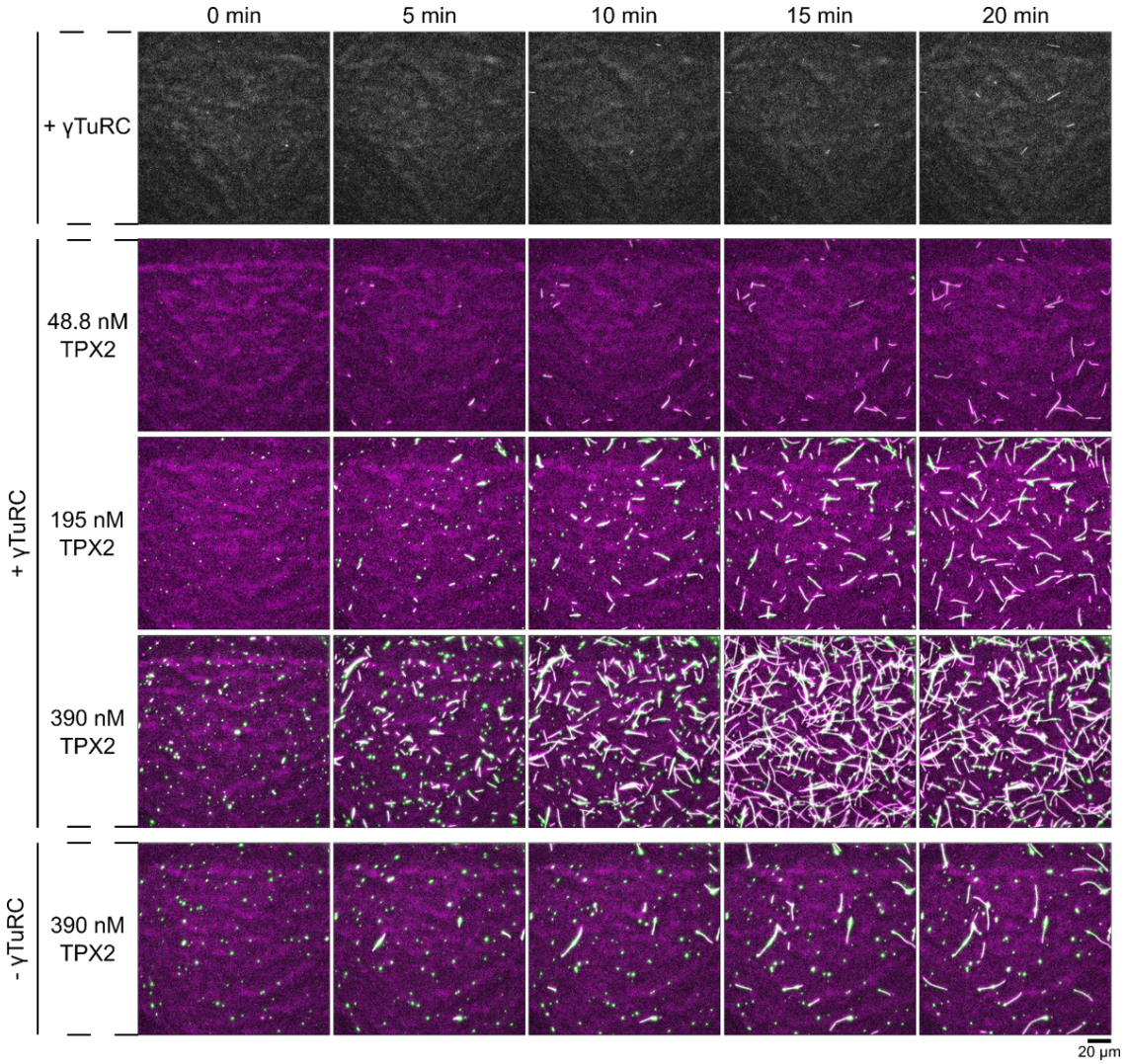

Figure 4.11: TPX2 promotes microtubule nucleation by γTuRC. Representative time series of merged TIRF microscopy images of a microtubule nucleation reaction performed in the presence of the indicated concentration of TPX2. Experiments were performed with mGFP-labelled TPX2 at 10 µM tubulin and at a surface density corresponding to 373 pM γTuRC. Microtubule nucleation in the presence of γTuRCs but in the absence of TPX2 (top panel) and spontaneous microtubule nucleation in the presence of 390 nM TPX2 (bottom panel) is shown for comparison. Field of view (164 µm x 164 µm). Microtubules are shown in magenta, chTOG-mGFP is shown in green. Images are shown with the same absolute intensity scale. Intensities in the images are directly comparable.

Quantification of microtubule nucleation kinetics and linear regression analysis again revealed a linear increase of microtubule number over time for all tested TPX2 concentrations (Figure 4.12, R^2 values as indicated). I found that the nucleation rate of γTuRC changes with the concentration of TPX2 in a dose dependent manner (note the different scales of the y-axis in Figure 4.12.). Nucleation rates varied between 1.3 microtubules per min and 9.9 microtubules per min for the lowest (48.8 nM) and highest (390 nM) TPX2 concentration tested. In the presence of TPX2, γTuRCs nucleate microtubules between 3- and 19-fold more efficiently. The rate of

microtubule nucleation by γTuRCs in the absence of TPX2 is around 0.53 microtubules per min and is shown for comparison (grey symbols).

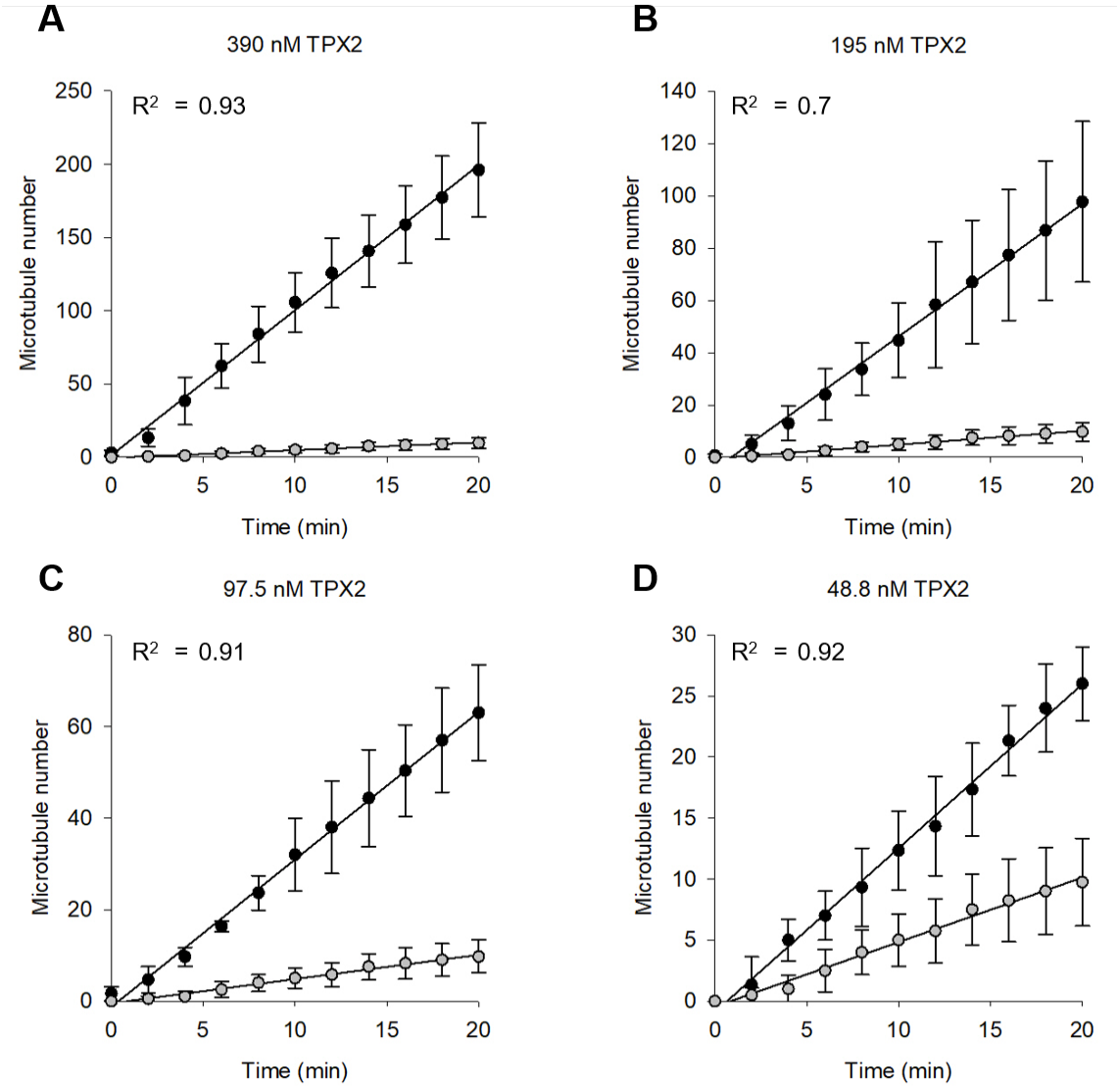

Figure 4.12: Quantification of γTuRC microtubule nucleation rates in the presence of different concentrations of TPX2. Plots of the average microtubule number over time (n=3) in the presence of different concentrations of TPX2 (black symbols) and in the absence of TPX2 (grey symbols). Experiments were performed at 373 pM γTuRC and 10 µM tubulin at the indicated TPX2 concentration. Error bars represent the standard deviation. Lines represent the linear regression. R^2 as indicated.

For better visualization of the different nucleation rates obtained at different TPX2 concentrations all plots from Figure 4.12 are combined and shown at the same scale in Figure 4.13 A. I verified that the γTuRC surface densities were comparable between the different experiments by quantification of mBFP fluorescence intensities (Figure 4.13 B)

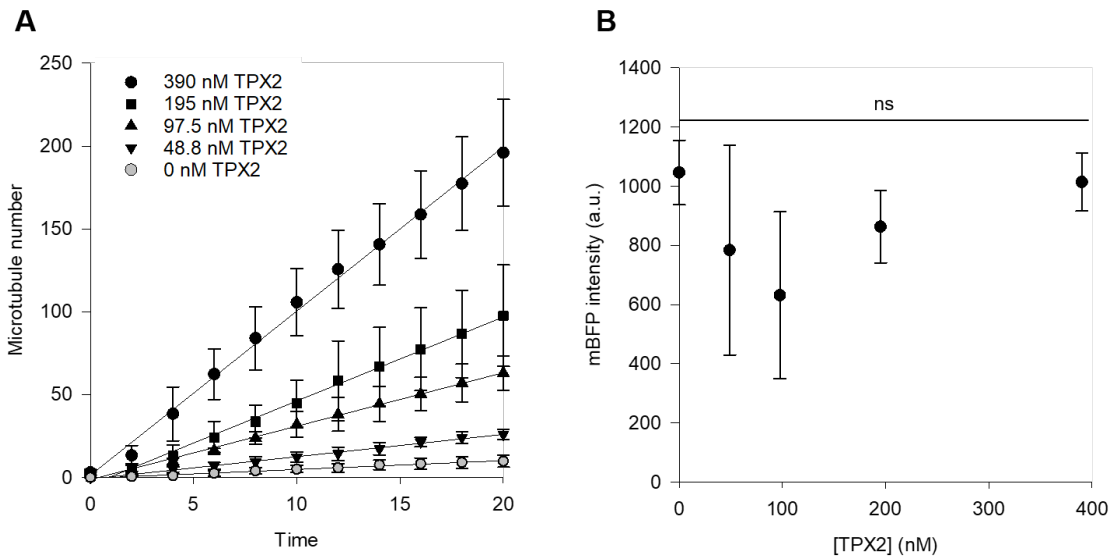

Figure 4.13: The microtubule nucleation rate is dependent on the TPX2 concentration. (A) Plots of the average microtubule number over time (n=3) in the presence of different concentrations of TPX2 (black symbols) and in the absence of TPX2 (grey symbols). Concentrations of TPX2 as indicated in the Figure. Experiments were performed in the presence of 10 µM tubulin and 373 pM γTuRC. Lines represent the linear regression. (B) Plot of the average γTuRC density (n=3) at different TPX2 concentrations. Quantification was performed using ImageJ. Field of view (164 µm x 164 µm). All error bars represent the standard deviation. Statistical analysis was performed using F-test. Significant differences are shown (ns, not significant; *p<0.05; **p<0.01; ***p<0.001; ****p<0.0001).

Next, I plotted the nucleation rate of γTuRCs against the TPX2 concentration in the assay (Figure 4.14 A). I found that the nucleation rate increased linearly with increasing TPX2 concentration. TPX2 has been shown to preferentially bind to microtubule ends but is known to bind to the whole microtubule lattice at high concentrations (Roostalu et al., 2015). I quantified the binding of TPX2 by measuring the GFP fluorescence intensity on γTuRC-nucleated microtubules at different TPX2 concentrations (Figure 4.14 B). I found that the binding of TPX2 to microtubules increased linearly with increasing TPX2 concentration. TPX2 is currently not known to have an effect on microtubule growth speed (Roostalu et al., 2015; Wieczorek et al., 2015). To verify that, I quantified the microtubule plus-end speeds of γTuRC-nucleated microtubules in the presence of TPX2 by kymograph analysis (Figure 4.14 C). Representative kymographs for all tested chTOG concentrations are shown in Figure 4.14 D. In contrast to the literature, the microtubule growth velocities increased weakly with increasing TPX2 concentration (Roostalu et al., 2015; Wieczorek et al., 2015).

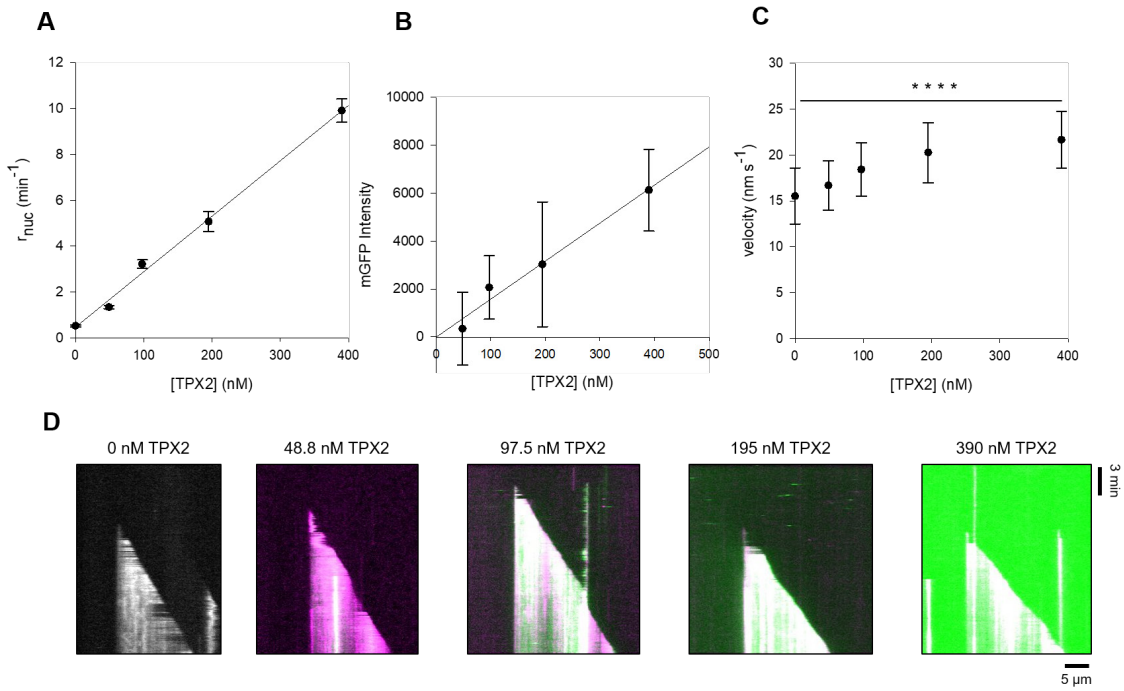

Figure 4.14: Dependence of growth speed and microtubule nucleation rate on the TPX2 concentration. (A) Plot of the average microtubule nucleation rate (n=3) against TPX2 concentration. (B) Plot of the average mGFP fluorescence intensity (n=3) against TPX2 concentration (C) Plot of the average microtubule plus-end growth velocity against TPX2 concentration: 0 nM TPX2 (n=27) 47 nM TPX2 (n=51), 97.5 nM TPX2 (n=49), 195 nM TPX2 (n=101), 390 nM TPX2 (n=106). All error bars represent the standard deviation. Statistical analysis was performed using F-test. Significant differences are shown (ns, not significant; *p<0.05; **p<0.01; ***p<0.001; ****p<0.0001). (C) Representative kymographs for each TPX2 concentration. Microtubules are shown in magenta, GFP-TPX2 is shown in green. Kymographs are shown with the same absolute intensity scale. Intensities in the images are directly comparable.

In summary, I found that TPX2 is able to promote microtubule nucleation by purified human γTuRCs *in vitro* in a dose-dependent manner without a strong effect on the microtubule growth velocity. This result suggests that TPX2 enhances microtubule nucleation by γTuRC through a distinct mechanism possibly related to its function as an anticatastrophe factor. My findings are in agreement with previous studies on spontaneous microtubule nucleation in the presence of TPX2, as well as nucleation from stabilized microtubule seed as templates which showed that TPX2 strongly enhances microtubule nucleation (Roostalu et al., 2015; Wieczorek et al., 2015).

4.2.2.3 Effect of EB3 on γTuRC-mediated microtubule nucleation

EBs are microtubule binding proteins which were shown to be anti-catastrophe factors *in vivo* (Komarova et al., 2009; Tirnauer et al., 2002). *In vitro*, EBs autonomously track growing microtubule-ends and were shown to stimulate catastrophes (Bieling et al., 2007; Vitre et al., 2008). Recently, it was shown that EB1 inhibits microtubule nucleation from microtubule seed templates (Wieczorek et al., 2015). Therefore, I next wanted to understand the potential effect of EBs on γTuRC-mediated microtubule nucleation.

For these experiments, I supplemented the assay buffer with GFP-tagged EB3 in a concentration range from 50 nM to 400 nM. GFP-EB3 (from here onwards, EB3) was provided by Johanna Roostalu (Surrey group, The Francis Crick institute). The construct is shown in Figure 4.15.

Figure 4.15: Scheme of cloning construct of GFP-EB3 used in this thesis. Purification of GFP-EB3 was conducted as described (Jha et al., 2017).

A representative time series of microtubule nucleation by human γTuRCs (373 pM) in the presence of three different EB3 concentrations and 12.5 µM tubulin is shown in Figure 4.16 (top three rows). In agreement with the literature, I could see microtubule plus-end tracking of EB3 at all tested concentrations (Bieling et al., 2007; Roth et al., 2019; Vitre et al., 2008). Microtubules in the presence of higher amounts of EB3 seemed more dynamic and showed more catastrophes. I could not observe a clear effect of EB3 on the number of microtubules nucleated in the presence of γTuRCs. For comparison, a parallel control in the presence of γTuRC but in the absence of EB3 is shown (Figure 4.16, top panel). Spontaneous microtubule nucleation in absence of γTuRC was low for all tested EB3 concentrations (Figure 4.16, bottom row).

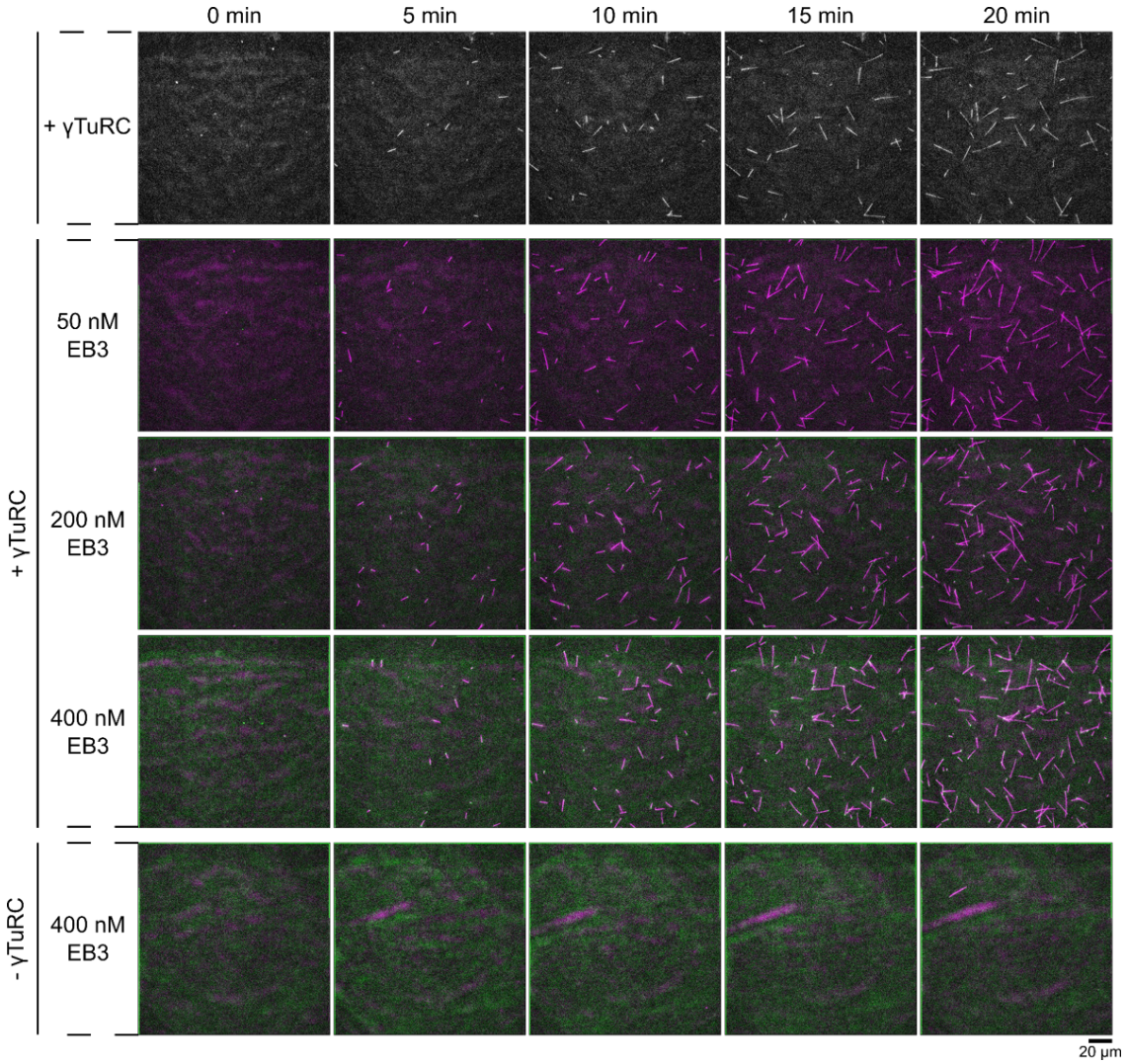

Figure 4.16: γTuRC-mediated microtubule nucleation in the presence of EB3. Representative time series of merged TIRF microscopy images of a microtubule nucleation reaction performed in the presence of the indicated concentration of EB3. Experiments were performed with mGFP-labelled EB3 at 12.5 µM tubulin and at a surface density corresponding to 373 pM γTuRC. Microtubule nucleation in the presence of γTuRCs but in the absence of EB3 (top panel) and spontaneous microtubule nucleation in the presence of 400 nM EB3 (bottom panel) is shown for comparison. Field of view (164 µm x 164 µm). Microtubules are shown in magenta, mGFP-EB3 is shown in green. Images are shown with the same absolute intensity scale. Intensities in the images are directly comparable.

I then quantified the number of microtubules nucleated by γTuRCs in the presence of different EB3 concentrations (Figure 4.16). For comparison increase of microtubule numbers in the presence of γTuRCs but in the absence of EB3 is also plotted in each Figure (grey symbols). Linear regression analysis revealed high R^2 values above 0.82 for all conditions confirming linearity.

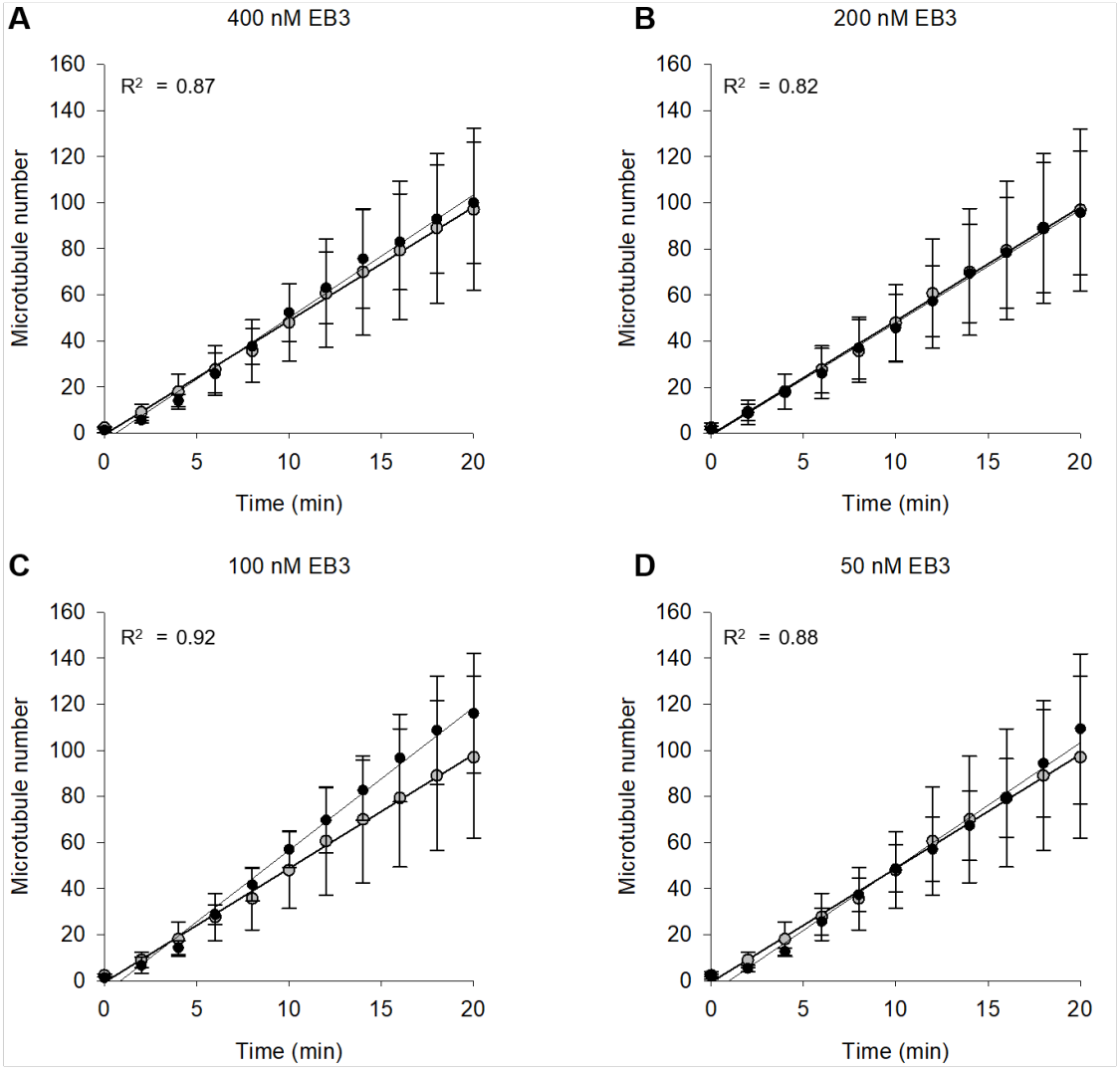

Figure 4.17: Quantification of γTuRC microtubule nucleation rates in the presence of different concentrations of EB3. Plots of the average microtubule number over time (n=3) in the presence of different concentrations of EB3 (black symbols) and in the absence of EB3 (grey symbols). Experiments were performed at 373 pM γTuRC and 12.5 µM tubulin at the indicated EB3 concentration. Error bars represent the standard deviation. Lines represent the linear regression. R^2 as indicated.

For better visualization of the similarity between the different nucleation rates obtained for the tested EB3 concentrations all plots from Figure 4.17 are combined and shown at the same scale in Figure 4.18 A. I could not find a statistical difference between nucleation rates obtained at different EB3 concentrations or in the absence of EB3 (Figure 4.18 B). To control for possible variations in the experiments, I first verified that the γTuRC density was the same (Figure 4.18 B). Then I analysed if EB3 has an effect on microtubule growth speeds by measuring the microtubule plus-end growth for all tested EB3 concentrations using kymograph analysis (Figure 4.18 D). I could not find a statistical difference in the mBFP fluorescence intensity or microtubule growth velocity for the different experiments. Representative kymographs

for all tested EB3 concentrations are shown in Figure 4.18 E. Higher EB3 concentrations increased the frequency of catastrophes as was previously reported for EB family members (Bieling et al., 2007; Komarova et al., 2009; Vitre et al., 2008). In summary, EB3 tracked growing microtubule ends under my assay conditions. EB3 did not have an effect on microtubule growth velocities but at high concentrations (>200 nM), EB3 increased the catastrophe frequency. I could not find an effect of EB3 on γTuRC-mediated microtubule nucleation.

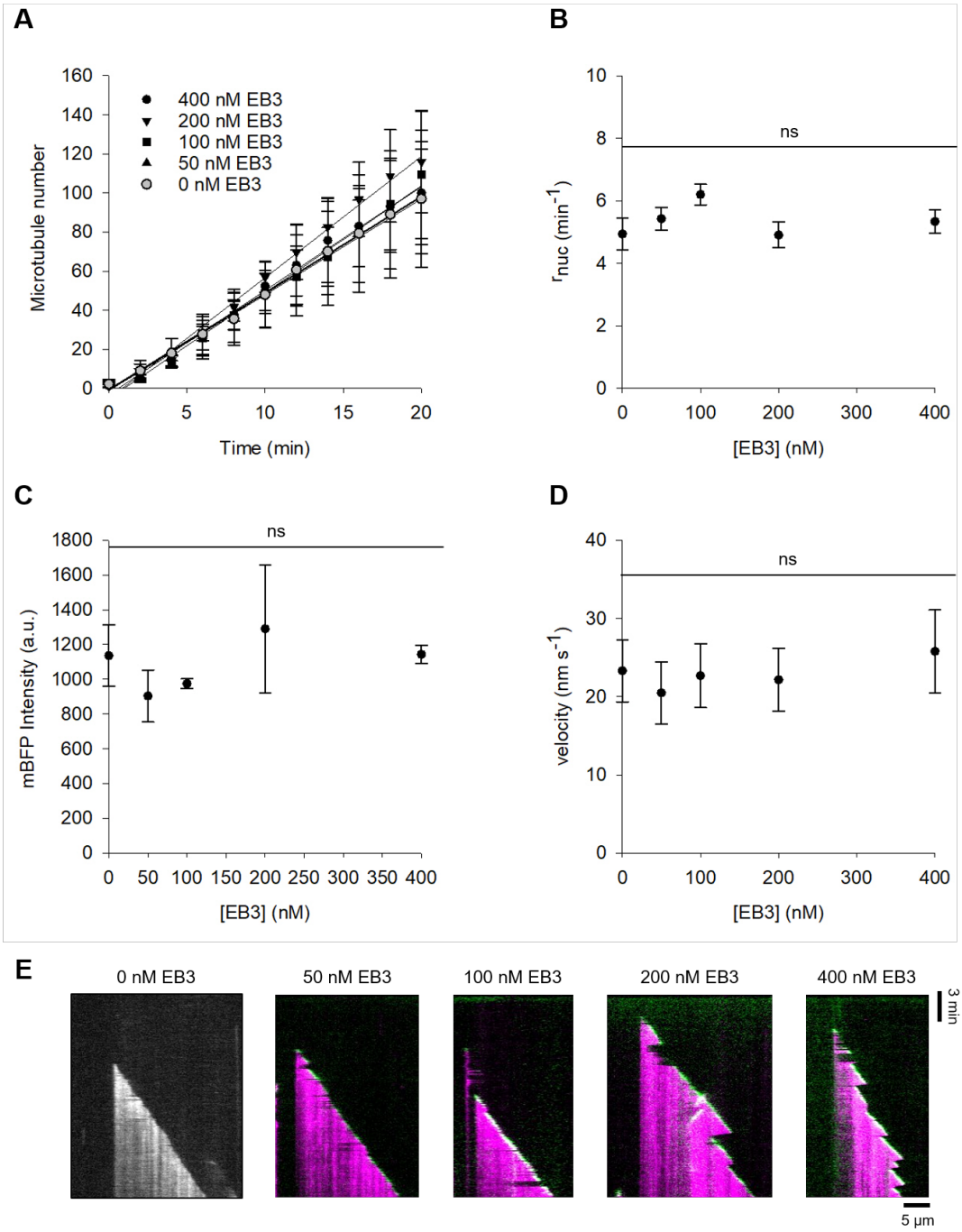

Figure 4.18: Characterization of EB3 in γTuRC-mediated microtubule nucleation. (A) Plot of the average microtubule number over time (n=3) in the presence of different EB3 concentrations. Concentrations of EB3 as indicated in the Figure. Lines represent the linear regression. (B) Plot of the average microtubule nucleation rate (n=3), (C) plot of the average γTuRC surface density (n=3) and (D) plot of the average microtubule plus-end growth velocity against EB3 concentration: 0 nM EB3 (n=177) 50 nM EB3 (n=50), 100 nM EB3 (n=138), 200 nM EB3 (n=125), 400 nM EB3 (n=204). Experiments were performed in the presence of 12.5 µM tubulin and 373 pM γTuRC. Quantification was performed using ImageJ. Field of view (164 µm x 164 µm). All error bars represent the standard deviation. Statistical analysis was performed using F-test. Significant differences are shown (ns, not significant; *p<0.05; **p<0.01; ***p<0.001; ****p<0.0001). (E) Representative kymographs for each EB3 concentration. Microtubules are shown in magenta, mGFP-EB3 is shown in green. Intensities are adjusted for best contrast and are not directly comparable.

4.3 Discussion

In cells, the γTuRC is thought to be regulated by activator proteins via a direct interaction. These might induce a conformational change which transforms the γTuRC from an inactive into an active nucleator. The γTuRC might be additionally or alternatively regulated by proteins that affect the dynamic properties of microtubules. These involve, for example, the acceleration of tubulin addition by microtubule polymerases or the increase of the microtubule lifetime by anticatastrophe factors (Brouhard and Rice, 2018; Farache et al., 2018; Roostalu and Surrey, 2017; Tovey et al., 2018). Due to the lack of assays that allow the observation of microtubule nucleation and elongation in real time, it has so far been impossible to simultaneously study the formation of new microtubules and microtubule dynamics. Therefore, it has been difficult to obtain direct information on the mechanisms that regulatory proteins employ to promote γTuRC-mediated microtubule nucleation. In this chapter, I applied the new microtubule nucleation assay developed in this thesis to study the regulation of human γTuRCs by different γTuRC-binders and microtubule binders.

4.3.1 Regulation of γTuRC by γTuRC binders

I first studied the roles of two γTuRC binders, CDK5Rap2 and Mzt1. Both are described in the literature to be potential allosteric activators of γTuRC (Choi et al., 2010; Cota et al., 2017; Dhani et al., 2013; Lin et al., 2016; Masuda and Toda, 2016; Nakamura et al., 2012). Specifically, I used the full-length Mzt1 and the evolutionary conserved domain of CDK5Rap2 that mediates binding of CDK5Rap2 to γTuRC (γTuNA) (Choi et al., 2010; Lin et al., 2015).

γTuNA was previously shown to stimulate microtubule nucleation by human γTuRCs *in vitro* and in cells (Choi et al., 2010; Cota et al., 2017; Muroyama et al., 2016). Here I found that 500 nM of γTuNA increased the nucleation efficiency of γTuRCs by 1.3-fold. This modest effect was unexpected, as it was previously shown that 10 nM of γTuNA enhance the microtubule nucleation activity of human γTuRCs by 7.1-fold *in vitro* (Choi et al., 2010). The different results could be due to differences in the assay conditions, e.g. differences between my assay buffer (BRB80 supplemented with 60 mM KCl, 0.02% Brij-35) compared to the published paper (BRB80) (Choi et al., 2010). The higher salt and the presence of detergent could decrease the binding of γTuNA to γTuRCs. Therefore, higher protein concentrations would be required to achieve the same stimulatory effect on γTuRC activity. Another reason for this discrepancy could be the expression system used to purify γTuNA. In the published experiments, γTuNA

was expressed and purified from human cells, while I expressed and purified γTuNA from *E. coli* (Choi et al., 2010). This means that the γTuNA used in this work lacks post-translational modifications which have been shown to be important for the stimulatory effect on γTuRC-mediated microtubule nucleation. Indeed, a phosphorylation-deficient mutant of γTuNA is unable to stimulate γTuRC-mediated microtubule nucleation in cells and *in vitro* (Choi et al., 2010; Cota et al., 2017; Muroyama et al., 2016). Thus, the phosphorylation of γTuNA/CDK5Rap2 seems to be crucial for its function and my experiments should therefore be repeated using eukaryotic protein expression systems, such as insect or human cells.

To my knowledge, the effects of Mzt1 on γTuRC-mediated microtubule nucleation have only been studied in yeast (Leong et al., 2019; Lin et al., 2016). In these publications, Mzt1 stimulated γTuRC activity in the presence of the yeast CDK5Rap2 homologues Spc110 or Mto1/2 (Leong et al., 2019; Lin et al., 2016). In *Candida albicans*, Mzt1 seems to bind to both γTuSCs and Spc110. γTuSCs and Spc110 also interact with each other independently. This 'bridging activity' of Mzt1 is thought to promote the oligomerization of γTuSCs into γTuRCs, which represents the first step for efficient microtubule nucleation (Lin et al., 2016). In contrast, Mzt1 in *Schizosaccharomyces pombe* has been shown to prevent the aggregation of γTuSCs and GCP3 but does not directly interact with Mto1. How Mzt1 increases microtubule nucleation efficiency of *Schizosaccharomyces pombe* γTuRCs is currently unknown, but it was suggested that it might be needed stabilize GCP3 within the γTuRCs (Leong et al., 2019).

In my hands, Mzt1 did not affect the microtubule nucleation activity of human γTuRCs. The protein used in this study was expressed and purified from *E. coli*. Therefore, the observed absence of an effect on γTuRC activity could potentially be due to the lack of post-translational modifications. However, it is currently not known if post-translational modifications are important for Mzt1 function (Teixidó-Travesa et al., 2012; Tovey and Conduit, 2018). The human γTuRC used in this thesis was found to contain Mzt2B (see Figure 2.23 for results from mass spectrometry analysis), which is a known paralogue of Mzt1. Mzt2B is thought to have an interphase specific role in γTuRC-mediated microtubule nucleation, while Mzt1 was shown to be important during interphase and mitosis (Hutchins et al., 2010; Teixidó-Travesa et al., 2010). Currently, it is not known how the binding of Mzt1 and Mzt2 to γTuRCs is regulated, e.g. whether Mzt1 and Mzt2 can bind to γTuRCs simultaneously, if they both bind to a different subset of γTuRCs or if there are cell type or cell cycle specific differences in the interaction of Mzt1 and Mzt2 with γTuRCs. It is therefore possible that the

endogenous Mzt2 might prevent the binding of the purified Mzt1 to γTuRCs under my assay conditions.

Alternatively, Mzt1 might not directly stimulate microtubule nucleation by human γTuRCs. It was recently suggested, that Mzt1 in human cells regulates the interaction of other regulatory proteins with γTuRCs (Cota et al., 2017). Overexpression of γTuNA in human cells strongly stimulates γTuRC-dependent microtubule nucleation at random locations in the cytoplasm. This stimulatory effect was completely abolished when Mzt1 was simultaneously knocked down, strongly indicating that Mzt1 is mediating CDK5Rap2 binding to γTuRCs (Cota et al., 2017).

In summary, it would be interesting to repeat the experiments presented in this thesis using proteins purified from other sources to re-evaluate the potential role of γTuNA/CDK5Rap2 as γTuRC activators. It would also be interesting to study the combination of Mzt1, γTuNA/CDK5Rap2 and γTuRC in order to understand if Mzt1 regulates the interaction of γTuNA/CDK5Rap2 with γTuRCs.

4.3.2 Regulation of γTuRCs by microtubule binders

In the last part of this chapter, I studied the effects of three different microtubule binders, chTOG, TPX2 and EB3, on γTuRC nucleation activity. All three microtubule binders are known to affect the dynamic properties of existing microtubules, albeit in different ways (Akhmanova and Steinmetz, 2015; Gouveia and Akhmanova, 2010; Gruss and Vernos, 2004; Howard and Hyman, 2007; Jiang and Akhmanova, 2011).

chTOG, a microtubule polymerase, is known to accelerate microtubule growth speeds, while TPX2 is an anti-catastrophe factor that stabilizes microtubules (Roostalu et al., 2015). EBs are plus-tip tracking proteins, known to increase catastrophe frequency *in vitro* and in some studies were shown to mildly promote microtubule growth (Komarova et al., 2009; Roth et al., 2019; Zhang et al., 2015). To my knowledge, these proteins have not been studied in combination with human γTuRCs.

4.3.2.1 Effect of EB3 on γTuRC-mediated microtubule nucleation

Conflicting results about the function of EBs in microtubule nucleation were reported in the literature. High concentrations of EB1 and the fission yeast homologue Mal3, were shown to induce spontaneous microtubule nucleation in solution (Sandblad et al., 2006; Vitre et al., 2008). In contrast, EB1 at end-tracking concentrations was shown to decrease the nucleation efficiency from stabilized microtubule seeds

(Wieczorek et al., 2015). In my experiments, I did not observe a significant effect of EB3 on γTuRC-mediated microtubule nucleation.

The different effects of EBs on microtubule nucleation might be due to the different concentrations of EBs used in those publications. At high concentrations, EB is known to not only bind microtubule ends but also the microtubule lattice (Maurer et al., 2011). The nucleation promoting effect found at high EB concentrations might therefore be a consequence of microtubule stabilization by lattice binding as was suggested previously (Wieczorek et al., 2015).

In my experiments, I used EB3 concentrations that displayed microtubule end-tracking behaviour but in the vast majority of the cases did not induce microtubule catastrophes that led to complete microtubule depolymerization. Therefore, EB3 most probably does not prevent the formation of the microtubule nucleus on γTuRC templates. This could also explain why EB3 in my experiments did not affect γTuRC-mediated microtubule nucleation.

Alternatively, the position of the tag on the EB protein might be important. It was previously shown that EB1 tagged with GFP on the C-terminus or on the N-terminus depict different behaviours in cells (Skube et al., 2010). N-terminal-tagging of EB1 alters the cellular localization and EB1 shows reduced binding to microtubules compared to C-terminally tagged EB1 (Skube et al., 2010). It is therefore possible that the position of the tag also alters the observed effect of EBs on microtubule nucleation. The EB3 used in this thesis was tagged on the N-terminus while in the literature either the untagged yeast homologue Mal3 or C-terminally tagged EB1 was used (Sandblad et al., 2006; Vitre et al., 2008; Wieczorek et al., 2015). Alternatively, EB1 and EB3 might affect microtubule nucleation from different templates differently due to structural differences between microtubules nucleated from microtubule seeds and γTuRCs (Kollman et al., 2011; Meurer-Grob et al., 2001). To better understand the effect of EBs on microtubule nucleation by γTuRCs it would be interesting in the future to repeat the experiments shown in this thesis with C-terminally tagged or untagged EB1 and EB3.

4.3.2.2 Effect of chTOG on γTuRC-mediated microtubule nucleation

The microtubule polymerases *Xenopus laevis* XMAP215, budding yeast Stu2 and the human chTOG were shown to mildly stimulate spontaneous microtubule nucleation in solutions of purified tubulin and GTP (Ghosh et al., 2013; Gunzelmann et al., 2018; Roostalu et al., 2015). It has also been shown that XMAP215 stimulates templated microtubule nucleation from microtubule seeds (Wieczorek et al., 2015). More

recently, XMAP215 and Stu2 were shown to have an effect on the microtubule nucleation efficiency of purified γTuRCs *in vitro* (Gunzelmann et al., 2018; Thawani et al., 2018). It was suggested that the effect of the microtubule polymerases on nucleation efficiency is due to the accelerated formation of a microtubule on the γTuRC (Gunzelmann et al., 2018; Thawani et al., 2018). However, this could not be shown directly due to the limitations of the assays used in these studies. In agreement with the published results, I found that chTOG promoted microtubule nucleation by γTuRCs synergistically by up to 12-fold. Using the new microtubule nucleation assay developed in this thesis, I was able to show that the rate of microtubule nucleation by γTuRCs is directly proportional to the chTOG-dependent microtubule growth velocity. This result strongly supports the current hypothesis of the role of microtubule polymerases in microtubule nucleation. The fast addition of tubulin dimers onto γTuRC templates probably facilitates the formation of the nascent microtubule and its transformation from an unstable oligomer into a stable elongation competent microtubule (Brouhard and Rice, 2018; Roostalu and Surrey, 2017).

Previous *in vitro* studies reported that the binding of XMAP215 and Stu2 via their C-terminus to γTuRCs is a prerequisite for efficient synergistic microtubule nucleation (Gunzelmann et al., 2018; Thawani et al., 2018). While this has not been directly studied in this thesis, I could observe a lower background GFP-fluorescence intensity in the presence of immobilized γTuRCs compared to a control assay performed in the absence of γTuRCs at the same chTOG concentration. The decreased GFP-background fluorescence could potentially be due to FRET between mGFP-tagged chTOG and mBFP-tagged γTuRCs if they are in close proximity (Heim and Tsien, 1996). This observation could suggest that γTuRCs and chTOG bind to each other. In the future it would be interesting to repeat the experiments performed in this thesis with a C-terminally truncated version of chTOG to confirm the proposed binding of chTOG to γTuRCs and to study the functional consequence on γTuRC-mediated microtubule nucleation in the new assay set up.

4.3.2.3 Effect of TPX2 on γTuRC-mediated microtubule nucleation

TPX2 was shown to promote spontaneous microtubule nucleation in solutions of purified tubulin and GTP (Alfaro-Aco et al., 2017; Brunet et al., 2004; Roostalu et al., 2015; Schatz et al., 2003). Kinetic studies with surface immobilized TPX2 further showed that this protein stabilizes the formation of short microtubule stubs, which do not elongate into a microtubule (Roostalu et al., 2015). TPX2 has also been shown to increase the efficiency of microtubule nucleation from microtubule seeds by

decreasing the minimal tubulin concentration needed for microtubule polymerization (Wieczorek et al., 2015).

To my knowledge, the effect of TPX2 on γTuRC-mediated microtubule nucleation has not been studied *in vitro*. My experiments showed that TPX2 strongly promoted γTuRC-mediated microtubule nucleation by up to 19-fold without a strong effect on microtubule growth velocity. This result is in agreement with a biochemical characterization showing that TPX2 reduces microtubule catastrophes and depolymerization speed without a strong effect on microtubule growth speeds (Roostalu et al., 2015; Wieczorek et al., 2015). More recently, a structural study showed that TPX2 promotes the association of tubulin subunits by binding to both longitudinal and lateral tubulin-tubulin interfaces in the microtubule lattice (Zhang et al., 2017). In agreement with the literature, my results suggest that TPX2 increases γTuRC-mediated microtubule nucleation through a different mechanism than the increase of microtubule growth velocities.

It was suggested in the literature that the C-terminus of TPX2 binds directly to γTuRCs and that the binding is essential for γTuRC-dependent microtubule nucleation (Alfaro-Aco et al., 2017). In the future it would be interesting to study a C-terminally truncated version of TPX2 to test if direct binding of TPX2 to γTuRCs is required to stimulate γTuRC-mediated microtubule nucleation.

5. Concluding remarks

The function of the microtubule cytoskeleton depends on its ability to arrange into ordered arrays and on the dynamicity of the micorutubule network (Bartolini and Gundersen, 2006; Muroyama and Lechler, 2017; Sanchez and Feldman, 2017). In part, this is achieved through the spatiotemporal regulation of the formation of new microtubules by γTuRCs (Kollman et al., 2011; Teixidó-Travesa et al., 2012). How γTuRC templates the formation of a new microtubule remains poorly understood. Studies in cells and *in vitro* found that γTuRCs are not constitutively active, as purified γTuRCs are poor nucleators, and in cells γTuRCs only nucleate microtubules at specific subcellular locations (MTOCs) (Choi et al., 2010; Gunawardane et al., 2000; Gunzelmann et al., 2018; Kollman et al., 2010, 2015; Leong et al., 2019; Lin et al., 2016, 2014; Moritz et al., 1998; Oegema et al., 1999; Thawani et al., 2018; Tovey and Conduit, 2018; Zheng et al., 1995). This led to the proposition that the efficiency of γTuRC-mediated microtubule nucleation is regulated by multiple mechanisms including regulatory factors, post-translational modifications and/or a conformational switch (Farache et al., 2018; Kollman et al., 2011; Tovey and Conduit, 2018).

Major limitations of previous *in vitro* studies have been the difficulty to obtain sufficient amount of γTuRCs, especially from higher eukaryotic systems and the lack of available assays that allow direct visualization and quantification of microtubule nucleation by γTuRCs in real-time. In the context of this thesis, I established a new procedure for the purification of human γTuRCs from a stable cell line and developed a novel TIRF-microscopy based real-time microtubule nucleation assay.

he new purification protocol is based on the affinity purification of γTuRCs, which are fluorescently-tagged on the γTuRC subunit GCP2. The tagging of the γTuRC did not interfere with the intracellular localization of the complex, and the tagged subunit integrated into the γTuRC without completely replacing endogenous GCP2. Currently, I do not know the copy number of tagged GCP2 within the complex or if all complexes contain the same copy number. Further characterization of the tagged γTuRC is necessary to better understand the possible heterogeneity of my purified γTuRC sample. The new purification procedure was not able to yield a completely pure γTuRC sample. It is not clear if the additional proteins present at the end of the purification are potential γTuRC regulatory factors or contaminant proteins. Future experiments will be needed to determine if these proteins have a function in γTuRC-mediated microtubule nucleation. It could also be interesting to purify the complex

from cells arrested during mitosis instead of asynchronous cells to see if the same or different additional proteins are co-purified. This way it could be possible to identify other potential regulatory factors and obtain information about differences in the regulation of γTuRCs between mitosis and interphase.

The relatively high yield of human γTuRC that can be obtained using the new purification protocol potentially opens up the possibility to study the structure of the γTuRC using cryo-EM. To date there is only one high-resolution structure of the γTuRC from *Saccharomyces cerevisiae* available (Kollman et al., 2010, 2015). Yeast γTuRCs, however, only contain GCP2/3 and lack the additional GCP4/5/6 (Choy et al., 2009; Geissler et al., 1996; Knop and Schiebel, 1997; Kollman et al., 2008, 2010, 2015; Sobel and Snyder, 1995; Soues and Adams, 1998). A high-resolution structure of human γTuRCs containing all subunits could help to reveal the subunit composition and positions of the GCPs within the complex. Experiments with the yeast γTuRC proposed a conformational switch as a possible regulatory mechanism. If the conformational switch exists, wheter it is specific to yeast or a general regulatory mechanism and if it is induced by the interaction of γTuRCs with αβ-tubulins or the interaction of the complex with γTuRC-binders remains to be determined. Cryo-EM of the complex in the presence and in the absence of γTuRC binders before and after microtubule nucleation might be able to reveal how γTuRCs facilitate microtubule nucleation.

Classically, it was thought that all γTuRCs within the same organism have the same subunit composition. However, quantifications of γTuRC subunit composition estimated the copy number of GCP6 to be less than one per complex suggesting that not all γTuRCs contain GCP6. Pull-downs of γTuRCs from human cells show that GCP4/5/6 co-immunoprecipitate in all pairwise combinations (Murphy et al., 1998, 2001). However, a more recent publication reports that less GCP4 can be found when γTuRC is immunoprecipitated via GCP6 compared to γ-tubulin while the level of GCP5 remains the same (Hutchins et al., 2010). Another study found GCP6-containing complexes which are only slightly smaller than γTuRCs after depletion of GCP4 or GCP5 from human cells (Cota et al., 2017). Appart from the γTuRC core components, it was shown that γTuRCs in mouse keratinocytes mutually exclusively bind to either NEDD1 or CDK5Rap2 (Muroyama et al., 2016). Mzt1 in *Drosophila melanogaster* was shown to be only expressed in the testis and in *Arabidopsis thaliana*, Mzt1 might only associate with a subset of all γTuRCs (Nakamura et al., 2012; Tovey et al., 2018). Thogether, this led to the speculation that different subpopulations of γTuRCs might exist within an organism (Tovey and Conduit, 2018).

Future work will be needed to further assess the possible heterogeneity of γTuRCs and what is the functional relevance of this.

In the second part of this thesis, I described the development of a new real-time TIRF-microscopy based γTuRC-mediated microtubule nucleation assay. In this assay purified fluorescent γTuRCs are immobilized to functionalized glass surfaces via the biotinylated AviTag on the GCP2 subunit. The assay set-up is based on previously described TIRF-assays used to study microtubule elongation from surface immobilized microtubule seeds and spontaneous microtubule nucleation in the absence of γTuRCs (Bieling et al., 2007, 2010; Roostalu et al., 2015). Using the new assay, the nucleation of individual microtubules by surface immobilized γTuRCs in the presence of GTP and tubulin can be observed in real-time using standard TIRF-microscopy. This set-up allows to differentiate between γTuRC-mediated microtubule nucleation, spontaneous background nucleation and microtubule elongation in the same nucleation reaction and thus the direct quantification of the kinetics of microtubule nucleation by γTuRC. It also allows for the addition of regulatory factors to test their effect on the efficiency of γTuRC-mediated microtubule nucleation.

Using the new assay, I found that fluorescently-tagged γTuRCs are active and able to stimulate microtubule nucleation above the level of spontaneous nucleation. The microtubules nucleated by γTuRCs stayed capped throughout the whole duration of a typical assay (20 min). This observation is in agreement with the function of the γTuRC as template for microtubule nucleation (Kollman et al., 2011). The number of microtubules nucleated by purified γTuRCs depended linearly on the amount of complexes attached to the glass surfaces and strongly on the concentration of tubulin in the assay. My results are in agreement with previous publications that showed that the efficiency of γTuRC-mediated microtubule nucleation depends linearly on the concentration of the complex and non-linearly on the tubulin concentration in the assay (Oegema et al., 1999; Zheng et al., 1995). I found that the increase of microtubule numbers over time was linear for all experimental conditions. This result suggests that γTuRCs have a constant probability to nucleate a microtubule at a given time point. This is in agreement with a recent publication which found a constant probability for microtubule nucleation from microtubule seeds as templates (Wieczorek et al., 2015).

At the highest tested tubulin concentration (20 µM tubulin) only 1% of all γTuRCs in a given field of view were able to nucleate a microtubule within 5 min. While it was surprising to find that only a small subpopulation of γTuRCs are able to nucleate microtubules, this observation is also in agreement with previous studies that found that purified γTuRCs are poor microtubule nucleators *in vitro* (Choi et al., 2010;

Gunawardane et al., 2000; Gunzelmann et al., 2018; Kollman et al., 2010, 2015; Leong et al., 2019; Lin et al., 2016, 2014; Moritz et al., 1998; Oegema et al., 1999; Thawani et al., 2018; Tovey and Conduit, 2018; Zheng et al., 1995). However, it is difficult to compare the efficiency of γTuRC-mediated microtubule nucleation found in this thesis with published data as different assays and experimental conditions were used (tubulin concentrations, temperature, buffer conditions, see Table 2). Another major difference is that other studies use endogenous γTuRCs purified while the complex in this thesis was purified from a stable cell line overexpressing a tagged γTuRC subunit. While the cells did not show any obvious defects upon expression of tagged GCP2 I cannot exclude that the tagging of the γTuRC interferes to some extend with its function as a microtubule nucleator. Additionally, in my assay set-up tagged γTuRCs are bound via the AviTag to functionalized glass surfaces. The attachment of the complex could potentially also decrease the efficiency of the γTuRC to nucleate microtubules due to possible sterical hindrances. It could be interesting to compare the activity of tagged purified γTuRCs with the activity of endogeneous complex purified from the same cell type using a different assay set-up to better assess the impact of the tag or the surface attachment on γTuRC-mediated microtubule nucleation.

I could not observe microtubule nucleation within 20 min at tubulin concentrations lower than 7.5 µM under my assay conditions. This tubulin concentration is in between the minimal concentration supporting the elongation of an existing microtubule (~2 µM) and the tubulin concentration needed for efficient spontaneous microtubule nucleation (≤ 20 µM). A similar result has been reported for microtubule nucleation from microtubule seed templates and was interpreted as the presence of a kinetic barrier for templated microtubule nucleation (Wieczorek et al., 2015). My results therefore suggest that γTuRC-mediated microtubule nucleation is also thermodynamically unfavourable and that first a nucleus needs to assemble on the γTuRC before a microtubule can elongate (see Figure 5.1). This observation is interesting because it could indicate structural differences between growing microtubule ends and templates or differences in the nucleotide state as was suggested in the literature (Brouhard and Rice, 2018; Roostalu and Surrey, 2017; Wieczorek et al., 2015).

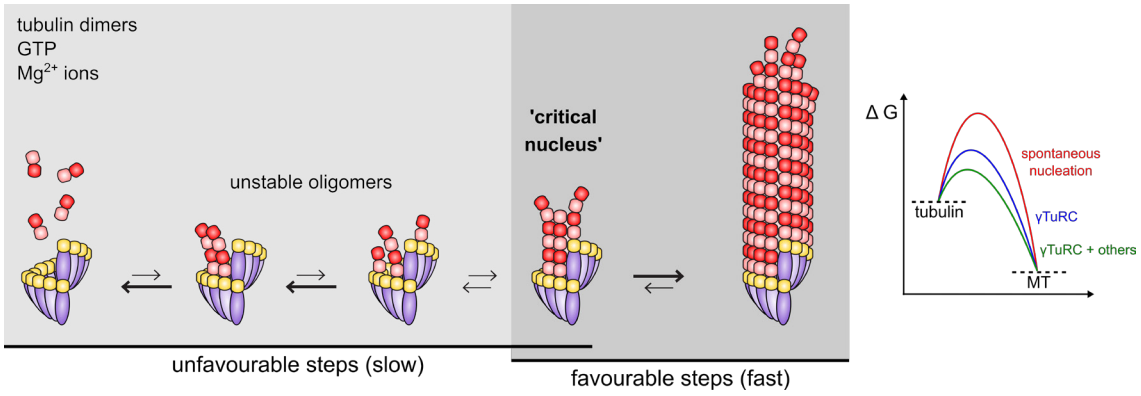

Figure 5.1: Hypothetical pathway of γTuRC-mediated microtubule nucleation. γTuRC-mediated microtubule nucleation might be hindered by a kinetic barrier. The kinetic barrier is lower than for spontaneous microtubule nucleation and can be further reduced by proteins which accelerate and/or stabilize the formation of the 'critical nucleus'.

An ongoing question in the field is the size of the 'critical nucleus' or the smallest stable tubulin oligomer which is needed to promote microtubule elongation. Using the kinetic data obtained from γTuRC-mediated microtubule nucleation experiments at different tubulin concentrations I estimated that the size of the critical nucleus in γTuRC-mediated microtubule nucleation is at least ~7 tubulin dimers. This nucleus size is similar to the estimates calculated from kinetic bulk measurements of spontaneous microtubule nucleation by spectrophotometry and kinetic models (nucleus size between 5 to 20 tubulin dimers) (Flyvbjerg and Jobs, 1997; Voter and Erickson, 1984). Measurements of spontaneously nucleated microtubule oligomers by negative stain electron microscopy report similar sizes in the range of three to a few tens of dimers in length (Mozziconacci et al., 2008; Portran et al., 2017; Voter and Erickson, 1984; Wang et al., 2005). While it remains unclear how accurate these estimations of the nucleus size really are, my result could indicate that the size of the critical nucleus for γTuRC templates is the same as for spontaneous nucleation. This suggests that the higher efficiency of the γTuRC to nucleate a microtubule compared to spontaneous microtubule nucleation is due to the more efficient formation of a critical nucleus due to the stabilization of tubulin dimer assembly by γ-tubulin. Notably, the nucleus size estimated from studies of microtubule nucleation from stabilized microtubule seeds using fluorescence microscopy and image analysis found that at least ~250 tubulin dimers need to assemble on the seed template before the microtubule switches to polymerization (Wieczorek et al., 2015). Currently, it is not known which of these methods is more accurate to estimate the size of the critical nucleus. Nevertheless, it is principally possible that the nucleus size varies between different templates as they have structural differences. For instance, microtubule

seeds present a β-tubulin surface and have a 14-protofilament structure, whereas γTuRC templates 13-protofilament microtubules and present a γ-tubulin surface (Kollman et al., 2011; Meurer-Grob et al., 2001). If the nucleus size varies between spontaneous nucleation and templated nucleation or between different templates will need further investigation.

γTuRCs can potentially be activated by different regulatory mechanisms including regulatory factors which directly bind to the complex and might induce a structural shift (Choy et al., 2009; Kollman et al., 2008, 2010, 2011, 2015). Alternatively, or additionally, the efficiency of γTuRC-mediated microtubule nucleation might be modulated by the activity of proteins that affect microtubule dynamics but do not necessarily directly interact with the complex (Alfaro-Aco et al., 2017; Brouhard and Rice, 2018; Gunzelmann et al., 2018; Roostalu and Surrey, 2017; Roostalu et al., 2015; Thawani et al., 2018; Wieczorek et al., 2015). Using the new assay, it is now possible to differentiate between a direct effect on the efficiency of γTuRC-mediated microtubule nucleation due to binding of a regulatory factor to γTuRC or a secondary effect due to changes in microtubule dynamicity, e.g. reduced catastrophe rates or accelerated microtubule growth velocities. The new microtubule nucleation assay allows to differentiate between these two possible regulatory mechanisms as microtubule nucleation and microtubule elongation can now be measured at the same time.

In the context of this thesis I studied the effect two known γTuRC-binders, Mzt1 and a fragment of CDK5Rap2 (termed γTuNA), on the activity of γTuRCs. In contrast to the literature, I only found a weak stimulatory effect of γTuNA on γTuRC-mediated microtubule nucleation (Choi et al., 2010; Muroyama et al., 2016). This result is most likely due to the lack of a phosphorylation site on γTuNA purified from *E. coli*. In my hands Mzt1, which also has been purified from *E. coli*, did not stimulate microtubule nucleation by γTuRCs. While this result might also be due to the lack of post-translational modifications it is also possible that Mzt1 does not have an effect on γTuRC-mediated microtubule nucleation. Alternatively, the Mzt2B, which co-purified with the γTuRC used in this thesis, might prevent the binding of recombinant Mzt1. More recently it was suggested that Mzt1 might bridge γTuRC and CDK5Rap2 together and thus regulates the activity of γTuRCs by modulating the binding of the complex with the activator (Cota et al., 2017). If Mzt1 only modulates the binding of CDK5Rap2 to γTuRCs or also the interaction of the complex with other regulatory factores remains to be determined. In the future it would be interesting to re-evaluate the role of these γTuRC binders on γTuRC activity individually and in combination.

Lastly, I studied the effect of three different microtubule binders, EB3, chTOG and TPX2, on γTuRC activity. I found that both chTOG and TPX2 synergistically increase the efficiency of γTuRC-mediated microtubule nucleation while EB3 was neutral. The results obtained for chTOG and TPX2 are in agreement with what has been observerd for microtubule nucleation from seed templates (Wieczorek et al., 2015). The synergistic effect of TPX2 and chTOG was interpreted in the literature as follows: the presence of γTuRC or other templates facilitates the formation of the weaker lateral contacts between incoming tubulin dimers which are less likely to form in solution. chTOG can than accelerate the longitudinal elongation of protofilaments which in turn increases the possibilities for lateral connections to form. Therefore, chTOG accelerates the transformation of an unstable oligomers into a stable nucleus (Brouhard and Rice, 2018; Roostalu and Surrey, 2017; Wieczorek et al., 2015). TPX2 instead did not show a strong effect on the microtubule plus-end growth velocity but is a known anti-catastrophe factor (Reid et al., 2016; Roostalu et al., 2015; Wieczorek et al., 2015). The effect of TPX2 on γTuRC-mediated microtubule nucleation might therefore be due to its activity as surpressor of microtubule dynamicity. TPX2 has also been shown to bind to lateral and longitudinal tubulin-tubulin interfaces (Zhang et al., 2017). The stimulatory effect of TPX2 could therefore also be due to TPX2 stabilizing tubulin-tubulin interactions.

In vitro experiments have shown that chTOG and TPX2 together can synergistically promote spontaneous microtubule nucleation in solution above the effect of the individual proteins (Roostalu et al., 2015). The synergy can be explained by the different mechanisms of how chTOG and TPX2 stimulate microtubule nucleation. It would be interesting to combine chTOG and TPX2 to observe their combined effect on microtubule nucleation by γTuRCs. Recently, it was suggested that both TPX2 and chTOG are also directly binding to γTuRCs, and that the binding is required to achieve the synergistic effect on microtubule nucleation (Alfaro-Aco et al., 2017; Gunzelmann et al., 2018; Thawani et al., 2018). While my results did not clearly indicate binding of TPX2 or chTOG to surface immobilized γTuRCs, further experiments with truncated versions of both proteins would be needed to rule out a possible direct interaction of these proteins with γTuRC.

The lack of an effect of EB3 on γTuRC-mediated microtubule nucleation was unexpected as it was reported before that EB1 inhibits microtubule nucleation from microtubule seed templates (Wieczorek et al., 2015). Further experiments will be needed to rule out if EBs do not have an effect on γTuRC-mediated microtubule nucleation, or if the discrepant results are due to different experimental conditions, e.g. assay conditions, N- or C-terminal tagging of EBs, EB1 versus EB3.

Appart from activation by direct binding partners and proteins regulating microtubule dynamicity, γTuRCs might also be regulated by post-translational modifications (Kollman et al., 2011; Teixidó-Travesa et al., 2012). So far, this possible regulatory mechanism has not been studied extensively. Using the new assay, it would be interesting to compare the nucleation activity of γTuRCs purified from different cell cycle stages (mitosis versus interphase) to better understand the impact of post-translational modifications on γTuRC nucleation efficiency. In the future, the assay might also be useful as a platform to test drugs which could inhibit γTuRC activity or to screen for new γTuRC interactors using cell extract.

In summary, the new γTuRC purification procedure and the new microtubule nucleation assay presented in this thesis will be useful tools to study γTuRC-mediated microtubule nucleation and the regulation of the complex in the future.

6. Material and Methods

6.1 Molecular biology

Cloning was performed using standard methods. DNA inserts were amplified from cDNA clones (Table 6) using either Kappa HiFi polymerase (Kapa Biosystems; KK 2101) or Phusion Hot Start polymerase (Finnzymes; F549L) according to manufactures recommendation. Primers were purchased from Sigma Aldrich (desalt grade). Primers used in this thesis are summarized in Table 7. Annealing temperatures were calculated using Serial Cloner freeware: (http://serialbasics.free.fr/Serial_Cloner.html).

PCR products were analyzed by agarose gels and prepared for downstream processing using the PCR cleanup kit from Quiagen (QIAquick PCR Purification Kit; 28104). PCR products and vectors were digested overnight at 37°C using standard restriction enzymes (all from New England Biolab, NEB, see Table 7). Vectors were dephosphorylated the next day by Antarctic Phosphatase (NEB; M0289S) treatment for 1 hour at 37°C. After heat inactivation at 65°C for 30 minutes, DNA was separated on agarose gels and purified using the Quiagen Gel Extraction Kit (QIAquick Gel Extraction Kit; 28704). DNA concentrations were measured using NanoDrop (NanoDrop ND 1000 Spectrophotometer, Thermo Scientific).

For restriction enzyme cloning, inserts and vectors were mixed in a 3:1 molar ratio and incubated with 10 U/µL T4 Ligase (NEB; M0202S) for four hours at 16°C in ligation buffer with ATP (NEB). 5 µL of ligation mix was transformed into 50 µL of *E. coli* DH5-alpha cells (Stratagene) by heat shock. Cells were incubated with DNA for 30 min on ice, heat shocked for 90 s followed by a 5 min incubation on ice. 1 mL of standard LB medium (10 g tryptone, 10 g NaCl, 5 g yeast extract, media kitchen, The Francis Crick Institute), was added and cells were incubated for 1 h at 37°C and 160 rpm. 100 µL of undiluted, 1:10 and 1:100 diluted transformation mixture was plated onto agar plates using either Ampicillin (100 µg/µL, Fischer) or Kanamycin (50 µg/µL, Fischer) as selection markers. Plates were incubated overnight at 37°C and at least 6 colonies were picked for 5 mL liquid overnight cultures (37°C, 160 rpm). Plasmid DNA was isolated using the Quiagen Miniprep kit (QIAprep Spin Miniprep Kit; 27104) and positive clones were selected using control restriction digests followed by agarose gel electrophoresis. Sequences were confirmed by sequencing at GATC-Biotech (http://www.gatc-biotech.com).

In-Fusion cloning was performed using a kit (In-Fusion® HD Cloning Plus, 638911) following manufactures instructions for Spin-Column purified PCR Fragments (Clontech). Vector and insert amounts for In-Fusion reactions were calculated using the In-Fusion molar ratio calculator online (https://www.takarabio.com/learning-centers/cloning/in-fusion-cloning-tools/in-fusion-molar-ratio-calculator). For proteins expressed in *E. coli*, 10 µL of ligation mix was transformed and processed as described above. For lentiviral constructs (Table 6) 10 µL of ligation mix was transformed into NEB stable competent *E. coli* (High efficiency) (NEB, C3040I) by heat shock and processed as described above.

Table 6: cDNA clones used in this thesis

Protein	Accession Number	Product code	Company
CDK5Rap2	NM_018249	EX-E1869-M43	Genecopoeia
NEDD1	NM_152905.3	custom made (codon optimized for insect cell expression)	LifeTechnolgoies
γ-tubulin	NM_001070	SC119462	Origene
GCP2	NM_001256617.1	SC115940	Origene
GCP3	NM_006322.6	SC322145	Origene
GCP4	NM_014444.4	SC115032	Origene
GCP5	NM_052903.6	SC127127	Origene
GCP6	NM_020461.4	RC213690	Origene
Mozart1	NM_001071775.3	SC315397	Origene

Table 7: Constructs cloned in this thesis. Mozart1 was cloned by Julian Gannon (Surrey group, The Francis Crick Institute).

Name	Protein	Tag	Primers	Plasmid	Method
pTC058	γTuNA$^{51-100}$	N-terminal AviTag-mBFP	FORWARD: GACGAATTCGGCGGCGGTGGCGGTGAAACAGTGTCTCCCACCAG REVERSE: GTCGCGGCCGCTTATTAAAGCTTGCTTTCCAAACGCAAC	pRSF-Duet	RD[1]: EcoRI NotI
pTC056	γTuNA$^{51-200}$	N-terminal AviTag-mBFP	FORWARD: GACGAATTCGGCGGCGGTGGCGGTGAAACAGTGTCTCCCACCAG REVERSE: GTCAAGCTTTTATTAGTAGATATGTTCAGTGGGGCCATG	pRSF-Duet	RD: EcoRI HindIII
pTC071	γTuNA$^{51-200}$	N-terminal GST-AviTag	FORWARD: AGGAGATATACCATGATGTCCCCTATACTAGGTTATTGGAA REVERSE: CACCGCCGCCGAATTCCTCGTGCCACTCGATCTTCTGAGCCTCGAAGATGTCGTTCAGACCGCCCTGAAAATACAGGTTTTCACCGCCACCGCCGCCTTTTGGAGGATGGTCGCCACC	pGEXNDE1	RD: NcoI EcoRI
pTC078	γTuNA$^{51-200}$	N-terminal GST	FORWARD: GGTGGTGGTGGAATTGAAACAGTGTCTCCCACCAGAG REVERSE: ACGATGAATTAAGCTGCTTATTAAAGCTTGCTTTCCAAACG	pGEXNDE1	In-Fusion: EcoRI HindIII
pTC037	ΔN-NEDD1[3]	N-terminal AviTag-mBFP	FORWARD: GACGAATTCGGTGGTGGTGGCGGTACTGTGGCTGTGCAAGAGAAG REVERSE: GTCAAGCTTTTATTAGAAGTGAGCACGCAGGC	pFastBacHta	RD: EcoRI HindIII
JG020	Mzt1	N-terminal GST	FORWARD: GAATTCTAGACCATATGGAAAACCTGTATTTTCAGGGCGCGAGTAGCAGCGGTGCTGGGGCGG REVERSE: TTGAGCTCGAGTCGACTTAGCTTGTCATATTTTCAGCAGCCTTCAGTGCTTCAGTAGCCTTGCG	pGEXNDE1	In-Fusion: Nde1 Sal1

[1] γTuNA is the N-terminal γTuRC-binding domain of CDK5Rap2 which contains the evolutionary conserved CM1 domain (amino acids 51-100)

[2] RD = Restriction Digest

[3] ΔN-NEDD is the C-terminal half of NEDD1 (amino acids 364-660)

Table 8: M13 primers for verification of insert integration into recombinant bacmids. (Bac-to-Bac manual, Thermo Fisher)

Primer	Sequence
M13 Forward	CCCAGTCACGACGTTGTAAAACG
M13 Reverse	AGCGGATAACAATTTCACACAGG

Table 9: Primers for N- and C-terminal tagging of GCP2. Constructs were cloned by Wei Ming Lim (Surrey group, The Francis Crick Institute).

Name	Protein	Tag	Primers	Plasmid	Method
pTC068	GCP2	N-terminal AviTag-mBFP	FORWARD mBFP: GGACTCAGATCTCGAATGGGTCTGAACGACATCTTCG FORWARD GCP2: AGTGAATTTCGGATTCACCATG	pLVX-Puro	In-Fusion: XhoI XbaI
			REVERSE mBFP: GAATCCGAAATTCACTTCCGCCTCCTCCGCCGCCCTGAAAATACAGGTTTTCTCCGCCTC CTCCGCCGTTCAGTTTATGACCCAGTTTGCT REVERSE GCP2: GGTAGAATTATCTAGTCACTGTGCGGTGACTGCGAC		
pTC069		C-terminal AviTag-mBFP	FORWARD mBFP: AGCGAAGAACTGATCAAAGAAAAC FORWARD GCP2: GGACTCAGATCTCGAATGAGTGAATTTCGGATTCACCAT	pLVX-Puro	In-Fusion: XhoI XbaI
			REVERSE mBFP: GGTAGAATTATCTAGTCAGTTCAGTTTATGACCCAGTTT REVERSE GCP2: TGATCAGTTCTTCGCTTCCGCCTCCTCCGCCCTCGTGCCACTCGATCTTCTGAGCCTCGA AGATGTCGTTCAGACCGCCCTGAAAATACAGGTTTTCTCCGCCTCCTCCGCCCTGTGCGG TGACTGCGACC		

Table 10: Primers for N- and C-terminal tagging of GCP4. Constructs were cloned by Wei Ming Lim (Surrey group, The Francis Crick Institute).

Name	Protein	Tag	Primers	Plasmid	Method
pTC066	GCP4	N-terminal AviTag-mBFP	FORWARD mBFP: GGACTCAGATCTCGAATGGGTCTGAACGACATCTTCG FORWARD GCP4: ATCCACGAACTGCTCTTGGCT	pLVX-Puro	In-Fusion: XhoI XbaI
			REVERSE mBFP: AGAGCAGTTCGTGGATTCCGCCTCCTCCGCCGCCCTGAAAATACAGGTTTTCTCCGCCTC CTCCGCCGTTCAGTTTATGACCCAGTTTGCT REVERSE GCP4: GGTAGAATTATCTAGTCACATCCCGAAACTGCCCAGA		
pTC067	GCP4	C-terminal AviTag-mBFP	FORWARD mBFP: AGCGAAGAACTGATCAAAGAAAAC FORWARD GCP4: GGACTCAGATCTCGAATGATCCACGAACTGCTCTTGG	pLVX-Puro	In-Fusion: XhoI XbaI
			REVERSE mBFP: GGTAGAATTATCTAGTCAGTTCAGTTTATGACCCAGTTT REVERSE GCP4: TGATCAGTTCTTCGCTTCCGCCTCCTCCGCCCTCGTGCCACTCGATCTTCTGAGCCTCGA AGATGTCGTTCAGACCGCCCTGAAAATACAGGTTTTCTCCGCCTCCTCCGCCCATCCCGA AACTGCCCAGAG		

Table 11: Primers for tagging of BirA. Constructs were cloned by Wei Ming Lim (Surrey group, The Francis Crick Institute).

Name	Protein	Tag	Primers	Plasmid	Method
pTC070	BirA	HA	FORWARD: CGGTGAATTCCTCGAATGTACCCATACGATGTTCCAGATTACGCTGGCGGAGGAGGCGG AAAGGATAACACCGTGCCACTG	pLVX-IRES-Hyg	In-Fusion: XhoI BamHI
			REVERSE: GAGAGGGGCGGGATCTTATTATTTTTCTGCACTACGCAGG		

6.2 Protein Expression

6.2.1 Protein expression in *E. coli*

Proteins were expressed in *E. coli* BL21 (DE3)-RIL competent cells (Stratagene; 230240). 100 ng of plasmid DNA was transformed into 50 µL of cells using the heat shock procedure described above. For selection, agar plates containing Chloramphenicol (50 µg/µL) and Kanamycin (50 µg/µL) or Ampicillin (100 µg/µL) were used. Agar plates were incubated overnight at 37°C. A single colony was picked for an overnight culture (400 mL LB media, supplemented with antibiotics and 2% glucose at 200 rpm and 25°C in a 2 L Erlenmeyer flask, prepared midday). On the next day, main culture (1 L LB media, supplemented with antibiotics in 5 L Erlenmeyer flask) was inoculated with overnight culture at an OD_{600} of 0.05 and left to grow to an OD_{600} of 0.6 at 25°C and 200 rpm. Cell density was monitored using a conventional spectrophotometer. When an OD_{600} of 0.6 was reached, cultured were transferred to 18°C and expression was induced with 0.1 mM Isopropyl β-D-1-thiogalactopyranoside (IPTG; Roche, 11411446001). For biotinylated proteins (AviTag), D-biotin (Sigma Aldrich; B4639) was added to a final concentration of 7 µg/mL. Cultures were harvested after 16-18h by centrifugation (30 min, 4000xg, 4°C, JLA 81000 rotor (Beckman)) and the supernatant was discarded. Pellets were resuspended in cold PBS (10 mM Na_2HPO_4, 18 mM KH2PO4, 27 mM KCl, 137 mM NaCl, pH 7.4), transferred into 50 ml Falcon tubes (Corning) and centrifuged again (15 min, 1,942xg). The supernatant was discarded. Pellets were flash frozen in liquid nitrogen and stored until further use at -80°C. Protein expression was confirmed by western blot and SDS-gel electrophoresis.

6.2.2 Insect cell culture and expression

For baculovirus mediated protein expression, *Sf21* (*Spodoptera frugiperda* 21) insect cells (originally provided by Imre Berger, EMBL Grenoble) were used. Cells were maintained in suspension culture in Sf-900 II SFM serum-free medium (Invitrogen) at $0.7x10^6$ cells/mL at 27°C and under constant shaking (120 rpm). Cells were grown in plastic Erlenmeyer flasks (Corning, Sigma Aldrich) of five times the cell culture volume. Cell density was maintained by counting cultures every 24h using a Neubauer improved cell counting chamber.

For generation of bavuloviruses, the Bac-to-Bac® Baculovirus Expression pFastBac system was used (Invitrogen/life technologies) according to the manufactures

recommendations. 100 ng vector DNA (pFastBac, (Fitzgerald et al., 2007) were transformed by heat shock (as described above) into *E. coli* DH10 MultiBac cells (Life technologies) for generation of recombinant bacmids. *E. coli* cells were grown in SOC media (Life technologies) for 4-8h at 37°C and plated onto agar plates containing Gentamycin (7 µg/mL), Teracyclin (10 µg/mL), Kanamycin (50 µg/mL), Bluo-Gal/X-Gal (0.1 mg/mL) and IPTG (40 µg/mL) as selection markers. Six positive colonies were selected by blue white screen (Ullmann, 1967) after 1 day of incubation at 37°C, re-streaked onto fresh plates and left for overnight incubation at 37°C. To verify presence of insert in the bacmid DNA a colony PCR using KAPA Hifi polymerase and M13 primers (Table 8, taken from the Bac-to-Bac manual, Thermo Fisher) was performed followed by analytical agarose gel electrophoresis (see below). Positive colonies were used to inoculate 10 mL overnight cultures in LB media supplemented with antibiotics (160 rpm, 37°C). DNA was isolated using the NucleoBond® Xtra Midi prep kit (Macherey-Nagel, 740410.10) and used the same day for baculovirus generation.

2 mL insect cell culture per well was transferred into 6 well plates (Corning) at a density of $0.3x10^6$ cells/mL and left to settle for 1h at 27°C. For transfection, 20 µL of freshly prepared bacmid DNA was mixed with 200 µL insect cell media and 14 µL FuGENE-HD (Promega; E2311) and incubated for 20 min at room temperature. Half of this mixture was added dropwise to each well containing seeded insect cells and mixed by moving the plates. Plates were kept in a sealed container and incubated for 72h at 25°C. Virus containing supernatant was added to 25 ml of *Sf21* suspension culture (density: $0.7x10^6$ cells/mL). Cell density was maintained until cells stopped to proliferate. The next day (48h after cells stop dividing) virus containing supernatant was harvested by centrifugation (700xg, 10 min, 4°C) and fetal bovine serum was added (10% final concentration, Sigma Aldrich; F7524). Mixture was filtered (PVDF membrane, 0.22 µM pore size, Millipore; SLGP033RS) and stored in the dark at 4°C. For long-term storage 1 mL aliquots were prepared, flash frozen in liquid nitrogen and stored at -80°C.

The exact virus titer was not determined, as virus amount for protein expression was always optimized empirically by small scale expression tests. Different virus amounts (25 to 500 µL) were added to 25 mL suspension cultures (density: $0.7x10^6$ cells/mL) and incubated for 72h. Samples were withdrawn daily and analyzed by SDS-gel electrophoresis and western blot to compare protein expression levels. Best condition (Highest expression level at lowest virus concentration) was chosen for large scale cultures (600 mL). Good expression was usually found 48-72h post infection at a 1:1000 dilution of virus.

Large scale cultures were harvested by centrifugation (700xg, 30 min, 4°C, JLA 81000 rotor (Beckman)) and the supernatant was discarded. Pellets were resuspended in cold PBS, transferred into 50 ml Falcon tubes (Corning) and centrifuged again (15 min, 700xg). Expression was controlled by SDS-gel electrophoresis and western blot. Since insect cell culture media contains biotin, no additional biotin was added for expression of biotinylated proteins (AviTag).

6.2.3 Mammalian cell culture and generation of stable HeLa-K cell lines

All cells used in this thesis have been negatively tested for mycoplasma. HeLa-K cells and U2OS cells were maintained at 37°C (10% CO2) in Dulbecco's Modified Eagle Medium (DMEM; Sigma Aldrich, D6429) supplemented with 10% fetal bovine serum (Sigma Aldrich; F7524), 50 U/mL Penicillin (Thermo Fisher) and 50 µg/mL Streptomycin (Thermo Fisher).

6.3 Generation of a stable HeLa-K cell lines expressing tagged GCP2 or GCP4

HeLa-K cells stably expressing N- or C-terminal AviTag-mBFP tagged GCP2 or GCP4 and HA-BirA were developed in collaboration with Jayant Asthana and Wei Ming Lim (both Surrey group, The Francis Crick Institute). Constructs were designed by myself and Wei Ming Lim performed the cloning. Cell culture work, lentiviral infection, flow cytometry, immunostaining and fluorescent microscopy screening were performed by Jayant Asthana and Wei Ming Lim. Western blot screen was performed by Wei Ming Lim and myself.

Lentiviral plasmids were cloned as described above using the primers and plasmids tabulated in the appendix. Lentiviruses were prepared in HEK293FT cells as described previously (Abella et al., 2016). HeLa-K cells were co-transduced with tagged GCP2 or GCP4 lentivirus and BirA lentivirus. Transduced cells were selected by antibiotic selection with hygromycin (50 µg/mL, Thermo Fisher) and puromycin (1 µg/mL, Thermo Fisher) for 72 h. Cells were sorted by flow cytometry (Flow cytometry facility, The Francis Crick Institute) and mBFP positive single cell colonies were screened for mBFP fluorescence and HA-BirA (immunostaining against HA-tag was performed as described (Asthana et al., 2013)) using fluorescence microscopy (spinning disc confocal, Nicon). Positive clones were grown at two different D-Biotin concentrations, 10 µM and 50 µM, and screened for *in vivo* biotinylation by HA-BirA using western blot (Figure 2.14, A and C). Clones C18 (GCP2) and C15 (GCP4) were

selected for large scale cell pellet production based on a second screen (Figure 2.14 B and D, see chapter 2, section 2.2.2.1).

6.3.1 Large scale production of human cell pellets

Large scale cell culture was performed by Cell Services Facility (The Francis Crick Institute). Every four weeks, fresh cells were revived from frozen vials. Pellets were stored at -80°C until further use.

Large scale culture of HeLa-K cells: Cells grown on one cell culture flask (175 cm^2, Thermo Fisher; 156502) were subdivided onto 7 cell culture flasks and left until confluent (~2 days). Then, cells were subdivided into 20 triple layer flasks (500 cm^2, Thermo Fisher; 10757811) and again allowed to become confluent (~4 days). Next, cells were subdivided into 100 triple layer flasks. D-biotin (cell culture grade, 1 mM stock prepared in 1xPBS in advance and stored at -20°C, Sigma Aldrich; B4639) was added to a final concentration of 50 µM and cells were grown for another ~3 days to get confluent. Cells were washed with PBS and trypsinised using 0.25% trypsin-EDTA solution (Sigma Aldrich; 25200056). Cells are harvested by centrifugation using a JS-4.2 rotor (Beckman, J6-MI centrifuge) at 283.7xg for 15 min at 4°C. Pellet is resuspended in PBS and spun in falcon tubes (Corning) in an Allegra X-30 table top centrifuge at 193xg at 4°C for 10 min to pellet sizes of 15 g each. Peer week 60±3 g of cell pellet are produced using this method.

Large scale culture of U2OS cells: Cells grown on one large flask were subdivided onto 4 large flasks and left until confluent (~2 days). Then cells were subdivided onto 20 large flasks and again allowed to become confluent (~3 days). Next cells were subdivided onto 35 triple layer flasks and left to get confluent (~3 days). Cells are harvested as described above. Per week 15±2 g of cell pellets were produced.

6.4 Gel electrophoresis

Sodium dodecyl sulphate polyacrylamide gel electrophoresis (SDS-PAGE) was performed using NuPAGE (Thermo Fisher) 10% Bis-Tris gels (NP0301) or 4-12% Bis-Tris gradient gels (NP0335). Protein gels were run using either NuPAGE 1x MOPS (NP0001) or 1x MES (NP0002) SDS Running buffer. Proteins were denatured by adding 1x NuPAGE LDS Sample Buffer (NP007) and heated at 65°C for 15 minutes. As size marker, Precision Plus Protein Dual Xtra prestained protein standard (BioRad, 1610377) was used. Gels were stained using Instant blue (Sigma Aldrich, ISB1L) or

0.25% coomassie brilliant blue (Bio-Safe Coomassie G-250 Stain, BioRad, 161-0786) in staining buffer (50% Methanol, 7% glacial acetic acid) for 1-3 h and left to destain overnight (staining buffer without coomassie). Staining of gels in SYPRO ruby (Thermo Scientific, S12000) was performed following manufacturer's instructions and imaged using a standard scanner after washing the gels in Milli-Q water.
Agarose gel electrophoresis was performed using standard methods (Viovy, 2000). 1x Tris-Acetate-EDTA buffer (50x TAE stock, 2 M Tris-HCl, 1 M glacial acetic acid, 0.05 M EDTA) was used as running buffer and resolved gels were stained with ethidium bromide (Thermo Fisher; 15585011). Amersham Imager 600 (GE Healthcare) was used to visualize DNA.

6.5 Western blotting

Protein gels were run as described above. For western blots against γTuRC subunits, Criterion XT Precast gels (3-8% Tris-Acetate, BioRad) and 1x XT Tricine running buffer (BioRad; 1610790) were used for better separation of protein bands in the high molecular weight range. Protein gels were transferred onto PVDF membrane (Immobilon-FL, pore size was 0.45 µM, Sigma Aldrich; 05317-10EA) using a tank-blotting chamber (BioRad) for 90 min at 400 mA in precooled transfer buffer (0.025 M Tris-HCl, 0.192 M Glycine, 0.25% SDS, 20% Methanol) at 4°C under constant stirring. Membranes were blocked in 5% nonfat milk dissolved in PBST buffer (PBS supplemented with 0.05% Tween-20) for 1h at room temperature. Blocking buffer was discarded and membranes were incubated with primary antibody diluted in blocking buffer overnight at 4°C. The next day, membranes were washed 3x in PBST for 10 min each and incubated for 45 min in horseradish peroxidase conjugated secondary antibody diluted in blocking solution. Western blots were washed 3x in PBST for 10 min each and imaged using an Amersham Imager 600 (GE Healthcare) or films (Amersham Hyperfilm ECL, Sigma Aldrich; 28906838) and a standard film developer. Protein bands were visualized using Clarity western ECL (BioRad; 1705060).
For detection of biotinylated proteins, horseradish peroxidase coupled streptavidin (streptavidin-HRP, Thermo Fisher; 21130) was used. Membranes were incubated with streptavidin-HRP (1:4000 in blocking buffer) after the first blocking step for 2h at room temperature. Unbound streptavidin-HRP was washed off 3x with PBST 10 min each and membranes were imaged as described above. For samples with low biotinylation levels better results were achieved when streptavidin-HRP was diluted in PBST containing 5% bovine serum albumin (BSA, Sigma Aldrich; A4503) and washing steps were performed with Milli-Q instead of PBST. Membranes were

washed with PBST before incubation with chemiluminescence reagent for imaging. All other commercial antibodies and dilutions used in this thesis are summarized in Table 12.

Table 12: List of commercial antibodies used for western blotting in this thesis.

Antibody	Product number	Company	Dilution
tRFP (anti-mBFP)	AB233	evrogen	1:2500
γ-tubulin	(GTU-88) ab11316	abcam	1:5000
GCP5	(E-1) sc-365837	Santa Cruz	1:50
GCP6	(H-9) sc-374063	Santa Cruz	1:50
HA	(F-7) sc-7392	Santa Cruz	1:200
γ-tubulin	ab18251	abcam	1:1000
goat anti-mouse-HRP	P0447	Agilent	1:5000
peroxidase polymer horse anti-rabbit IgG	WB-1000-.8	Vector	1:5000

Except GCP5 and GCP6 antibodies (see Table 14) commercial antibodies against γTuRC subunits performed poorly or were completely unspecific in my hands. Therefore, I started to design peptide antibodies and protein fragments for custom-made polyclonal rabbit antibodies. This part of the project was taken over by Julian Gannon (Surrey group, The Francis Crick Institute). Serum containing specific antibodies against GCP2 (raised against amino acids 1-155, Pettingill) and GCP4 (raised against the full-length protein, Covalab) could be obtained and antibodies were affinity purified by Julian Gannon. Anti-GCP2 was used 1:1000 and anti-GCP4 1:5000 diluted. A full list of all peptides, protein fragments and full-length proteins tested for polyclonal antibody production in rabbits is shown in the appendix.

6.6 Protein purification

All proteins were purified using an ÄKTA purifier (ÄKTApurifier, GE-Healthcare). Purified proteins were separated on protein gels followed by staining with coomassie or instant blue as described above to test for purity. Protein concentration was measured by NanoDrop (NanoDrop ND 1000 Spectrophotometer, Thermo Scientific) or Bradford assay (Quick Start Bradford, BioRad; 5000205) using BSA as standard (Thermo Scientific; 23209).

6.6.1 Tubulin purification and labelling

Pig brain tubulin was purified as described (Castoldi and Popov, 2003). Covalent labelling of tubulin with CF640R-N-hydroxysuccinimide ester (NHS, Sigma-Aldrich;

SCJ4600044) and biotin-NHS (Thermo Fisher; 20217) was performed as described (Hyman et al., 1991).

6.6.2 Purification of antibodies

Antibodies were cloned, expressed and purified by Julian Gannon (Surrey Group, The Francis Crick Institute). Briefly, full-length proteins and protein fragments used for the immunization of rabbits were expressed with an N-terminal His-tag. Proteins for the purification of antibodies from rabbit serum were produced with an N-terminal maltose binding protein (MBP)-tag. Proteins were expressed in *E. coli* BL21 (DE3)-CodonPlus (0.5 mM IPTG, His-tagged proteins (2 h), MBP-tag proteins (1 h) at 37 C).

His-tagged proteins were insoluble and therefore purified as inclusion bodies using 10 mM Tris, pH 8 containing 6 M Guanidine Hydrochloride and 1 mL of Ni-NTA resin (Thermo Fisher, R90101), following the manufacturer's instructions. Proteins were eluted with 250 mM imidazole and dialysed into PBS overnight. The precipitate was resuspended in PBS to a concentration of 1 mg/ml. MBP-tagged proteins were purified in PBS Tween supplemented with 0.5% Tween20 using 1 mL of amylose resin (NEB, E8021S), following the manufacturer's instructions. Purified proteins were immediately used to for immobilization on freshly prepared CNBr beads and left to bind overnight at 4°C. This affinity column was used for the purification of antibodies from rabbit serum.

Typically, antibodies were purified from 5 mL rabbit serum by incubation with the affinity column at 4°C for 3 h. The resin was washed with phosphate buffer pH 7.5 supplemented with 0.1% Tween20 and 0.5 M NaCl, followed by another wash with PBS. Antibodies were eluted with 100 mM glycine at pH 2.5. Elution fractions were immediately neutralised by addition of 1 M Tris pH 8.5. Peak fractions containing the antibody were pooled, aliquoted and stored at -20. The specificity of antibodies was tested by western blot against lysates obtained from different human cells, lysates from the stable cell lines containing tagged GCP2 or GCP4 developed in this thesis (see chapter 2 section 2.2.2), and control lysates in which GCP2 and GCP4 were depleted by RNAi as described (Cota et al., 2017). Western blots are shown in the appendix Figure 7.1).

6.6.3 Purification of AviTag-mBFP-γTuRC binders (Bio-γTuRC binders)

Lysis buffer for CDK5Rap2-fragments (Bio-γTuNA$^{51-100}$, Bio-γTuNA$^{51-200}$):
50 mM NaPi, 500 mM KCl, 5 mM $MgCl_2$, 1 mM EDTA, 1 mM βME, pH 7.4

AviTag-mBFP-CDK5Rap2 fragments were expressed in *E. coli* as described before. For purification, cell pellets were resuspended in lysis buffer supplemented with DNaseI (stock concentration 2 mg/mL in 20% glycerol and 75 mM NaCl, Sigma Aldrich; DN25) at a final concentration of 10 µg/mL and cOmplete EDTA-free protease inhibitor tablets (1x per 50 mL lysate, Sigma Aldrich; COEDTAF-RO) on ice. Cells were then lysed by passing the lysate 3x through a pre-cooled microfluidizer and clarified by centrifugation at 4°C in a Ti70 rotor at 256,630.8xg for 45 min. Clarified lysate was filtered (PVDF membrane, 0.45 µM pore size, Millipore; SLHV033RS) and buffer exchanged over HiPrep 26/10 desalting columns (1x column per 15 mL lysate, GE Healthcare; 17508701) to remove biotin. Protein containing fractions were pooled, supplemented with pre-dissolved cOmplete EDTA-free protease inhibitor tablets (1x per 50 mL lysate) and loaded onto 1 mL monomeric avidin beads (Thermo Fisher; 20228) packed into a column using a pressure pump at 0.5 mL/min in the cold room. Column was washed with 20 mL lysis buffer, 20 mL ATP-wash buffer (lysis buffer supplemented with 5 mM ATP) and 20 mL wash buffer (lysis buffer but 1 mM $MgCl_2$) at a flow rate of 1 mL/min. Proteins were eluted in elution buffer (wash buffer supplemented with 5 mM D-biotin, Sigma Aldrich; B4501) at 0.5 mL/min and fractionated in 1 mL fractions. Protein containing fractions were pooled and buffer exchanged using HiPrep 26/10 desalting columns (1x column per 15 mL sample volume). Protein containing fractions were pooled and concentrated using Vivaspin concentrators of appropriate molecular weight cut-off (Sartorius). Pure proteins were then centrifuged in a TLA110 rotor at 267008xg for 10 min at 4°C to remove aggregates, snap frozen and stored in liquid nitrogen.

Lysis buffer for Bio-ΔN-NEDD1:
50 mM HEPES, 250 mM KCl, 5 mM $MgCl_2$, 1 mM EDTA, 1 mM βME, pH 7.4

Protein was expressed in *Sf21* cells as described before and purified using the same protocol as above but cells were lysed on ice by douncing (120 strokes) in a dounce tissue grinder (Wheaton, Thermo; 11521305).

6.6.4 Purification of GST-AviTag- and GST-γTuRC binders

GST-Mzt1 was cloned and purified by Julian Gannon (Surrey Group, The Francis Crick Institute).

Lysis buffer for GST-AviTag-γTuNA$^{51-200}$, GST-γTuNA$^{51-200}$ and GST-Mzt1:
50 mM HEPES, 250 mM KCl, 10 mM $MgCl_2$, 1 mM EDTA, 5 DTT, 5 mM ATP, pH 7.4

GST-AviTag and GST-γTuRC binders were expressed in *E. coli* as described before. For purification, cell pellets were resuspended in lysis buffer supplemented with DNaseI (stock concentration 2 mg/mL in 20% glycerol and 75 mM NaCl, Sigma Aldrich; DN25) at a final concentration of 10 µg/mL and cOmplete EDTA-free protease inhibitor tablets (1x per 50 mL lysate, Sigma Aldrich; COEDTAF-RO) on ice. Cells were then lysed by passing the lysate 3x through a pre-cooled microfluidizer and clarified by centrifugation at 4°C in a Ti70 rotor at 256,630.8xg for 45 min. Clarified lysate was filtered (PVDF membrane, 0.45 µM pore size, Millipore; SLHV033RS) and loaded onto 1 mL prepacked GSTrap HP column (GE Healthcare; 17-5281-01) using a pressure pump at 0.5 mL/min in the cold room. Column was washed with 20 mL lysis buffer followed by 20 mL storage buffer (lysis buffer without ATP) at a flow rate of 1 mL/min. Proteins were eluted in elution buffer (storage buffer supplemented with 40 mM reduced glutathione at pH 8, Fisher; 70-18-8) at 0.5 mL/min and fractionated in 1 mL fractions. Protein containing fractions were pooled and buffer exchanged into storage buffer using HiPrep 26/10 desalting columns (1x column per 15 mL sample volume). Protein containing fractions were pooled and concentrated using Vivaspin concentrators of appropriate molecular weight cut-off (Sartorius). Pure proteins were then centrifuged in a TLA110 rotor at 267008xg for 10 min at 4°C to remove aggregates, snap frozen and stored in liquid nitrogen.
GST-Mozart1 was provided by Julian Gannon (Surrey laboratory) and purified using the same protocol with modifications. Protein was dialyzed overnight instead of buffer exchanged. Dialyzed protein was further purified by size exclusion chromatography using a HiLoad 16/600 Superdex 200 prep grade column (GE Healthcare).

6.6.5 Purification of human chTOG-GFP, GFP-TPX2 and GFP-EB3

Purified chTOG-GFP, GFP-TPX2 and GFP-EB3 were provided by Johanna Roostalu (Surrey laboratory). Purification of chTOG-GFP and GFP-TPX2 was conducted as described (Roostalu et al., 2015). GFP-EB3 was purified as described (Jha et al.,

2017). TPX2 storage buffer was 50 mM HEPES, pH 7.5, 300 mM KCl, 2 mM $MgCl_2$, 50 mM glutamate, 50 mM arginine, 250 mM sucrose, 5 mM βME (Roostalu et al., 2015).

6.7 Purification of native γTuRC

6.7.1 Purification of native γTuRC via AviTag-mBFP-γTuNA$^{51-200}$

Preparation of affinity purification column

1.5 mg of Bio-γTuNA$^{51-200}$ was bound to 1 mL of monomeric avidin beads (Thermo Fisher; 20228). Beads were washed with at least 10 column volumes of Bio-γTuNA$^{51-200}$ storage buffer to remove unbound protein. Beads were then equilibrated with at least 10 column volumes of γTuRC lysis buffer. Affinity purification column was always prepared fresh and used on the same day.

Native γTuRC purification

γTuRC was purified from 10 g U2OS cell pellet. Cells were lysed on ice in 10 mL lysis buffer (50 mM HEPES, 150 mM NaCl, 5 mM $MgCl_2$, 1 mM EGTA, 1 mM DTT, 0.1 mM GTP, 0.5% IGEPAL (IGEPAL CA-630, Sigma Aldrich, I3021), pH 7.2) using a dounce tissue homogenizer. Lysate was clarified by centrifugation using a Ti70 rotor at 256,630xg for 45 min at 4°C. Supernatant was recovered, filtered (PVDF membrane, 0.45 µM pore size, Millipore; SLHV033RS) and loaded onto the affinity purification column at 0.5 mL/min in the cold room. Beads were washed at 1 mL/min with a total of 40 mL wash buffer (50 mM HEPES, 150 mM NaCl, 1 mM $MgCl_2$, 1 mM EGTA, 1 mM DTT, 0.1 mM GTP, 0.01% IGEPAL, pH 7.4). γTuRC and Bio-γTuNA$^{51-200}$ were eluted with elution buffer (wash buffer supplemented with 5 mM D-Biotin) at 0.5 mL/min.

6.7.2 Purification of native γTuRC via GST-γTuNA$^{51-200}$

Preparation of affinity purification column

24 mg GST-γTuNA$^{51-200}$ was bound to 1 mL glutathione beads (Thermo Fisher, 16100). Beads were washed with at least 3x5 mL of the GST-AviTag-CDK5Rap2-long storage buffer to remove unbound protein. Beads were then equilibrated with at

least 10 column volumes of γTuRC lysis buffer. Affinity purification column was always prepared fresh and used on the same day.

Native γTuRC purification

γTuRC was purified from 15 g U2OS cells pellet. Cells were lysed on ice in 15 mL lysis buffer (50 mM HEPES, 150 mM KCl, 5 mM $MgCl_2$, 1 mM EGTA, 1 mM DTT, 0.1 mM GTP, pH 7.2) using a dounce tissue homogenizer. Lysate was ammonium sulfate precipitated as described below and AS supernatant (resuspended in 5 mL resuspension buffer (lysis buffer containing 1 mM $MgCl_2$)) was incubated for 2 h with the affinity purification column. Colum was washed by gravity with 40 mL resuspension buffer. γTuRC and GST-γTuNA$^{51-200}$ were eluted by incubation of beads with 5 mL elution buffer for 30 min (resuspension buffer supplemented with 40 mM reduced glutathione at pH 8.0). Elution was repeated 4x in total (20 mL), elutions were pooled and concentrated to 5 mL. Concentrated elution was subjected to size exclusion chromatography using a Superose 6 XK 16/70 pg column (GE Healthcare). Fraction size was 1.5 mL.

6.7.3 Ammonium sulfate precipitation of human cell lysate

Ammonium sulphate precipitation was conducted as described in (Zheng et al., 1995, 1998). In short, 5 g of human cell pellet (U2OS or HeLA-K) was resuspened in 5 mL γTuRC lysis buffer and lysed using a dounce tissue grinder (120 strokes) on ice. Lysate is clarified twice by centrifugation at 17,000xg and 4°C for 15 min each using a JA-20 rotor. Supernatant was collected and brought to 15% ammonium sulphate by addition of cold saturated ammonium sulphate solution. Mixture was incubated for 10 min on ice, followed by centrifugation for 15 min using a JA-20 rotor at 4°C. Pellet was discarded and supernatant was brought to 25% ammonium sulphate by addition of cold saturated ammonium sulphate solution. Mixture was again incubated for 10 min on ice followed by centrifugation for 15 min using a JA-20 rotor at 4°C. Supernatant was discarded and pellet was incubated with 5 mL γTuRC lysis buffer for 10 min on ice. Pellet was resuspended and centrifuged to remove aggregates in a cooled table-top centrifuge (Heraeus Fresco 17 Microcentrifuge) for 10 min at maximal velocity (17,000xg). Supernatant containing γTuRC was collected and used immediately. If smaller cell pellet amounts (less than 5 g) were processed, all centrifugation steps were conducted using a cooled table top centrifuge at maximal velocity.

6.7.4 Optimization of γTuRC lysis conditions

Comparison of different lysis buffers: For each condition, 0.5 g U2OS cell pellet was lysed on ice in 1.25 mL of the corresponding lysis buffer using a dounce tissue grinder (120 strokes). A sample was kept and residual lysate was clarified by centrifugation in an Optima MAX-XP Ultracentrifuge using a TLA110 rotor at 278,088xg for 10 min at 4°C. Supernatant was recovered. Samples from lysate and supernatant were then analysed by western blot. All buffers contained 5 mM MgCl2, 1 mM EGTA, 1 mM DTT, 0.1 mM GTP. Buffering agent (50 mM HEPES, pH 7.2 or 80 mM PIPES, pH 6.8) and salt concentration (150 mM KCl or 75 mM KCl) were used.

Comparison of centrifugation speeds and IGEPAL: For each condition, 0.25 mg U2OS cell pellet was lysed in 0.25 mL of either lysis buffer without IGEPAL or lysis buffer supplemented with 0.5% IGEPAL using a dounce tissue grinder (120 strokes). A sample was kept and residual lysate was clarified at 4°C by centrifugation in an Optima MAX-XP Ultracentrifuge using a TLA110 rotor at 278,088xg for 10 min (high speed centrifugation, HS) or twice for 15 min each in a cooled table top centrifuge at 17,000xg at 4°C (low speed centrifugation, LS). Supernatant was recovered. Samples from lysate and supernatant were then analysed by western blot. Lysis buffer contained 50 mM HEPES, pH 7.2, 5 mM $MgCl_2$, 1 mM EGTA, 1 mM DTT, 0.1 mM GTP.

6.7.5 Size exclusion chromatography analysis of human cell lysate

1 g of U2OS cell pellet was lysed on ice in 2.5 mL lysis buffer using a dounce tissue grinder (120 strokes). Lysate was clarified by centrifugation at 4°C either once in an Optima MAX-XP Ultracentrifuge using a TLA110 rotor at 278,088xg for 10 min (high speed centrifugation, HS) or twice for 15 min each in a cooled table top centrifuge at 17,000xg (low speed centrifugation, LS). Supernatant was recovered and filtered (0.45 µM, PVDF membrane, Millipore; SLHV033RS). Protein concentration was measured using NanoDrop and supernatant was diluted to 2 mg/mL total protein. From there, 0.5 mL of protein solution was subjected to size exclusion chromatography using a Superose 6 10/300 GL column (GE Healthcare). Fractions were analysed by western blot. Fraction size was 0.5 mL. For analysis of AS precipitated lysates, 1 g of human cell pellet was AS precipitated as described before and AS supernatant (1 mL resuspension volume) was processed as described above.

All buffers contained 5 mM $MgCl_2$, 1 mM EGTA, 1 mM DTT, 0.1 mM GTP. Buffering agent (50 mM HEPES, pH 7.2 or 80 mM PIPES, pH 6.8), salt concentration (150 mM KCl or 75 mM KCl) and addition of IGEPAL (0.5%) as described in Figure 2.5.

6.7.6 Small scale pull-down of γTuRC from human cells

Preparation of affinity purification beads

For ease of handling all steps were performed in Micro Bio Spin Chromatography columns (BioRad, 7326204). Washes were performed by gravity flow.
For native γTuRC pull-downs from U2OS cell lysate, 200 µg of γTuRC-binder was bound to 100 µL of monomeric avidin beads (Thermo Fisher; 20228), SoftLink Soft Release Avidin resin (Promega, V2011), BcMag monomeric avidin magnetic beads (Bioclone, MMI-102) or glutathione beads (Thermo Fisher, 16100). Beads were washed with at least 10 column voumes of the storage buffer of the corresponding γTuRC-binder to remove unbound protein. Beads were then equilibrated with at least 10 column volumes of γTuRC lysis buffer. Affinity purification beads were always prepared fresh and used on the same day.

Comparison of biotinylated γTuRC-binders

For each condition, 1 g of U2OS cells was resuspended in 1 mL lysis buffer (50 mM HEPES, pH 7.2, 150 mM NaCl, 5 mM $MgCl_2$, 1 mM EGTA, 1 mM DTT, 0.5% IGEPAL 0.1 mM GTP), clarified using a cooled table top centrifuge (Heraeus Fresco 17 Microcentrifuge) at maximal velocity (17,000xg) for 10 min and incubated with affinity purification beads for 2 h in the cold room using a rotator. Beads were washed with 5 mL lysis buffer and γTuRC and γTuRC-binders were eluted twice by incubating the beads for 30 min each with 0.5 mL elution buffer (lysis buffer supplemented with 5 mM D-biotin, 1 mM $MgCl_2$ and 0.01% IGEPAL). Elutions were pooled. Beads were washed once more with 1 mL elution buffer and samples of elution and beads were analyzed by western blot.

Comparison of elution conditions

For each condition, 1 g human cell pellet was resuspended in 1 mL γTuRC lysis buffer (50 mM HEPES, pH 7.2, 150 mM KCl, 5 mM $MgCl_2$, 1 mM EGTA, 1 mM DTT, 0.1 mM GTP) and ammonium sulphate precipitated as described above. AS supernatant (1

mL resuspension volume) was incubated with beads as described above. All elution buffers contained 5 mM D-biotin, 1 mM $MgCl_2$, 1 mM EGTA, 1 mM DTT, 0.1 mM GTP. Salt concentration (150 mM or 250 mM) and addition of IGEPAL (0.5%) as indicated in Figure 2.7

Comparison of bead materials

Experiment was performed essentially as described in section 0 using the following buffer for elution: 50 mM HEPES, pH 7.2, 250 mM KCl, 1 mM $MgCl_2$, 1 mM EGTA, 1 mM DTT, 0.1 mM GTP, 0.5% IGEPAL, 5 mM D-Biotin.

Pull down of γTuRC via GST-γTuNA $^{51\text{-}200}$: Experiment was performed as described in section 0 using the following lysis buffer: 50 mM HEPES, pH 7.4, 150 mM KCl, 5 mM $MgCl_2$, 1 mM EGTA, 1 mM DTT, 0.1 mM GTP. For elution, lysis buffer (1 mM $MgCl_2$) was supplemented with 40 mM reduced glutathione and pH was increased to pH 8.0.

6.8 Purification of tagged γTuRC from HeLA-K cells

γTuRC was purified from a stable HeLa-K cell line co-expressing GCP2-mBFP-AviTag and HA-BirA. Cloning, cell line preparation and cell culture was performed as described above.

Lysis buffer:
50 mM HEPES, 150 mM KCl, 5 mM $MgCl_2$, 1 mM EGTA, 1 mM DTT, 0.1 mM GTP, pH 7.4

Storage buffer:
50 mM HEPES, 150 mM KCl, 1 mM $MgCl_2$, 1 mM EGTA, 1 mM DTT, 0.1 mM GTP, 0.02% Brij-35 (v/v, 10% stock solution, Thermo Fisher; 28316), pH 7.4

Wash buffer:
50 mM HEPES, 200 mM KCl, 1 mM $MgCl_2$, 1 mM EGTA, 1 mM DTT, 0.1 mM GTP, 0.2% Brij-35, pH 7.4

Elution buffer:
Storage buffer supplemented with 5 mM D-biotin (Sigma Aldrich; B4501)

For purification, 60 g of cell pellets were thawed in a water bath at room temperature. On ice, 2.5 mL lysis buffer and 1x cOmplete EDTA-free protease inhibitor tablet is added per 5 g of cell pellet. Pellets are resuspended and about ~100 mg DNaseI (Sigma Aldrich; DN25) is added in powder. Cells are lysed on ice using a polytron tissue dispenser (Blending cycle: Three rounds of $6.6x10^3$ rpm for 90 s each. Lysate is incubated on ice for 90 s between each round). When smaller amounts are processed (less than 30 g cell pellet) cells are lysed on ice by douncing (120 strokes) in a dounce tissue grinder of appropriate size.

Lysate is clarified twice by centrifugation at 17,000xg and 4°C for 15 min each using a JA-20 rotor. Clarified lysate is filtered through three sets of filters with decreasing pore size: 1.2 µM (cellulose acetate membrane, GE Healthcare; FP30/1.2 CA-S), 0.8 µM (cellulose acetate membrane, GE-Healthcare; FP 30/0.8 CA-S) and 0.45 µM (PVDF membrane, Millipore; SLHV033RS). Then lysate is buffer exchanged into storage buffer over HiPrep 26/10 desalting columns (1x column per 15 mL lysate, GE Healthcare; 17508701) to remove biotin. Protein containing fractions were pooled, supplemented with pre-dissolved cOmplete EDTA-free protease inhibitor tablets (2x per 50 mL lysate) and loaded onto a 1 mL HiTrap SP Sepharose FF column (SP FF, GE Healthcare; 17505401) connected in tandem with 1 mL Streptavidin mutein matrix beads (Sigma Aldrich; 3708152001) packed into a Tricorn 5/50 column (GE Healthcare; 28-4064-09) using a pressure pump at 0.5 mL/min in the cold room. Once lysate finished loading, SP FF column was disconnected and Streptavidin mutein matrix column was transferred to an ÄKTA purifier (GE Healthcare). Column was washed with 30 mL storage buffer, 30 mL wash buffer followed by another 30 mL storage buffer at a flow rate of 1 mL/min. Proteins were eluted with elution buffer at 0.5 mL/min and fractionated into 0.5 mL fractions.

γTuRC containing fractions (first two 2 fractions of elution peak) were pooled and buffer exchanged using a HiTrap Desalting column (2 mL sample volume per column, GE Healthcare, 17140801). Protein containing fractions were pooled and concentrated using Amicon centrifugal units (MWCO 30,000, Millipore; UFC803008) to 0.5 mL final volume. Sample is spun in a cooled table top centrifuge at maximum speed (17,000xg, Heraeus Fresco 17 Microcentrifuge) for 10 min and subjected to size exclusion chromatography using a Superose 6 10/300 GL column (GE Healthcare). Elution from size exclusion chromatography column is fractionated in 0.5 mL fractions. γTuRC peak fractions are pooled (~2 mL) and concentrated to ~0.2 mg/mL using Amicon centrifugal units. Purified protein was spun in a TLA120 rotor at 278088.3xg for 10 min at 4°C to remove aggregates, snap frozen in 3 µL aliquots and stored in liquid nitrogen.

6.8.1 Characterization of tagged γTuRC

Negative stain of fluorescently tagged γTuRC

Negative staining of γTuRC complexes was performed by Julia Locke (Alessandro Costa group, The Francis Crick Institute). A 4 µL droplet of freeze/thawed purified γTuRC (final concentration of 0.2 mg/mL) was applied to a freshly glow-discharged carbon-coated grid (C300Cu100, EM Resolution) and incubated for 2 min. The grid was stained with consecutive applications onto three 50 µL droplets of 2% uranyl acetate solution for 30 s each. Then, the grid was blotted dry and stored until imaged on a 120 keV G2 Spirit transmission electron microscope (FEI) equipped with a 2k×2k Ultrascan-1000 camera (Gatan). The Micrographs were collected at a pixel size of 3.45 Å at the specimen level.

LC-MS/MS analysis of fluorescently tagged γTuRC

Purified γTuRC was separated on SDS-Page (4-12% Bis-Tris gel, Invitrogen) as described above. Protein bands were cut and then analysed by the Francis Crick Institute Mass Spectrometry Proteomics facility. Proteins were in-gel digested with trypsin using a Janus automated liquid handling workstation (Perkin Elmer). Tryptic peptides were analysed using a Q Exactive Orbitrap mass spectrometer coupled to an Ultimate 3000 HPLC equipped with an EasySpray nanosource (Thermo Fisher Scientific). Peak lists were extracted from the raw data using Mascot Distiller, and searched with Mascot v2.4.1 (Matrix Science) against the Uniprot all species database. Search results were collated using Scaffold 4 (Proteome Software) and results are summarized in Table 13.

Table 13: LC-MS/MS results for each γTuRC subunit.

γTuRC subunits	Accession number	Unique peptide count	Sequence coverage (%)
GCP6	GCP6_HUMAN	49	43
GCP5	GCP5_HUMAN	49	43
GCP2-mBFP-Avitag	GCP2_HUMAN(+1)	48	55
GCP3	GCP3_HUMAN(+1)	37	37
GCP2	GCP2_HUMAN (+1)	29	33
GCP4	GCP4_HUMAN	17	33
γ-tubulin	TBG1_HUMAN	27	57

6.8.2 Optimization of tagged γTuRC purification

Ammonium sulphate precipitation of tagged γTuRC

For γTuRC purification with ammonium sulphate precipitation, γTuRC was purified from 30 g of HeLa-K cell pellet as described above with following modifications: SP FF cation exchange column was not used. 1 mL monomeric avidin beads were used instead of streptavidin mutein matrix beads. Instead of Brij-35, storage buffer contained 0.05% IGEPAL, wash buffer and elution buffer contained 0.5% IGEPAL and 250 mM KCl. AS precipitation was performed as described below and γTuRC conaining pellet was resuspended in 30 mL storage buffer. Elution was not buffer exchanged and concentrated using Vivaspin concentrators.

Streptavidin mutein matrix and monomeric avidin beads comparison

Experiment was performed with fluorescently tagged γTuRC using 5 g of HeLa-K cell pellet and 100 µL of streptavidin mutein matrix beads (Sigma Aldrich; 3708152001) and monomeric avidin beads (Thermo Fisher; 20228). Cell pellet was resuspended in lysis buffer (50 mM HEPES, pH 7.4, 150 mM KCl, 5 mM MgCl2, 1 mM EGTA, 1 mM DTT, 0.1 mM GTP) and ammonium sulphate precipitated as described above. 2.5 mL AS supernatant (resuspended in 5 mL lysis buffer) was incubated with each type of beads for 2 h in the cold room using a rotator. Beads were washed with 5 mL lysis buffer and γTuRC was eluted twice by incubating the beads for 30 min each with 0.5 mL elution buffer (lysis buffer, 1 mM $MgCl_2$, supplemented with 5 mM biotin and 0.02% Brij-35). Beads were washed once more with 1 mL elution buffer and samples of elution and beads were analyzed by western blot.

Cation exchange column

5 g HeLa-K cell pellet was resuspended in lysis buffer (50 mM HEPES, pH 7.4, 150 mM KCl, 5 mM MgCl2, 1 mM EGTA, 1 mM DTT, 0.1 mM GTP) and ammonium sulphate precipitated as described above. A sample of the AS supernatant (resuspended in 5 mL lysis buffer) was withdrawn and residual AS supernatant was flown through a 1 mL HiTrap SP Sepharose FF column (SP FF, GE Healthcare; 17505401). Input and flow through was compared by western blot.

6.9 Glass preparation

Glass was prepared as described (Bieling et al., 2010), with modifications. 22 x 22 mm coverslips (Menzel Gläser; #1.5) are marked with a 'C' on the lower right corner to decipher one side from another. Coverslips are then loaded in porcelain racks and sonicated in 3 M NaOH for 30 min. Coverslips are then rinsed with Milli-Q water, placed in an empty 1 L beaker and sonicated in Piranha solution (180 mL 95-97% H2SO4 + 120 mL 30% H2O2) for 45 min in a fume hood. Coverslips are washed by submerging in 4x1 L Milli-Q water, sonicated for 5 min, followed by washing by submersion in 4x1 L Milli-Q water. Coverslips are spin dried and one half is placed with their marked side up in clean glass petri dishes placed on a hot plate at 75°C. 2-3 drops of GOPTS (Sigma Aldrich; 440167) is added and the rest of the coverslips are placed marked side down on top to create a GOPTS sandwich, before they are placed in an oven at 75 °C for 30 min. Coverslips are taken out and left to cool for 15 min before being separated with a pair of razor blades and tossed into a beaker filled with 300 mL acetone. After 15 min coverslips are transferred into a second acetone beaker avoiding the slides drying at mid-air. During that 15 min, 0.1 g biotin-CONH-PEG-NH2 (Rapp Polymere; 133000-25-20) and 1 g HO-PEG-NH2 (Rapp Polymere; 10300-20) are combined at room temperature, and left rotating on rollers. Coverslips are spin dried and one half is placed with their marked side up in clean petri dishes on a hot plate at 75°C. About ~50 mg of PEG mix is added on top and the rest of the coverslips are placed marked side down on top to create a PEG sandwich, before they are placed in an oven at 75°C. Once the PEG has melted, bubbles are removed by gently pressing down on the sandwiches with forceps. Sandwiches are incubated overnight at 75°C. Coverslips are separated with a pair of razor blades on a hot plate at 75°C and tossed in Milli-Q water. Coverslips are sonicated for 30 min and washed with Milli-Q water until solution stops foaming. Coverslips are then spin dried and stored between lens cleaning tissue at 4°C for a maximum of 2 months.

6.10 Preparation of flow cells

Glass cover slips (76x26 mm, VWR, 631-1550P) were used for flow cell assembly. Two strips of double-sided tape (~2 cm, from Tesa) are placed ~5 mm apart parallel to one another on each coverslip. Tape is pressed down using forceps, then 10 µL of 2 mg/mL poly(L-lysine)-PEG (PLL, SuSoS) is spread between the tape using a pipette tip and left to dry for 20 min to 1h. Slides are washed with water and dried with N_2. Backs of double sided tapes are removed and a quarter of a coverslip, prepared as

described above, is placed on top with their marked side facing down. Coverslips are cut into quarters using a glass cutter. Edges of the flow cells are sealed by gently pressing down on the coverslip with forceps. Flow cells are used immediately or stored at 4°C and used within 24 h.

6.11 *In vitro* microscopy assay

All TIRF microscopy experiments were performed on a custom TIRFM microscope (Cairn Research, Faversham, UK) based on a Nikon Ti-E frame with a 60x 1.49 N.A. objective lens. The sample was excited using a 360°TIRF illumination. Images were acquired with an Andor iXon Ultra 888 EMCCD camera. The microscope chamber was kept at 33°C. Images were captured every 5 s for a total time of 20 minutes.

In vitro microscopy buffers

Pre-assay buffer: 80 mM PIPES, 60 mM KCl, 1 mM EGTA, 1 mM $MgCl_2$, 1 mM GTP, 5 mM βME, 0.15% (w/v) methylcellulose (4,000 cp, Sigma Aldrich) 1% (w/v) glucose, 0.02% (v/v) Brij-35.

Final assay buffer composition: 50% 2x Pre-Assay buffer stock diluted to 1x by addition of BRB80 (80 mM PIPES, 1 mM EGTA, 1 mM $MgCl_2$), and supplemented with 1 mg/mL BSA (20 mg/mL stock in BRB80, Sigma Aldrich, 05470), 1 mg/mL glucose oxidase (25 mg/mL stock in BRB80, Serva, 22778), 0.2 mg/mL catalase (6 mg/mL stock in BRB80, Sigma-Aldrich, c40) and tubulin mix (unlabelled and CF640R-labelled tubulin, labelling ratio 5.42%, final tubulin concentration is indicated for each experiment). For assays with γTuRC-binders or microtubule binders 2.9% of protein solution was added. Proteins concentrations were altered by predilution in their storage buffers (see above). chTOG-GFP was diluted in pre-assay buffer, and final assay buffer was spun in a TLA100 rotor (278088xg) for 10 min at 4°C after addition of chTOG-GFP. GFP-EB3 was diluted in BRB80. Final assay buffer volume was 70 µL.

γTuRC storage buffer: 50 mM HEPES, 150 mM KCl, 1 mM $MgCl_2$, 1 mM EGTA, 1 mM DTT, 0.1 mM GTP, 0.02% Brij-35, pH 7.4.

γTuRC nucleation assay

The assay is based on a published surface nucleation assay using microtubule binders (Roostalu et al., 2015) with modifications. All incubation steps were performed at room temperature. 50 µL 5% Pluronic F127 (Sigma Aldrich; P2443) in MilliQ water was flown through the flow cell and left to incubate for 10 min. Flow cell was washed with 2x50 µL pre-buffer (see above) supplemented with 0.2 mg/mL κ-casein (5 mg/mL stock in BRB80, Sigma Aldrich, C0406). Next, 50 µL pre-buffer supplemented with 0.2 mg/mL κ-casein and 0.05 mg/mL NeutrAvidin (5 mg/mL stock in 1xPBS and 20% glycerol, Thermo Fisher, A2666) was flown through the flow cell, and incubated for 3 min. Meanwhile, 1 µL of γTuRC (prediluted in γTuRC storage and kept on ice without loss of activity) was added to 54 µL γTuRC storage buffer on ice. Flow cell was washed with 2x50 µL of γTuRC storage buffer and 50 µL of γTuRC solution was flown through. γTuRC was left to bind for 5 min. In the meantime, final assay buffer was mixed on ice. Unbound γTuRC was removed by washing the flow cell with 2x50 µL of pre-buffer. 30 µL of final assay buffer was flown through the flow cell and left to incubate for 1 min. Another 30 µL of final assay buffer was flown through and flow cell was sealed using Korasilon paste (medium viscosity, Sigma Aldrich, 769681). Imaging was started 2 min after slide was transferred onto the TIRF microscope.

Microtubule seed assay

Seed assays were performed with fluorescently-labelled biotinylated GMPCPP stabilized microtubule seeds as described for γTuRC assay but instead of γTuRC, stabilized seeds were bound to the glass surface. Microtubule seeds were prepared as described (Bieling et al., 2010; Roostalu et al., 2015) by mixing 6.7 µM tubulin, 5 µM biotinylated tubulin and 7.1 µM CF640R-labelled tubulin and 0.5 µM GMPCPP (Jena bioscience, NU-405S) in a final volume of 60 µL BRB80. Mixture is kept on ice for 5 min and seeds are polymerized for 1 h at 37°C in a waterbath. 440 µL prewarmed BRB80 was added to the solution, and the reaction was spun at 17,000xg in a table top centrifuge for 10 min. The supernatant was discarded, and 500 µL fresh, prewarmed BRB80 was added followed by another spin at 17,000xg for 2 min. Supernatant was discarded, and pellet was resuspended in 500 µL prewarmed BRB80. Microtubule seeds were kept wrapped in foil at room temperature and used on the same day. For assays, 1 µL of the seeds solution was added to 54 µL of BRB80 and 50 µL of this solution was flown through the flow cell (pre-washed with 2x50 µL BRB80). ‘seeds’ were incubated for 3 min.

Temperature measurement in the flow cell

Flow cell for temperature measurement was prepared as described above. To create a flow cell of appropriate size to accommodate the thermistor needed for temperature measurement, three strips of double-sided tape were layered on top of each other. This results in a flow cell of approximately 6-fold more volume than flow cells used for experiments. For the temperature measurement a γTuRC assay was simulated by performing the same steps as described above but all protein containing solutions were replaced by the appropriate buffer solution. Flow cell was placed on the microscope objective, thermistor was introduced into the flow cell and the temperature increase within the flow cell was followed manually.

6.12 Live cell imaging

Live cell imaging was conducted by Jayant Asthana and Wei Ming Lim (both Surrey group, The Francis Crick Institute). BFP-GCP2-Avitag (clone15) and BFP-GCP-4-Avitag (clone 8) expressing HeLa-K cells were seeded at a density of 0.5×10^5 cells/ml on a ibidi 8 Well µ-Slide (ibidi, 80826). Cells were allowed to attach to the surface for 18 h, Imaging was performed at 37°C in phenol red free Dulbecco's minimal essential medium supplemented with 25 mM HEPES to keep the pH constant. Cells were observed for BFP localization using a 100x immersion objective in a spinning disc confocal microscope (Nikon).

6.13 Image analysis

Image processing was performed using ImageJ (https://imagej.nih.gov/ij/) to generate kymographs and to merge image sequences from different channels. For multi-colour imaging, a calibration grid was used to correct for camera drifts. Images were aligned using a MatLab based script as described (Maurer et al., 2014) and images were merged based on the alignment of the grid images of different channels/cameras. Background was subtracted using the build in background subtraction tool (ImageJ, "rolling ball" method) for clarity.

Measuring microtubule growth rates

Microtubule growth rates were measured directly from kymographs using the built in Resclice function in ImageJ. Lines were drawn manually along growing plus- and

minus-ends for microtubule growth rates. Values were calculated from the slope of the line.

Microtubule nucleation rate analysis

For each assay, microtubule numbers were counted manually at 10 different time points over the duration of the whole assay (20 min) using ImageJ and the build in ROI Manager tool. Only γTuRC nucleated microtubules were counted. For assays at high γTuRC concentration or tubulin concentration it was not possible to confidently count microtubule numbers for the whole assay duration due to high microtubule densities. Instead 10 time points for a shorter time period were counted (see Figures for specific times). Microtubule nucleation rates represent the slope of the linear regression for each condition. Linear regression fit was performed using a build in function of Sigmaplot.

6.14 Statistics

All error bars represent standard deviations. If not stated otherwise, all experiments presented in this thesis have been performed at least in triplicates. Linear regression and curve fitting were performed in Sigmaplot. Statistical significance was assessed using Prism software (GraphPad).

6.15 General computer software

DNA sequencing data was analysed using Ape, primers and cloning strategies were designed using Serial cloner and SnapGene software. Image analysis was performed using ImageJ. Data analysis was performed using Microsoft Excel, Sigmaplot (version 14) and MatLab. Metamorph was used as microscope control software for confocal and TIRF microscopes. Word processing was performed using Microsoft Word. Figures were created and arranged using Microsoft Power Point and Inkscape free software (https://inkscape.org/).

7. Appendix

Verification of specificity of GCP2 and GCP4 antibodies

Verification of antibodies using specific siRNAs was performed by Julian Gannon as described (Cota et al., 2017)

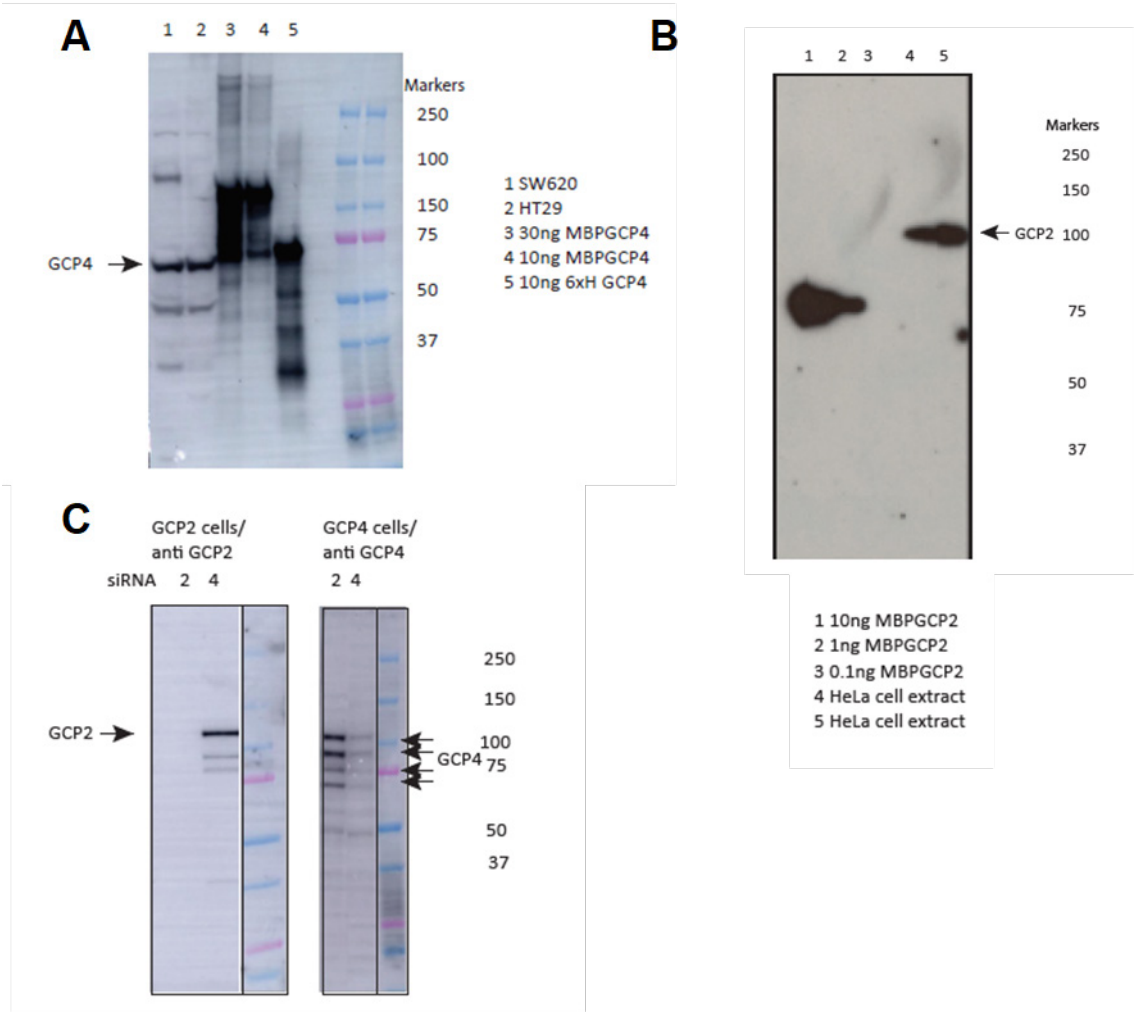

Figure 7.1: Specificity verification or polyclonal rabbit antibodies. Courtesy of Julian Gannon (Surrey group, The Francis Crick Institute). Polyclonal antibodies were tested against purified proteins and cell lysates as indicated. (A) Verification of anti-GCP4 specificity. (B) Verification of anti-GCP2 specificity. (C) anti-GCP2 and anti-GCP4 were tested for specificity against tagged GCP4 or tagged GCP2 overexpressed in stable HeLa-K cell lines (see chapter 6.3). anti-GCP4 antibody was produced against full-length GCP4. anti-GCP2 was produced against a GCP2 fragment (amino acids 1-155). See table Table 14.

Table 14: List of antibodies tested in this thesis. Peptide antibodies were raised in three rabbits, full-length and fragment antibodies in two rabbits. Full-length GCP3 was expressed but not send for antibody production. Full-length GCP5 and GCP6 could not be expressed in *E. coli*. Antibodies against GCP2 and GCP4 used in this thesis are marked in green.

Protein	Antigen	Sequence length (amino acids)	Specificity	Company
GCP2	Peptide	868-883	poor	Pettingill
	Protein fragment	1-155	good	Pettingill
GCP3	Peptide	627-641	poor	Pettingill
	Full-length protein	1-907	not tested	Covalab
	Protein fragment	1-159	poor	Pettingill
		709-907	poor	Pettingill
GCP4	Peptide	549-562	poor	Pettingill
	Full-length protein	1-666	poor	Pettingill
			poor	Biogenes
			good	Covalab
	Protein fragment	1-158	poor	Pettingill
		468-666	poor	Pettingill
GCP5	Peptide	974-989	poor	Pettingill
	Protein fragment	1-159	poor	Pettingill
			not tested	Biogenes
GCP6	Peptide	1664-1678	poor	Pettingill
	Protein fragment	1-159	poor	Pettingill
		668-842	poor	Pettingill
		153-335	good	Biogenes
	Protein fragments	153-335 and 668-842	good	Covalab

8. References

Abella, J.V.G., Galloni, C., Pernier, J., Barry, D.J., Kjær, S., Carlier, M.-F., and Way, M. (2016). Isoform diversity in the Arp2/3 complex determines actin filament dynamics. Nat. Cell Biol. *18*, 76–86.

Abraham, V.C., Krishnamurthi, V., Taylor, D.L., and Lanni, F. (1999). The Actin-Based Nanomachine at the Leading Edge of Migrating Cells. Biophys. J. *77*, 1721–1732.

Ahuja, R., Pinyol, R., Reichenbach, N., Custer, L., Klingensmith, J., Kessels, M.M., and Qualmann, B. (2007). Cordon-Bleu Is an Actin Nucleation Factor and Controls Neuronal Morphology. Cell *131*, 337–350.

Akashi, T., Yoon, Y., and Oakley, B.R. (1997). Characterization of gamma-tubulin complexes in Aspergillus nidulans and detection of putative gamma-tubulin interacting proteins. Cell Motil. Cytoskeleton *37*, 149–158.

Akhmanova, A., and Steinmetz, M.O. (2008). Tracking the ends: a dynamic protein network controls the fate of microtubule tips. Nat. Rev. Mol. Cell Biol. *9*, 309–322.

Akhmanova, A., and Steinmetz, M.O. (2015). Control of microtubule organization and dynamics: two ends in the limelight. Nat. Rev. Mol. Cell Biol. *16*, 711–726.

Al-Bassam, J., and Chang, F. (2011). Regulation of microtubule dynamics by TOG-domain proteins XMAP215/Dis1 and CLASP. Trends Cell Biol. *21*, 604–614.

Al-Bassam, J., Larsen, N.A., Hyman, A.A., and Harrison, S.C. (2007). Crystal structure of a TOG domain: conserved features of XMAP215/Dis1-family TOG domains and implications for tubulin binding. Struct. Lond. Engl. 1993 *15*, 355–362.

Aldaz, H., Rice, L.M., Stearns, T., and Agard, D.A. (2005). Insights into microtubule nucleation from the crystal structure of human γ-tubulin. Nature *435*, 523–527.

Alfaro-Aco, R., Thawani, A., and Petry, S. (2017). Structural analysis of the role of TPX2 in branching microtubule nucleation. J Cell Biol *216*, 983–997.

Allen, C., and Borisy, G.G. (1974). Structural polarity and directional growth of microtubules of Chlamydomonas flagella. J. Mol. Biol. *90*, 381–402.

Alushin, G.M., Lander, G.C., Kellogg, E.H., Zhang, R., Baker, D., and Nogales, E. (2014). High-Resolution Microtubule Structures Reveal the Structural Transitions in αβ-Tubulin upon GTP Hydrolysis. Cell *157*, 1117–1129.

Alvarado-Kristensson, M., Rodríguez, M.J., Silió, V., Valpuesta, J.M., and Carrera, A.C. (2009). SADB phosphorylation of γ-tubulin regulates centrosome duplication. Nat. Cell Biol. *11*, 1081–1092.

Amann, K.J., and Pollard, T.D. (2001). Direct real-time observation of actin filament branching mediated by Arp2/3 complex using total internal reflection fluorescence microscopy. Proc. Natl. Acad. Sci. *98*, 15009–15013.

Amos, L.A., and Klug, A. (1974). Arrangement of Subunits in Flagellar Microtubules. J. Cell Sci. *14*, 523–549.

Anders, A., Lourenço, P.C.C., and Sawin, K.E. (2006). Noncore Components of the Fission Yeast γ-Tubulin Complex. Mol. Biol. Cell *17*, 5075–5093.

Andersen, J.S., Wilkinson, C.J., Mayor, T., Mortensen, P., Nigg, E.A., and Mann, M. (2003). Proteomic characterization of the human centrosome by protein correlation profiling. Nature *426*, 570–574.

Arnal, I., and Wade, R.H. (1995). How does taxol stabilize microtubules? Curr. Biol. *5*, 900–908.

Asthana, J., Kapoor, S., Mohan, R., and Panda, D. (2013). Inhibition of HDAC6 Deacetylase Activity Increases Its Binding with Microtubules and Suppresses Microtubule Dynamic Instability in MCF-7 Cells. J. Biol. Chem. *288*, 22516–22526.

Atherton, J., Jiang, K., Stangier, M.M., Luo, Y., Hua, S., Houben, K., van Hooff, J.J.E., Joseph, A.-P., Scarabelli, G., Grant, B.J., et al. (2017). A structural model for microtubule minus-end recognition and protection by CAMSAP proteins. Nat. Struct. Mol. Biol. *24*, 931–943.

Atherton, J., Stouffer, M., Francis, F., and Moores, C.A. (2018). Microtubule architecture in vitro and in cells revealed by cryo-electron tomography. Acta Crystallogr. Sect. Struct. Biol. *74*, 572–584.

Avidor-Reiss, T., and Gopalakrishnan, J. (2013). Building a centriole. Curr. Opin. Cell Biol. *25*, 72–77.

Ayaz, P., Ye, X., Huddleston, P., Brautigam, C.A., and Rice, L.M. (2012). A TOG:αβ-tubulin complex structure reveals conformation-based mechanisms for a microtubule polymerase. Science *337*, 857–860.

Ayaz, P., Munyoki, S., Geyer, E.A., Piedra, F.-A., Vu, E.S., Bromberg, R., Otwinowski, Z., Grishin, N.V., Brautigam, C.A., and Rice, L.M. (2014). A tethered delivery mechanism explains the catalytic action of a microtubule polymerase. ELife *3*.

Baas, P.W., Deitch, J.S., Black, M.M., and Banker, G.A. (1988). Polarity orientation of microtubules in hippocampal neurons: uniformity in the axon and nonuniformity in the dendrite. Proc. Natl. Acad. Sci. *85*, 8335–8339.

Baas, P.W., Black, M.M., and Banker, G.A. (1989). Changes in microtubule polarity orientation during the development of hippocampal neurons in culture. J. Cell Biol. *109*, 3085–3094.

Bacallao, R., Antony, C., Dotti, C., Karsenti, E., Stelzer, E.H., and Simons, K. (1989). The subcellular organization of Madin-Darby canine kidney cells during the formation of a polarized epithelium. J. Cell Biol. *109*, 2817–2832.

Bahtz, R., Seidler, J., Arnold, M., Haselmann-Weiss, U., Antony, C., Lehmann, W.D., and Hoffmann, I. (2012). GCP6 is a substrate of Plk4 and required for centriole duplication. J Cell Sci *125*, 486–496.

Bartolini, F., and Gundersen, G.G. (2006). Generation of noncentrosomal microtubule arrays. J. Cell Sci. *119*, 4155–4163.

Bayliss, R., Sardon, T., Vernos, I., and Conti, E. (2003). Structural Basis of Aurora-A Activation by TPX2 at the Mitotic Spindle. Mol. Cell *12*, 851–862.

Beese, L., Stubbs, G., and Cohen, C. (1987). Microtubule structure at 18 A resolution. J. Mol. Biol. *194*, 257–264.

Bieling, P., Laan, L., Schek, H., Munteanu, E.L., Sandblad, L., Dogterom, M., Brunner, D., and Surrey, T. (2007). Reconstitution of a microtubule plus-end tracking system *in vitro*. Nature *450*, 1100–1105.

Bieling, P., Telley, I.A., Hentrich, C., Piehler, J., and Surrey, T. (2010). Chapter 28 - Fluorescence Microscopy Assays on Chemically Functionalized Surfaces for

Quantitative Imaging of Microtubule, Motor, and +TIP Dynamics. In Methods in Cell Biology, L.W. and J.J. Correia, ed. (Academic Press), pp. 555–580.

Bischoff, F.R., and Ponstingl, H. (1991a). Mitotic regulator protein RCC1 is complexed with a nuclear ras-related polypeptide. Proc. Natl. Acad. Sci. *88*, 10830–10834.

Bischoff, F.R., and Ponstingl, H. (1991b). Catalysis of guanine nucleotide exchange on Ran by the mitotic regulator RCC1. Nature *354*, 80.

Bischoff, F.R., Klebe, C., Kretschmer, J., Wittinghofer, A., and Ponstingl, H. (1994). RanGAP1 induces GTPase activity of nuclear Ras-related Ran. Proc. Natl. Acad. Sci. *91*, 2587–2591.

Borisy, G.G., Olmsted, J.B., and Klugman, R.A. (1972). In Vitro Aggregation of Cytoplasmic Microtubule Subunits. Proc. Natl. Acad. Sci. *69*, 2890–2894.

Bornens, M. (2012). The Centrosome in Cells and Organisms. Science *335*, 422–426.

Bouissou, A., Vérollet, C., Sousa, A., Sampaio, P., Wright, M., Sunkel, C.E., Merdes, A., and Raynaud-Messina, B. (2009). γ-Tubulin ring complexes regulate microtubule plus end dynamics. J. Cell Biol. *187*, 327–334.

Braun, M., Drummond, D.R., Cross, R.A., and McAinsh, A.D. (2009). The kinesin-14 Klp2 organizes microtubules into parallel bundles by an ATP-dependent sorting mechanism. Nat. Cell Biol. *11*, 724–730.

Bré, M.H., Pepperkok, R., Hill, A.M., Levilliers, N., Ansorge, W., Stelzer, E.H., and Karsenti, E. (1990). Regulation of microtubule dynamics and nucleation during polarization in MDCK II cells. J. Cell Biol. *111*, 3013–3021.

Brouhard, G.J. (2015). Dynamic instability 30 years later: complexities in microtubule growth and catastrophe. Mol. Biol. Cell *26*, 1207–1210.

Brouhard, G.J., and Rice, L.M. (2014). The contribution of αβ-tubulin curvature to microtubule dynamics. J. Cell Biol. *207*, 323–334.

Brouhard, G.J., and Rice, L.M. (2018). Microtubule dynamics: an interplay of biochemistry and mechanics. Nat. Rev. Mol. Cell Biol. *19*, 451.

Brouhard, G.J., Stear, J.H., Noetzel, T.L., Al-Bassam, J., Kinoshita, K., Harrison, S.C., Howard, J., and Hyman, A.A. (2008). XMAP215 is a processive microtubule polymerase. Cell *132*, 79–88.

Brunet, S., Sardon, T., Zimmerman, T., Wittmann, T., Pepperkok, R., Karsenti, E., and Vernos, I. (2004). Characterization of the TPX2 Domains Involved in Microtubule Nucleation and Spindle Assembly in Xenopus Egg Extracts. Mol. Biol. Cell *15*, 5318–5328.

Brunet, S., Dumont, J., Lee, K.W., Kinoshita, K., Hikal, P., Gruss, O.J., Maro, B., and Verlhac, M.-H. (2008). Meiotic regulation of TPX2 protein levels governs cell cycle progression in mouse oocytes. PloS One *3*, e3338.

Bu, W., and Su, L.-K. (2003). Characterization of Functional Domains of Human EB1 Family Proteins. J. Biol. Chem. *278*, 49721–49731.

Bugnard, E., Zaal, K.J.M., and Ralston, E. (2005). Reorganization of microtubule nucleation during muscle differentiation. Cell Motil. Cytoskeleton *60*, 1–13.

Busch, K.E., and Brunner, D. (2004). The Microtubule Plus End-Tracking Proteins mal3p and tip1p Cooperate for Cell-End Targeting of Interphase Microtubules. Curr. Biol. *14*, 548–559.

Calarco, P.G. (2000). Centrosome precursors in the acentriolar mouse oocyte. Microsc. Res. Tech. *49*, 428–434.

Cao, Y.-N., Zheng, L.-L., Wang, D., Liang, X.-X., Gao, F., and Zhou, X.-L. (2018). Recent advances in microtubule-stabilizing agents. Eur. J. Med. Chem. *143*, 806–828.

Carazo-Salas, R.E., Guarguaglini, G., Gruss, O.J., Segref, A., Karsenti, E., and Mattaj, I.W. (1999). Generation of GTP-bound Ran by RCC1 is required for chromatin-induced mitotic spindle formation. Nature *400*, 178–181.

Carlier, M.F. (1989). Role of nucleotide hydrolysis in the dynamics of actin filaments and microtubules. Int. Rev. Cytol. *115*, 139–170.

Carlier, M.F., and Pantaloni, D. (1978). Kinetic analysis of cooperativity in tubulin polymerization in the presence of guanosine di- or triphosphate nucleotides. Biochemistry *17*, 1908–1915.

Carlier, M.F., and Pantaloni, D. (1981). Kinetic analysis of guanosine 5'-triphosphate hydrolysis associated with tubulin polymerization. Biochemistry *20*, 1918–1924.

Casenghi, M., Meraldi, P., Weinhart, U., Duncan, P.I., Körner, R., and Nigg, E.A. (2003). Polo-like Kinase 1 Regulates Nlp, a Centrosome Protein Involved in Microtubule Nucleation. Dev. Cell *5*, 113–125.

Cassimeris, L., and Spittle, C. (2001). Regulation of microtubule-associated proteins. In International Review of Cytology, (Academic Press), pp. 163–226.

Castoldi, M., and Popov, A.V. (2003). Purification of brain tubulin through two cycles of polymerization–depolymerization in a high-molarity buffer. Protein Expr. Purif. *32*, 83–88.

Caudron, N., Valiron, O., Usson, Y., Valiron, P., and Job, D. (2000). A reassessment of the factors affecting microtubule assembly and disassembly in Vitro11Edited by A. Klug. J. Mol. Biol. *297*, 211–220.

Chabin-Brion, K., Marceiller, J., Perez, F., Settegrana, C., Drechou, A., Durand, G., and Poüs, C. (2001). The Golgi Complex Is a Microtubule-organizing Organelle. Mol. Biol. Cell *12*, 2047–2060.

Chang, F., Drubin, D., and Nurse, P. (1997). cdc12p, a Protein Required for Cytokinesis in Fission Yeast, Is a Component of the Cell Division Ring and Interacts with Profilin. J. Cell Biol. *137*, 169–182.

Charrier, E.E., and Janmey, P.A. (2016). Mechanical properties of intermediate filament proteins. Methods Enzymol. *568*, 35–57.

Chen, J., Kanai, Y., Cowan, N.J., and Hirokawa, N. (1992). Projection domains of MAP2 and tau determine spacings between microtubules in dendrites and axons. Nature *360*, 674.

Chen, J.V., Buchwalter, R.A., Kao, L.-R., and Megraw, T.L. (2017a). A Splice Variant of Centrosomin Converts Mitochondria to Microtubule-Organizing Centers. Curr. Biol. *27*, 1928-1940.e6.

Chen, J.W.C., Chen, Z.A., Rogala, K.B., Metz, J., Deane, C.M., Rappsilber, J., and Wakefield, J.G. (2017b). Cross-linking mass spectrometry identifies new interfaces of Augmin required to localise the γ-tubulin ring complex to the mitotic spindle. Biol. Open *6*, 654–663.

Cheng, F., and Eriksson, J.E. (2017). Intermediate Filaments and the Regulation of Cell Motility during Regeneration and Wound Healing. Cold Spring Harb. Perspect. Biol. *9*, a022046.

Chesarone, M.A., DuPage, A.G., and Goode, B.L. (2010). Unleashing formins to remodel the actin and microtubule cytoskeletons. Nat. Rev. Mol. Cell Biol. *11*, 62–74.

Choi, Y.-K., and Qi, R.Z. (2014). Chapter Seven - Assaying Microtubule Nucleation by the γ-Tubulin Ring Complex. In Methods in Enzymology, Ronald D. Vale, ed. (Academic Press), pp. 119–130.

Choi, Y.-K., Liu, P., Sze, S.K., Dai, C., and Qi, R.Z. (2010). CDK5RAP2 stimulates microtubule nucleation by the -tubulin ring complex. J. Cell Biol. *191*, 1089–1095.

Choy, R.M., Kollman, J.M., Zelter, A., Davis, T.N., and Agard, D.A. (2009). Localization and orientation of the γ-Tubulin Small Complex components using protein tags as labels for single particle EM. J. Struct. Biol. *168*, 571–574.

Chrétien, D., Fuller, S.D., and Karsenti, E. (1995). Structure of growing microtubule ends: two-dimensional sheets close into tubes at variable rates. J. Cell Biol. *129*, 1311–1328.

Chrétien, D., Buendia, B., Fuller, S.D., and Karsenti, E. (1997). Reconstruction of the Centrosome Cycle from Cryoelectron Micrographs. J. Struct. Biol. *120*, 117–133.

Cianfrocco, M.A., DeSantis, M.E., Leschziner, A.E., and Reck-Peterson, S.L. (2015). Mechanism and Regulation of Cytoplasmic Dynein. Annu. Rev. Cell Dev. Biol. *31*, 83–108.

Colombié, N., Vérollet, C., Sampaio, P., Moisand, A., Sunkel, C., Bourbon, H.-M., Wright, M., and Raynaud-Messina, B. (2006). The Drosophila γ-Tubulin Small Complex Subunit Dgrip84 Is Required for Structural and Functional Integrity of the Spindle Apparatus. Mol. Biol. Cell *17*, 272–282.

Conduit, P.T., Wainman, A., and Raff, J.W. (2015). Centrosome function and assembly in animal cells. Nat. Rev. Mol. Cell Biol. *16*, 611–624.

Cooper, J.A., Buhle, E.L., Walker, S.B., Tsong, T.Y., and Pollard, T.D. (1983). Kinetic evidence for a monomer activation step in actin polymerization. Biochemistry *22*, 2193–2202.

Corthésy-Theulaz, I., Pauloin, A., and Pfeffer, S.R. (1992). Cytoplasmic dynein participates in the centrosomal localization of the Golgi complex. J. Cell Biol. *118*, 1333–1345.

Cota, R.R., Teixidó-Travesa, N., Ezquerra, A., Eibes, S., Lacasa, C., Roig, J., and Lüders, J. (2017). MZT1 regulates microtubule nucleation by linking γTuRC assembly to adapter-mediated targeting and activation. J Cell Sci *130*, 406–419.

Cote, R.H., and Borisy, G.G. (1981). Head-to-tail polymerization of microtubules in vitro. J. Mol. Biol. *150*, 577–599.

Courtemanche, N. (2018). Mechanisms of formin-mediated actin assembly and dynamics. Biophys. Rev. *10*, 1553–1569.

Courtois, A., Schuh, M., Ellenberg, J., and Hiiragi, T. (2012). The transition from meiotic to mitotic spindle assembly is gradual during early mammalian development. J. Cell Biol. *198*, 357–370.

Coutts, A.S., Weston, L., and Thangue, N.B.L. (2009). A transcription co-factor integrates cell adhesion and motility with the p53 response. Proc. Natl. Acad. Sci. *106*, 19872–19877.

Cross, R.A., and McAinsh, A. (2014). Prime movers: the mechanochemistry of mitotic kinesins. Nat. Rev. Mol. Cell Biol. *15*, 257–271.

Cukier, C.D., Tourdes, A., El-Mazouni, D., Guillet, V., Nomme, J., Mourey, L., Milon, A., Merdes, A., and Gervais, V. (2017). NMR secondary structure and interactions of recombinant human MOZART1 protein, a component of the gamma-tubulin complex. Protein Sci. *26*, 2240–2248.

Dammermann, A., Desai, A., and Oegema, K. (2003). The minus end in sight. Curr. Biol. *13*, R614–R624.

Dammermann, A., Müller-Reichert, T., Pelletier, L., Habermann, B., Desai, A., and Oegema, K. (2004). Centriole Assembly Requires Both Centriolar and Pericentriolar Material Proteins. Dev. Cell *7*, 815–829.

David-Pfeuty, T., Erickson, H.P., and Pantaloni, D. (1977). Guanosinetriphosphatase activity of tubulin associated with microtubule assembly. Proc. Natl. Acad. Sci. *74*, 5372–5376.

Dehmelt, L., and Halpain, S. (2004). The MAP2/Tau family of microtubule-associated proteins. Genome Biol. 10.

Delgehyr, N., Sillibourne, J., and Bornens, M. (2005). Microtubule nucleation and anchoring at the centrosome are independent processes linked by ninein function. J. Cell Sci. *118*, 1565–1575.

Derivery, E., and Gautreau, A. (2010). Generation of branched actin networks: assembly and regulation of the N-WASP and WAVE molecular machines. BioEssays News Rev. Mol. Cell. Dev. Biol. *32*, 119–131.

Desai, A., and Mitchison, T.J. (1997). MICROTUBULE POLYMERIZATION DYNAMICS. Annu. Rev. Cell Dev. Biol. *13*, 83–117.

Détraves, C., Mazarguil, H., Lajoie-Mazenc, I., Julian, M., Raynaud-Messina, B., and Wright, M. (1997). Protein complexes containing gamma-tubulin are present in mammalian brain microtubule protein preparations. Cell Motil. *36*, 179–189.

Detrich, H.W., Jordan, M.A., Wilson, L., and Williams, R.C. (1985). Mechanism of microtubule assembly. Changes in polymer structure and organization during assembly of sea urchin egg tubulin. J. Biol. Chem. *260*, 9479–9490.

Dhani, D.K., Goult, B.T., George, G.M., Rogerson, D.T., Bitton, D.A., Miller, C.J., Schwabe, J.W.R., and Tanaka, K. (2013). Mzt1/Tam4, a fission yeast MOZART1 homologue, is an essential component of the γ-tubulin complex and directly interacts with GCP3Alp6. Mol. Biol. Cell *24*, 3337–3349.

Dictenberg, J.B., Zimmerman, W., Sparks, C.A., Young, A., Vidair, C., Zheng, Y., Carrington, W., Fay, F.S., and Doxsey, S.J. (1998). Pericentrin and γ-Tubulin Form a Protein Complex and Are Organized into a Novel Lattice at the Centrosome. J. Cell Biol. *141*, 163–174.

Doxsey, S.J., Stein, P., Evans, L., Calarco, P.D., and Kirschner, M. (1994). Pericentrin, a highly conserved centrosome protein involved in microtubule organization. Cell *76*, 639–650.

Drechsel, D.N., Hyman, A.A., Cobb, M.H., and Kirschner, M.W. (1992). Modulation of the dynamic instability of tubulin assembly by the microtubule-associated protein tau. Mol. Biol. Cell *3*, 1141–1154.

Duncan, T., and Wakefield, J.G. (2011). 50 ways to build a spindle: the complexity of microtubule generation during mitosis. Chromosome Res. *19*, 321–333.

Dyachuk, V., Bierkamp, C., and Merdes, A. (2016). Non-centrosomal Microtubule Organization in Differentiated Cells. In The Microtubule Cytoskeleton, J. Lüders, ed. (Vienna: Springer Vienna), pp. 27–41.

Efimov, A., Kharitonov, A., Efimova, N., Loncarek, J., Miller, P.M., Andreyeva, N., Gleeson, P., Galjart, N., Maia, A.R.R., McLeod, I.X., et al. (2007). Asymmetric CLASP-Dependent Nucleation of Noncentrosomal Microtubules at the trans-Golgi Network. Dev. Cell *12*, 917–930.

Ehler, E., Rothen, B.M., Hammerle, S.P., Komiyama, M., and Perriard, J.C. (1999). Myofibrillogenesis in the developing chicken heart: assembly of Z-disk, M-line and the thick filaments. J. Cell Sci. *112*, 1529–1539.

Ems-McClung, S.C., Zheng, Y., and Walczak, C.E. (2004). Importin α/β and Ran-GTP Regulate XCTK2 Microtubule Binding through a Bipartite Nuclear Localization Signal. Mol. Biol. Cell *15*, 46–57.

Erickson, H.P. (2000). Gamma-tubulin nucleation: template or protofilament? Nat. Cell Biol. *2*, E93-96.

Erickson, H.P., and Pantaloni, D. (1981). The role of subunit entropy in cooperative assembly. Nucleation of microtubules and other two-dimensional polymers. Biophys. J. *34*, 293–309.

Eriksson, J.E., Dechat, T., Grin, B., Helfand, B., Mendez, M., Pallari, H.-M., and Goldman, R.D. (2009). Introducing intermediate filaments: from discovery to disease. J. Clin. Invest. *119*, 1763–1771.

Erlemann, S., Neuner, A., Gombos, L., Gibeaux, R., Antony, C., and Schiebel, E. (2012). An extended γ-tubulin ring functions as a stable platform in microtubule nucleation. J. Cell Biol. *197*, 59–74.

Etienne-Manneville, S. (2018). Cytoplasmic Intermediate Filaments in Cell Biology. Annu. Rev. Cell Dev. Biol. *34*, 1–28.

Evangelista, M., Pruyne, D., Amberg, D.C., Boone, C., and Bretscher, A. (2002). Formins direct Arp2/3-independent actin filament assembly to polarize cell growth in yeast. Nat. Cell Biol. *4*, 32–41.

Evans, L., Mitchison, T., and Kirschner, M. (1985). Influence of the centrosome on the structure of nucleated microtubules. J. Cell Biol. *100*, 1185–1191.

Eyers, P.A., Erikson, E., Chen, L.G., and Maller, J.L. (2003). A Novel Mechanism for Activation of the Protein Kinase Aurora A. Curr. Biol. *13*, 691–697.

Fant, X., Srsen, V., Espigat-Georger, A., and Merdes, A. (2009). Nuclei of Non-Muscle Cells Bind Centrosome Proteins upon Fusion with Differentiating Myoblasts. PLOS ONE *4*, e8303.

Farache, D., Jauneau, A., Chemin, C., Chartrain, M., Remy, M.-H., Merdes, A., and Haren, L. (2016). Functional Analysis of Gamma-tubulin Complex Proteins Indicates Specific Lateral Association via their N-terminal Domains. J. Biol. Chem. jbc.M116.744862.

Farache, D., Emorine, L., Haren, L., and Merdes, A. (2018). Assembly and regulation of γ-tubulin complexes. Open Biol. *8*, 170266.

Farhadi, L., Fermino Do Rosario, C., Debold, E.P., Baskaran, A., and Ross, J.L. (2018). Active Self-Organization of Actin-Microtubule Composite Self-Propelled Rods. Front. Phys. *6*.

Fava, F., Raynaud-Messina, B., Leung-Tack, J., Mazzolini, L., Li, M., Guillemot, J.C., Cachot, D., Tollon, Y., Ferrara, P., and Wright, M. (1999). Human 76p A New

Member of the γ-Tubulin–Associated Protein Family. J. Cell Biol. *147*, 857–868.

Feierbach, B., and Chang, F. (2001). Roles of the fission yeast formin for3p in cell polarity, actin cable formation and symmetric cell division. Curr. Biol. *11*, 1656–1665.

Ferreira, J.G., Pereira, A.L., and Maiato, H. (2014). Chapter Two - Microtubule Plus-End Tracking Proteins and Their Roles in Cell Division. In International Review of Cell and Molecular Biology, K.W. Jeon, ed. (Academic Press), pp. 59–140.

Fink, G., Hajdo, L., Skowronek, K.J., Reuther, C., Kasprzak, A.A., and Diez, S. (2009). The mitotic kinesin-14 Ncd drives directional microtubule–microtubule sliding. Nat. Cell Biol. *11*, 717–723.

Firat-Karalar, E.N., and Welch, M.D. (2011). New mechanisms and functions of actin nucleation. Curr. Opin. Cell Biol. *23*, 4–13.

Fish, K.N. (2009). Total Internal Reflection Fluorescence (TIRF) Microscopy. Curr. Protoc. Cytom. Editor. Board J Paul Robinson Manag. Ed. Al *0 12*, Unit12.18.

Fitzgerald, D.J., Schaffitzel, C., Berger, P., Wellinger, R., Bieniossek, C., Richmond, T.J., and Berger, I. (2007). Multiprotein Expression Strategy for Structural Biology of Eukaryotic Complexes. Structure *15*, 275–279.

Fletcher, D.A., and Mullins, R.D. (2010). Cell mechanics and the cytoskeleton. Nature *463*, 485–492.

Flyvbjerg, H., and Jobs, E. (1997). Microtubule dynamics. II. Kinetics of self-assembly. Phys. Rev. E *56*, 7083–7099.

Fong, K.-W., Choi, Y.-K., Rattner, J.B., and Qi, R.Z. (2008). CDK5RAP2 Is a Pericentriolar Protein That Functions in Centrosomal Attachment of the -Tubulin Ring Complex. Mol. Biol. Cell *19*, 115–125.

Fong, K.-W., Au, F.K.C., Jia, Y., Yang, S., Zhou, L., and Qi, R.Z. (2017). Microtubule plus-end tracking of end-binding protein 1 (EB1) is regulated by CDK5 regulatory subunit-associated protein 2. J. Biol. Chem. *292*, 7675–7687.

Forth, S., Hsia, K.-C., Shimamoto, Y., and Kapoor, T.M. (2014). Asymmetric Friction of Nonmotor MAPs Can Lead to Their Directional Motion in Active Microtubule Networks. Cell *157*, 420–432.

Franker, M.A.M., and Hoogenraad, C.C. (2013). Microtubule-based transport – basic mechanisms, traffic rules and role in neurological pathogenesis. J. Cell Sci. *126*, 2319–2329.

Fujita, A., Vardy, L., Garcia, M.A., and Toda, T. (2002). A Fourth Component of the Fission Yeast γ-Tubulin Complex, Alp16, Is Required for Cytoplasmic Microtubule Integrity and Becomes Indispensable When γ-Tubulin Function Is Compromised. Mol. Biol. Cell *13*, 2360–2373.

Fujiwara, I., Takahashi, S., Tadakuma, H., Funatsu, T., and Ishiwata, S. (2002). Microscopic analysis of polymerization dynamics with individual actin filaments. Nat. Cell Biol. *4*, 666.

Fygenson, D.K., Braun, E., and Libchaber, A. (1994). Phase diagram of microtubules. Phys. Rev. E *50*, 1579–1588.

Gapud, E.J., Bai, R., Ghosh, A.K., and Hamel, E. (2004). Laulimalide and Paclitaxel: A Comparison of Their Effects on Tubulin Assembly and Their Synergistic Action When Present Simultaneously. Mol. Pharmacol. *66*, 113–121.

Gard, D.L., and Kirschner, M.W. (1987). A microtubule-associated protein from Xenopus eggs that specifically promotes assembly at the plus-end. J. Cell Biol. *105*, 2203–2215.

Gardner, M.K., Charlebois, B.D., Jánosi, I.M., Howard, J., Hunt, A.J., and Odde, D.J. (2011). Rapid microtubule self-assembly kinetics. Cell *146*, 582–592.

Gardner, M.K., Zanic, M., and Howard, J. (2013). Microtubule catastrophe and rescue. Curr. Opin. Cell Biol. *25*, 14–22.

Garrett, S., Auer, K., Compton, D.A., and Kapoor, T.M. (2002). hTPX2 Is Required for Normal Spindle Morphology and Centrosome Integrity during Vertebrate Cell Division. Curr. Biol. *12*, 2055–2059.

Gavilan, M.P., Gandolfo, P., Balestra, F.R., Arias, F., Bornens, M., and Rios, R.M. (2017). The Centrosome Controls the Number and Spatial Distribution of Microtubules by Negatively Regulating Alternative MTOCs. BioRxiv 153304.

Gavilan, M.P., Gandolfo, P., Balestra, F.R., Arias, F., Bornens, M., and Rios, R.M. (2018). The dual role of the centrosome in organizing the microtubule network in interphase. EMBO Rep. *19*.

Geisler, N., and Weber, K. (1982). The amino acid sequence of chicken muscle desmin provides a common structural model for intermediate filament proteins. EMBO J. *1*, 1649–1656.

Geissler, S., Pereira, G., Spang, A., Knop, M., Souès, S., Kilmartin, J., and Schiebel, E. (1996). The spindle pole body component Spc98p interacts with the gamma-tubulin-like Tub4p of Saccharomyces cerevisiae at the sites of microtubule attachment. EMBO J. *15*, 3899–3911.

Gekko, K., and Timasheff, S.N. (1981). Mechanism of protein stabilization by glycerol: preferential hydration in glycerol-water mixtures. Biochemistry *20*, 4667–4676.

Ghosh, S., Hentrich, C., and Surrey, T. (2013). Micropattern-controlled local microtubule nucleation, transport, and mesoscale organization. ACS Chem. Biol. *8*, 673–678.

Gigant, B., Curmi, P.A., Martin-Barbey, C., Charbaut, E., Lachkar, S., Lebeau, L., Siavoshian, S., Sobel, A., and Knossow, M. (2000). The 4 Å X-Ray Structure of a Tubulin:Stathmin-like Domain Complex. Cell *102*, 809–816.

Gimona, M., Djinovic-Carugo, K., Kranewitter, W.J., and Winder, S.J. (2002). Functional plasticity of CH domains. FEBS Lett. *513*, 98–106.

Gittes, F. (1993). Flexural rigidity of microtubules and actin filaments measured from thermal fluctuations in shape. J. Cell Biol. *120*, 923–934.

Goley, E.D., Rammohan, A., Znameroski, E.A., Firat-Karalar, E.N., Sept, D., and Welch, M.D. (2010). An actin-filament-binding interface on the Arp2/3 complex is critical for nucleation and branch stability. Proc. Natl. Acad. Sci. *107*, 8159–8164.

Gombos, L., Neuner, A., Berynskyy, M., Fava, L.L., Wade, R.C., Sachse, C., and Schiebel, E. (2013). GTP regulates the microtubule nucleation activity of γ-tubulin. Nat. Cell Biol. *15*, 1317–1327.

Gomez-Ferreria, M.A., Bashkurov, M., Helbig, A.O., Larsen, B., Pawson, T., Gingras, A.-C., and Pelletier, L. (2012). Novel NEDD1 phosphorylation sites regulate γ-tubulin binding and mitotic spindle assembly. J. Cell Sci. *125*, 3745–3751.

Görlich, D., Panté, N., Kutay, U., Aebi, U., and Bischoff, F.R. (1996). Identification of different roles for RanGDP and RanGTP in nuclear protein import. EMBO J. *15*, 5584–5594.

Goshima, G., and Kimura, A. (2010). New look inside the spindle: microtubule-dependent microtubule generation within the spindle. Curr. Opin. Cell Biol. *22*, 44–49.

Goshima, G., Wollman, R., Goodwin, S.S., Zhang, N., Scholey, J.M., Vale, R.D., and Stuurman, N. (2007). Genes Required for Mitotic Spindle Assembly in Drosophila S2 Cells. Science *316*, 417–421.

Goshima, G., Mayer, M., Zhang, N., Stuurman, N., and Vale, R.D. (2008). Augmin: a protein complex required for centrosome-independent microtubule generation within the spindle. J. Cell Biol. *181*, 421–429.

Gould, R.R., and Borisy, G.G. (1977). The pericentriolar material in Chinese hamster ovary cells nucleates microtubule formation. J. Cell Biol. *73*, 601–615.

Gouveia, S.M., and Akhmanova, A. (2010). Chapter One - Cell and Molecular Biology of Microtubule Plus End Tracking Proteins: End Binding Proteins and Their Partners. In International Review of Cell and Molecular Biology, K.W. Jeon, ed. (Academic Press), pp. 1–74.

Gräf, R., Euteneuer, U., Ho, T.-H., and Rehberg, M. (2003). Regulated expression of the centrosomal protein DdCP224 affects microtubule dynamics and reveals mechanisms for the control of supernumerary centrosome number. Mol. Biol. Cell *14*, 4067–4074.

Grimaldi, A.D., Zanic, M., and Kaverina, I. (2015). Encoding the microtubule structure: Allosteric interactions between the microtubule +TIP complex master regulators and TOG-domain proteins. Cell Cycle Georget. Tex *14*, 1375–1378.

Groen, A.C., Cameron, L.A., Coughlin, M., Miyamoto, D.T., Mitchison, T.J., and Ohi, R. (2004). XRHAMM Functions in Ran-Dependent Microtubule Nucleation and Pole Formation during Anastral Spindle Assembly. Curr. Biol. *14*, 1801–1811.

Groen, A.C., Maresca, T.J., Gatlin, J.C., Salmon, E.D., and Mitchison, T.J. (2009). Functional Overlap of Microtubule Assembly Factors in Chromatin-Promoted Spindle Assembly. Mol. Biol. Cell *20*, 2766–2773.

Gruss, O.J., and Vernos, I. (2004). The mechanism of spindle assembly functions of Ran and its target TPX2. J. Cell Biol. *166*, 949–955.

Gruss, O.J., Carazo-Salas, R.E., Schatz, C.A., Guarguaglini, G., Kast, J., Wilm, M., Le Bot, N., Vernos, I., Karsenti, E., and Mattaj, I.W. (2001). Ran Induces Spindle Assembly by Reversing the Inhibitory Effect of Importin α on TPX2 Activity. Cell *104*, 83–93.

Gruss, O.J., Wittmann, M., Yokoyama, H., Pepperkok, R., Kufer, T., Silljé, H., Karsenti, E., Mattaj, I.W., and Vernos, I. (2002). Chromosome-induced microtubule assembly mediated by TPX2 is required for spindle formation in HeLa cells. Nat. Cell Biol. *4*, 871–879.

Guerin, C.M., and Kramer, S.G. (2009). RacGAP50C directs perinuclear γ-tubulin localization to organize the uniform microtubule array required for Drosophila myotube extension. Dev. Camb. Engl. *136*, 1411–1421.

Guesdon, A., Bazile, F., Buey, R.M., Mohan, R., Monier, S., García, R.R., Angevin, M., Heichette, C., Wieneke, R., Tampé, R., et al. (2016). EB1 interacts with

outwardly curved and straight regions of the microtubule lattice. Nat. Cell Biol. *18*, 1102–1108.

Guillet, V., Knibiehler, M., Gregory-Pauron, L., Remy, M.-H., Chemin, C., Raynaud-Messina, B., Bon, C., Kollman, J.M., Agard, D.A., Merdes, A., et al. (2011). Crystal structure of γ-tubulin complex protein GCP4 provides insight into microtubule nucleation. Nat. Struct. Mol. Biol. *18*, 915–919.

Gunawardane, R.N., Martin, O.C., Cao, K., Zhang, L., Dej, K., Iwamatsu, A., and Zheng, Y. (2000). Characterization and Reconstitution of Drosophila γ-Tubulin Ring Complex Subunits. J. Cell Biol. *151*, 1513–1524.

Gunawardane, R.N., Zheng, Y., Oegema, K., and Wiese, C. (2001). Purification and reconstitution of Drosophila γ-tubulin complexes. In Methods in Cell Biology, T.N.D. Robert E. Palazzo, ed. (Academic Press), pp. 1–25.

Gunawardane, R.N., Martin, O.C., and Zheng, Y. (2003). Characterization of a New γTuRC Subunit with WD Repeats. Mol. Biol. Cell *14*, 1017–1026.

Gunzelmann, J., Rüthnick, D., Lin, T., Zhang, W., Neuner, A., Jäkle, U., and Schiebel, E. (2018). The microtubule polymerase Stu2 promotes oligomerization of the γ-TuSC for cytoplasmic microtubule nucleation. ELife *7*, e39932.

Hamel, E., Lustbader, J., and Lin, C.M. (1984). Deoxyguanosine nucleotide analogues: potent stimulators of microtubule nucleation with reduced affinity for the exchangeable nucleotide site of tubulin. Biochemistry *23*, 5314–5325.

Hamel, E., Day, B.W., Miller, J.H., Jung, M.K., Northcote, P.T., Ghosh, A.K., Curran, D.P., Cushman, M., Nicolaou, K.C., Paterson, I., et al. (2006). Synergistic effects of peloruside A and laulimalide with taxoid site drugs, but not with each other, on tubulin assembly. Mol. Pharmacol. *70*, 1555–1564.

Hannak, E., Oegema, K., Kirkham, M., Gönczy, P., Habermann, B., and Hyman, A.A. (2002). The kinetically dominant assembly pathway for centrosomal asters in *Caenorhabditis elegans* is γ-tubulin dependent. J. Cell Biol. *157*, 591–602.

Haren, L., Remy, M.-H., Bazin, I., Callebaut, I., Wright, M., and Merdes, A. (2006). NEDD1-dependent recruitment of the γ-tubulin ring complex to the centrosome is necessary for centriole duplication and spindle assembly. J. Cell Biol. *172*, 505–515.

Haren, L., Stearns, T., and Lüders, J. (2009). Plk1-Dependent Recruitment of γ-Tubulin Complexes to Mitotic Centrosomes Involves Multiple PCM Components. PLoS ONE *4*, e5976.

Harris, E.S., Li, F., and Higgs, H.N. (2004). The Mouse Formin, FRLα, Slows Actin Filament Barbed End Elongation, Competes with Capping Protein, Accelerates Polymerization from Monomers, and Severs Filaments. J. Biol. Chem. *279*, 20076–20087.

Hayashi, I., and Ikura, M. (2003). Crystal Structure of the Amino-terminal Microtubule-binding Domain of End-binding Protein 1 (EB1). J. Biol. Chem. *278*, 36430–36434.

Hayward, D., Metz, J., Pellacani, C., and Wakefield, J.G. (2014). Synergy between Multiple Microtubule-Generating Pathways Confers Robustness to Centrosome-Driven Mitotic Spindle Formation. Dev. Cell *28*, 81–93.

Heim, R., and Tsien, R.Y. (1996). Engineering green fluorescent protein for improved brightness, longer wavelengths and fluorescence resonance energy transfer. Curr. Biol. *6*, 178–182.

Helmke, K.J., Heald, R., and Wilbur, J.D. (2013). Interplay between spindle architecture and function. Int. Rev. Cell Mol. Biol. *306*, 83–125.

Hendershott, M.C., and Vale, R.D. (2014). Regulation of microtubule minus-end dynamics by CAMSAPs and Patronin. Proc. Natl. Acad. Sci. U. S. A. *111*, 5860–5865.

Herrmann, H., and Aebi, U. (1998). Intermediate filament assembly: fibrillogenesis is driven by decisive dimer-dimer interactions. Curr. Opin. Struct. Biol. *8*, 177–185.

Hesse, M., Magin, T.M., and Weber, K. (2001). Genes for intermediate filament proteins and the draft sequence of the human genome: novel keratin genes and a surprisingly high number of pseudogenes related to keratin genes 8 and 18. J. Cell Sci. *114*, 2569–2575.

Higashida, C., Miyoshi, T., Fujita, A., Oceguera-Yanez, F., Monypenny, J., Andou, Y., Narumiya, S., and Watanabe, N. (2004). Actin Polymerization-Driven Molecular Movement of mDia1 in Living Cells. Science *303*, 2007–2010.

Higgs, H.N., and Pollard, T.D. (1999). Regulation of Actin Polymerization by Arp2/3 Complex and WASp/Scar Proteins. J. Biol. Chem. *274*, 32531–32534.

Himes, R.H., Burton, P.R., and Gaito, J.M. (1977). Dimethyl sulfoxide-induced self-assembly of tubulin lacking associated proteins. J. Biol. Chem. *252*, 6222–6228.

Hirokawa, N., Noda, Y., Tanaka, Y., and Niwa, S. (2009). Kinesin superfamily motor proteins and intracellular transport. Nat. Rev. Mol. Cell Biol. *10*, 682–696.

Holmes, K.C., Popp, D., Gebhard, W., and Kabsch, W. (1990). Atomic model of the actin filament. Nature *347*, 44–49.

Honnappa, S., John, C.M., Kostrewa, D., Winkler, F.K., and Steinmetz, M.O. (2005). Structural insights into the EB1–APC interaction. EMBO J. *24*, 261–269.

Honnappa, S., Gouveia, S.M., Weisbrich, A., Damberger, F.F., Bhavesh, N.S., Jawhari, H., Grigoriev, I., van Rijssel, F.J.A., Buey, R.M., Lawera, A., et al. (2009). An EB1-Binding Motif Acts as a Microtubule Tip Localization Signal. Cell *138*, 366–376.

Horesh, D., Sapir, T., Francis, F., Grayer Wolf, S., Caspi, M., Elbaum, M., Chelly, J., and Reiner, O. (1999). Doublecortin, a Stabilizer of Microtubules. Hum. Mol. Genet. *8*, 1599–1610.

Horio, T. (2007). Role of microtubules in tip growth of fungi. J. Plant Res. *120*, 53–60.

Horio, T., Uzawa, S., Jung, M.K., Oakley, B.R., Tanaka, K., and Yanagida, M. (1991). The fission yeast gamma-tubulin is essential for mitosis and is localized at microtubule organizing centers. J. Cell Sci. *99 (Pt 4)*, 693–700.

Howard, J., and Hyman, A.A. (2007). Microtubule polymerases and depolymerases. Curr. Opin. Cell Biol. *19*, 31–35.

Hsia, K.-C., Wilson-Kubalek, E.M., Dottore, A., Hao, Q., Tsai, K.-L., Forth, S., Shimamoto, Y., Milligan, R.A., and Kapoor, T.M. (2014). Reconstitution of the augmin complex provides insights into its architecture and function. Nat. Cell Biol. *16*, 852–863.

Hurtado, L., Caballero, C., Gavilan, M.P., Cardenas, J., Bornens, M., and Rios, R.M. (2011). Disconnecting the Golgi ribbon from the centrosome prevents directional cell migration and ciliogenesis. J. Cell Biol. *193*, 917–933.

Hutchins, J.R.A., Toyoda, Y., Hegemann, B., Poser, I., Hériché, J.-K., Sykora, M.M., Augsburg, M., Hudecz, O., Buschhorn, B.A., Bulkescher, J., et al. (2010).

Systematic Analysis of Human Protein Complexes Identifies Chromosome Segregation Proteins. Science *328*, 593–599.

Hyman, A., and Karsenti, E. (1998). The role of nucleation in patterning microtubule networks. J. Cell Sci. *111 (Pt 15)*, 2077–2083.

Hyman, A., Drechsel, D., Kellogg, D., Salser, S., Sawin, K., Steffen, P., Wordeman, L., and Mitchison, T. (1991). [39] Preparation of modified tubulins. In Methods in Enzymology, (Academic Press), pp. 478–485.

Hyman, A.A., Salser, S., Drechsel, D.N., Unwin, N., and Mitchison, T.J. (1992). Role of GTP hydrolysis in microtubule dynamics: information from a slowly hydrolyzable analogue, GMPCPP. Mol. Biol. Cell *3*, 1155–1167.

Hyman, A.A., Chrétien, D., Arnal, I., and Wade, R.H. (1995). Structural changes accompanying GTP hydrolysis in microtubules: information from a slowly hydrolyzable analogue guanylyl-(alpha,beta)-methylene-diphosphonate. J. Cell Biol. *128*, 117–125.

Inoue, D., Mahmot, B., Kabir, A.M.R., Farhana, T.I., Tokuraku, K., Sada, K., Konagaya, A., and Kakugo, A. (2015). Depletion force induced collective motion of microtubules driven by kinesin. Nanoscale *7*, 18054–18061.

Ismail, A.M., Padrick, S.B., Chen, B., Umetani, J., and Rosen, M.K. (2009). The WAVE regulatory complex is inhibited. Nat. Struct. Mol. Biol. *16*, 561–563.

Izaurralde, E., Kutay, U., von Kobbe, C., Mattaj, I.W., and Görlich, D. (1997). The asymmetric distribution of the constituents of the Ran system is essential for transport into and out of the nucleus. EMBO J. *16*, 6535–6547.

Izumi, N., Fumoto, K., Izumi, S., and Kikuchi, A. (2008). GSK-3β Regulates Proper Mitotic Spindle Formation in Cooperation with a Component of the γ-Tubulin Ring Complex, GCP5. J. Biol. Chem. *283*, 12981–12991.

Janmey, P.A., Euteneuer, U., Traub, P., and Schliwa, M. (1991). Viscoelastic properties of vimentin compared with other filamentous biopolymer networks. J. Cell Biol. *113*, 155–160.

Janski, N., Masoud, K., Batzenschlager, M., Herzog, E., Evrard, J.-L., Houlné, G., Bourge, M., Chabouté, M.-E., and Schmit, A.-C. (2012). The GCP3-interacting proteins GIP1 and GIP2 are required for γ-tubulin complex protein localization, spindle integrity, and chromosomal stability. Plant Cell *24*, 1171–1187.

Jha, R., Roostalu, J., Cade, N.I., Trokter, M., and Surrey, T. (2017). Combinatorial regulation of the balance between dynein microtubule end accumulation and initiation of directed motility. EMBO J. *36*, 3387–3404.

Jiang, K., and Akhmanova, A. (2011). Microtubule tip-interacting proteins: a view from both ends. Curr. Opin. Cell Biol. *23*, 94–101.

Jiang, K., Hua, S., Mohan, R., Grigoriev, I., Yau, K.W., Liu, Q., Katrukha, E.A., Altelaar, A.F.M., Heck, A.J.R., Hoogenraad, C.C., et al. (2014). Microtubule minus-end stabilization by polymerization-driven CAMSAP deposition. Dev. Cell *28*, 295–309.

Job, D., Valiron, O., and Oakley, B. (2003). Microtubule nucleation. Curr. Opin. Cell Biol. *15*, 111–117.

Johmura, Y., Soung, N.-K., Park, J.-E., Yu, L.-R., Zhou, M., Bang, J.K., Kim, B.-Y., Veenstra, T.D., Erikson, R.L., and Lee, K.S. (2011). Regulation of microtubule-based microtubule nucleation by mammalian polo-like kinase 1. Proc. Natl. Acad. Sci. *108*, 11446–11451.

Johnson, K.A., and Borisy, G.G. (1977). Kinetic analysis of microtubule self-assembly in vitro. J. Mol. Biol. *117*, 1–31.

Jolly, A.L., Kim, H., Srinivasan, D., Lakonishok, M., Larson, A.G., and Gelfand, V.I. (2010). Kinesin-1 heavy chain mediates microtubule sliding to drive changes in cell shape. Proc. Natl. Acad. Sci. U. S. A. *107*, 12151–12156.

Jordan, M.A., Thrower, D., and Wilson, L. (1992). Effects of vinblastine, podophyllotoxin and nocodazole on mitotic spindles. Implications for the role of microtubule dynamics in mitosis. J. Cell Sci. *102 (Pt 3)*, 401–416.

Joshi, H.C., Palacios, M.J., McNamara, L., and Cleveland, D.W. (1992). γ-Tubulin is a centrosomal protein required for cell cycle-dependent microtubule nucleation. Nature *356*, 80.

Jourdain, L., Curmi, P., Sobel, A., Pantaloni, D., and Carlier, M.-F. (1997). Stathmin: A Tubulin-Sequestering Protein Which Forms a Ternary T2S Complex with Two Tubulin Molecules. Biochemistry *36*, 10817–10821.

Kabsch, W., Mannherz, H.G., Suck, D., Pai, E.F., and Holmes, K.C. (1990). Atomic structure of the actin: DNase I complex. Nature *347*, 37–44.

Kalab, P., Pu, R.T., and Dasso, M. (1999). The Ran GTPase regulates mitotic spindle assembly. Curr. Biol. *9*, 481–484.

Kalab, P., Weis, K., and Heald, R. (2002). Visualization of a Ran-GTP Gradient in Interphase and Mitotic Xenopus Egg Extracts. Science *295*, 2452–2456.

Kaláb, P., Pralle, A., Isacoff, E.Y., Heald, R., and Weis, K. (2006). Analysis of a RanGTP-regulated gradient in mitotic somatic cells. Nature *440*, 697–701.

Kamasaki, T., Osumi, M., and Mabuchi, I. (2007). Three-dimensional arrangement of F-actin in the contractile ring of fission yeast. J. Cell Biol. *178*, 765–771.

Kasai, M., Asakura, S., and Oosawa, F. (1962). The G-F equilibrium in actin solutions under various conditions. Biochim. Biophys. Acta *57*, 13–21.

Kawamura, E., Himmelspach, R., Rashbrooke, M.C., Whittington, A.T., Gale, K.R., Collings, D.A., and Wasteneys, G.O. (2006). MICROTUBULE ORGANIZATION 1 regulates structure and function of microtubule arrays during mitosis and cytokinesis in the Arabidopsis root. Plant Physiol. *140*, 102–114.

Keating, T.J., and Borisy, G.G. (2000). Immunostructural evidence for the template mechanism of microtubule nucleation. Nat. Cell Biol. *2*, 352.

Kelleher, J.F., Atkinson, S.J., and Pollard, T.D. (1995). Sequences, structural models, and cellular localization of the actin-related proteins Arp2 and Arp3 from Acanthamoeba. J. Cell Biol. *131*, 385–397.

Kellogg, E.H., Hejab, N.M.A., Howes, S., Northcote, P., Miller, J.H., Díaz, J.F., Downing, K.H., and Nogales, E. (2017). Insights into the Distinct Mechanisms of Action of Taxane and Non-Taxane Microtubule Stabilizers from Cryo-EM Structures. J. Mol. Biol. *429*, 633–646.

Khodjakov, A., and Rieder, C.L. (1999). The Sudden Recruitment of γ-Tubulin to the Centrosome at the Onset of Mitosis and Its Dynamic Exchange Throughout the Cell Cycle, Do Not Require Microtubules. J. Cell Biol. *146*, 585–596.

Khodjakov, A., Cole, R.W., Oakley, B.R., and Rieder, C.L. (2000). Centrosome-independent mitotic spindle formation in vertebrates. Curr. Biol. *10*, 59–67.

Khodjakov, A., Copenagle, L., Gordon, M.B., Compton, D.A., and Kapoor, T.M. (2003). Minus-end capture of preformed kinetochore fibers contributes to spindle morphogenesis. J. Cell Biol. *160*, 671–683.

Khrapunovich-Baine, M., Menon, V., Yang, C.-P.H., Northcote, P.T., Miller, J.H., Angeletti, R.H., Fiser, A., Horwitz, S.B., and Xiao, H. (2011). Hallmarks of Molecular Action of Microtubule Stabilizing Agents EFFECTS OF EPOTHILONE B, IXABEPILONE, PELORUSIDE A, AND LAULIMALIDE ON MICROTUBULE CONFORMATION. J. Biol. Chem. *286*, 11765–11778.

Kikkawa, M., Ishikawa, T., Nakata, T., Wakabayashi, T., and Hirokawa, N. (1994). Direct visualization of the microtubule lattice seam both in vitro and in vivo. J. Cell Biol. *127*, 1965–1971.

Kim, J., and Park, S.-J. (2018). Roles of end-binding 1 protein and gamma-tubulin small complex in cytokinesis and flagella formation of Giardia lamblia. MicrobiologyOpen e748.

Kirmse, R., Portet, S., Mücke, N., Aebi, U., Herrmann, H., and Langowski, J. (2007). A Quantitative Kinetic Model for the in Vitro Assembly of Intermediate Filaments from Tetrameric Vimentin. J. Biol. Chem. *282*, 18563–18572.

Kirschner, M., and Mitchison, T. (1986). Beyond self-assembly: from microtubules to morphogenesis. Cell *45*, 329–342.

Kitamura, E., Tanaka, K., Komoto, S., Kitamura, Y., Antony, C., and Tanaka, T.U. (2010). Kinetochores Generate Microtubules with Distal Plus Ends: Their Roles and Limited Lifetime in Mitosis. Dev. Cell *18*, 248–259.

Knop, M., and Schiebel, E. (1997). Spc98p and Spc97p of the yeast γ-tubulin complex mediate binding to the spindle pole body via their interaction with Spc110p. EMBO J. *16*, 6985–6995.

Kobielak, A., Pasolli, H.A., and Fuchs, E. (2004). Mammalian formin-1 participates in adherens junctions and polymerization of linear actin cables. Nat. Cell Biol. *6*, 21–30.

Koffa, M.D., Casanova, C.M., Santarella, R., Köcher, T., Wilm, M., and Mattaj, I.W. (2006). HURP is part of a Ran-dependent complex involved in spindle formation. Curr. Biol. CB *16*, 743–754.

Kollman, J.M., Zelter, A., Muller, E.G.D., Fox, B., Rice, L.M., Davis, T.N., and Agard, D.A. (2008). The Structure of the γ-Tubulin Small Complex: Implications of Its Architecture and Flexibility for Microtubule Nucleation. Mol. Biol. Cell *19*, 207–215.

Kollman, J.M., Polka, J.K., Zelter, A., Davis, T.N., and Agard, D.A. (2010). Microtubule nucleating γ-TuSC assembles structures with 13-fold microtubule-like symmetry. Nature *466*, 879–882.

Kollman, J.M., Merdes, A., Mourey, L., and Agard, D.A. (2011). Microtubule nucleation by γ-tubulin complexes. Nat. Rev. Mol. Cell Biol. *12*, 709–721.

Kollman, J.M., Greenberg, C.H., Li, S., Moritz, M., Zelter, A., Fong, K.K., Fernandez, J.-J., Sali, A., Kilmartin, J., Davis, T.N., et al. (2015). Ring closure activates yeast γTuRC for species-specific microtubule nucleation. Nat. Struct. Mol. Biol. *22*, 132–137.

Komarova, Y., De Groot, C.O., Grigoriev, I., Gouveia, S.M., Munteanu, E.L., Schober, J.M., Honnappa, S., Buey, R.M., Hoogenraad, C.C., Dogterom, M., et al. (2009). Mammalian end binding proteins control persistent microtubule growth. J. Cell Biol. *184*, 691–706.

Korn, E.D., Carlier, M.F., and Pantaloni, D. (1987). Actin polymerization and ATP hydrolysis. Science *238*, 638–644.

Kosco, K.A., Pearson, C.G., Maddox, P.S., Wang, P.J., Adams, I.R., Salmon, E.D., Bloom, K., and Huffaker, T.C. (2001). Control of microtubule dynamics by Stu2p is essential for spindle orientation and metaphase chromosome alignment in yeast. Mol. Biol. Cell *12*, 2870–2880.

Kovar, D.R., and Pollard, T.D. (2004). Insertional assembly of actin filament barbed ends in association with formins produces piconewton forces. Proc. Natl. Acad. Sci. U. S. A. *101*, 14725–14730.

Kovar, D.R., Wu, J.-Q., and Pollard, T.D. (2005). Profilin-mediated Competition between Capping Protein and Formin Cdc12p during Cytokinesis in Fission Yeast. Mol. Biol. Cell *16*, 2313–2324.

Kronja, I., Kruljac-Letunic, A., Caudron-Herger, M., Bieling, P., and Karsenti, E. (2009). XMAP215–EB1 Interaction Is Required for Proper Spindle Assembly and Chromosome Segregation in Xenopus Egg Extract. Mol. Biol. Cell *20*, 2684–2696.

Kuchnir Fygenson, D., Flyvbjerg, H., Sneppen, K., Libchaber, A., and Leibler, S. (1995). Spontaneous nucleation of microtubules. Phys. Rev. E *51*, 5058–5063.

Lansky, Z., Braun, M., Lüdecke, A., Schlierf, M., ten Wolde, P.R., Janson, M.E., and Diez, S. (2015). Diffusible Crosslinkers Generate Directed Forces in Microtubule Networks. Cell *160*, 1159–1168.

Lawo, S., Bashkurov, M., Mullin, M., Ferreria, M.G., Kittler, R., Habermann, B., Tagliaferro, A., Poser, I., Hutchins, J.R.A., Hegemann, B., et al. (2009). HAUS, the 8-Subunit Human Augmin Complex, Regulates Centrosome and Spindle Integrity. Curr. Biol. *19*, 816–826.

Lawo, S., Hasegan, M., Gupta, G.D., and Pelletier, L. (2012). Subdiffraction imaging of centrosomes reveals higher-order organizational features of pericentriolar material. Nat. Cell Biol. *14*, 1148–1158.

Lazarus, J.E., Moughamian, A.J., Tokito, M.K., and Holzbaur, E.L.F. (2013). Dynactin Subunit p150Glued Is a Neuron-Specific Anti-Catastrophe Factor. PLoS Biol. *11*.

Lebensohn, A.M., and Kirschner, M.W. (2009). Activation of the WAVE complex by coincident signals controls actin assembly. Mol. Cell *36*, 512–524.

Lee, J.C., and Timasheff, S.N. (1975). The reconstitution of microtubules from purified calf brain tubulin. Biochemistry *14*, 5183–5187.

Lee, J.C., and Timasheff, S.N. (1977). In vitro reconstitution of calf brain microtubules: effects of solution variables. Biochemistry *16*, 1754–1764.

Leong, S.L., Lynch, E.M., Zou, J., Tay, Y.D., Borek, W.E., Tuijtel, M.W., Rappsilber, J., and Sawin, K.E. (2019). Reconstitution of Microtubule Nucleation In Vitro Reveals Novel Roles for Mzt1. Curr. Biol. *29*, 2199-2207.e10.

Li, W., Moriwaki, T., Tani, T., Watanabe, T., Kaibuchi, K., and Goshima, G. (2012). Reconstitution of dynamic microtubules with Drosophila XMAP215, EB1, and Sentin. J Cell Biol *199*, 849–862.

Lidke, D.S., Lidke, K.A., Rieger, B., Jovin, T.M., and Arndt-Jovin, D.J. (2005). Reaching out for signals: filopodia sense EGF and respond by directed retrograde transport of activated receptors. J. Cell Biol. *170*, 619–626.

Ligon, L.A., Shelly, S.S., Tokito, M., and Holzbaur, E.L.F. (2002). The Microtubule Plus-End Proteins EB1 and Dynactin Have Differential Effects on Microtubule Polymerization. Mol. Biol. Cell *14*, 1405–1417.

Lin, T., Neuner, A., and Schiebel, E. (2015). Targeting of γ-tubulin complexes to microtubule organizing centers: conservation and divergence. Trends Cell Biol. *25*, 296–307.

Lin, T., Neuner, A., Flemming, D., Liu, P., Chinen, T., Jäkle, U., Arkowitz, R., and Schiebel, E. (2016). MOZART1 and γ-tubulin complex receptors are both required to turn γ-TuSC into an active microtubule nucleation template. J Cell Biol jcb.201606092.

Lin, T.-C., Neuner, A., Schlosser, Y.T., Scharf, A.N., Weber, L., and Schiebel, E. (2014). Cell-cycle dependent phosphorylation of yeast pericentrin regulates γ-TuSC-mediated microtubule nucleation. ELife *3*, e02208.

Lindeboom, J.J., Nakamura, M., Hibbel, A., Shundyak, K., Gutierrez, R., Ketelaar, T., Emons, A.M.C., Mulder, B.M., Kirik, V., and Ehrhardt, D.W. (2013). A mechanism for reorientation of cortical microtubule arrays driven by microtubule severing. Science *342*, 1245533.

Liu, L., and Wiese, C. (2008). Xenopus NEDD1 is required for microtubule organization in Xenopus egg extracts. J. Cell Sci. *121*, 578–589.

Liu, P., Choi, Y.-K., and Qi, R.Z. (2014a). NME7 is a functional component of the γ-tubulin ring complex. Mol. Biol. Cell *25*, 2017–2025.

Liu, T., Tian, J., Wang, G., Yu, Y., Wang, C., Ma, Y., Zhang, X., Xia, G., Liu, B., and Kong, Z. (2014b). Augmin triggers microtubule-dependent microtubule nucleation in interphase plant cells. Curr. Biol. CB *24*, 2708–2713.

Löwe, J., Li, H., Downing, K.H., and Nogales, E. (2001). Refined structure of alpha beta-tubulin at 3.5 A resolution. J. Mol. Biol. *313*, 1045–1057.

Lüders, J., Patel, U.K., and Stearns, T. (2006). GCP-WD is a γ-tubulin targeting factor required for centrosomal and chromatin-mediated microtubule nucleation. Nat. Cell Biol. *8*, 137–147.

Lynch, E.M., Groocock, L.M., Borek, W.E., and Sawin, K.E. (2014). Activation of the γ-Tubulin Complex by the Mto1/2 Complex. Curr. Biol. *24*, 896–903.

Lyon, A.S., Morin, G., Moritz, M., Yabut, K.C.B., Vojnar, T., Zelter, A., Muller, E., Davis, T.N., and Agard, D.A. (2016). Higher-order oligomerization of Spc110p drives γ-tubulin ring complex assembly. Mol. Biol. Cell *27*, 2245–2258.

Machesky, L.M., and Insall, R.H. (1998). Scar1 and the related Wiskott–Aldrich syndrome protein, WASP, regulate the actin cytoskeleton through the Arp2/3 complex. Curr. Biol. *8*, 1347–1356.

Machesky, L.M., Atkinson, S.J., Ampe, C., Vandekerckhove, J., and Pollard, T.D. (1994). Purification of a cortical complex containing two unconventional actins from Acanthamoeba by affinity chromatography on profilin-agarose. J. Cell Biol. *127*, 107–115.

MacNeal, R.K., and Purich, D.L. (1978). Stoichiometry and role of GTP hydrolysis in bovine neurotubule assembly. J. Biol. Chem. *253*, 4683–4687.

Mahoney, N.M., Goshima, G., Douglass, A.D., and Vale, R.D. (2006). Making Microtubules and Mitotic Spindles in Cells without Functional Centrosomes. Curr. Biol. *16*, 564–569.

Maia, A.R.R., Zhu, X., Miller, P., Gu, G., Maiato, H., and Kaverina, I. (2013). Modulation of Golgi-associated microtubule nucleation throughout the cell cycle. Cytoskeleton *70*, 32–43.

Maiato, H., and Sunkel, C.E. (2004). Kinetochore–microtubule interactions during cell division. Chromosome Res. *12*, 585–597.

Mandelkow, E.M., Mandelkow, E., and Milligan, R.A. (1991). Microtubule dynamics and microtubule caps: a time-resolved cryo-electron microscopy study. J. Cell Biol. *114*, 977–991.

Manning, J., and Kumar, S. (2007). NEDD1: Function in microtubule nucleation, spindle assembly and beyond. Int. J. Biochem. Cell Biol. *39*, 7–11.

Manning, J.A., Shalini, S., Risk, J.M., Day, C.L., and Kumar, S. (2010). A Direct Interaction with NEDD1 Regulates γ-Tubulin Recruitment to the Centrosome. PLoS ONE *5*, e9618.

Martin, M.A., Osmani, S.A., and Oakley, B.R. (1997). The role of γ-tubulin in mitotic spindle formation and cell cycle progression in Aspergillus nidulans. J. Cell Sci. *110*, 623–633.

Martin, O.C., Gunawardane, R.N., Iwamatsu, A., and Zheng, Y. (1998). Xgrip109: A γ Tubulin–Associated Protein with an Essential Role in γ Tubulin Ring Complex (γTuRC) Assembly and Centrosome Function. J. Cell Biol. *141*, 675–687.

Masuda, H., and Toda, T. (2016). Synergistic role of fission yeast Alp16GCP6 and Mzt1MOZART1 in γ-tubulin complex recruitment to mitotic spindle pole bodies and spindle assembly. Mol. Biol. Cell *27*, 1753–1763.

Masuda, H., Mori, R., Yukawa, M., and Toda, T. (2013). Fission yeast MOZART1/Mzt1 is an essential γ-tubulin complex component required for complex recruitment to the microtubule organizing center, but not its assembly. Mol. Biol. Cell *24*, 2894–2906.

Mattila, P.K., and Lappalainen, P. (2008). Filopodia: molecular architecture and cellular functions. Nat. Rev. Mol. Cell Biol. *9*, 446–454.

Maurer, S.P., Bieling, P., Cope, J., Hoenger, A., and Surrey, T. (2011). GTPγS microtubules mimic the growing microtubule end structure recognized by end-binding proteins (EBs). Proc. Natl. Acad. Sci. *108*, 3988–3993.

Maurer, S.P., Fourniol, F.J., Bohner, G., Moores, C.A., and Surrey, T. (2012). EBs Recognize a Nucleotide-Dependent Structural Cap at Growing Microtubule Ends. Cell *149*, 371–382.

Maurer, S.P., Cade, N.I., Bohner, G., Gustafsson, N., Boutant, E., and Surrey, T. (2014). EB1 Accelerates Two Conformational Transitions Important for Microtubule Maturation and Dynamics. Curr. Biol. *24*, 372–384.

May, R.C., and Machesky, L.M. (2001). Phagocytosis and the actin cytoskeleton. J. Cell Sci. *114*, 1061–1077.

May, R.C., Caron, E., Hall, A., and Machesky, L.M. (2000). Involvement of the Arp2/3 complex in phagocytosis mediated by FcgammaR or CR3. Nat. Cell Biol. *2*, 246–248.

McIntosh, J.R., O'Toole, E., Morgan, G., Austin, J., Ulyanov, E., Ataullakhanov, F., and Gudimchuk, N. (2018). Microtubules grow by the addition of bent guanosine triphosphate tubulin to the tips of curved protofilaments. J Cell Biol *217*, 2691–2708.

McNally, F.J., and Roll-Mecak, A. (2018). Microtubule-severing enzymes: From cellular functions to molecular mechanism. J Cell Biol *217*, 4057–4069.

Melchior, F., Paschal, B., Evans, J., and Gerace, L. (1993). Inhibition of nuclear protein import by nonhydrolyzable analogues of GTP and identification of the small GTPase Ran/TC4 as an essential transport factor. J. Cell Biol. *123*, 1649–1659.

Mennella, V., Keszthelyi, B., McDonald, K.L., Chhun, B., Kan, F., Rogers, G.C., Huang, B., and Agard, D.A. (2012). Subdiffraction-resolution fluorescence microscopy reveals a domain of the centrosome critical for pericentriolar material organization. Nat. Cell Biol. *14*, 1159–1168.

Meunier, S., and Vernos, I. (2016). Acentrosomal Microtubule Assembly in Mitosis: The Where, When, and How. Trends Cell Biol. *26*, 80–87.

Meurer-Grob, P., Kasparian, J., and Wade, R.H. (2001). Microtubule structure at improved resolution. Biochemistry *40*, 8000–8008.

Miller, P.M., Folkmann, A.W., Maia, A.R.R., Efimova, N., Efimov, A., and Kaverina, I. (2009). Golgi-derived CLASP-dependent Microtubules Control Golgi Organization and Polarized Trafficking in Motile Cells. Nat. Cell Biol. *11*, 1069–1080.

Mimori-Kiyosue, Y., Shiina, N., and Tsukita, S. (2000). The dynamic behavior of the APC-binding protein EB1 on the distal ends of microtubules. Curr. Biol. *10*, 865–868.

Mimori-Kiyosue, Y., Grigoriev, I., Lansbergen, G., Sasaki, H., Matsui, C., Severin, F., Galjart, N., Grosveld, F., Vorobjev, I., Tsukita, S., et al. (2005). CLASP1 and CLASP2 bind to EB1 and regulate microtubule plus-end dynamics at the cell cortex. J. Cell Biol. *168*, 141–153.

Mirigian, M., Mukherjee, K., Bane, S.L., and Sackett, D.L. (2013). Chapter 14 - Measurement of In Vitro Microtubule Polymerization by Turbidity and Fluorescence. In Methods in Cell Biology, J.J. Correia, and L. Wilson, eds. (Academic Press), pp. 215–229.

Mishra, R.K., Chakraborty, P., Arnaoutov, A., Fontoura, B.M.A., and Dasso, M. (2010). The Nup107-160 complex and γ-TuRC regulate microtubule polymerization at kinetochores. Nat. Cell Biol. *12*, 164–169.

Mitchison, T.J. (1992). Compare and contrast actin filaments and microtubules. Mol. Biol. Cell *3*, 1309–1315.

Mitchison, T., and Kirschner, M. (1984a). Dynamic instability of microtubule growth. Nature *312*.

Mitchison, T., and Kirschner, M. (1984b). Microtubule assembly nucleated by isolated centrosomes. Nature *312*, 232.

Mitchison, T., Evans, L., Schulze, E., and Kirschner, M. (1986). Sites of microtubule assembly and disassembly in the mitotic spindle. Cell *45*, 515–527.

Mogensen, M.M., Malik, A., Piel, M., Bouckson-Castaing, V., and Bornens, M. (2000). Microtubule minus-end anchorage at centrosomal and non-centrosomal sites: the role of ninein. J. Cell Sci. *113*, 3013–3023.

Mollinari, C., Kleman, J.-P., Jiang, W., Schoehn, G., Hunter, T., and Margolis, R.L. (2002). PRC1 is a microtubule binding and bundling protein essential to maintain the mitotic spindle midzone. J. Cell Biol. *157*, 1175–1186.

Moore, M.S., and Blobel, G. (1993). The GTP-binding protein Ran/TC4 is required for protein import into the nucleus. Nature *365*, 661.

Moores, C.A., Yu, M., Guo, J., Beraud, C., Sakowicz, R., and Milligan, R.A. (2002). A Mechanism for Microtubule Depolymerization by KinI Kinesins. Mol. Cell *9*, 903–909.

Moores, C.A., Perderiset, M., Francis, F., Chelly, J., Houdusse, A., and Milligan, R.A. (2004). Mechanism of Microtubule Stabilization by Doublecortin. Mol. Cell *14*, 833–839.

Moores, C.A., Perderiset, M., Kappeler, C., Kain, S., Drummond, D., Perkins, S.J., Chelly, J., Cross, R., Houdusse, A., and Francis, F. (2006). Distinct roles of doublecortin modulating the microtubule cytoskeleton. EMBO J. *25*, 4448–4457.

Mori, Y., Inoue, Y., Tanaka, S., Doda, S., Yamanaka, S., Fukuchi, H., and Terada, Y. (2015a). Cep169, a Novel Microtubule Plus-End-Tracking Centrosomal Protein, Binds to CDK5RAP2 and Regulates Microtubule Stability. PLOS ONE *10*, e0140968.

Mori, Y., Taniyama, Y., Tanaka, S., Fukuchi, H., and Terada, Y. (2015b). Microtubule-bundling activity of the centrosomal protein, Cep169, and its binding to microtubules. Biochem. Biophys. Res. Commun. *467*, 754–759.

Moritz, M., Braunfeld, M.B., Sedat, J.W., Alberts, B., and Agard, D.A. (1995). Microtubule nucleation by γ-tubulin-containing rings in the centrosome. Nature *378*, 638.

Moritz, M., Zheng, Y., Alberts, B.M., and Oegema, K. (1998). Recruitment of the γ-Tubulin Ring Complex to Drosophila Salt-stripped Centrosome Scaffolds. J. Cell Biol. *142*, 775–786.

Moritz, M., Braunfeld, M.B., Guénebaut, V., Heuser, J., and Agard, D.A. (2000). Structure of the γ-tubulin ring complex: a template for microtubule nucleation. Nat. Cell Biol. *2*, 365–370.

Moseley, J.B., Sagot, I., Manning, A.L., Xu, Y., Eck, M.J., Pellman, D., and Goode, B.L. (2003). A Conserved Mechanism for Bni1- and mDia1-induced Actin Assembly and Dual Regulation of Bni1 by Bud6 and Profilin. Mol. Biol. Cell *15*, 896–907.

Mountain, V., Simerly, C., Howard, L., Ando, A., Schatten, G., and Compton, D.A. (1999). The Kinesin-Related Protein, Hset, Opposes the Activity of Eg5 and Cross-Links Microtubules in the Mammalian Mitotic Spindle. J. Cell Biol. *147*, 351–366.

Mozziconacci, J., Sandblad, L., Wachsmuth, M., Brunner, D., and Karsenti, E. (2008). Tubulin Dimers Oligomerize before Their Incorporation into Microtubules. PLoS ONE *3*.

Müller-Reichert, T., Chrétien, D., Severin, F., and Hyman, A.A. (1998). Structural changes at microtubule ends accompanying GTP hydrolysis: Information from a slowly hydrolyzable analogue of GTP, guanylyl (α,β)methylenediphosphonate. Proc. Natl. Acad. Sci. *95*, 3661–3666.

Mullins, R.D., Heuser, J.A., and Pollard, T.D. (1998). The interaction of Arp2/3 complex with actin: Nucleation, high affinity pointed end capping, and formation of branching networks of filaments. Proc. Natl. Acad. Sci. *95*, 6181–6186.

Murata, T., Sonobe, S., Baskin, T.I., Hyodo, S., Hasezawa, S., Nagata, T., Horio, T., and Hasebe, M. (2005). Microtubule-dependent microtubule nucleation based on recruitment of gamma-tubulin in higher plants. Nat. Cell Biol. *7*, 961–968.

Muroyama, A., and Lechler, T. (2017). Microtubule organization, dynamics and functions in differentiated cells. Development *144*, 3012–3021.

Muroyama, A., Seldin, L., and Lechler, T. (2016). Divergent regulation of functionally distinct γ-tubulin complexes during differentiation. J. Cell Biol. *213*, 679–692.

Murphy, S.M., Urbani, L., and Stearns, T. (1998). The Mammalian γ-Tubulin Complex Contains Homologues of the Yeast Spindle Pole Body Components Spc97p and Spc98p. J. Cell Biol. *141*, 663–674.

Murphy, S.M., Preble, A.M., Patel, U.K., O'Connell, K.L., Dias, D.P., Moritz, M., Agard, D., Stults, J.T., and Stearns, T. (2001). GCP5 and GCP6: Two New Members of the Human γ-Tubulin Complex. Mol. Biol. Cell *12*, 3340–3352.

Musa, H., Orton, C., Morrison, E.E., and Peckham, M. (2003). Microtubule assembly in cultured myoblasts and myotubes following nocodazole induced microtubule depolymerisation. J. Muscle Res. Cell Motil. *24*, 301–308.

Müsch, A. (2004). Microtubule Organization and Function in Epithelial Cells. Traffic *5*, 1–9.

Nachury, M.V., Maresca, T.J., Salmon, W.C., Waterman-Storer, C.M., Heald, R., and Weis, K. (2001). Importin β Is a Mitotic Target of the Small GTPase Ran in Spindle Assembly. Cell *104*, 95–106.

Nakamura, N. (2010). Emerging new roles of GM130, a cis-Golgi matrix protein, in higher order cell functions. J. Pharmacol. Sci. *112*, 255–264.

Nakamura, M., Yagi, N., Kato, T., Fujita, S., Kawashima, N., Ehrhardt, D.W., and Hashimoto, T. (2012). Arabidopsis GCP3-interacting protein 1/MOZART 1 is an integral component of the γ-tubulin-containing microtubule nucleating complex. Plant J. *71*, 216–225.

Nakaoka, Y., Kimura, A., Tani, T., and Goshima, G. (2015). Cytoplasmic Nucleation and Atypical Branching Nucleation Generate Endoplasmic Microtubules in Physcomitrella patens. Plant Cell *27*, 228–242.

Nashchekin, D., Fernandes, A.R., and St Johnston, D. (2016). Patronin/Shot Cortical Foci Assemble the Noncentrosomal Microtubule Array that Specifies the Drosophila Anterior-Posterior Axis. Dev. Cell *38*, 61–72.

Nawrotek, A., Knossow, M., and Gigant, B. (2011). The Determinants That Govern Microtubule Assembly from the Atomic Structure of GTP-Tubulin. J. Mol. Biol. *412*, 35–42.

Neuhaus, J.-M., Wanger, M., Keiser, T., and Wegner, A. (1983). Treadmilling of actin. J. Muscle Res. Cell Motil. *4*, 507–527.

Neumayer, G., Belzil, C., Gruss, O.J., and Nguyen, M.D. (2014). TPX2: of spindle assembly, DNA damage response, and cancer. Cell. Mol. Life Sci. *71*, 3027–3047.

Newton, C.N., Wagenbach, M., Ovechkina, Y., Wordeman, L., and Wilson, L. (2004). MCAK, a Kin I kinesin, increases the catastrophe frequency of steady-state HeLa cell microtubules in an ATP-dependent manner in vitro. FEBS Lett. *572*, 80–84.

Nogales, E. (2001). Structural Insights into Microtubule Function. Annu. Rev. Biophys. Biomol. Struct. *30*, 397–420.

Nogales, E., Whittaker, M., Milligan, R.A., and Downing, K.H. (1999). High-resolution model of the microtubule. Cell *96*, 79–88.

Oakley, C.E., and Oakley, B.R. (1989). Identification of gamma-tubulin, a new member of the tubulin superfamily encoded by mipA gene of Aspergillus nidulans. Nature *338*, 662–664.

Oakley, B.R., Oakley, C.E., Yoon, Y., and Jung, M.K. (1990). γ-tubulin is a component of the spindle pole body that is essential for microtubule function in Aspergillus nidulans. Cell *61*, 1289–1301.

Oakley, B.R., Paolillo, V., and Zheng, Y. (2015). γ-Tubulin complexes in microtubule nucleation and beyond. Mol. Biol. Cell *26*, 2957–2962.

O'Connell, C.B., Lončarek, J., Kaláb, P., and Khodjakov, A. (2009). Relative contributions of chromatin and kinetochores to mitotic spindle assembly. J. Cell Biol. *187*, 43–51.

Oda, T., Aihara, T., and Wakabayashi, K. (2016). Early nucleation events in the polymerization of actin, probed by time-resolved small-angle x-ray scattering. Sci. Rep. *6*, 34539.

Oegema, K., Wiese, C., Martin, O.C., Milligan, R.A., Iwamatsu, A., Mitchison, T.J., and Zheng, Y. (1999). Characterization of Two Related Drosophila γ-tubulin Complexes that Differ in Their Ability to Nucleate Microtubules. J. Cell Biol. *144*, 721–733.

Okada, K., Bartolini, F., Deaconescu, A.M., Moseley, J.B., Dogic, Z., Grigorieff, N., Gundersen, G.G., and Goode, B.L. (2010). Adenomatous polyposis coli protein nucleates actin assembly and synergizes with the formin mDia1. J. Cell Biol. *189*, 1087–1096.

Oosawa, F., and Asakura, S. (1975). Thermodynamics of the polymerization of protein (London ; New York: Academic Press).

Oriola, D., Needleman, D.J., and Brugués, J. (2018). The Physics of the Metaphase Spindle. Annu. Rev. Biophys. *47*, 655–673.

Oriolo, A.S., Wald, F.A., Canessa, G., and Salas, P.J.I. (2007). GCP6 Binds to Intermediate Filaments: A Novel Function of Keratins in the Organization of Microtubules in Epithelial Cells. Mol. Biol. Cell *18*, 781–794.

O'Toole, E., Greenan, G., Lange, K.I., Srayko, M., and Müller-Reichert, T. (2012). The Role of γ-Tubulin in Centrosomal Microtubule Organization. PLoS ONE *7*, e29795.

Padrick, S.B., Cheng, H.-C., Ismail, A.M., Panchal, S.C., Doolittle, L.K., Kim, S., Skehan, B.M., Umetani, J., Brautigam, C.A., Leong, J.M., et al. (2008). Hierarchical regulation of WASP/WAVE proteins. Mol. Cell *32*, 426–438.

Petry, S., and Vale, R.D. (2015). Microtubule nucleation at the centrosome and beyond. Nat. Cell Biol. *17*, 1089–1093.

Petry, S., Groen, A.C., Ishihara, K., Mitchison, T.J., and Vale, R.D. (2013). Branching microtubule nucleation in Xenopus egg extracts mediated by augmin and TPX2. Cell *152*, 768–777.

Piehl, M., Tulu, U.S., Wadsworth, P., and Cassimeris, L. (2004). Centrosome maturation: Measurement of microtubule nucleation throughout the cell cycle by using GFP-tagged EB1. Proc. Natl. Acad. Sci. U. S. A. *101*, 1584–1588.

Pinyol, R., Scrofani, J., and Vernos, I. (2013). The Role of NEDD1 Phosphorylation by Aurora A in Chromosomal Microtubule Nucleation and Spindle Function. Curr. Biol. *23*, 143–149.

Pizon, V., Gerbal, F., Diaz, C.C., and Karsenti, E. (2005). Microtubule-dependent transport and organization of sarcomeric myosin during skeletal muscle differentiation. EMBO J. *24*, 3781–3792.

Podolski, M., Mahamdeh, M., and Howard, J. (2014). Stu2, the Budding Yeast XMAP215/Dis1 Homolog, Promotes Assembly of Yeast Microtubules by Increasing Growth Rate and Decreasing Catastrophe Frequency. J. Biol. Chem. *289*, 28087–28093.

Pollard, T.D., and Borisy, G.G. (2003). Cellular Motility Driven by Assembly and Disassembly of Actin Filaments. Cell *112*, 453–465.

Pollard, T.D., and Cooper, J.A. (2009). Actin, a Central Player in Cell Shape and Movement. Science *326*, 1208–1212.

Popov, A.V., Severin, F., and Karsenti, E. (2002). XMAP215 Is Required for the Microtubule-Nucleating Activity of Centrosomes. Curr. Biol. *12*, 1326–1330.

Portet, S., Mücke, N., Kirmse, R., Langowski, J., Beil, M., and Herrmann, H. (2009). Vimentin Intermediate Filament Formation: In Vitro Measurement and Mathematical Modeling of the Filament Length Distribution during Assembly. Langmuir *25*, 8817–8823.

Portran, D., Schaedel, L., Xu, Z., Théry, M., and Nachury, M.V. (2017). Tubulin acetylation protects long-lived microtubules against mechanical ageing. Nat. Cell Biol. *19*, 391–398.

Pring, M., Evangelista, M., Boone, C., Yang, C., and Zigmond, S.H. (2003). Mechanism of Formin-Induced Nucleation of Actin Filaments. Biochemistry *42*, 486–496.

Pruyne, D., Evangelista, M., Yang, C., Bi, E., Zigmond, S., Bretscher, A., and Boone, C. (2002). Role of Formins in Actin Assembly: Nucleation and Barbed-End Association. Science *297*, 612–615.

Qualmann, B., and Kessels, M.M. (2009). New players in actin polymerization – WH2-domain-containing actin nucleators. Trends Cell Biol. *19*, 276–285.

Quinlan, M.E., Heuser, J.E., Kerkhoff, E., and Mullins, R.D. (2005). Drosophila Spire is an actin nucleation factor. Nature *433*, 382–388.

Rale, M.J., Kadzik, R.S., and Petry, S. (2018). Phase Transitioning the Centrosome into a Microtubule Nucleator. Biochemistry *57*, 30–37.

Ravelli, R.B.G., Gigant, B., Curmi, P.A., Jourdain, I., Lachkar, S., Sobel, A., and Knossow, M. (2004). Insight into tubulin regulation from a complex with colchicine and a stathmin-like domain. Nature *428*, 198.

Reichl, E.M., Ren, Y., Morphew, M.K., Delannoy, M., Effler, J.C., Girard, K.D., Divi, S., Iglesias, P.A., Kuo, S.C., and Robinson, D.N. (2008). Interactions between myosin and actin crosslinkers control cytokinesis contractility dynamics and mechanics. Curr. Biol. CB *18*, 471–480.

Reid, T.A., Schuster, B.M., Mann, B.J., Balchand, S.K., Plooster, M., McClellan, M., Coombes, C.E., Wadsworth, P., and Gardner, M.K. (2016). Suppression of microtubule assembly kinetics by the mitotic protein TPX2. J Cell Sci *129*, 1319–1328.

Reilein, A., Yamada, S., and Nelson, W.J. (2005). Self-organization of an acentrosomal microtubule network at the basal cortex of polarized epithelial cells. J. Cell Biol. *171*, 845–855.

Rice, L.M., Montabana, E.A., and Agard, D.A. (2008). The lattice as allosteric effector: Structural studies of αβ- and γ-tubulin clarify the role of GTP in microtubule assembly. Proc. Natl. Acad. Sci. U. S. A. *105*, 5378–5383.

Riehlman, T.D., Olmsted, Z.T., Branca, C.N., Winnie, A.M., Seo, L., Cruz, L.O., and Paluh, J.L. (2013). Functional replacement of fission yeast γ-tubulin small complex proteins Alp4 and Alp6 by human GCP2 and GCP3. J. Cell Sci. *126*, 4406–4413.

Rios, R.M. (2014). The centrosome–Golgi apparatus nexus. Philos. Trans. R. Soc. Lond. B Biol. Sci. *369*, 20130462.

Rivero, S., Cardenas, J., Bornens, M., and Rios, R.M. (2009). Microtubule nucleation at the cis-side of the Golgi apparatus requires AKAP450 and GM130. EMBO J. *28*, 1016–1028.

Robert, A., Hookway, C., and Gelfand, V.I. (2016). Intermediate filament dynamics: What we can see now and why it matters. BioEssays News Rev. Mol. Cell. Dev. Biol. *38*, 232–243.

Robinson, J., and Engelborghs, Y. (1982). Tubulin polymerization in dimethyl sulfoxide. J. Biol. Chem. *257*, 5367–5371.

Rogers, G.C., Rusan, N.M., Peifer, M., and Rogers, S.L. (2008). A Multicomponent Assembly Pathway Contributes to the Formation of Acentrosomal Microtubule Arrays in Interphase Drosophila Cells. Mol. Biol. Cell *19*, 3163–3178.

Romero, S., Le Clainche, C., Didry, D., Egile, C., Pantaloni, D., and Carlier, M.-F. (2004). Formin Is a Processive Motor that Requires Profilin to Accelerate Actin Assembly and Associated ATP Hydrolysis. Cell *119*, 419–429.

Roostalu, J., and Surrey, T. (2017). Microtubule nucleation: beyond the template. Nat. Rev. Mol. Cell Biol. *18*, nrm.2017.75.

Roostalu, J., Cade, N.I., and Surrey, T. (2015). Complementary activities of TPX2 and chTOG constitute an efficient importin-regulated microtubule nucleation module. Nat. Cell Biol. *17*, 1422–1434.

Roth, D., Fitton, B.P., Chmel, N.P., Wasiluk, N., and Straube, A. (2019). Spatial positioning of EB family proteins at microtubule tips involves distinct nucleotide-dependent binding properties. J Cell Sci *132*, jcs219550.

Roubin, R., Acquaviva, C., Chevrier, V., Sedjaï, F., Zyss, D., Birnbaum, D., and Rosnet, O. (2013). Myomegalin is necessary for the formation of centrosomal and Golgi-derived microtubules. Biol. Open *2*, 238–250.

Rouiller, I., Xu, X.-P., Amann, K.J., Egile, C., Nickell, S., Nicastro, D., Li, R., Pollard, T.D., Volkmann, N., and Hanein, D. (2008). The structural basis of actin filament branching by the Arp2/3 complex. J. Cell Biol. *180*, 887–895.

Safer, D., Golla, R., and Nachmias, V.T. (1990). Isolation of a 5-kilodalton actin-sequestering peptide from human blood platelets. Proc. Natl. Acad. Sci. U. S. A. *87*, 2536–2540.

Sagot, I., Rodal, A.A., Moseley, J., Goode, B.L., and Pellman, D. (2002a). An actin nucleation mechanism mediated by Bni1 and profilin. Nat. Cell Biol. *4*, 626–631.

Sagot, I., Klee, S.K., and Pellman, D. (2002b). Yeast formins regulate cell polarity by controlling the assembly of actin cables. Nat. Cell Biol. *4*, 42–50.

Sampaio, P., Rebollo, E., Varmark, H., Sunkel, C.E., and González, C. (2001). Organized microtubule arrays in γ-tubulin-depleted Drosophila spermatocytes. Curr. Biol. *11*, 1788–1793.

Sanchez, A.D., and Feldman, J.L. (2017). Microtubule-organizing centers: from the centrosome to non-centrosomal sites. Curr. Opin. Cell Biol. *44*, 93–101.

Sánchez-Huertas, C., and Lüders, J. (2015). The Augmin Connection in the Geometry of Microtubule Networks. Curr. Biol. *25*, R294–R299.

Sandblad, L., Busch, K.E., Tittmann, P., Gross, H., Brunner, D., and Hoenger, A. (2006). The Schizosaccharomyces pombe EB1 homolog Mal3p binds and stabilizes the microtubule lattice seam. Cell *127*, 1415–1424.

Sanders, A.A.W.M., and Kaverina, I. (2015). Nucleation and dynamics of Golgi-derived microtubules. Front. Neurosci. *9*.

Sanders, A.A.W.M., Chang, K., Zhu, X., Thoppil, R.J., Holmes, W.R., and Kaverina, I. (2017). Nonrandom γ-TuNA-dependent spatial pattern of microtubule nucleation at the Golgi. Mol. Biol. Cell *28*, 3181–3192.

Sawin, K.E., and Tran, P.T. (2006). Cytoplasmic microtubule organization in fission yeast. Yeast *23*, 1001–1014.

Sawin, K.E., Lourenco, P.C.C., and Snaith, H.A. (2004). Microtubule Nucleation at Non-Spindle Pole Body Microtubule-Organizing Centers Requires Fission Yeast Centrosomin-Related Protein mod20p. Curr. Biol. *14*, 763–775.

Schatten, H., and Sun, Q.-Y. (2010). The role of centrosomes in fertilization, cell division and establishment of asymmetry during embryo development. Semin. Cell Dev. Biol. *21*, 174–184.

Schatz, C.A., Santarella, R., Hoenger, A., Karsenti, E., Mattaj, I.W., Gruss, O.J., and Carazo-Salas, R.E. (2003). Importin α-regulated nucleation of microtubules by TPX2. EMBO J. *22*, 2060–2070.

Schek, H.T., Gardner, M.K., Cheng, J., Odde, D.J., and Hunt, A.J. (2007). Microtubule Assembly Dynamics at the Nanoscale. Curr. Biol. CB *17*, 1445–1455.

Schirenbeck, A., Bretschneider, T., Arasada, R., Schleicher, M., and Faix, J. (2005). The Diaphanous-related formin dDia2 is required for the formation and maintenance of filopodia. Nat. Cell Biol. *7*, 619–625.

Schlüter, K., Jockusch, B.M., and Rothkegel, M. (1997). Profilins as regulators of actin dynamics. Biochim. Biophys. Acta BBA - Mol. Cell Res. *1359*, 97–109.

Schnackenberg, B.J., Khodjakov, A., Rieder, C.L., and Palazzo, R.E. (1998). The disassembly and reassembly of functional centrosomes in vitro. Proc. Natl. Acad. Sci. *95*, 9295–9300.

Schnorrer, F., Luschnig, S., Koch, I., and Nüsslein-Volhard, C. (2002). γ-Tubulin37C and γ-tubulin ring complex protein 75 Are Essential for bicoid RNA Localization during Drosophila Oogenesis. Dev. Cell *3*, 685–696.

Scrofani, J., Sardon, T., Meunier, S., and Vernos, I. (2015). Microtubule Nucleation in Mitosis by a RanGTP-Dependent Protein Complex. Curr. Biol. *25*, 131–140.

Sdelci, S., Schütz, M., Pinyol, R., Bertran, M.T., Regué, L., Caelles, C., Vernos, I., and Roig, J. (2012). Nek9 Phosphorylation of NEDD1/GCP-WD Contributes to Plk1 Control of γ-Tubulin Recruitment to the Mitotic Centrosome. Curr. Biol. *22*, 1516–1523.

Sept, D., and McCammon, J.A. (2001). Thermodynamics and Kinetics of Actin Filament Nucleation. Biophys. J. *81*, 667–674.

Severson, A.F., Baillie, D.L., and Bowerman, B. (2002). A Formin Homology Protein and a Profilin Are Required for Cytokinesis and Arp2/3-Independent Assembly of Cortical Microfilaments in C. elegans. Curr. Biol. *12*, 2066–2075.

Sharp, D.J., McDonald, K.L., Brown, H.M., Matthies, H.J., Walczak, C., Vale, R.D., Mitchison, T.J., and Scholey, J.M. (1999). The Bipolar Kinesin, KLP61F, Cross-links Microtubules within Interpolar Microtubule Bundles of Drosophila Embryonic Mitotic Spindles. J. Cell Biol. *144*, 125–138.

Sikirzhytski, V., Renda, F., Tikhonenko, I., Magidson, V., McEwen, B.F., and Khodjakov, A. (2018). Microtubules assemble near most kinetochores during early prometaphase in human cells. J. Cell Biol. *217*, 2647–2659.

Silljé, H.H.W., Nagel, S., Körner, R., and Nigg, E.A. (2006). HURP Is a Ran-Importin β-Regulated Protein that Stabilizes Kinetochore Microtubules in the Vicinity of Chromosomes. Curr. Biol. *16*, 731–742.

Skube, S.B., Chaverri, J.M., and Goodson, H.V. (2010). Effect of GFP tags on the localization of EB1 and EB1 fragments in vivo. Cytoskelet. Hoboken Nj *67*, 1–12.

Slep, K.C., Rogers, S.L., Elliott, S.L., Ohkura, H., Kolodziej, P.A., and Vale, R.D. (2005). Structural determinants for EB1-mediated recruitment of APC and spectraplakins to the microtubule plus end. J. Cell Biol. *168*, 587–598.

Smith, B.A., Daugherty-Clarke, K., Goode, B.L., and Gelles, J. (2013). Pathway of actin filament branch formation by Arp2/3 complex revealed by single-molecule imaging. Proc. Natl. Acad. Sci. U. S. A. *110*, 1285–1290.

Sobel, S.G., and Snyder, M. (1995). A highly divergent gamma-tubulin gene is essential for cell growth and proper microtubule organization in Saccharomyces cerevisiae. J. Cell Biol. *131*, 1775–1788.

Song, J.-G., King, M.R., Zhang, R., Kadzik, R.S., Thawani, A., and Petry, S. (2018). Mechanism of how augmin directly targets the γ-tubulin ring complex to microtubules. J Cell Biol jcb.201711090.

Soues, S., and Adams, I.R. (1998). SPC72: a spindle pole component required for spindle orientation in the yeast Saccharomyces cerevisiae. J. Cell Sci. *111*, 2809–2818.

Spiegelman, B.M., Penningroth, S.M., and Kirschner, M.W. (1977). Turnover of tubulin and the N site GTP in chinese hamster ovary cells. Cell *12*, 587–600.

Stearns, T., and Kirschner, M. (1994). In vitro reconstitution of centrosome assembly and function: The central role of γ-tubulin. Cell *76*, 623–637.

Stearns, T., Evans, L., and Kirschner, M. (1991). γ-Tubulin is a highly conserved component of the centrosome. Cell *65*, 825–836.

Steinert, P.M., and Roop, D.R. (1988). Molecular and Cellular Biology of Intermediate Filaments. Annu. Rev. Biochem. *57*, 593–625.

Steinmetz, M.O., Goldie, K.N., and Aebi, U. (1997). A Correlative Analysis of Actin Filament Assembly, Structure, and Dynamics. J. Cell Biol. *138*, 559–574.

Steinmetz, M.O., Kammerer, R.A., Jahnke, W., Goldie, K.N., Lustig, A., and van Oostrum, J. (2000). Op18/stathmin caps a kinked protofilament-like tubulin tetramer. EMBO J. *19*, 572–580.

Strome, S., Powers, J., Dunn, M., Reese, K., Malone, C.J., White, J., Seydoux, G., and Saxton, W. (2001). Spindle Dynamics and the Role of γ-Tubulin in Early *Caenorhabditis elegans* Embryos. Mol. Biol. Cell *12*, 1751–1764.

Su, L.-K., and Qi, Y. (2001). Characterization of Human MAPRE Genes and Their Proteins. Genomics *71*, 142–149.

Suetsugu, S., Miki, H., Yamaguchi, H., Obinata, T., and Takenawa, T. (2001). Enhancement of branching efficiency by the actin filament-binding activity of N-WASP/WAVE2. J. Cell Sci. *114*, 4533–4542.

Sui, H., and Downing, K.H. (2010). Structural basis of interprotofilament interaction and lateral deformation of microtubules. Struct. Lond. Engl. 1993 *18*, 1022–1031.

Sulimenko, V., Hájková, Z., Klebanovych, A., and Dráber, P. (2017). Regulation of microtubule nucleation mediated by γ-tubulin complexes. Protoplasma *254*, 1187–1199.

Takahashi, M., Yamagiwa, A., Nishimura, T., Mukai, H., and Ono, Y. (2002). Centrosomal Proteins CG-NAP and Kendrin Provide Microtubule Nucleation Sites by Anchoring γ-Tubulin Ring Complex. Mol. Biol. Cell *13*, 3235–3245.

Tassin, A.M., Maro, B., and Bornens, M. (1985). Fate of microtubule-organizing centers during myogenesis in vitro. J. Cell Biol. *100*, 35–46.

Taylor, K.R., Holzer, A.K., Bazan, J.F., Walsh, C.A., and Gleeson, J.G. (2000). Patient Mutations in Doublecortin Define a Repeated Tubulin-binding Domain. J. Biol. Chem. *275*, 34442–34450.

Teixidó-Travesa, N., Villén, J., Lacasa, C., Bertran, M.T., Archinti, M., Gygi, S.P., Caelles, C., Roig, J., and Lüders, J. (2010). The γTuRC Revisited: A Comparative Analysis of Interphase and Mitotic Human γTuRC Redefines the Set of Core Components and Identifies the Novel Subunit GCP8. Mol. Biol. Cell *21*, 3963–3972.

Teixidó-Travesa, N., Roig, J., and Lüders, J. (2012). The where, when and how of microtubule nucleation – one ring to rule them all. J. Cell Sci. *125*, 4445–4456.

Telley, I.A., Bieling, P., and Surrey, T. (2011). Reconstitution and Quantification of Dynamic Microtubule End Tracking In Vitro Using TIRF Microscopy. In Microtubule Dynamics: Methods and Protocols, A. Straube, ed. (Totowa, NJ: Humana Press), pp. 127–145.

Thawani, A., Kadzik, R.S., and Petry, S. (2018). XMAP215 is a microtubule nucleation factor that functions synergistically with the γ-tubulin ring complex. Nat. Cell Biol. *20*, 575–585.

Thomas, N.E., Shashikala, S., and Sengupta, S. (2010). Cytoplasmic gamma-tubulin complex from brain contains nonerythroid spectrin. J. Cell. Biochem. *110*, 1334–1341.

Tirnauer, J.S., Grego, S., Salmon, E.D., and Mitchison, T.J. (2002). EB1–Microtubule Interactions in Xenopus Egg Extracts: Role of EB1 in Microtubule Stabilization and Mechanisms of Targeting to Microtubules. Mol. Biol. Cell *13*, 3614–3626.

Tobacman, L.S., and Korn, E.D. (1983). The kinetics of actin nucleation and polymerization. J. Biol. Chem. *258*, 3207–3214.

Torosantucci, L., De Luca, M., Guarguaglini, G., Lavia, P., and Degrassi, F. (2008). Localized RanGTP Accumulation Promotes Microtubule Nucleation at Kinetochores in Somatic Mammalian Cells. Mol. Biol. Cell *19*, 1873–1882.

Tournebize, R., Popov, A., Kinoshita, K., Ashford, A.J., Rybina, S., Pozniakovsky, A., Mayer, T.U., Walczak, C.E., Karsenti, E., and Hyman, A.A. (2000). Control of microtubule dynamics by the antagonistic activities of XMAP215 and XKCM1 in Xenopus egg extracts. Nat. Cell Biol. *2*, 13–19.

Tovey, C.A., and Conduit, P.T. (2018). Microtubule nucleation by γ-tubulin complexes and beyond. Essays Biochem. *62*, 765–780.

Tovey, C.A., Tubman, C.E., Hamrud, E., Zhu, Z., Dyas, A.E., Butterfield, A.N., Fyfe, A., Johnson, E., and Conduit, P.T. (2018). γ-TuRC Heterogeneity Revealed by Analysis of Mozart1. Curr. Biol. *0*.

Trieselmann, N., Armstrong, S., Rauw, J., and Wilde, A. (2003). Ran modulates spindle assembly by regulating a subset of TPX2 and Kid activities including Aurora A activation. J. Cell Sci. *116*, 4791–4798.

Tsai, M.-Y., Wiese, C., Cao, K., Martin, O., Donovan, P., Ruderman, J., Prigent, C., and Zheng, Y. (2003). A Ran signalling pathway mediated by the mitotic kinase Aurora A in spindle assembly. Nat. Cell Biol. *5*, 242–248.

Tulu, U.S., Fagerstrom, C., Ferenz, N.P., and Wadsworth, P. (2006). Molecular Requirements for Kinetochore-Associated Microtubule Formation in Mammalian Cells. Curr. Biol. *16*, 536–541.

Uehara, R., Nozawa, R., Tomioka, A., Petry, S., Vale, R.D., Obuse, C., and Goshima, G. (2009). The augmin complex plays a critical role in spindle microtubule generation for mitotic progression and cytokinesis in human cells. Proc. Natl. Acad. Sci. *106*, 6998–7003.

Vaart, B. van der, Akhmanova, A., and Straube, A. (2009). Regulation of microtubule dynamic instability. Biochem. Soc. Trans. *37*, 1007–1013.

Vale, R.D. (2003). The Molecular Motor Toolbox for Intracellular Transport. Cell *112*, 467–480.

Vasioukhin, V., Bauer, C., Yin, M., and Fuchs, E. (2000). Directed Actin Polymerization Is the Driving Force for Epithelial Cell–Cell Adhesion. Cell *100*, 209–219.

Vemu, A., Atherton, J., Spector, J.O., Moores, C.A., and Roll-Mecak, A. (2017). Tubulin isoform composition tunes microtubule dynamics. Mol. Biol. Cell *28*, 3564–3572.

Venkatram, S., Tasto, J.J., Feoktistova, A., Jennings, J.L., Link, A.J., and Gould, K.L. (2004). Identification and Characterization of Two Novel Proteins Affecting Fission Yeast γ-tubulin Complex Function. Mol. Biol. Cell *15*, 2287–2301.

Vérollet, C., Colombié, N., Daubon, T., Bourbon, H.-M., Wright, M., and Raynaud-Messina, B. (2006). Drosophila melanogaster γ-TuRC is dispensable for targeting γ-tubulin to the centrosome and microtubule nucleation. J. Cell Biol. *172*, 517–528.

Vignaud, T., Blanchoin, L., and Théry, M. (2012). Directed cytoskeleton self-organization. Trends Cell Biol. *22*, 671–682.

Vinh, D.B.N., Kern, J.W., Hancock, W.O., Howard, J., and Davis, T.N. (2002). Reconstitution and Characterization of Budding Yeast γ-Tubulin Complex. Mol. Biol. Cell *13*, 1144–1157.

Viovy, J.-L. (2000). Electrophoresis of DNA and other polyelectrolytes: Physical mechanisms. Rev. Mod. Phys. *72*, 813–872.

Vitre, B., Coquelle, F.M., Heichette, C., Garnier, C., Chrétien, D., and Arnal, I. (2008). EB1 regulates microtubule dynamics and tubulin sheet closure in vitro. Nat. Cell Biol. *10*, 415–421.

Vogt, N., Koch, I., Schwarz, H., Schnorrer, F., and Nüsslein-Volhard, C. (2006). The γTuRC components Grip75 and Grip128 have an essential microtubule-anchoring function in the Drosophila germline. Development *133*, 3963–3972.

Voter, W.A., and Erickson, H.P. (1984). The kinetics of microtubule assembly. Evidence for a two-stage nucleation mechanism. J. Biol. Chem. *259*, 10430–10438.

Wainman, A., Buster, D.W., Duncan, T., Metz, J., Ma, A., Sharp, D., and Wakefield, J.G. (2009). A new Augmin subunit, Msd1, demonstrates the importance of mitotic spindle-templated microtubule nucleation in the absence of functioning centrosomes. Genes Dev. *23*, 1876–1881.

Walker, R.A., O'Brien, E.T., Pryer, N.K., Soboeiro, M.F., Voter, W.A., Erickson, H.P., and Salmon, E.D. (1988). Dynamic instability of individual microtubules analyzed by video light microscopy: rate constants and transition frequencies. J. Cell Biol. *107*, 1437–1448.

Wang, H.-W., and Nogales, E. (2005). Nucleotide-dependent bending flexibility of tubulin regulates microtubule assembly. Nature *435*, 911–915.

Wang, H., Robinson, R.C., and Burtnick, L.D. (2010a). The structure of native G-actin. Cytoskeleton *67*, 456–465.

Wang, H.-W., Long, S., Finley, K.R., and Nogales, E. (2005). Assembly of GMPCPP-Bound Tubulin into Helical Ribbons and Tubes and Effect of Colchicine. Cell Cycle *4*, 1157–1160.

Wang, S., Wu, D., Quintin, S., Green, R.A., Cheerambathur, D.K., Ochoa, S.D., Desai, A., and Oegema, K. (2015). NOCA-1 functions with γ-tubulin and in parallel to Patronin to assemble non-centrosomal microtubule arrays in C. elegans. ELife *4*, e08649.

Wang, Z., Wu, T., Shi, L., Zhang, L., Zheng, W., Qu, J.Y., Niu, R., and Qi, R.Z. (2010b). Conserved Motif of CDK5RAP2 Mediates Its Localization to Centrosomes and the Golgi Complex. J. Biol. Chem. *285*, 22658–22665.

Wang, Z., Zhang, C., and Qi, R.Z. (2014). A newly identified myomegalin isoform functions in Golgi microtubule organization and ER–Golgi transport. J Cell Sci *127*, 4904–4917.

Wegner, A. (1976). Head to tail polymerization of actin. J. Mol. Biol. *108*, 139–150.

Weisenberg, R.C. (1972). Microtubule Formation in vitro in Solutions Containing Low Calcium Concentrations. Science *177*, 1104–1105.

Weisenberg, R.C., Broisy, G.G., and Taylor, E.William. (1968). Colchicine-binding protein of mammalian brain and its relation to microtubules. Biochemistry *7*, 4466–4479.

Weston, L., Coutts, A.S., and La Thangue, N.B. (2012). Actin nucleators in the nucleus: an emerging theme. J. Cell Sci. *125*, 3519–3527.

Widlund, P.O., Stear, J.H., Pozniakovsky, A., Zanic, M., Reber, S., Brouhard, G.J., Hyman, A.A., and Howard, J. (2011). XMAP215 polymerase activity is built by combining multiple tubulin-binding TOG domains and a basic lattice-binding region. Proc. Natl. Acad. Sci. U. S. A. *108*, 2741–2746.

Wieczorek, M., Bechstedt, S., Chaaban, S., and Brouhard, G.J. (2015). Microtubule-associated proteins control the kinetics of microtubule nucleation. Nat. Cell Biol. *17*, 907–916.

Wiese, C. (2008). Distinct Dgrip84 Isoforms Correlate with Distinct γ-Tubulins in Drosophila. Mol. Biol. Cell *19*, 368–377.

Wiese, C., and Zheng, Y. (2000). A new function for the γ -tubulin ring complex as a microtubule minus-end cap. Nat. Cell Biol. *2*, 358–364.

Wiese, C., Wilde, A., Moore, M.S., Adam, S.A., Merdes, A., and Zheng, Y. (2001). Role of Importin-β in Coupling Ran to Downstream Targets in Microtubule Assembly. Science *291*, 653–656.

van den Wildenberg, S.M.J.L., Tao, L., Kapitein, L.C., Schmidt, C.F., Scholey, J.M., and Peterman, E.J.G. (2008). The Homotetrameric Kinesin-5 KLP61F Preferentially Crosslinks Microtubules into Antiparallel Orientations. Curr. Biol. *18*, 1860–1864.

Wittmann, T., Wilm, M., Karsenti, E., and Vernos, I. (2000). Tpx2, a Novel Xenopus Map Involved in Spindle Pole Organization. J. Cell Biol. *149*, 1405–1418.

Woodruff, J.B., Ferreira Gomes, B., Widlund, P.O., Mahamid, J., Honigmann, A., and Hyman, A.A. (2017). The Centrosome Is a Selective Condensate that Nucleates Microtubules by Concentrating Tubulin. Cell *169*, 1066-1077.e10.

Wu, J., and Akhmanova, A. (2017). Microtubule-Organizing Centers. Annu. Rev. Cell Dev. Biol. *33*, 51–75.

Wu, J., de Heus, C., Liu, Q., Bouchet, B.P., Noordstra, I., Jiang, K., Hua, S., Martin, M., Yang, C., Grigoriev, I., et al. (2016). Molecular Pathway of Microtubule Organization at the Golgi Apparatus. Dev. Cell *39*, 44–60.

Xiong, Y., and Oakley, B.R. (2009). In vivo analysis of the functions of -tubulin-complex proteins. J. Cell Sci. *122*, 4218–4227.

Yajima, H., Ogura, T., Nitta, R., Okada, Y., Sato, C., and Hirokawa, N. (2012). Conformational changes in tubulin in GMPCPP and GDP-taxol microtubules observed by cryoelectron microscopy. J. Cell Biol. *198*, 315–322.

Zanic, M., Stear, J.H., Hyman, A.A., and Howard, J. (2009). EB1 Recognizes the Nucleotide State of Tubulin in the Microtubule Lattice. PLOS ONE *4*, e7585.

Zanic, M., Widlund, P.O., Hyman, A.A., and Howard, J. (2013). Synergy between XMAP215 and EB1 increases microtubule growth rates to physiological levels. Nat. Cell Biol. *15*, 688–693.

Zhang, J., and Megraw, T.L. (2007). Proper Recruitment of γ-Tubulin and D-TACC/Msps to Embryonic Drosophila Centrosomes Requires Centrosomin Motif 1. Mol. Biol. Cell *18*, 4037–4049.

Zhang, L., Keating, T.J., Wilde, A., Borisy, G.G., and Zheng, Y. (2000). The Role of Xgrip210 in γ-Tubulin Ring Complex Assembly and Centrosome Recruitment. J. Cell Biol. *151*, 1525–1536.

Zhang, R., Alushin, G.M., Brown, A., and Nogales, E. (2015). Mechanistic Origin of Microtubule Dynamic Instability and Its Modulation by EB Proteins. Cell *162*, 849–859.

Zhang, R., Roostalu, J., Surrey, T., and Nogales, E. (2017). Structural insight into TPX2-stimulated microtubule assembly. ELife *6*, e30959.

Zhang, X., Chen, Q., Feng, J., Hou, J., Yang, F., Liu, J., Jiang, Q., and Zhang, C. (2009). Sequential phosphorylation of Nedd1 by Cdk1 and Plk1 is required for targeting of the γTuRC to the centrosome. J. Cell Sci. *122*, 2240–2251.

Zheng, Y., Jung, M.K., and Oakley, B.R. (1991). γ-Tubulin is present in Drosophila melanogaster and homo sapiens and is associated with the centrosome. Cell *65*, 817–823.

Zheng, Y., Wong, M.L., Alberts, B., and Mitchison, T. (1995). Nucleation of microtubule assembly by a γ-tubulin-containing ring complex. Nature *378*, 578–583.

Zheng, Y., Lie Wong, M., Alberts, B., and Mitchison, T. (1998). [19] purification and assay of γ tubulin ring complex. In Methods in Enzymology, R.B. Valee, ed. (Academic Press), pp. 218–228.

Zhu, X., and Kaverina, I. (2013). Golgi as an MTOC: making microtubules for its own good. Histochem. Cell Biol. *140*, 361–367.

Zhu, H., Coppinger, J.A., Jang, C.-Y., Yates, J.R., and Fang, G. (2008). FAM29A promotes microtubule amplification via recruitment of the NEDD1–γ-tubulin complex to the mitotic spindle. J. Cell Biol. *183*, 835–848.

Zhu, H., Fang, K., and Fang, G. (2009). FAM29A, a target of Plk1 regulation, controls the partitioning of NEDD1 between the mitotic spindle and the centrosomes. J. Cell Sci. *122*, 2750–2759.

Zimmerman, W.C., Sillibourne, J., Rosa, J., and Doxsey, S.J. (2004). Mitosis-specific Anchoring of γ Tubulin Complexes by Pericentrin Controls Spindle Organization and Mitotic Entry. Mol. Biol. Cell *15*, 3642–3657.

Zuchero, J.B., Coutts, A.S., Quinlan, M.E., Thangue, N.B.L., and Mullins, R.D. (2009). p53-cofactor JMY is a multifunctional actin nucleation factor. Nat. Cell Biol. *11*, 451–459.

Zwetsloot, A.J., Tut, G., and Straube, A. (2018). Measuring microtubule dynamics. Essays Biochem. EBC20180035.